Syntheses, Characterisation and Quadratic Nonlinear Optical Properties of Ruthenium(II) Ammine Complexes and Related Organic Compounds

A thesis submitted to the University of Manchester for the degree of Doctor of Philosophy in the Faculty of Science and Engineering

July 2001

James Harris

Department of Chemistry, University of Manchester, Oxford Road, Manchester, M13 9PL, UK

ProQuest Number: 10729374

All rights reserved

INFORMATION TO ALL USERS
The quality of this reproduction is dependent upon the quality of the copy submitted.

In the unlikely event that the author did not send a complete manuscript
and there are missing pages, these will be noted. Also, if material had to be removed,
a note will indicate the deletion.

ProQuest 10729374

Published by ProQuest LLC (2017). Copyright of the Dissertation is held by the Author.

All rights reserved.
This work is protected against unauthorized copying under Title 17, United States Code
Microform Edition © ProQuest LLC.

ProQuest LLC.
789 East Eisenhower Parkway
P.O. Box 1346
Ann Arbor, MI 48106 – 1346

E81Pu

Th 22446

JOHN RYLANDS
UNIVERSITY
LIBRARY OF
MANCHESTER

Table of Contents

List of Figures

List of Tables

Abstract

The salts *trans*-$[Ru^{II}(NH_3)_4(L_D)(L_A)][PF_6]_3$ [L_D = NH_3 and L_A = *N*-methyl-2,7-diazapyrenium ($Medap^+$), *N*-(2-pyrimidyl)-4,4′-bipyridinium ($PymQ^+$), *N*-methyl-4-[*trans*-2-(4-pyridyl)ethenyl]pyridinium ($Mebpe^+$) and *N*-phenyl-4-[*trans*-2-(4-pyridyl)ethenyl]pyridinium ($Phbpe^+$); L_D = pyridine (py) and L_A = $Medap^+$, $PymQ^+$, $Mebpe^+$ or $Phbpe^+$; L_D = 1-methylimidazole (mim) and L_A = $Medap^+$, $PymQ^+$, $Mebpe^+$ or $Phbpe^+$] have been prepared. The complexes in these salts show intense $d\pi(Ru^{II})\rightarrow\pi^*(L_A)$ metal-to-ligand charge-transfer (MLCT) absorptions (λ_{max} = 560–700 nm). A single crystal X-ray structure of *trans*-$[Ru^{II}(NH_3)_4py(Medap^+)][PF_6]_3\bullet 4MeCN$ has been determined. Molecular first hyperpolarizabilities (β = 579–1068 × 10^{-30} esu) and two-level model static first hyperpolarizabilities (β_0 = 51–336 × 10^{-30} esu) have been obtained from hyper-Rayleigh scattering (HRS) studies at 1064 nm. β_0 generally increases as the MLCT absorption energy E_{max} decreases.

The salts *trans*-$[Ru^{II}(NH_3)_4(L_D)(L_A)][PF_6]_3$ [L_D = NH_3 and L_A = *N*-methyl-4,4′-bipyridinium (MeQ^+), *N*-phenyl-4,4′-bipyridinium (PhQ^+), *N*-(4-acetylphenyl)-4,4′-bipyridinium ($AcPhQ^+$), *N*-(2,4-dinitrophenyl)-4,4′-bipyridinium ($DNPhQ^+$), $Mebpe^+$, $Phbpe^+$ or $Medap^+$; L_D = mim and L_A = MeQ^+, PhQ^+, $AcPhQ^+$, $PymQ^+$, $Mebpe^+$ or $Phbpe^+$; L_D = 4-(dimethylamino)pyridine (dmap) and L_A = MeQ^+, PhQ^+ or $AcPhQ^+$; L_D = py and L_A = $PymQ^+$, $Mebpe^+$ or $Phbpe^+$; L_D = 4-(dimethylamino)benzonitrile and L_A = MeQ^+] have been studied by using electroabsorption (Stark) spectroscopy, yielding dipole moment changes $\Delta\mu_{12}$ for the MLCT excitations. β_0 values calculated according to the two-level model by using $\beta_0 = 3\Delta\mu_{12}(\mu_{12})^2/(E_{max})^2$ (μ_{12} = transition dipole moment) are mostly in good agreement with the HRS β_0 values. The electroabsorption results confirm the unusually large magnitudes of β_0 in these complex salts and also that *N*-arylation enhances β_0.

The cations 4-(4-dimethylaminophenyl)-*N*-(R)-pyridinium [R = Me, Ph, 2,4-dinitrophenyl (DNPh) or 2-pyrimidyl (Pym)], *trans*-4-(R_1)-*N*-R_2-4′-stilbazolium [R_1 = NMe_2 and R_2 = Me, Ph, DNPh or Pym; R_1 = OMe and R_2 = Me, Ph, DNPh or Pym], *trans*-*N*-R-4-(dimethylaminophenyl-4-buta-1,3-dienyl)pyridinium [R = Me, Ph, DNPh or Pym] and *trans*-4-[(4-dimethylaminophenyl)iminomethyl]-*N*-R-pyridinium [R = Me or Ph] have been prepared. These chromophores show intense $\pi(NMe_2/OMe)\rightarrow\pi^*$(pyridinum) charge-transfer absorptions (λ_{max} = 375–580 nm). Fluorescence-free β values (166–435 and 50–1396 × 10^{-30} esu) and β_0 values (51–227 and 23–446 × 10^{-30} esu) were obtained from femtosecond HRS at 800 and 1300 nm with PF_6^- salts. Single crystal X-ray structures of 7 salts have been determined. [*Trans*-4-dimethylamino-*N*-phenyl-4′-stilbazolium]PF_6 and [*trans*-4-[(4-dimethylaminophenyl)-iminomethyl]-*N*-phenyl-pyridinium]PF_6 crystallise in the noncentrosymmetric space group *Cc*, and give Kurtz powder test second harmonic generation efficiencies at 1907 nm of *ca.* 470 and 240 times that of urea, respectively.

The salts *cis*-$[Ru^{II}(NH_3)_4(L_A)_2][PF_6]_4$ [L_A = MeQ^+, PhQ^+, $AcPhQ^+$ or $PymQ^+$] *trans*-$[Ru^{II}(NH_3)_4(L_{A1})(L_{A2})][PF_6]_4$ [L_{A1} = L_{A2} = MeQ^+, PhQ^+, $AcPhQ^+$ or $PymQ^+$; L_{A1} = MeQ^+ and L_{A2} = PhQ^+, $AcPhQ^+$ or $PymQ^+$] have been prepared. The cis complexes exhibit two intense MLCT bands (λ_{max} = 497–644 nm) and interesting ligand-based electrochemistry. The trans complexes show one broad MLCT band (λ_{max} = 595–639 nm).

Declaration

I hereby declare that no portion of this work referred to in this thesis has been submitted in support of an application for another degree or qualification of this or any other university or other institute of learning.

Copyright

(1) Copyright in text of this thesis rests with the Author. Copies (by any process) either in full, or of extracts, may be made **only** in accordance with instructions given by the Author and lodged in the John Rylands University Library of Manchester. Details may be obtained from the Librarian. This page must form part of any such copies made. Further copies (by any process) of copies made in accordance with such instructions may not be made without the permission (in writing) of the Author.

(2) The ownership of any intellectual property rights which may be described in this thesis is vested in the University of Manchester, subject to any prior agreement to the contrary, and may not be made available for use by third parties without the written permission of the University, which will prescribe the terms and conditions of any such agreement.

Further information on the conditions under which disclosures and exploitation may take place is available from the Head of the Department of Chemistry.

Author History

James Harris graduated from the University of Manchester in July 1997 with a first class honours degree in chemistry. Since September 1997 he has been studying the second-order nonlinear optical properties of ruthenium ammine complexes and related purely organic compounds under the supervision of Dr. B. J. Coe at the University of Manchester.

Publications

1. "Ruthenium (II) Ammine Centres as Efficient Electron Donor Groups for Quadratic Non-Linear Optics", B. J. Coe, J. A. Harris, J. P. Essex-Lopresti, S. Houbrechts, A. Persoons, *J. Chem. Soc. Chem. Commun.*, 1997, 1645–1646.

2. "Enhancement of Molecular Quadratic Hyperpolarizabilities in Ruthenium (II) 4,4'-Bipyridinium Complexes by *N*-Phenylation", B. J. Coe, J. A. Harris, L. J. Harrington, J. C. Jeffery, L. H. Rees, S. Houbrechts and A. Persoons, *Inorg. Chem.*, 1998, **37**, 3391–3399.

3. "Tuning of Charge-Transfer Absorption and Molecular Quadratic Non-Linear Optical Properties in Ruthenium (II) Ammine Complexes", B. J. Coe, J. A. Harris, I. Asselberghs, A. Persoons, J. C. Jeffery, L. H. Rees, T. Gelbrich and M. B. Hursthouse, *J. Chem. Soc. Dalton Trans.*, 1999, 3617–3625.

4. "Tuning the Hyperpolarizabilities of Asymmetrically Substituted Trans-Tetra-Ammineruthenium(II) Complexes", S. Houbrechts, I. Asselberghs, A. P. Persoons, B. J. Coe, J. A. Harris, L. J. Harrington, M. C. Chamberlain, J. P. Essex-Lopresti, S. Gaines, *Proc. SPIE-Int. Soc. Opt. Eng.* (Organic Nonlinear Optical Materials), 1999, **3796**, 209–218.

5. "Large Molecular Hyperpolarizabilities in Donor/Acceptor-Substituted Trans-Tetraammine ruthenium(II) Complexes", S. Houbrechts, I. Asselberghs, A. Persoons, B. J. Coe, J. A. Harris, L. J. Harrington, J. P. Essex-Lopresti, *Mol. Cryst. Liq. Cryst. Science & Tech., Sect. B: Nonlinear Opt.*, 1999, **22(1-4)**, 161-164.

6. "Trans-4-[(4-dimethylaminophenyl)iminomethyl]-*N*-phenylpyridinium Hexafluoro-phosphate" B. J. Coe, J. A. Harris, T. Gelbrich and M. B. Hursthouse, *Acta Crystallogr.* 2000, **C56**, 1487–1489.

7. "A Comparison of the Pentaammine(pyridyl)ruthenium(II) and 4-(Dimethylamino)phenyl Groups as Electron Donors for Quadratic Non-linear Optics" B. J. Coe, J. A. Harris, K. Clays, A. Persoons, K. Wostyn and B. S. Brunschwig, *J. Chem. Soc. Chem. Commun.*, 2001, 1548–1549.

8. "Trans-4-[(4-dimethylaminophenyl)iminomethyl]-*N*-methylpyridinium Para-Toluene-Sulfonate" B. J. Coe, J. A. Harris, S. J. Coles and M. B. Hursthouse, *Acta Crystallogr.* 2001, **C57**, 857–858.

Presentations/Posters

"Enhancement and Tuning of Molecular Quadratic Hyperpolarizabilities in Ruthenium(II) Ammine Complexes" James A. Harris, Benjamin J. Coe, Jonathan P. Essex-Lopresti, Inge Asselberghs, Stephan Houbrechts, André Persoons, Bruce S. Brunschwig, Thomas Gelbrich and Michael B. Hursthouse, The Royal Society of Chemistry (Dalton Division) 34th International Conference on Coordination Chemistry, 9-14 July 2000.

Acknowledgements

Thanks are due to many people who have helped me over the past 4 years, making the time pass quickly and pleasantly. In particular thanks are due to:

Ben Coe, my supervisor for his ideas, patience and general support throughout the last four years at Manchester. Philip Day, my advisor, for our initial meetings and all his help and advice. Chris McDonald, for his thoughts and ideas in the lab. In particular his general football knowledge was invaluable, helping the time pass during those slow filtrations and for educating me about the finer points of the beautiful game. Lathe Jones, also for his thoughts in the lab and for putting up with all my questions about Australia. My friends and colleagues in Manchester and in the department of chemistry for their support.

Bruce Brunschwig and everyone in Brookhaven National Labs, New York, USA for allowing me to carry out the electroabsorption (Stark) studies on the ruthenium ammine complexes. Everyone at BNL was very accommodating and made me feel very welcome indeed. In particular I'd like to thank Dave Thompson for our trips around Long Island, without which I would not have seen the beautiful scenery on offer.

The technical support staff; Maurice Hart, Martin Jennings and their co-workers in the microanalytical labs, Val Boote in mass spectrometry and finally Ian Preece and John Friend in NMR.

The EPSRC for the financial support of this work.

Ombretta for her love and support during the writing of this thesis. And finally, my family to whom I dedicate this thesis for their support both financially and emotionally over the many years I have spent studying in Manchester.

To my family

Abbreviations

1D	One-Dimensional
2,2′-bpy	2,2′-Bipyridine
2D	Two-Dimensional
3D	Three-Dimensional
4,4′-bpy	4,4′-Bipyridine
A	Electron Acceptor
$AcPhQ^+$	*N*-(4-Acetylphenyl)-4,4′-bipyridinium
acpy	4-Acetylpyridine
BBO	*β*-Barium Borate
BLA	Bond Length Alternation
C–510	Coumarin–510
C–523	Coumarin–523
CT	Charge Transfer
D	Electron Donor
DANS	4-Dimethylamino-4′-nitrostilbene
DAST	4-Dimethylamino-*N*-methyl-stilbazolium Tosylate
dmabn	4-(Dimethylamino)benzonitrile
dmap	4-(Dimethylamino)pyridine
DMF	Dimethylformamide
dmit	2-thioxo-1,3-dithiole-4,5-dithiolato
DMSO	Dimethylsulphoxide
DNPh	2,4-Dinitrophenyl
$DNPhQ^+$	*N*-(2,4-Dinitrophenyl)-4,4′-bipyridinium
$dnppic^+$	*N*-(2,4-Dinotrophenyl)-4-picolinium
EFISHG	Electric Field Induced Second Harmonic Generation
E-O	Electro-Optical
FT	Fourier Transform
HOMO	Highest Occupied Molecular Orbital
HRS	Hyper-Rayleigh Scattering
ICT	Intramolecular Charge-Transfer
ILCT	Intra Ligand Charge-Transfer
IR	Infra-Red
isn	Isonicotinamide
ITO	Indium-Tin Oxide
KDP	Potassium Dihydrogen Phosphate
KTP	Potassium Titanyl Phosphate
L_A	Acceptor substituted ligand
LB	Langmuir-Blodgett
L_D	Donor substituted ligand
LMCT	Ligand-to-Metal-Charge-Transfer
LUMO	Lowest Unoccupied Molecular Orbital
Me	Methyl
$Mebpe^+$	*N*-Methyl-4-[*trans*-2-(4-pyridyl)ethenyl]pyridinium
$Medap^+$	*N*-Methyl-2,7-diazapyrenium
$mepic^+$	*N*-Methyl-4-picolinium
MeQ^+	*N*-Methyl-4,4′-bipyridinium
mim	1-Methylimidazole
MLCT	Metal-to-Ligand Charge-Transfer
MO	Molecular Orbital
NEt_2	Diethylamino
NIR	Near Infra-Red
NLO	Nonlinear Optical
NMe_2	Dimethylamino
NMR	Nuclear Magnetic Resonance
OMe	Methoxy
OTs	Tosylate
Ph	Phenyl
$Phbpe^+$	*N*-Phenyl-4-[*trans*-2-(4-pyridyl)ethenyl]pyridinium
phen	1,10-Phenathroline

PhQ^+	*N*-Phenyl-4,4′-bipyridinium
$ppic^+$	*N*-Phenyl-4-picolinium
PTZ	Phenothiazine
py	Pyridine
py-4-COOH	Pyridine-4-carboxylic acid
py-4-NH_2	4-Aminopyridine
pyca	Pyridine-4-carboxaldehyde
Pym	2-Pyrimidyl
$pympic^+$	*N*-(2-Pyrimidyl)-4-picolinium
$PymQ^+$	*N*-(2-Pyrimidyl)-4,4′-bipyridinium
pz	Pyrazine
SCE	Saturated Calomel Electrode
SHG	Second Harmonic Generation
SOS	Sum Over States
TCNQ	7,7′,8,8′-Tetracyanoquinodimethane
TFA	Trifluoroacetic Acid
THF	Tetrahydrofuran
THG	Third Harmonic Generation
UV	Ultra-Violet
UV/Vis	Ultra-Violet/Visible
ZINDO	Zerner Intermediate Neglect of Differential Overlap
$\Delta\mu_{12}$	Dipole moment change upon charge transfer excitation
β	Molecular first hyperpolarizability
β_0	Static molecular first hyperpolarizability
μ_{12}	Transition dipole moment

Chapter 1. Introduction

The field of nonlinear optics is relatively new; only since the availability of lasers[1] in the 1960s have the many nonlinear optical (NLO) effects been observed[2] and studied. A number of simple inorganic materials[3] (see section 1.3) have been developed over the past three decades for use in devices, but their suitability is not ideal. Molecular materials have received a great deal of attention for NLO applications because they promise higher optical nonlinearities and better processing properties than the traditional inorganics. Purely organic materials have generated the most interest in this field, but metallo-organic compounds also possess great potential for uses in novel NLO devices (see section 1.7).

1.1 Physical Origins of NLO Effects

NLO effects originate from the interaction of the electric field of light with the electronic charges within a material. Sufficiently strong interactions can result in the production of light beams with propagation characteristics (*e.g.* frequency, phase, amplitude, polarization) different from those of the incident light.

When light with a very strong electric field is incident on a molecule, the charges within the molecule can be displaced, leading to an induced polarization response. If the molecule has a dipole moment (*i.e.* the electronic charges are more easily displaced in one direction than another), then an asymmetric polarization is produced. This induced polarization can be described by the equation

$$P = P_0 + \alpha E + \beta E^2 + \gamma E^3 + ... \quad (1)$$

where P_0 is the static polarization (the polarization of the molecule in the absence of any field), E is the electric field of the incident light, α is the polarizability, β is the first hyperpolarizability and γ is the second hyperpolarizability. Since α is much larger than β and γ, NLO effects only become significant when very strong electric fields are used. It is for this reason that NLO effects were not observed until the invention of lasers.

The β coefficient gives rise to second-order (quadratic) effects such as the Pockels effect, second harmonic generation (SHG) and three-wave mixing. The γ coefficient gives rise to third-order (cubic) effects such as third harmonic generation (THG), optical bistability, the optical Kerr effect, degenerate four-wave mixing and phase conjugation. Table 1 gives a summary of common NLO effects, listing input and output frequencies.

Table 1. Some common NLO effects.

Input frequencies	Output frequency	Effect
0, ω	ω	DC electro–optical effect (Pockels effect)
ω, ω	2ω	SHG
ω_1, ω_2	$\omega_1 \pm \omega_2$	Sum and difference frequency generation
ω, ω, ω	3ω	THG
ω, ω, ω	ω	Optical bistability
ω, ω, ω	ω	Optical Kerr effect
ω, ω, ω	ω	Degenerate four-wave mixing
ω, ω, ω	ω	Phase conjugation

The origin of the most widely studied NLO effect, SHG, can be demonstrated simply if we express the electric field of light as $E = E_0 \cos(\omega t)$, where E_0 is the amplitude of the electric field of the incident light, ω is the angular frequency and t is time. Equation 1 now becomes

$$P = P_0 + \alpha E_0 \cos(\omega t) + \beta E_0^2 \cos^2(\omega t) + \gamma E_0^3 \cos^3(\omega t) + ... \quad (2)$$

Given that $\cos^2(\omega t) = 1/2 + 1/2\cos(2\omega t)$ and considering only up to the second-order, then equation 2 becomes

$$P = \left[P_0 + 1/2\beta E_0^2\right] + \alpha E_0 \cos(\omega t) + 1/2\beta E_0^2 \cos(2\omega t) + ... \quad (3)$$

The frequency doubled component 2ω gives rise to SHG which is a special example of three-wave mixing where the two input frequencies are the same. It is called three-wave mixing because two photons of frequency ω combine to generate a single photon of

frequency of 2ω. This type of analysis can be extended to the third-order contribution and thus THG can be explained.

NLO effects are generally observed in bulk or macroscopic materials, for which the bulk polarization can be expressed as

$$P = P_0 + \chi^{(1)}E + \chi^{(2)}E^2 + \chi^{(3)}E^3 + ... \quad (4)$$

where P_0 is the intrinsic static bulk polarization of the material and $\chi^{(2)}$ and $\chi^{(3)}$ are the bulk second and third-order susceptibilities which are analogous to the coefficients in equation 1, except that the χ terms take into account local field effects. For a non-zero $\chi^{(2)}$ (required for quadratic NLO effects to be observed in bulk materials) the individual molecules must be arranged in a noncentrosymmetric fashion, *i.e.* the molecules must be arranged so that their β coefficients are additive. This study is concerned only with (largely molecular) second-order NLO properties, and third-order effects will hence not be discussed any further.

The development of novel molecular NLO materials begins with chemistry. An active molecule must be designed, synthesised and investigated to ensure that it has the correct properties before being incorporated into a bulk structure (see section 1.6). For second-order effects, several techniques exist to measure β (see section 1.4), allowing the establishment of detailed molecular structure-property relationships.

1.2 Practical Uses for NLO effects[4]

Applications of NLO materials lie primarily in the areas of optical communications, signal processing and data storage. The trend towards an increased emphasis on optical operation is expected to greatly improve the performance of computing devices, *etc.* The most common practical uses of second-order NLO effects are as follows:

1. The electro-optic effect (Pockels effect) is used for modulating and switching laser beams. Electro-optic modulators can convert an electrical signal into an amplitude

or phase modulation of a laser beam for use in telecommunications. At present there is only a small market for such devices made from potassium dihydrogen phosphate (KDP) or lithium niobate ($LiNbO_3$).

2. SHG is used for the generation of new laser sources. An example is the frequency doubling of a Nd:YAG laser (fundamental at 1064 nm) using KDP to produce light in the green region of the visible spectrum (532 nm). There is particular interest in the development of materials capable of frequency doubling low-power diode lasers from the near infra-red to the blue region of the visible spectrum, for use in optical data storage where decreasing the wavelength leads to an increase in data storage capacity.
3. Sum and difference frequency generation can allow the mixing of a laser beam (usually in the infra-red) carrying information, *e.g.* as an amplitude modulation (*i.e.* an optical signal), with a pump beam of a fixed intensity. This interaction can be used to convert the information-carrying beam to a wavelength where detection and processing may be much easier than at the original wavelength.

1.3 Established Inorganic NLO Materials

Following the first observations of NLO effects in quartz,[2a] there was much interest in inorganic crystalline materials. NLO effects were subsequently observed in KDP,[3a] $LiNbO_3$,[3b] silver mercury iodide (Ag_2HgI_4)[5] and lead titanate ($PbTiO_3$).[5]

Materials such as $LiNbO_3$ and KDP are used widely in current NLO devices. $LiNbO_3$ is used in waveguide applications, although it only has a moderately high NLO coefficient. SHG devices for operation with laser diodes have been demonstrated,[6] and a number of companies are producing electro-optic waveguide devices for rapid modulation and switching of light. Unfortunately, the material has to be grown from a non-congruent melt at high temperature, which can lead to difficulties in maintaining the proper composition. Furthermore, $LiNbO_3$ is susceptible to optical damage at high laser powers.

Table 2. Early NLO materials.

Year	Material	Relative SHG (1064 nm)[a]	References
1961	Quartz	1	2a
1962	KDP	16	3a
1963	ADP	15	7
1964	$LiNbO_3$	600	3b
1968	Ag_2HgI_4	1500	5
1968	$PbTiO_3$	2400	5

[a] Measured using the Kurtz powder test (see section 1.4.1).

KDP has been used to produce frequency-doublers and electro-optic shutters for use in high-power laser systems. Like $LiNbO_3$, it has a relatively low NLO coefficient, but large, high-quality single crystals grown from solution are of sufficient quality to be used in very high-powered laser systems.

Potassium titanyl phosphate (KTP) is relatively new to the NLO field, but has shown great promise. The main selling point of KTP is its SHG efficiency which is approximately thirty times that of KDP and three times that of $LiNbO_3$.[8] Highly efficient frequency-doubling has been demonstrated and waveguides have been made using ion-exchange methods.[9] The main problems are the limited size of the KTP crystals that can be grown and optical damage; cumulative exposure to incident radiation in high-power applications leads to discoloration of the material.

β-Barium borate (BBO) is another recently developed material having reasonable optical nonlinearity and high damage thresholds. It is of particular interest because its wide transparency range (approx. 200 nm to 2600 nm) makes it a good candidate for SHG and sum and difference frequency generation in the UV region.

1.4 Measurement of NLO Properties of Molecular Compounds

The study of organic molecular materials gained momentum following the observation of NLO effects in urea. It was found to have an SHG efficiency some 400 times that of quartz.[3b,5] Subsequently, various techniques have been developed to obtain information about the second-order NLO properties of molecules and molecular materials.

1.4.1 Kurtz-Powder Technique[5]

A laser is directed onto a powdered sample and the second harmonic light is collected, filtered, detected and compared with the signal from a reference sample (usually quartz or urea) to obtain a measure of the SHG efficiency. This technique is rather crude, since the magnitude of the response depends on the particle size and recrystallisation from a range of solvents can lead to different results due to polymorphism. The measured SHG efficiency depends upon both the molecular (β) and the bulk ($\chi^{(2)}$) NLO responses, and therefore powder testing is not a reliable probe of structure-property relationships.[10] Furthermore, an absence of SHG may simply indicate a centrosymmetric crystal structure, rather than a lack of NLO activity at the molecular level.

1.4.2 Electric Field Induced Second Harmonic Generation (EFISHG)[11]

In the EFISHG experiment a liquid or solution sample is subjected to a high voltage dc pulse which aligns the constituent molecules and thus allows SHG in what was previously an isotropic medium. Most materials are dissolved in an appropriate solvent, and methods have been developed to distinguish between contributions of the solvent and the solute.[11a] All molecular species will produce an EFISHG signal as it is formally a third-order process and as such the second hyperpolarizability (γ) is a component. γ is normally determined from THG experiments, then subtracted from the EFISHG response to

determine $\mu\beta$ (the vectoral projection of β along the molecular dipole moment direction). In compounds exhibiting significant charge-transfer (CT), $\mu\beta$ is much greater than γ, so the third-order contribution is usually ignored. EFISHG gives a projection of the β vector along the molecular dipole (μ) direction and therefore can be used to investigate structure-property relationships.

Unfortunately, the application of EFISHG is limited to neutral compounds. The presence of ionic species makes it impossible to apply high electric fields to a solution. Also, it is not possible to use EFISHG with molecules that have no net dipole moment (*e.g.* octupolar molecules – see section 1.5.5).

1.4.3 Hyper-Rayleigh Scattering (HRS)[12]

The HRS technique determines β by detecting the incoherently scattered second harmonic light generated from an isotropic solution. HRS arises from orientational fluctuations of asymmetric molecules in solution that give rise to local asymmetry, on a microscopic scale, in a macroscopically isotropic liquid.[12b] The light scattered from such a system has a component at the second harmonic that depends only on the β of the solute molecules and varies quadratically with incident intensity. For a solvent-solute system, this relation can be expressed by

$$\frac{I_{2\omega}}{I_{\omega}^2} = g(N_S\beta_S^2 + N_s\beta_s^2) \qquad (5)$$

where N_S and N_s are the concentrations of the solvent and solute, respectively, and g is an instrumental factor which takes into account the scattering geometry, collection efficiency and photomultiplier gain. The ratio $I_{2\omega}/I_{\omega}^2$ is determined for a dilution series of the solute and is plotted *vs.* the corresponding number density of the solute. For molecules non-absorbing at the second harmonic, $I_{2\omega}/I_{\omega}^2$ depends linearly upon the solute concentration and thus the slope equals $g\beta_s^2$. In cases where absorption does occur at the second

harmonic frequency, a Lambert-Beer correction must be included in equation 5. However, if very dilute solutions (10^{-4}–10^{-5} mol dm^{-3}) are used, such that concentration × pathlength × absorption coefficient < 0.05, then the correction factor is negligible and a linear dependence is observed. To obtain a value of β_s^2, a second series of a reference chromophore is measured, giving a slope of $g\beta_{\text{ref}}^2$. Once $g\beta_{\text{ref}}^2$ is known, then β_s^2 can be calculated from the ratio of both slopes (equation 6).

$$\frac{g\beta_s^2}{g\beta_{\text{ref}}^2} = \frac{\text{sample slope}}{\text{reference slope}} \tag{6}$$

HRS determines the average first hyperpolarizability in laboratory coordinates $\langle\beta^2\rangle$ which is related to the hyperpolarizability in the molecular reference system by a summation of weighted products of tensor components.[13] For example, the relation between the average hyperpolarizability in laboratory coordinates and the hyperpolarizability in the molecular reference system in a C_{2v} molecule can be expressed by

$$\langle\beta^2\rangle = \langle\beta_{zzz}^2\rangle + \langle\beta_{xzz}^2\rangle \tag{7}$$

$\langle\beta_{zzz}^2\rangle$ and $\langle\beta_{xzz}^2\rangle$ are defined by equations 8 and 9.

$$\langle\beta_{zzz}^2\rangle = \frac{1}{7}\beta_{333}^2 + \frac{6}{35}\beta_{333}\beta_{322} + \frac{9}{35}\beta_{322}^2 \tag{8}$$

$$\langle\beta_{xzz}^2\rangle = \frac{1}{35}\beta_{333}^2 - \frac{2}{105}\beta_{333}\beta_{322} + \frac{11}{105}\beta_{322}^2 \tag{9}$$

The letter indices refer to the laboratory frame and the number indices refer to the molecular frame.

Specific Advantages of the HRS technique are:

1. Values of β can be obtained directly, without the need to independently determine the dipole moment, μ, and the second hyperpolarizability, γ.
2. Experimental simplicity compared to EFISHG. There is no need for a dc field to be applied, so HRS can be used to study molecules with no net dipole moment and also ionic molecules. The latter has important implications for metal complexes which are often charged and may have a range of oxidation states.
3. Sensitivity to non-vector components of the β tensor (EFISHG only determines one component of β).

However, because of the inherently low intensity of the scattered second harmonic light, HRS requires sensitive detection equipment and a high intensity fundamental. High intensity of the fundamental can lead to problems[14] such as stimulated Raman or Brillouin scattering, self focusing or dielectric breakdown. Furthermore, the quadratic dependence of the HRS signal means that it is only possible to find the magnitude of β (*i.e.* not the sign), and HRS can also give unreliable results with molecules that luminesce in the region of the second harmonic.[15]

1.5 Organic Molecular NLO Materials[16]

Molecular materials have several advantages over the currently used inorganic crystals, such as larger bulk optical nonlinearities, faster response times and higher resistance to optical damage. For example, urea has an optical damage threshold of 500 GW/cm^2 at 1064 nm (for 10 ns pulses), compared to 0.5 GW/cm^2 for KDP under the same conditions. Furthermore, organic crystals often have high intrinsic birefringence which can facilitate phase matching (whereby the second harmonic and fundamental beams interfere in a constructive manner) for processes such as SHG, and they also have lower dielectric permittivities than established inorganics. The latter is important in applications such as electro-optic modulation where high frequency electric fields are placed across a sample. The maximum frequency that can be achieved is determined by (amongst other things) the

capacitance of the sample which is related to the dielectric permittivity of the molecules making up the material. By comparison with their inorganic counterparts, molecular NLO materials can suffer from disadvantages such as volatility, low thermal stability, mechanical weakness and low solubility, but these factors are of relatively minor significance.

In organic materials it is often possible to achieve the non-centrosymmetric arrangements which are critical for non-zero values of $\chi^{(2)}$. The NLO properties of molecular species may also be tuned via chemical synthesis, and molecules can be incorporated into Langmuir-Blodgett films (see section 1.6.2) or polymers (see section 1.6.3), providing routes to bulk materials other than single crystals. Various organic compounds have received a great deal of attention for their NLO properties over the past 30 years.[17] Using techniques for measuring β such as EFISHG and HRS (see section 1.4), structure-property relationships have been elucidated, and it is now a relatively simple matter to design molecules with very large β values. The same cannot be said for metallo-organic molecular materials which have received comparatively little attention until very recently.

Since NLO effects result from interactions between the electric field of light and polarizable electronic charges within a molecule, it is no great surprise that molecules containing a π-conjugated system often have large β values (the electrons in π-bonds are much more mobile than those involved in σ-bonds). In order for the induced polarization response to be asymmetric (a requirement for second-order NLO effects), the molecule must have a permanent dipole moment. This can be achieved by the introduction of an electron donor group (D) or an electron acceptor group (A), or both D and A groups if they are positioned so that their effects are additive (Figure 1). Typical electron donor groups are amino, hydroxy and alkoxy groups and typical electron acceptors are carboxyl, carbonyl, nitrile, nitro and nitroso groups.

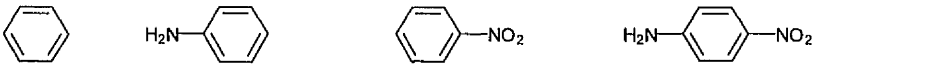

1. Symmetrical $\beta = 0$ **2.** Donor only $\beta = 2 \times 10^{-30}$ esu **3.** Acceptor only $\beta = 1 \times 10^{-30}$ esu **4.** Donor and acceptor $\beta = 20 \times 10^{-30}$ esu

Figure 1. Electron Donor and Acceptor-Substituted Benzenes.

Hence, in order for a molecule to have an especially large β it must possess a D group linked via a π-conjugated polarizable bridge to an A group. Such molecules are sometimes referred to as DπA systems. A good example of a DπA molecule is 4-dimethylamino-4′-nitrostilbene (DANS, **5**) which has a large β and is often used as a benchmark to evaluate the NLO properties of new chromophores.

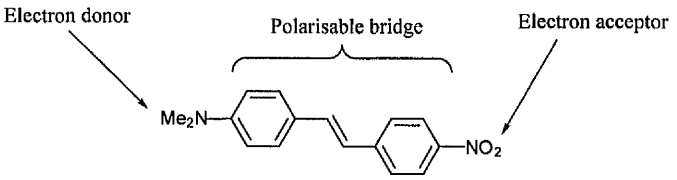

5. $CHCl_3$; λ_{max} = 430 nm; $\beta_{1907} = 73 \times 10^{-30}$ esu; $\beta_0 = 55 \times 10^{-30}$ esu; $\mu\beta_{1900} = 313 \times 10^{-48}$ esu[18]

1.5.1 The Two-Level Model

A widely useful two-level model,[19] developed by Oudar and Chemla, represents a simple theoretical description of the first hyperpolarizability of one-dimensional CT molecules. This model describes β in terms of a CT excitation between the ground and excited states, and can be used as a guide for the design of second-order NLO chromophores. For SHG, the dominant component of β is given by

$$\beta(-2\omega;\omega,\omega) = \frac{3\Delta\mu_{12}\mu_{12}^2}{(\hbar\omega_{CT})^2}\frac{\omega_{CT}}{[1-(2\omega)^2(\omega_{CT}^2)^{-1}][\omega_{CT}^2-\omega^2]} \qquad (10)$$

$$= \beta_0 \frac{\omega_{CT}}{[1-(2\omega)^2(\omega_{CT}^2)^{-1}][\omega_{CT}^2-\omega^2]}$$

where $\hbar\omega_{CT}$ is the energy of the CT excitation (E_{CT}), $\Delta\mu_{12}$ is the change in dipole moment between the ground state and the lowest energy excited state, μ_{12} is the electronic transition moment, ω is the angular frequency of the incident light and β_0 is the static first hyperpolarizability (the intrinsic β of the molecule in the absence of any field). A dispersion contribution is needed to compensate for the enhancement of β due to resonance effects. Unfortunately, the two-level model breaks down when ω_{CT} is close to the

fundamental or the second harmonic frequencies of the incident light: in the limiting cases of $\omega_{CT} = \omega$ or 2ω the dispersion factor is infinite and therefore $\beta_0 = 0$. Unless damping corrections are included, the two-level model can only be used to provide an estimate of β_0 when ω_{CT} is well removed from the fundamental or the second harmonic frequencies. When this is the case, β_0 can be used to quantitatively compare the optical nonlinearities of different molecules, although the accuracy of β_0 decreases significantly as ω_{CT} approaches ω or 2ω. It should be noted, however, that several two-level descriptions are available, and depending on which conventions are used to define the hyperpolarizability, values calculated from equation 10 can change by a constant factor of 0.5 or 2.[20] Other factors such as solvent and fundamental wavelength must also be considered when comparing experimental data (see section 1.5.3).

According to the two-level model, it is evident that there are several ways in which to increase β_0. Since β_0 is proportional to $\Delta\mu_{12}\mu_{12}/E_{CT}^2$, lowering the energy of the CT excitation or increasing $\Delta\mu_{12}$ or μ_{12} can all lead to increases in β_0.

UV/visible/NIR spectroscopy can be used as an indirect means of predicting the changes in β of a particular system. For instance, if two molecules are similar except for their acceptor groups then the two-level model predicts that the molecule with the lower energy CT absorption will have the larger β value, providing that the extinction coefficients for the absorptions are similar (extinction coefficient is related to the oscillator strength of an absorption). Correspondingly, if two molecules have CT absorption bands at the same energy, then the molecule with the larger extinction coefficient is expected to have the larger β value.

For a molecular NLO material to have a long operational lifetime it is essential that it operates 'off-resonance', *i.e.* it does not absorb the laser fundamental or second harmonic light. The two-level model predicts that β will increase as E_{CT} decreases, so sacrifices in the magnitude of β may have to be made in order maintain the necessary transparency. This is commonly referred to as the 'efficiency/transparency trade-off'. Consequently, it does not appear that one molecular material will fit all situations; rather it seems that they will be 'tailored' to operate at specific wavelengths.

1.5.2 Bond Length Alternation (BLA)[21]

A simple model has recently been proposed which correlates β with the degree of ground state polarization (amount of charge separation in the ground state).[18, 22] The latter property depends on the molecular structure and also on the environment of the molecule (*e.g.* the polarity of the bulk medium). In D/A polyenes, the ground state polarization can be related to a geometrical parameter, the bond length alternation (BLA), which is defined as the average of the difference in length between adjacent carbon-carbon bonds in a polymethine ($(CH)_n$) chain. Polyenes have alternating double and single bonds (with average distances of 1.34 Å and 1.45 Å, respectively) and thus show a high degree of BLA (+0.11 Å). The convention dictates that the neutral form has a positive BLA whilst the charge-separated form has a negative BLA (the double and single bond pattern is now reversed relative to the neutral form) (Figure 2).

Figure 2. Limiting canonical forms of a simple polyene.

Substituted polyenes with weak D/A groups have a ground state dominated by the neutral form and therefore have a high degree of BLA. As the strength of the D/A groups increases, the contribution of the neutral form to the ground state decreases and thus the degree of BLA decreases. When the two extreme resonance forms contribute equally to the ground state structure, the molecule exhibits zero BLA. This situation is called the cyanine limit; cyanine molecules can be represented by two degenerate resonance forms (Figure 3), resulting in a structure with virtually no BLA.

Figure 3. Resonance forms of a cyanine molecule.

There have been a number of theoretical[23] and experimental[24] studies correlating β with the extent of ground state polarization, and thus BLA, which all come to essentially the same conclusion. On going from the neutral polyene case towards the cyanine limit, β increases, peaks in a positive sense, then decreases and passes through zero at the cyanine limit. From this point going towards the charge-separated limit, β continues to decrease, peaks in a negative sense and then increases in a positive sense to become smaller in the charge-separated structure (Figure 4).

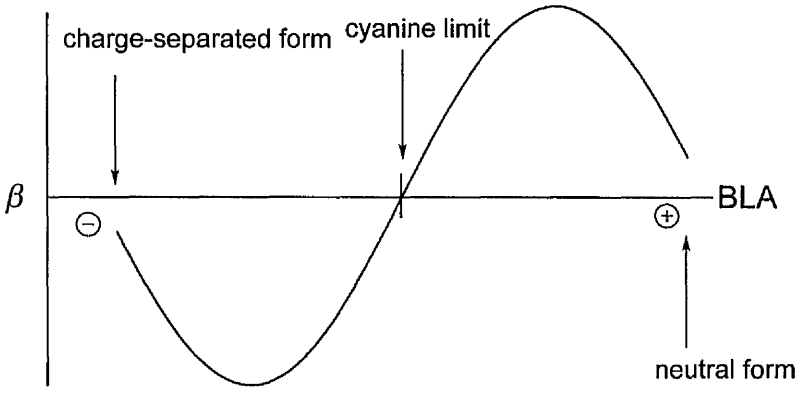

Figure 4. Plot of β versus BLA for a simple donor-acceptor polyene.

E_{CT} can be correlated in a similar way, *i.e.* it decreases as the BLA approaches the cyanine limit and increases as the ground state becomes more charge-separated or neutral in character.

1.5.3 Comparing β values

There are many problems in comparing β values obtained by different groups using different techniques. The most important of these arise from dispersion effects, the measurement of different tensor components, the errors associated with the measurement technique and different physical processes contributing to optical nonlinearity. In order to even attempt to compare β values, the fundamental wavelength, the solvent and the wavelength of the CT absorption compared to the fundamental/second harmonic wavelength must be noted.

The CT absorption wavelength will determine the amount of dispersion of the NLO response. Measurements are frequently available at only one wavelength and the degree to which the results are influenced by molecular resonances close to the fundamental/second harmonic wavelength is often difficult to quantify. It is possible to compensate for some dispersion effects in certain cases. For example, the two-level model (see section 1.5.1) can be used with some reliability for one-dimensional CT molecules, and the three-level model is used for octupolar species (see section 1.5.5).

The associated errors of the different techniques (*ca.* 10–15% for HRS and EFISHG) must also be taken into account; for example, β values of 100 and 113×10^{-30} esu are not significantly different if the error of the technique is 10%. The tensorial character of β is another practical complication. Experimental techniques only provide access to specific components of β or combinations of components of β. Solubility can also pose problems, since the compound under investigation must be sufficiently soluble to allow the detected NLO response to be distinguished from that of the solvent.

1.5.4 Strategies for increasing β

For a given bridge length, β can be maximised by having the correct combination of D and A groups. If the two limiting resonance forms are very different in energy (high energy CT), then the lower energy form will dominate the ground state structure and the molecule will exhibit a high degree of BLA. Changing the relative contributions of the resonance forms requires an understanding of the factors that influence their relative energies. In organic molecules there are two principal factors that determine the energies of the resonance forms:

1. A coulombic term that is destabilizing when charge is separated. Stabilisation can be achieved by increasing the strengths of the D/A groups or by placing the molecules in a more polar solvent.
2. A term associated with the topology of the molecule. If the neutral form of a molecule is aromatic, then charge-separation will interrupt the aromaticity and yield

a higher energy quinoidal resonance form. This results in an additional destabilisation due to loss of aromatic stabilisation, and will therefore further bias towards the neutral resonance form. Conversely, if the neutral form is quinoidal then the molecule will gain aromatic stabilisation in the charge-separated form.

Molecules based on the stilbene structure have a very large BLA, typically greater than 0.10 Å. Calculations have shown that β is maximised at a BLA of about 0.04 Å, so such molecules are not sufficiently polarized to maximise β. It has been proposed that the large BLA is due to the loss of aromatic stabilisation in the charge-separated resonance form.[22a,b]

A strategy to solve this problem was proposed and involves the design of molecules in which loss of aromaticity at one end (*e.g.* the donor end) on CT is offset by an accompanying gain in aromaticity at the other end. Examples of such molecules, where the acceptor groups gain aromaticity on charge separation, are compounds with 3-phenyl-5-isoxazolone, **6**, or N,N′-diethyl-thiobarbituric acid, **7**, A groups.[25] These molecules have very large β values and because they are not charged it is possible to induce polar order by electric field poling, leading to non-centrosymmetric bulk arrangements (see section 1.6). A large dipole moment, μ, in addition to a large β is desirable for electric field poling. Therefore, $\mu\beta$ can be considered as a molecular figure of merit. Both these molecules have $\mu\beta$ values greater than 10000×10^{-48} esu (measured by EFISHG at 1907 nm) which are very impressive when compared to that of DANS which has a $\mu\beta$ of 313×10^{-48} esu at 1900 nm.[18]

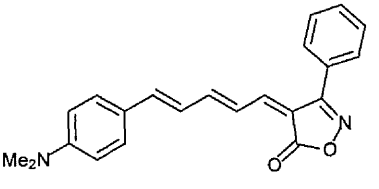

6.

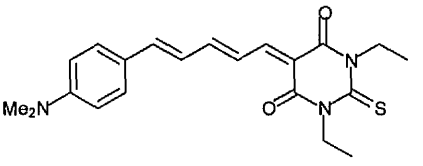

7.

An alternative approach is to replace strongly aromatic benzene rings with heteroaromatic rings that have smaller aromatic stabilisation energies. This approach has been successful using the low aromaticity thiazole[26] and thiophene[26] rings. Replacement of the benzene rings in DANS derivatives with thiophene rings results in a large increase in $\mu\beta$.[27]

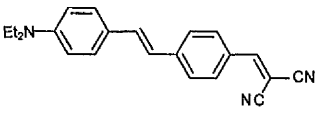

8. dioxane; λ_{max} = 468 nm; $\mu\beta_{1907} = 1100 \times 10^{-48}$ esu

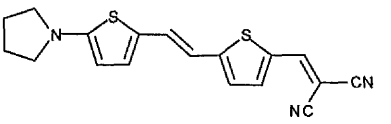

9. dioxane; λ_{max} = 584 nm; $\mu\beta_{1907} = 2600 \times 10^{-48}$ esu

Lower aromatic stabilisation energies are not the only benefit of replacing benzene rings with heteroaromatics. The aromaticity of heteroaromatics also affects the electronic coupling between the D and A substituents, and the electron-rich or electron-deficient nature of the heterocyclic ring system plays an important role in determining the overall electron donating/accepting ability of the D/A substituents. As expected, electron-rich heterocycles act as auxiliary electron donors and electron-deficient heterocycles as auxiliary acceptors.[28] Therefore, a molecule containing a donor attached to an electron-rich heterocycle, *e.g.* thiophene and an acceptor attached to an electron-deficient heterocycle, *e.g.* thiazole will have enhanced NLO properties compared to its benzene-derived analogue.

A recent study employing this strategy[29] revealed that the CT absorption energies of chromophores containing thiazole and thiophene rings are highly dependent on the position of the auxiliary donors/acceptors, as well as on the nature of the rings themselves.

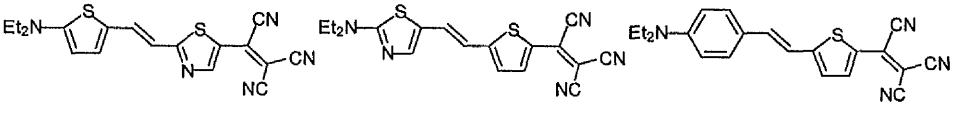

10. λ_{max}[dioxane] = 702 nm; auxiliary-donor/acceptor

11. λ_{max}[dioxane] = 622 nm; auxiliary-donor/acceptor reversed

12. λ_{max}[dioxane] = 640 nm; Only auxiliary-donor

Comparison of compound **12** with **11** indicates that replacing the benzene ring on the donor end with an electron-deficient heterocycle decreases the overall donating ability and counteracts the effects of the reduced aromatic stabilisation energy.

A further way of increasing β is to increase $\Delta\mu_{12}$,[30] by extending the conjugation length between the D and A groups. Such a structural change also decreases the energy gap between the ground and excited states and so would appear to be the best tactic to increase β. Several studies[31] in this area have yielded promising results. Dulcic *et al.*[32] studied a series of DπA compounds and found that $\mu\beta_0$ showed a strong dependence on conjugation length.

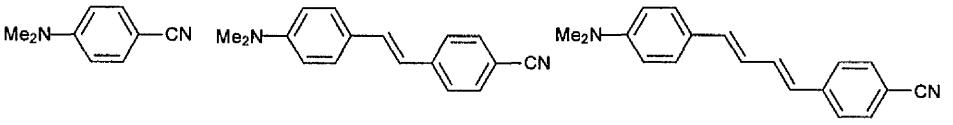

13. λ_{max}[DMSO] = 297 nm; $\mu\beta_0 = 90 \times 10^{-48}$ esu

14. λ_{max}[DMSO] = 390 nm; $\mu\beta_0 = 820 \times 10^{-48}$ esu

15. λ_{max}[DMSO] = 410 nm; $\mu\beta_0 = 1700 \times 10^{-48}$ esu

An increase in conjugation length can involve additional double bonds and/or additional phenylene rings. However, experimental data obtained by Oudar[19b] for a series of stilbene derivatives show that double bonds are more effective at increasing $\mu\beta$ than are phenylene rings.

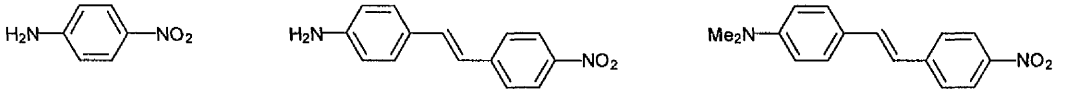

16. $\beta_{1064} = 34.5 \times 10^{-30}$ esu; **17.** $\beta_{1064} = 260 \times 10^{-30}$ esu; **18.** $\beta_{1064} = 450 \times 10^{-30}$ esu;

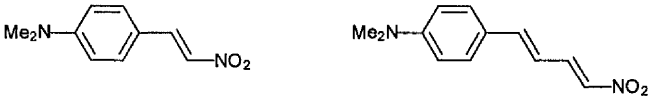

19. $\beta_{1064} = 220 \times 10^{-30}$ esu; **20.** $\beta_{1064} = 650 \times 10^{-30}$ esu;

These experimental results also agree with MO calculations. Morley *et al.*[33] calculated the β values for some DπA polyene systems, and the results show that β increases rapidly with conjugation length. However, similar calculations on related polyphenyls show that β appears to plateau after 5 phenyl rings. The effect of adding additional rings on β peaks for 3 rings and thereafter additional rings lead to decreasing returns. However, experimental data on polyphenyl systems shows a decrease in β for three ring systems which may be attributed to ring twisting.[34] Unfortunately, increasing the

conjugation length in polyenes decreases the thermal stability; chromophores with thermal stabilities greater than 200 °C are often required to meet the demands of material processing and device applications. Recently[35] a strategy for increasing the thermal stabilities of polyene chromophores by locking the configuration of the polyene has been investigated. In these studies, the π-conjugated polyene chains are fully embedded into plane-rigidified annulated rings (**21** and **23**). These configuration-locked chromophores have slightly blue-shifted CT bands compared to their corresponding non-rigidified analogues, and the configurational locking leads to dramatic increases in thermal stability.

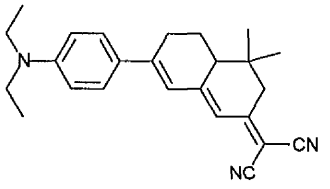

21. λ_{max}(dioxane) = 496 nm;
Td = >350 °C

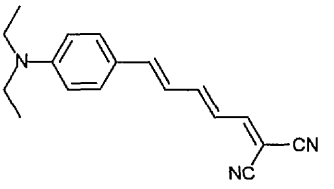

22. λ_{max}(dioxane) = 508 nm;
Td = 252 °C

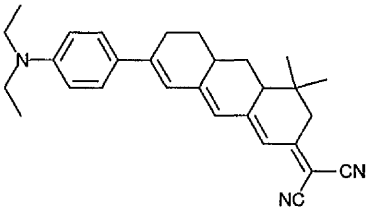

23. λ_{max}(dioxane) = 518 nm;
Td = 343 °C

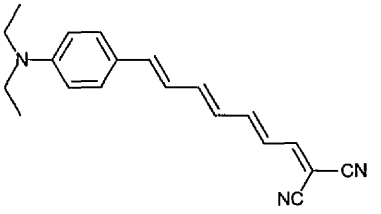

24. λ_{max}(dioxane) = 528 nm;
Td = 170 °C

1.5.5 Octupolar Molecules

In the early 90s, Zyss and co-workers introduced octupolar molecules possessing second-order NLO behaviour. Octupolar molecules are non-polar molecules that combine second-order NLO properties with a strict cancellation of all vector-like observables, including ground and excited state dipole moments.[36] Such systems usually possess three-fold rotational symmetry (C_3, D_3, D_{3h}; 2D-molecules) or tetrahedral or octahedral symmetry (T_d, O_h; 3-D molecules). 1,3,5-triamino-2,4,6-trinitrobenzene, **25**, is regarded as the prototypical octupolar molecule and as such has been studied extensively.[36c,d,37]

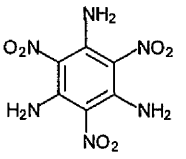

25.

Octupolar systems, therefore, cannot be described by the two-level model because $\Delta\mu_{12} = 0$. Instead, the two-level model must be extended to a three-level model[36d] which describes β in terms of a CT excitation between the ground and two degenerate excited states.

$$\beta = \frac{\mu_{12}^2 \mu_{22'}}{\hbar^2 \omega_{CT}^2} \frac{\omega_{CT}^4}{[\omega_{CT}^2 - 4\omega^2][\omega_{CT}^2 - \omega^2]} \tag{11}$$

μ_{12} is the transition moment from the ground state to the first degenerate excited state, $\mu_{22'}$ is the transition moment connecting the two excited states, ω_{CT} is the angular frequency of the CT transition and ω is the angular frequency of the incident light.

The advantages of using non-polar species for NLO purposes include an increased likelihood of non-centrosymmetric crystallization, no dipolar interactions, an increased ratio of off-diagonal versus diagonal β tensor components and an improved efficiency/transparency trade-off.

Due to the development of the HRS technique, it has become possible to experimentally evaluate the β values of octupolar molecules. Molecules with three-fold rotational symmetry have been the most widely studied, but other symmetries have also been investigated.

Lambert *et al.*[38] used truxenone as the central connecting moiety, as it is a good electron acceptor, has C_3 symmetry allowing three chromophores to be attached and has a planar π-electron system which may facilitate strong electronic coupling between the attached chromophores.

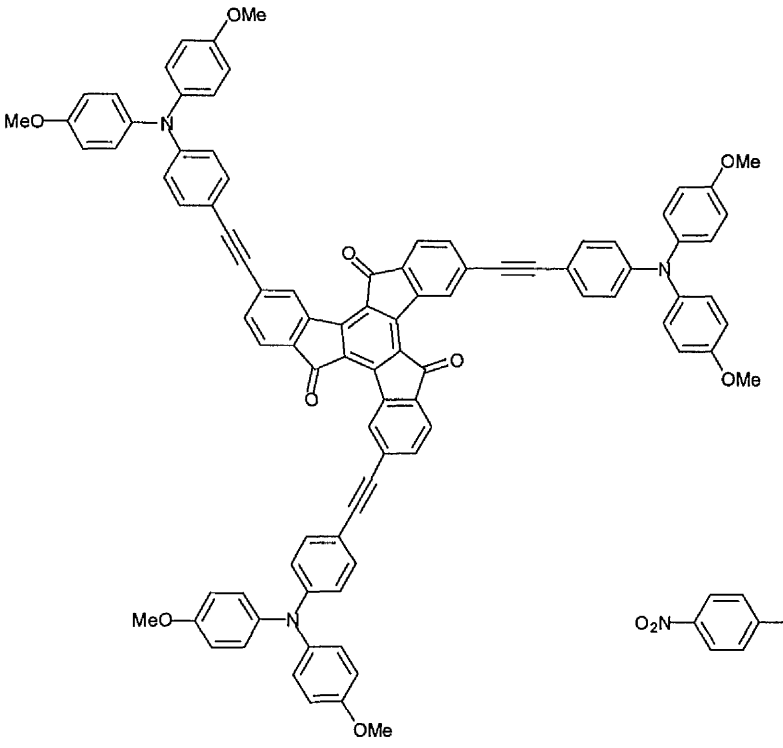

26. $CHCl_3$; λ_{max} = 509 nm;
$\beta_{1500} = 355 \times 10^{-30}$ esu;
$\beta_0 = 169 \times 10^{-30}$ esu

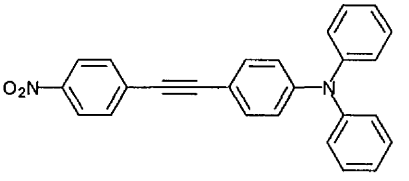

27. $CHCl_3$; λ_{max} = 418 nm;
$\mu\beta_{1300} = 315 \times 10^{-48}$ esu;
$\beta_0 = 28 \times 10^{-30}$ esu[39]

Although **26** actually has C_3 symmetry, Lambert *et al.* assumed a symmetry of D_{3d} because this is the approximate symmetry of the localised transition moments of the chromophores branches. In this case, β reduces to two non-zero components, $\beta_{xxx} = -\beta_{xyy}$, if Kleinman symmetry is valid.[19c,40] **26** has a lower energy CT absorption and a much larger β value compared to **27** which is attributed in part to the stronger electron accepting abilities of the truxenone unit.

Wortmann *et al.*[41] have followed many different strategies to optimise the β values of octupolar molecules with three-fold symmetry; increasing acceptor strength, decreasing steric hindrance to ensure planarity of the molecule and extending conjugation lengths. They have also investigated branched cyanine molecules. Cyanines are known to have large linear polarizabilities, but because they are symmetrical, they do not exhibit second-order NLO effects. Branching removes the centre of symmetry and gives rise to non-vanishing β values.[42]

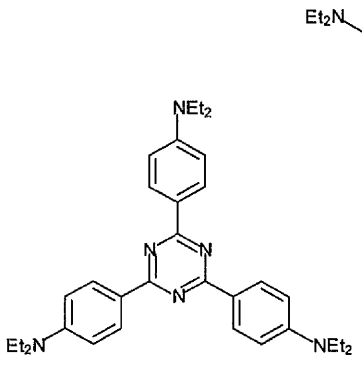

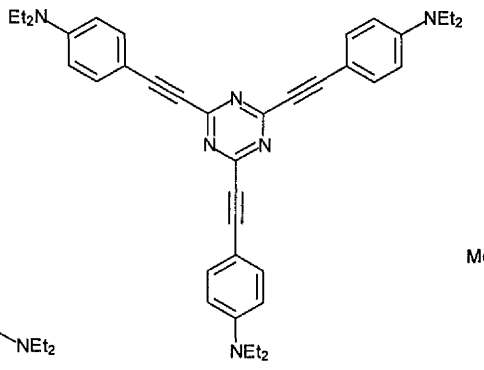

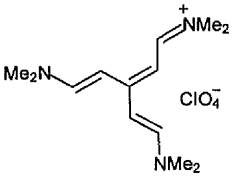

28. acetone; $\lambda_{max} = 375$ nm; $\beta_{1064} = 436 \times 10^{-30}$ esu; $\beta_0 = 191 \times 10^{-30}$ esu

29. acetone; $\lambda_{max} = 425$ nm; $\beta_{1064} = 1087 \times 10^{-30}$ esu; $\beta_0 = 331 \times 10^{-30}$ esu

30. acetonitrile; $\lambda_{max} = 430$ nm; $\beta_{1064} = 275 \times 10^{-30}$ esu; $\beta_0 = (\beta_{zzz}^2 + \beta_{yyy}^2)^{1/2} = 81 \times 10^{-30}$ esu

Compounds **28** and **29** have approximate D_{3h} symmetry, so β reduces to one non-vanishing component β_{zzz}. **30** has approximate C_{3h} symmetry and in this case β reduces to two non-vanishing components. The central 1,3,5-triazinyl unit acts as an electron-acceptor group and also has the additional benefit of lowering steric hindrance between the chromophoric arms. As with 1-D CT organic chromophores, extension of the conjugation lengths in the octupolar molecules leads to significant increases in β.

Wortmann *et al.*[43] have recently investigated similar compounds based on a 1,3,5-tricyanobenzene central unit. **32** has the largest β reported to date for an octupolar molecule. Wortmann *et al.* re-measured the β of **29** in the same solvent ($\lambda_{max} = 418$ nm; $\beta_{1064} = 1139 \times 10^{-30}$ esu; $\beta_0 = 371 \times 10^{-30}$ esu); the 1,3,5-triazinyl and 1,3,5-tricyanobenzene units have similar acceptor strengths, so the large increase in β between **29** and **32** was attributed to unusually effective conjugation through the 1,3,5-tricyanobenzene central core.

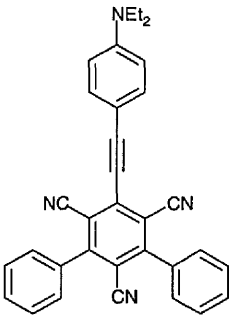

31. dioxane; $\lambda_{max} = 466$ nm;
$\beta_{1064} = 4093 \times 10^{-30}$ esu;
$\beta_0 = 767 \times 10^{-30}$ esu

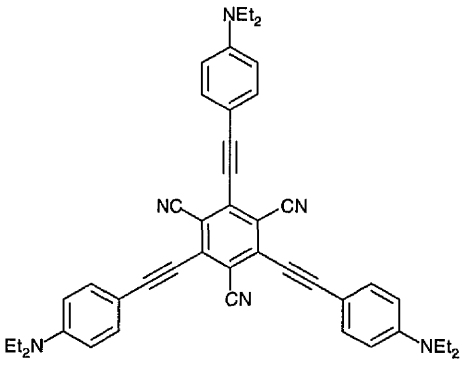

32. dioxane; $\lambda_{max} = 476$ nm;
$\beta_{1064} = 7219 \times 10^{-30}$ esu;
$\beta_0 = 1152 \times 10^{-30}$ esu

Zyss *et al.*[44] have studied octupolar molecules derived from a 1,3,5-triazinyl unit with stilbazolium chromophoric arms. Unfortunately, the β value of **33** could not be evaluated because of strong two-photon fluorescence in the region of the second harmonic (670 nm). Compounds **34** and **35** both have fairly large β values, with the difference between them accounted for by an increase in donor strength as evidenced by the decrease in CT energy.

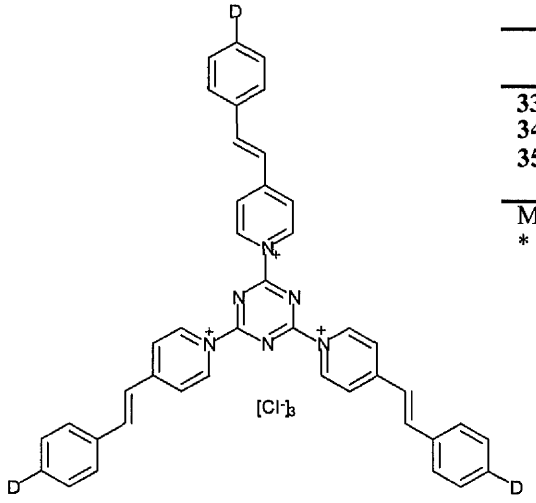

	D	λ_{max} /nm	β_{1340} (10^{-30} esu)	β_0 (10^{-30} esu)
33	NMe_2	547	*	
34	MeO	440	19	9
35	MeS	470	46	20

Measurements in DMSO
* fluorescence

Blanchard-Desce *et al.*[45] have studied a series of twisted biphenyl derivatives. The *ortho* substituents cause the phenyl rings to adopt a twisted arrangement which has a D_{2d} or 'quasi-tetrahedral' symmetry. Due to symmetry reasons, β reduces to one non-vanishing component, β_{xyz}.

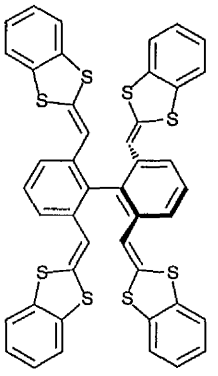

36. $CHCl_3$;λ_{max} = 320 nm;
$\beta_{1064} = 50 \times 10^{-30}$ esu

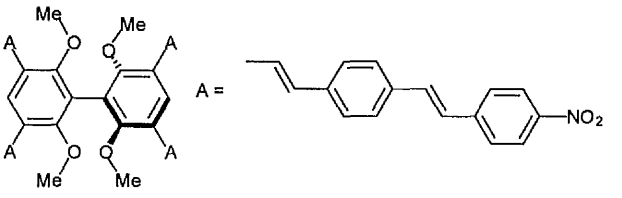

37. $CHCl_3$; λ_{max} = 401 nm;
$\beta_{1340} = 145 \times 10^{-30}$ esu

1.6 Solid State NLO Materials

Creating suitable solid-state forms of molecular NLO materials so that bulk $\chi^{(2)}$ values are maximized is challenging. The size of the $\chi^{(2)}$ coefficient depends on both the magnitude of the molecular β value and on the relative orientations of the molecules within the solid. For a non-zero $\chi^{(2)}$ the molecules must be arranged in a non-centrosymmetric fashion, and to maximise $\chi^{(2)}$ they must also be aligned so that the major β coefficients of the molecules are additive. For applications such as SHG the situation is further complicated by the need for phase matching, whereby the second harmonic and fundamental beams interfere in a constructive manner. There are several ways to prepare high $\chi^{(2)}$ materials at present, including growing single crystals, fabricating polymers or Langmuir-Blodgett (LB) films.

1.6.1 Single Crystals

Unfortunately, it is currently not possible to accurately predict from a molecular structure how a compound will crystallize. Nevertheless, there is much that a synthetic chemist can do to influence the way in which molecules arrange themselves. Highly polar DπA molecules tend to align in antiparallel pairs to minimise energies. This undesirable

tendency can be counteracted in a number of ways, *e.g.* substitution of bulky side groups (which do not themselves detract from the β value). The inclusion of chiral centres[46] within substituent groups will ensure a non-centrosymmetric crystal structure (although this can still involve effective dipole cancellation), and the incorporation of groups which encourage hydrogen bonding[46a,47] may also be advantageous since the relatively strong forces involved in hydrogen bonding may be sufficient to overcome dipolar forces. Unfortunately, single crystal growth is very time consuming and in general is not appropriate for the formation of thin films suitable for use in wave-guide devices.

1.6.2 LB films

The main attraction of the LB technique lies in the ability to build up on a substrate a film of accurately controlled thickness and composition, in which dipolar molecules are highly ordered. LB films can be deposited a monolayer at a time, allowing complex structures to be engineered. It is possible, by careful design, to make multi-layers having very high NLO coefficients. Interleaved LB film structures (Figure 5) can be designed so that the molecular optical nonlinearities from adjacent monolayers are additive.

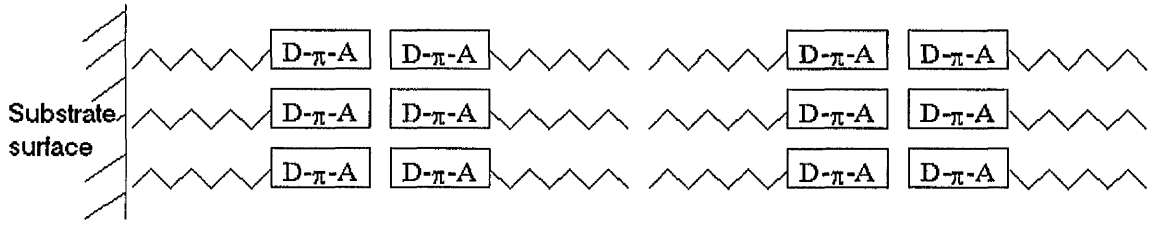

Figure 5. Schematic of an interleaved LB film.

However, there are drawbacks to the LB approach. Firstly, the molecules have to be specifically designed to be suitable for LB deposition, requiring the attachment of a hydrophobic chain or chains to the molecule. Such groups do not contribute to the β of the molecule, and act to dilute the overall bulk $\chi^{(2)}$ of the film. Also, the process of making

films in monolayer steps which are thick enough to guide light (*i.e.* > 1 μm) is both time-consuming and tedious and with present technology would prove to be an expensive manufacturing step. Studies on such thick films have revealed high optical losses because of scattering within the film caused by boundaries between crystalline domains. Nevertheless, the LB technique does hold great promise for fabricating NLO devices and good results have been obtained.[48] It is anticipated that the remaining problems of optical and mechanical quality will be overcome in time.

1.6.3 Polymer Films

The use of polymeric compounds is another way of forming ordered thin films having high optical nonlinearities. Molecules with large β values can be incorporated into polymers in two ways, either by simply mixing the two components together to make a 'guest-host' system, or by attaching the active molecules to the polymer chain to make a 'side-chain' polymer (Figure 6).

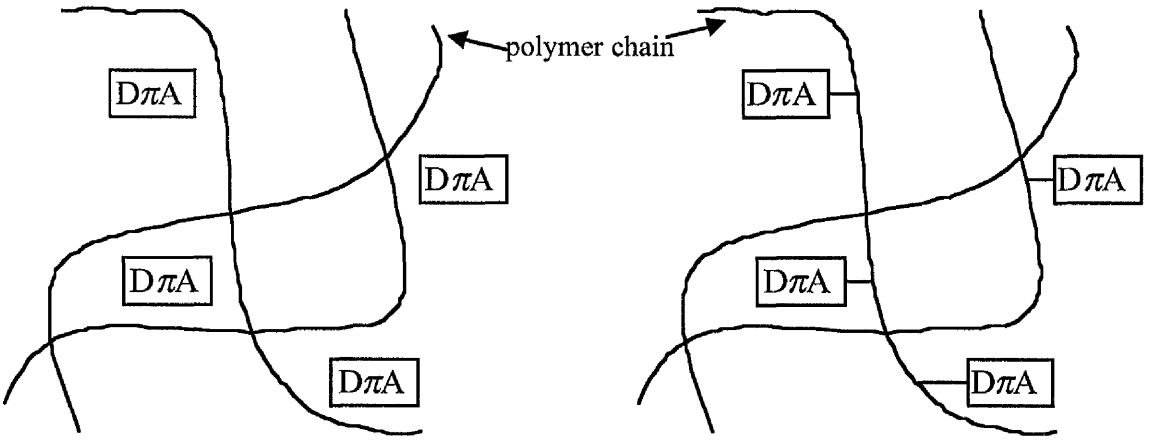

Figure 6. Schematic of guest-host and side-chain polymer systems.

In guest-host systems, a degree of orientational order can be obtained by poling the material using a strong dc electric field at elevated temperatures (above the glass transition temperature, T_g). Above its T_g a polymer adopts a rubbery state, so the guest molecules can move to a certain extent to align their dipoles with the field direction. With the field

still in place, the material is then cooled, 'locking' the dipolar molecules in place. Figure 6 is an idealised picture of what can be achieved by this method; in practice only a small amount of ordering can be created. Poled guest-host polymers have the advantage that in principle any non-ionic NLO molecule can be incorporated and standard techniques of polymer processing can be used to fabricate devices, thereby facilitating mass production. However, such materials do have disadvantages. For example, the inactive polymer matrix dilutes the NLO response, and the concentration of active molecules is limited by their solubility in the polymer matrix. The degree of orientation is also limited by thermal effects and over time, chain motion may allow a relaxation of the NLO molecules back into a centrosymmetric arrangement.

Side-chain polymers require more demanding synthetic chemistry, but they avoid the problem of relaxation of the NLO molecules which are directly attached to the polymer chain. Higher chromophores concentrations can be achieved and the same processing techniques can be used as with the guest-host systems.

In addition to these two types of polymers, work is being carried out to investigate the properties of various other types of polymers for NLO applications.[49] The following systems are being investigated because they have various attractive features such as higher concentrations of active molecules or decreased relaxation rates.

1. Main-chain polymers in which the NLO molecule is incorporated into the polymer chain itself.
2. Crossed-linked systems in which the polymer chains are immobilized by cross linkages between chains.
3. Sol-gel glasses in which suitable organic NLO molecules are suspended in inorganic glasses formed by polymerisation techniques.
4. Organic glasses formed from suitable organic NLO molecules when cooled appropriately.

1.7 *Metallo-organic Molecular NLO Materials*

Metal complexes have received relatively little attention compared to purely organic molecules for NLO effects. Interest in this field only took off in the late 1980s when the first reports of metal complexes with large SHG efficiencies were published.[52–57]

Depending on their oxidation state, metal centres can act as extremely powerful D/A groups compared to conventional organic substituents. Metal complexes can therefore possess intense, low-energy metal-to-ligand or ligand-to-metal CT absorptions (MLCT and LMCT, respectively). Such optical absorption bands are often associated with large second-order NLO activities. Redox activity may also provide an effective means of switching NLO responses.[50]

Changing the ligands attached to a D/A metal centre allows for 'fine tuning'/optimisation of β. Ligand changes can also influence the crystallographic factors that affect bulk efficiencies. For example, incorporation of a chiral ligand will ensure that, if resolved, the metal complex will crystallize in a noncentrosymmetric arrangement. The counter-ions of metal complex salts can also be varied readily, providing another means to modify bulk structures. Compared with purely organic compounds, the incorporation of transition metal ions can in some cases lead to increased solubility, thereby increasing the processability of a material.

A number of illustrative examples of transition metal complexes possessing second-order NLO properties are briefly discussed in the following sections. Further details may be found in a number of reviews published in the last few years.[10,51]

1.7.1 Metallocene Complexes

In 1987, Green *et al.*[52] showed that (*Z*)-1-ferrocenyl-2-(4-nitrophenyl)ethane, **38**, has an excellent SHG efficiency, and thus demonstrated the potential of organometallic compounds in the field of second-order NLO materials. The cis isomer was studied because it crystallizes in a noncentrosymmetric space group. By contrast the trans isomer

of **38** crystallizes in a centrosymmetric arrangement. Recently, chiral derivatives of (*E*)-1-ferrocenyl-2-(4-nitrophenyl)ethane, *e.g.* **39**, have been studied.[53] The chirality means that **39** crystallizes noncentrosymmetrically and thus bulk SHG can be observed (100 times that of a urea standard). However, the observed β values for **39** and related complexes were lower than expected,[54] a result attributed to poor coupling between the metal centre and the 4-nitrophenyl substituent due to the molecular shape.

Compound **40** was made and studied as part of a series of ferrocenyl *N*-methylpyridinium salts in which the SHG activity depends critically on the nature of the counter anion.[55,56] As with purely organic NLO chromophores, elongation of conjugated bridges, as well as addition of D groups to the metallocene rings has been found to lead to increases in β.[57,54]

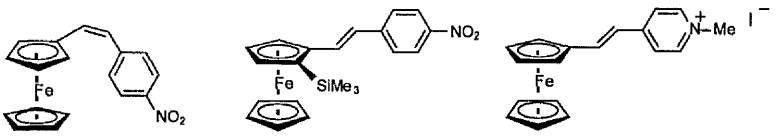

38. SHG_{1064} = 62 × urea; **39**. SHG_{1907} = 100 × urea; **40**. SHG_{1907} = 220 × urea;

For DπA metallocenes, in contrast to most organic chromophores, two intense optical transitions are observed in the low-energy region of the UV/visibleNIR spectrum (Figure 7). If design guidelines are to be developed, it is essential to ascertain how these absorptions contribute to the molecular NLO responses. Marder *et al.*[54] first suggested that the transitions correspond to MLCT [dπ(M)$\rightarrow\pi^*$(L) on bridge; lowest energy absorption] and ILCT (intra-ligand CT) ($\pi\rightarrow\pi^*$ on acceptor group; higher energy) and that both transitions should contribute to the NLO response. However, a theoretical study using a combination of Zerner intermediate neglect of differential overlap (ZINDO) and sum-over-states (SOS) techniques by Marks *et al.*[58] suggests that the NLO response is dependent only on the MLCT transition [dπ(M)$\rightarrow\pi^*$(L) on acceptor; lowest energy absorption]. Recently, Marder *et al.*[59] have refined their models, describing the absorption spectra by using a variety of techniques such as UV/visible/NIR, photoelectron and Stark spectroscopies and electrochemistry. These studies indicate that the lowest energy

absorption is an MLCT transition [$d\pi(M) \rightarrow \pi^*(L)$ on acceptor], as opposed to a transition involving a π^* orbital on the bridge (as originally suggested). The higher energy absorption is still considered to correspond to an ILCT process, and the NLO response is dependent on both transitions. The orbital situation is obviously rather complicated and thus the two-level model cannot be meaningfully applied to such complexes.

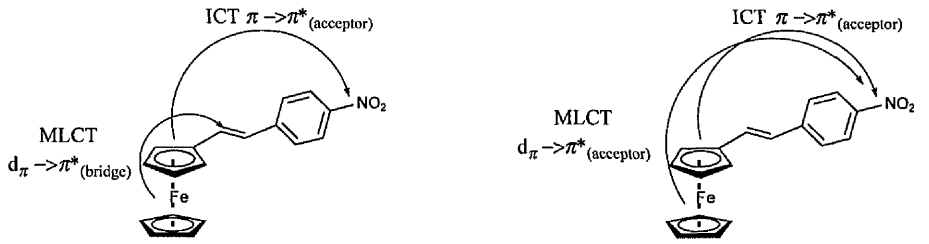

Figure 7. CT transitions in ferrocene derivatives.

As with DπA organic chromophores, the presence of heteroaromatics in the conjugated bridge can be highly beneficial for increasing the first hyperpolarizabilities of metallocene chromophores. Lin *et al.*[60] have carried out solvatochromic and electrochemical studies on ferrocenylethylene complexes that incorporate heteroaromatics such as thiophene and furan. These complexes exhibit pronounced solvatochromic behaviour, indicative of high β values. The π-D-A interactions are more pronounced in the thiophene derivative compared to their furan or benzene analogues.

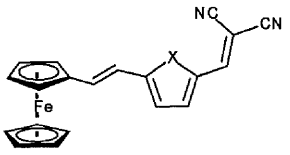

41. X = O
42. X = S

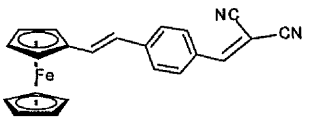

43.

If the presence of one metal centre can afford large β values with the potential for tunability, then it follows that two metal centres may offer further benefits. Hence, heterobimetallic molecules incorporating ferrocenyl subunits[61] (**44–50**) have been studied. In these complexes, it was found that the type of linkage to the metal carbonyl fragment

affects the magnitude of β. In the cases of **49** and **50**, the carbonyl fragments are π-bonded, involving the same orbitals which delocalise the charge. Hence, one might expect a larger β than for a similar compound bound primarily via σ-bonds, *e.g.* **46-48** *vs.* **49**.

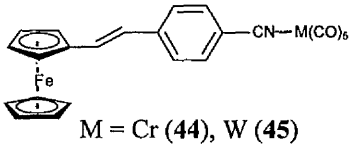

M = Cr (**44**), W (**45**)

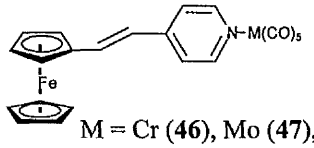

M = Cr (**46**), Mo (**47**), W (**48**)

No.	M	β_{1064} (10^{-30} esu)	λ_{max}[$CHCl_3$] (nm)
44	Cr	271	481
45	W	375	487
46	Cr	63	401
47	Mo	95	487
48	W	101	491
49(n = 1)	Cr	193	304
50(n = 2)	Cr	300	334

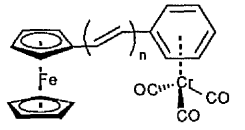

n = 1 (**49**), n = 2 (**50**)

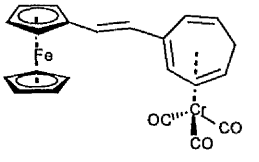

51. CH_2Cl_2; λ_{max} = 670 nm; $\beta_{1064} = 320 \times 10^{-30}$ esu; $\beta_0 = 113 \times 10^{-30}$ esu

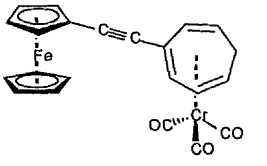

52. CH_2Cl_2; λ_{max} = 600 nm; $\beta_{1064} = 570 \times 10^{-30}$ esu; $\beta_0 = 105 \times 10^{-30}$ esu

Further studies on related heterobimetallic complexes also show that bridging C=C bonds are better than C≡C for enhancing β (**51** *vs.* **52**). In the case of **51** and **52** the β_0 values are very similar but such effects have also been observed in purely organic chromophores, and in gold σ-acetylide complexes.

Despite their rather complicated electronic structures, metallocene derivatives have received, and continue to receive, a great deal of attention for their NLO properties. Molecules with very large values of $\mu\beta$, comparable with the best purely organic chromophores, are known (*e.g.* **53**).

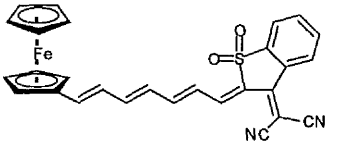

53. $CHCl_3$; $\mu\beta_{1907} = 11200 \times 10^{-48}$ esu[62]

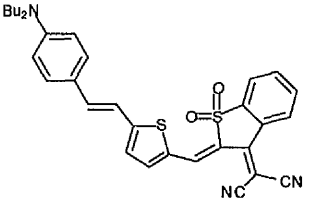

54. CH_2Cl_2; $\mu\beta_{1907} = 15000 \times 10^{-48}$ esu; $\mu\beta_0 = 5000 \times 10^{-48}$ esu[63]

1.7.2 Half-Sandwich Complexes

It has been predicted that having a metal centre in the plane of a conjugated backbone should lead to especially large β values, due to increased metal-ligand π-coupling.[54] Wenseleers *et al.*[64] have recently studied a range of compounds consisting of a transition metal D centre coordinated by a η^5-cyclopentadienyl ring, a PPh_3 or dppe [1,2-bis(diphenylphosphino)ethane, $Ph_2P(CH_2)_2PPh_2$] ligand and a conjugated nitrile ligand. The metal was varied (M = Co^{III}, Ni^{II}, Fe^{II} and Ru^{II}), whilst keeping the acceptor-substituted ligand the same. It is likely that the larger β values for the Ru and Fe complexes compared with their Ni analogue arise from more effective $d\pi(M)\rightarrow\pi^*(L)$ back-donation.

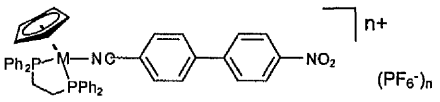

55-58

No.	n	M	β_{1064} (10^{-30} esu)	$\lambda_{max}[CH_2Cl_2]$ (nm)
55	2	Co	–	420
56	1	Ni	45	299
57	1	Ru	85	293
58	1	Fe	240	372

Organometallic σ-alkynyl complexes with the metal atom in the plane of the conjugated backbone have been extensively studied by a number of groups. Such complexes are especially attractive due to their ease of synthesis, high stability and potential as building blocks for oligomeric and polymeric materials. Chromophores containing a variety of different metals such as Ru,[65] Au[66] and Ni[66a,67] have been investigated (*e.g.* **59–61**), with the Ru complexes (see section 1.8) having the largest β values because they contain the strongest D groups. The first hyperpolarizabilities increase with increasing ligand acceptor strength and conjugation length, paralleling established trends in purely organic chromophores.

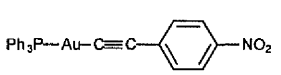

59. THF; λ_{max} = 338 nm; $\beta_{1064} = 22 \times 10^{-30}$ esu; $\beta_0 = 12 \times 10^{-30}$ esu

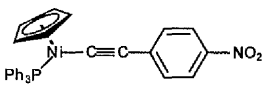

60. THF; λ_{max} = 439, 368 nm; $\beta_{1064} = 221 \times 10^{-30}$ esu; $\beta_0 = 59 \times 10^{-30}$ esu

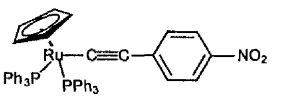

61. THF; λ_{max} = 460, 382 nm; $\beta_{1064} = 468 \times 10^{-30}$ esu; $\beta_0 = 96 \times 10^{-30}$ esu

Since the MLCT absorptions of the gold complexes are far removed from the second harmonic wavelength, their study allows the elucidation of some structure-property relationships that are not clear in the ruthenium complexes because of resonance effects. In common with other studies, C=C bonds are better linking groups than C≡C bonds in terms of β enhancement in these gold derivatives.

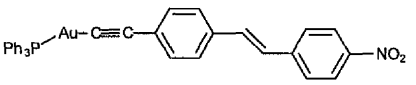

62. THF; λ_{max} = 386, 303 nm;
$\beta_{1064} = 120 \times 10^{-30}$ esu;
$\beta_0 = 49 \times 10^{-30}$ esu

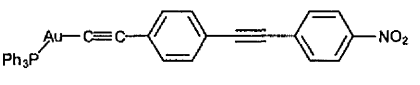

63. THF; λ_{max} = 362, 301 nm;
$\beta_{1064} = 59 \times 10^{-30}$ esu;
$\beta_0 = 28 \times 10^{-30}$ esu

Bifunctional σ-acetylide ligands have also been used to make heterobimetallic complexes which have large β values (*e.g.* **64, 65**).[65b,68] It has been suggested that **65** has a slightly larger β than **64** because the tungsten pentacarbonyl group is a better electron accepting group than its Cr counterpart due to increased M→CO π-back bonding.

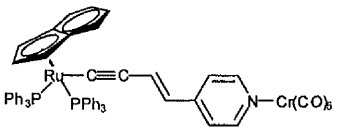

64. CH_2Cl_2; λ_{max} = 451 nm;
$\beta_{1064} = 260 \times 10^{-30}$ esu;
$\beta_0 = 60 \times 10^{-30}$ esu

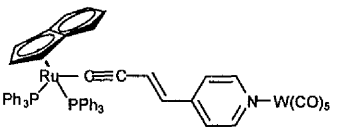

65. CH_2Cl_2; λ_{max} = 462 nm
$\beta_{1064} = 535 \times 10^{-30}$ esu;
$\beta_0 = 71 \times 10^{-30}$ esu

1.7.3 Schiff base complexes

Rather than acting as terminal D/A groups, transition metals have been used in a different manner to augment the NLO properties of organic Schiff base chromophores. Simple organic compounds such as **66** with D and A groups connected via a polarizable π-bridge appear to be ideal candidates for second-order NLO effects. Unfortunately, due to noncoplanarity of the aryl rings and the imine double bond, the NLO activity of such compounds is not maximized. However, cyclometalation forces the metalated ring and the imine bond to become coplanar, hence maximizing the D/A interaction and increasing the NLO activity.

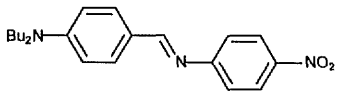

66. $CHCl_3$; λ_{max} = 416 nm;
$\beta_{1340} = 69 \times 10^{-30}$ esu;
$\beta_0 = 38 \times 10^{-30}$ esu

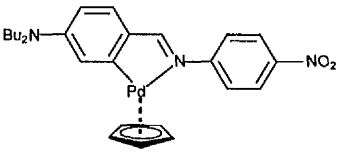

67. $CHCl_3$; λ_{max} = 483 nm;
$\beta_{1340} = 167 \times 10^{-30}$ esu;
$\beta_0 = 70 \times 10^{-30}$ esu

Espinet *et al.*[69] have studied a series of platinum(II) and palladium(II) Schiff base complexes and compared their β values to those of the corresponding free imines. They found that, depending on the amount of electron density at the metal, β can be increased by as much as *ca.* 80% on complexation.

1.7.4 Carbonyl Complexes

In 1986, Frazier *et al.*[70] studied metal carbonyl complexes having the form $[M(CO)_n(\eta\text{-arene})L_{3-n}]$ (where M = Cr, Mo, W; L = phosphane; n = 0–3) by the Kurtz powder technique. These complexes were expected to show significant second-order NLO responses because they exhibit intense CT absorptions in the low energy region of the visible spectrum. Unfortunately, centrosymmetric crystallizations give rise to vanishing SHG efficiencies.

More recently, Beck *et al.*[71] studied a series of rhenium complexes of the form *fac*-$ReBr(CO)_3L_2$ (where L = a pyridine-based ligand, *e.g.* **68**). In such complexes, the rhenium centre acts as an inductive electron acceptor and substantial β values are observed, having two significant components, β_{xxz} and β_{zzz}. The separate tensor elements cannot be measured directly by HRS, but were calculated by tensor addition, assuming the ligands to be separate molecules, orientated 90° to one another. This treatment results in β_{xyz} and β_{yyz} vanishing and $\beta_{xxz} = \beta_{zzz}$.

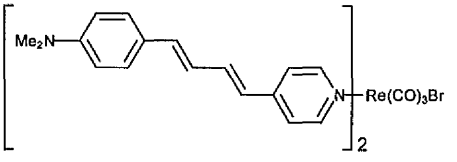

68. $CHCl_3$; λ_{max} = 438 nm; $\beta_{1500} = 208 \times 10^{-30}$ esu;
$\beta_{zzz} = \beta_{xxz} = 104 \times 10^{-30}$ esu

1.7.5 Square Planar Complexes

Recently Chen *et al.*[72] have made a rare series of D/A substituted nickel(II) bis-dithiolene complexes (*e.g.* **69**) which have all the necessary attributes for large optical nonlinearities, such as intense, low-energy CT absorptions.

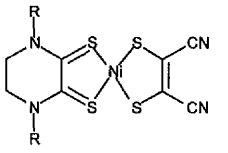

R = 2-ethylhexyl

69. $CHCl_3$; λ_{max} = 829 nm;
$\beta_{0(calc)} = 37 \times 10^{-30}$ esu

Transition dipole moments, ground state and excited state dipole moments were determined via spectroscopic methods, and used to calculate β values by using the two-level model.

Extremely large β values have been recorded for push-pull metal-containing porphyrin complexes (*e.g.* **70**).[73a] These results compare well with DπA polyenes with very large β values (*e.g.* **71** and **72**).[25]

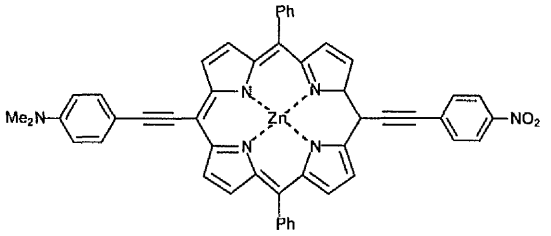

70. $CHCl_3$; λ_{max} = 675, 450 nm;
$\beta_{1064} = 4933 \times 10^{-30}$ esu;
$\beta_0 = 800 \times 10^{-30}$ esu;
$\mu\beta_0 = 9840 \times 10^{-48}$ esu

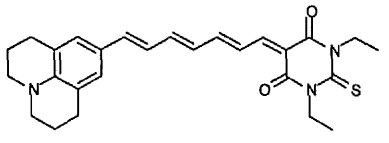

71. $CHCl_3$; λ_{max} = 686 nm;
$\beta_{1907} = 2169 \times 10^{-30}$ esu;
$\beta_0 = 911 \times 10^{-30}$ esu;
$\mu\beta_0 = 8019 \times 10^{-48}$ esu

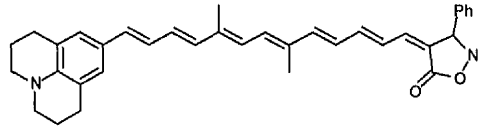

72. $CHCl_3$; λ_{max} = 647nm;
$\beta_{1907} = 1781 \times 10^{-30}$ esu;
$\beta_0 = 849 \times 10^{-30}$ esu;
$\mu\beta_0 = 13600 \times 10^{-48}$ esu

1.7.6 Group 6 cumulenylidenes

Heck *et al.*[74] have studied a range of group 6 cumulenylidenes (*e.g.* **73–76**), varying the metal centre, conjugation length and type of bridge in order to develop an understanding of the second-order NLO properties. In such compounds, β depends strongly on the conjugated chain length and addition of a conjugated alkene end unit does not greatly affect β_0, whilst insertion of a cumulated C_2 unit causes a three-fold increase in β_0 (**74** *vs.* **76**).

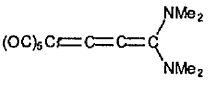

73. DMF; λ_{max} = 372 nm;
$\beta_{1064} = 21 \times 10^{-30}$ esu;
$\beta_0 = 10 \times 10^{-30}$ esu

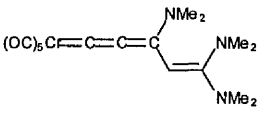

74. DMF; λ_{max} = 388 nm;
$\beta_{1064} = 22 \times 10^{-30}$ esu;
$\beta_0 = 9 \times 10^{-30}$ esu

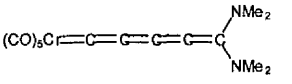

75. DMF; λ_{max} = 424 nm;
$\beta_{1064} = 100 \times 10^{-30}$ esu;
$\beta_0 = 31 \times 10^{-30}$ esu

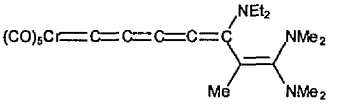

76. DMF; λ_{max} = 414 nm;
$\beta_{1064} = 125 \times 10^{-30}$ esu;
$\beta_0 = 40 \times 10^{-30}$ esu

1.7.7 Sesquifulvalene Complexes

An interesting class of compounds based on the two-ring sesquifulvalene system has been extensively studied and found to have large β values. Sesquifulvalene behaves like a polyene with alternating bond lengths. In the ground state, the structure is best described by the non-polar resonance form I, but upon CT excitation the resulting structure is better represented by resonance form II. Sesquifulvalene is very reactive and so cannot be studied directly, but it can be stabilized by metal complexation.

I II

The five-membered ring can be stabilized by coordination to (Cp)M (M = Ru, Fe) or (η^4–C_4H_4)Co fragments, and the seven-membered ring can be left uncoordinated as a free tropylium cation or bound to $Cr(CO)_3$ or $Ru(Cp)^+$ moieties. Hence, the five-membered ring unit can act as an electron donor, whilst the seven-membered ring is an acceptor. Heck *et al.*[75] have studied such complexes extensively, investigating the effect of varying the D/A groups and changing the bridge between the two rings (*e.g.* **77–80**).

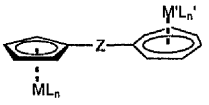

	ML_n	Z	$M'L_n'$
77	FeCp	–	–
78	FeCp*	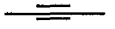	$Cr(CO)_3$
79	RuCp	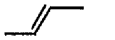	RuCp*
80	$Co(C_4R_4)$	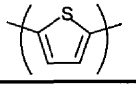	$Mo(CO)_3$

R = aryl, Cp = η^5-C_5H_5, Cp* = η^5-C_5Me_5

The same researchers have also recently prepared benzanellated and cumulogous sesquifulvalene derivatives (*e.g.* **81–83**).[76] In these complexes, the donor strength of the Mn centre was tuned by substituting a carbonyl ligand with a more electron-donating triphenylphosphine.

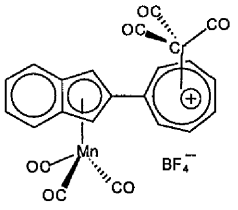

81. CH_3NO_2; λ_{max} = 435 nm;
$\beta_{1064} = 112 \times 10^{-30}$ esu;
$\beta_0 = 31 \times 10^{-30}$ esu

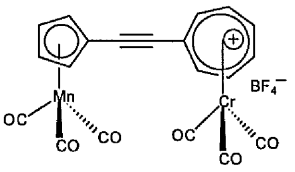

82. CH_2Cl_2; λ_{max} = 449 nm;
$\beta_{1064} = 224 \times 10^{-30}$ esu;
$\beta_0 = 58 \times 10^{-30}$ esu

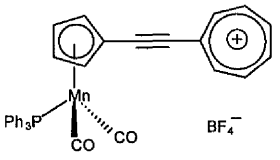

83. CH_2Cl_2; λ_{max} = 751 nm;
$\beta_{1064} = 226 \times 10^{-30}$ esu;
$\beta_0 = 31 \times 10^{-30}$ esu

1.8 *Ruthenium Complexes For Second-Order Nonlinear Optics*

Organoruthenium complexes have been studied quite extensively for their second-order NLO properties. Ruthenium(II) is popular because it has highly polarizable, electron-rich dπ orbitals and thus can act as a powerful electron donor. Also, Ru(II) has a rich and versatile synthetic chemistry that provides many opportunities to design promising chromophores for NLO effects. Many and varied Ru(II) compounds have been studied such as ruthenocene derivatives, bimetallics, aromatic σ-acetylides, octupolar complexes and ammine pyridyl complexes.

1.8.1 Ruthenocene Derivatives

Since the original study by Green *et al.* (see section 1.7.1), there has been much interest in ferrocene derivatives (*e.g.* **85**), and ruthenium analogues of many of the promising chromophores have also been studied.

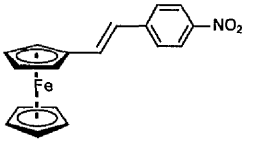

84. *p*-dioxane; λ_{max} = 496, 356 nm; β_{1910} *ca.* 31-34 × 10^{-30} esu[17b,54,57,77]

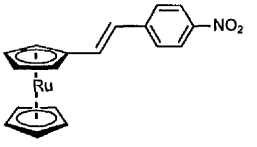

85. *p*-dioxane; λ_{max} = 390, 350 nm; β_{1910} = 12–16 × 10^{-30} esu [17b,54,57,77]

85. *p*-dioxane; λ_{max} = 390, 350 nm; β_{1910} = 12–16 × 10^{-30} esu [17b,54,57,77]

Replacement of iron by ruthenium results in ruthenium(II) has a higher ionisation potential than iron(II), *i.e.* the ruthenocenyl group is a weaker electron donor than ferrocenyl. Chiral ruthenocene derivatives have also been investigated, with some showing significant bulk NLO properties (*e.g.* **86**).

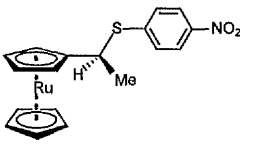

86. SHG_{1064} = 27 × urea[78]

Bourgault *et al.*[79] studied the second-order NLO properties of a number of complexes featuring ferrocenyl or ruthenocenyl groups (*e.g.* **87**, **88**), establishing the electron donor strength order dibutylamino > methoxyphenyl > ferrocenyl > ruthenocenyl. Coordination of the 2,2′-bipyridine moieties of **87–90** to rhenium carbonyl or tetrahedral zinc/mercury centres revealed the electron acceptor strength order $Re(CO)_3Br$ > $ZnCl_2$ > $Zn(OAc)_2$ > $HgCl_2$ > $Hg(OAc)_2$.

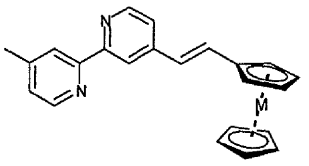

M = Fe **87**.
M = Ru **88**.

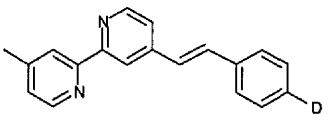

D = MeO **89**.
D = NMe_2 **90**.

1.8.2 σ-acetylides

Transition metal σ-acetylides are an important class of NLO compounds which have been studied particularly extensively,[65-68] the ruthenium complexes having especially large β_0 values (*e.g.* **91–95**).

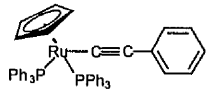

91. THF; λ_{max} = 310 nm;
$\beta_{1064} = 89 \times 10^{-30}$ esu
$\beta_0 = 45 \times 10^{-30}$ esu[65f,68a]

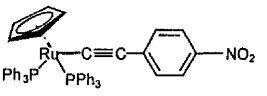

92. THF; λ_{max} = 460, 382 nm;
$\beta_{1064} = 468 \times 10^{-30}$ esu
$\beta_0 = 96 \times 10^{-30}$ esu[65c,68b]

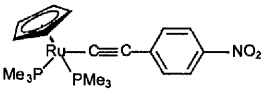

93. THF; λ_{max} = 477, 279 nm;
$\beta_{1064} = 248 \times 10^{-30}$ esu
$\beta_0 = 39 \times 10^{-30}$ esu[65c,68b]

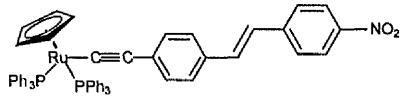

94. THF; λ_{max} = 476, 341 nm;
$\beta_{1064(HRS)} = 1455 \times 10^{-30}$ esu;
$\beta_{1064(EFISHG)} = 1464 \times 10^{-30}$ esu;
$\beta_{0(HRS)} = 232 \times 10^{-30}$ esu;
$\beta_{0(EFISHG)} = 234 \times 10^{-30}$ esu[65c,68b]

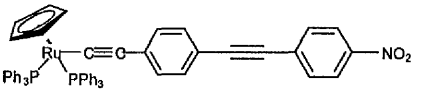

95. THF; λ_{max} = 446, 340 nm;
$\beta_{1064} = 865 \times 10^{-30}$ esu;
$\beta_0 = 212 \times 10^{-30}$ esu[65f,68a]

JOHN RYLANDS
UNIVERSITY
LIBRARY
MANCHESTER

It was expected that PMe_3 ligands would increase the electron density at the Ru centre and therefore increase β_0 compared with the analogous PPh_3 complexes. However, an opposite effect has been found (**93** *vs.* **92**). As in other systems, alkenyl linkages are found to be better than alkynyl groups for β enhancement. Biphenyl derivatives, although having increased conjugation lengths have higher energy MLCT absorptions compared to their phenyl analogues, but nonetheless, **96** has a larger β_0 value than **92**.

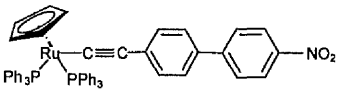

96. THF; λ_{max} = 448, 310 nm;
$\beta_{1064} = 560 \times 10^{-30}$ esu;
$\beta_0 = 134 \times 10^{-30}$ esu[65f,68a]

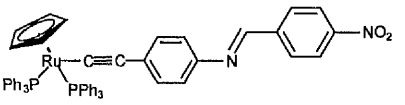

97. THF; λ_{max} = 496, 298 nm;
$\beta_{1064(HRS)} = 840 \times 10^{-30}$ esu;
$\beta_{1064(EFISH)} = 760 \times 10^{-30}$ esu;
$\beta_{0(HRS)} = 86 \times 10^{-30}$ esu;
$\beta_{0(EFISH)} = 78 \times 10^{-30}$ esu[65c,68b]

The Schiff base complex **97** has a lower β than expected, due to a loss of coplanarity of the conjugated bridge. Indenyl analogues have also been made; the indenyl group is a better electron donor than cyclopentadienyl, so the complexes have larger β_0 values than their Cp analogues (*e.g.* **98** *vs.* **92**).

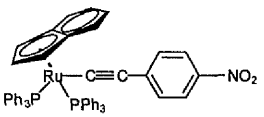

98. CH_2Cl_2; λ_{max} = 476 nm;
$\beta_{1064} = 746 \times 10^{-30}$ esu;
$\beta_0 = 119 \times 10^{-30}$ esu[68a,b]

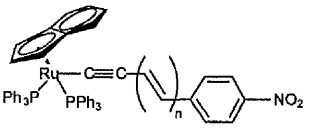

CH_2Cl_2;	**99**. n = 1;	**100**. n = 2.
λ_{max} /nm	507;	523;
$\beta_{1064} \times 10^{-30}$ esu	1257;	1320;
$\beta_0 \times 10^{-30}$ esu	89	34[65c,68b]

The complexes **99** and **100** absorb strongly near the second harmonic (532 nm) when measured in $CHCl_3$ so their β_0 values are underestimated. Hence, **100** appears to have a smaller β_0 than **99**, despite its extended conjugated system.

1.8.3 Bimetallics

Ruthenium has also been incorporated into bimetallic σ-acetylide complexes (*e.g.* **101–103**).[68] The β values of these complexes are strongly resonance enhanced, and the tungsten pentacarbonyl complex has an increased β_0 compared to its chromium analogue. The β_0 values of these compounds are among the largest reported for organometallic complexes.

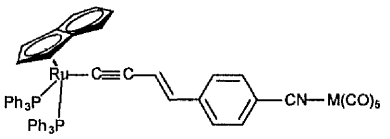

101. M = Cr; CH_2Cl_2;
λ_{max} = 442nm;
$\beta_{1064} = 465 \times 10^{-30}$ esu;
$\beta_0 = 119 \times 10^{-30}$ esu

102. M = W; CH_2Cl_2;
λ_{max} = 456 nm
$\beta_{1064} = 700 \times 10^{-30}$ esu;
$\beta_0 = 150 \times 10^{-30}$ esu

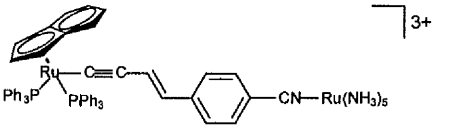

103. acetone; λ_{max} = 442 nm;
$\beta_{1064} = 315 \times 10^{-30}$ esu;
$\beta_0 = 80 \times 10^{-30}$ esu

A series of cyanide-bridged ruthenium indenyl bimetallics and heterobimetallics has also been investigated,[68] and an increase in β_0 is again observed on going from chromium to tungsten in the acceptor group.

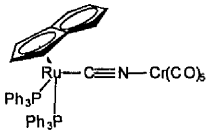

104. CH_2Cl_2; λ_{max} = 392 nm;
$\beta_{1064} = 25 \times 10^{-30}$ esu;
$\beta_0 = 10 \times 10^{-30}$ esu

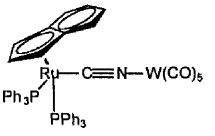

105. CH_2Cl_2; λ_{max} = 392 nm;
$\beta_{1064} = 40 \times 10^{-30}$ esu;
$\beta_0 = 15 \times 10^{-30}$ esu

Related ruthenium pentaammine cyanide-bridged metal carbonyl heterobimetallics have been studied by Denning *et al.*[80]

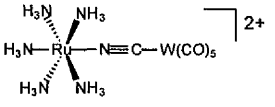

106. acetone; λ_{max} = 708 nm;
$\beta_{1064} = 130 \times 10^{-30}$ esu;
$\beta_0 = 56 \times 10^{-30}$ esu

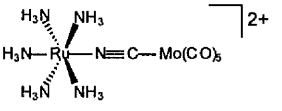

107. acetone; λ_{max} = 693 nm;
$\beta_{1064} = 225 \times 10^{-30}$ esu;
$\beta_0 = 90 \times 10^{-30}$ esu

Mixed-valence compounds display characteristic, low-energy inter-valence CT transitions, in which the D and A groups are both metal atoms. Since low energy, highly solvatochromic CT absorptions are a good indicator of NLO activity, it is unsurprising that the Ru(II)/Ru(III) compounds **108–110** possess large β_0 values.[68,81] **111** would be expected to have a smaller β_0 than **109** because the Os(III) centre is a weaker electron acceptor than its Ru(III) counterpart. However, the available data are in different solvents, so are not directly comparable.

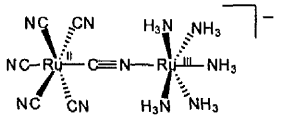

108. $MeNO_2$; λ_{max} = 684 nm ;
$\beta_{1064} = 209 \times 10^{-30}$ esu;
$\beta_0 = 81 \times 10^{-30}$ esu

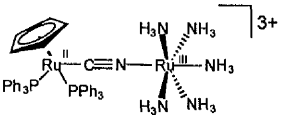

109. $MeNO_2$; λ_{max} = 716 nm;
$\beta_{1064} = 157 \times 10^{-30}$ esu;
$\beta_0 = 78 \times 10^{-30}$ esu

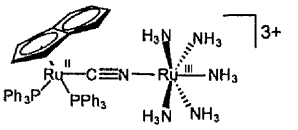

110. acetone; λ_{max} = 621 nm;
$\beta_{1064} = 108 \times 10^{-30}$ esu;
$\beta_0 = 26 \times 10^{-30}$ esu

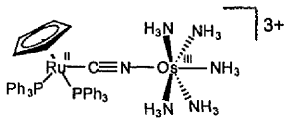

111. dmso; λ_{max} = 440 nm;
$\beta_{1064} = 65 \times 10^{-30}$ esu;
$\beta_0 = 16 \times 10^{-30}$ esu

1.8.4 Octupolar Complexes

In the early 1990s, Zyss *et al.* first demonstrated the second order NLO properties of octupolar metal complexes.[82] They investigated the ruthenium(II) tris(2,2′-bipyridine) and tris(1,10-phenanthroline) complexes by HRS at 1064 nm. **112** and **113** have been investigated extensively for their luminescence properties and their capacity for engaging in electron and energy-transfer processes.[83] They possess D_3 symmetry, exhibit MLCT absorptions near 450 nm [$d\pi(Ru^{II}) \rightarrow \pi^*$(2,2′-bpy, phen); ethanol] and appear to have large β values; β_{HRS} *ca.* 210 and 170×10^{-30} esu for **112** and **113**, respectively. However, these large β values seem to be mainly due to two-photon excited luminescence. **112** was recently re-examined by Morrison *et al.*[81a] who found a much lower value (β_{HRS} *ca.* 25 × 10^{-30} esu).

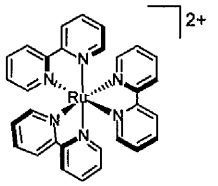

112.

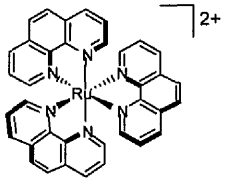

113.

In an attempt to increase the β of **112,** extension of the π-conjugated system was carried out and strong acceptor groups were introduced.[84] The presence of the extended π-systems and the nitro groups red-shifts the MLCT absorption to 508 nm in acetone, but unfortunately **114** is not sufficiently soluble to allow β measurements by HRS.

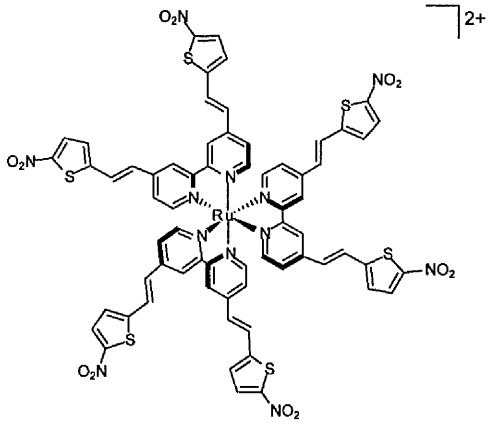

114.

Related complexes of 2,2′-bipyridine ligands bearing π-donor substituents have also been investigated by Zyss *et al.*[85] As well as MLCT bands, these complexes exhibit intense intra-ligand CT absorptions (ε *ca.* 120,000–150,000 M^{-1} cm^{-1}), which are sensitive to the nature of the D group.

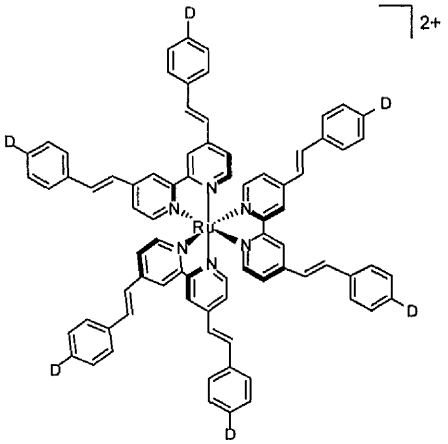

	D	β_{1340} (10^{-30} esu)	$\lambda_{max}(CHCl_3)$ /nm
115	NBu_2	1130	500–510*
116	N(Me)(Oct)	1000	380, 482

*broad ICT

Initial HRS measurements on the salt **115** at 1340 nm in $CHCl_3$ gave a huge β of 2200×10^{-30} esu, enhanced by two-photon excited luminescence. Subsequent measurements afforded reduced, but still large, β values (**115**: $\beta_{1340} = 1130 \times 10^{-30}$ esu; **116**: $\beta_{1340} = 1000 \times 10^{-30}$ esu).[86]

Vance and Hupp[87] investigated the symmetry of selected optical transitions of a ruthenium(II) complex related to **115** (D = NEt_2, **117**) by using resonant HRS and electroabsorption (Stark) spectroscopy. The large first hyperpolarizabilities of such complexes had previously been ascribed to an octupolar electronic structure. Vance and Hupp probed whether the octupolar symmetry is maintained in the relevant molecular excited states or whether lower symmetry dipolar excited states are created, such that the second-order NLO response arises from a more conventional mechanism. The experimental results indicate that the large β values are most likely from additive resonant/near resonant dipolar responses and not a direct result of an octupolar ground state geometry. Thus, **117** and related complexes can be thought of as a superposition of either three or six equivalent chromophores.

Matsuo *et al.*[88] have studied the SHG of amphiphilic derivative of **112** in LB films. The β value of the disubstituted **118** is estimated at *ca.* 70×10^{-30} esu.

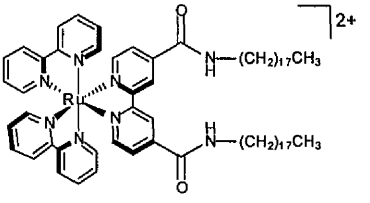

118.

Humphrey *et al.*[65e] have prepared octupolar ruthenium(II) complexes with D_{3h} symmetry based around a central benzene core with three alkynyl benzene arms (**119** and **120**).

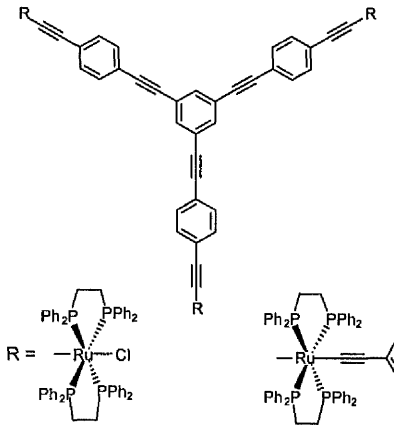

119. THF; λ_{max} = 414 nm; $\beta_{1064} = 94 \times 10^{-30}$ esu

120. THF; λ_{max} = 411 nm; $\beta_{1064} = 93 \times 10^{-30}$ esu

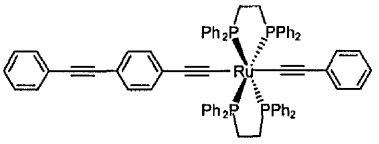

121. THF; λ_{max} = 383 nm; $\beta_{1064} = 34 \times 10^{-30}$ esu

This study showed that there is no enhancement of β on extending the π-system through the metal, but on going from the linear complex **121** to the octupolar complex **120**, a three-fold increase in β_{1064} occurs with little loss of optical transparency. The β_{1064} values are among the largest for octupolar molecules lacking a formal acceptor group and it is expected that replacing the arene ring with an acceptor such as 2,4,6-trinitrophenyl or 2,4,6-triazinyl groups will further increase β.[41]

1.8.5 Complexes previously studied in the Coe group

Ru ammine centres behave as electron acceptors when the metal is in the +3 oxidation state,[89] but as electron donors when in the +2 oxidation state.[90,91] $[Ru(NH_3)_5]^{n+}$ (n = 2 or 3) centres have been coordinated to the coumarin laser dyes C–510 and C–523.

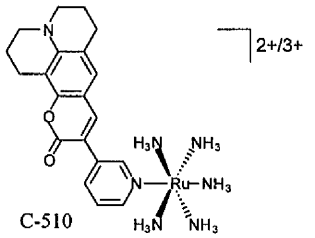

C-510

124/126

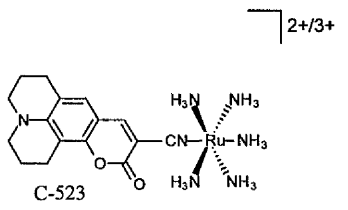

C-523

125/127

Table 3. Data for a series of ruthenium-coumarin dye complexes.

No.	Compound	λ_{max} /nm	β_{1064} (10^{-30} esu)	β_0 (10^{-30} esu)
122	C–510*	418	114	33
123	C–523*	444	132	32
124	$[Ru^{II}(NH_3)_5(C–510)](PF_6)_2$	430	120	35
125	$[Ru^{II}(NH_3)_5(C–523)](PF_6)_2$	498	420	41
126	$[Ru^{III}(NH_3)_5(C–510)](PF_6)_3$	438	137	37
127	$[Ru^{III}(NH_3)_5(C–523)](PF_6)_3$	460	240	49

*NLO data for coumarins recorded by EFISHG in $CHCl_3$;[92] NLO data for complexes **124–127** recorded by HRS. λ_{max} and HRS data recorded in acetonitrile.

The free dyes exhibit intense, broad absorptions in the violet region due to intra-molecular CT (ICT) excitations, corresponding to electron transfers from the tertiary amino donors to the vinyl lactone acceptor groups. Complexation of the dyes results in red-shifts of these ICT bands (C–510, 12–20 nm; C–523, 16–54 nm). The complexes **125** and **127** are highly solvatochromic which is a good indication of large second-order NLO responses.

The β values are large, but strongly resonance enhanced for the complexes of C–523 and thus the two-level model probably underestimates the β_0 values. In the case of C–510, complexation does not significantly enhance β_0, in agreement with the very slight red-shifting of the ICT absorption band. For C–523, complexation enhances β, with a larger apparent increase in the Ru(III) complex, **127**. However, HRS data at a longer wavelength are required in order to give more reliable comparisons of the β_0 values.

A series of complexes *trans*-$[Ru^{II}(NH_3)_4L_AL_D]^{n+}$ [L_D = 4-(dimethylamino)-pyridine (dmap), 1-methylimidazole (mim), NH_3, 4-(dimethylamino)benzonitrile (dmabn) or phenothiazine (PTZ); L_A = an acceptor-substituted ligand; n = 2, 3 (**128–149**)] were prepared and their β values measured by HRS. All of these complexes show intense $d\pi(Ru^{II})\rightarrow\pi^*(L)$ absorptions in the region 320–690 nm in acetonitrile. Some of the complexes show two MLCT absorptions, with the lower energy band corresponding to a $d\pi(Ru^{II})\rightarrow\pi^*(L_A)$ excitation and the higher energy band to a $d\pi(Ru^{II})\rightarrow\pi^*(L_D)$ transition. The lower energy MLCT band is strongly influenced by the nature of the trans L_D ligand; for a given L_A, the MLCT energy increases in the order L_D = dmap < mim < NH_3 < dmabn < PTZ. This is a consequence of the increasing stability of the Ru-based HOMO as the basicity of L_D decreases. Similarly, for a given L_D, the MLCT energy increases in the order

L_A = $DNPhQ^+$ < $AcPhQ^+$ < PhQ^+ < MeQ^+ < pyca < acpy < isn, a reflection of the steadily decreasing stability of the ligand-based LUMO as delocalisation length and acceptor strength decrease. As with the coumarin complexes **125** and **127**, **128–148** are highly solvatochromic. First hyperpolarizabilities were measured by HRS at 1064 nm in acetonitrile and corrected by using the two-level model. The 4,4′-bipyridinium-based complexes (**133–149**) showed the largest β_0 values (β_{1064} ranging from 419–1273 × 10^{-30} esu, β_0 ranging from 12–354 × 10^{-30} esu), which are at least twice as large as those of their acpy, pyca or isn analogues. This effect is a result of both increased conjugation length and the fact that a pyridinium group is a much stronger electron acceptor than a 4-acetyl, formyl or ethyl ester group. Since some of these complexes absorb strongly close to 532 nm, some of the β_0 values are underestimated by the two-level model.

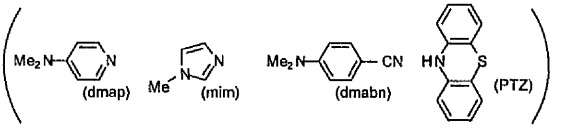

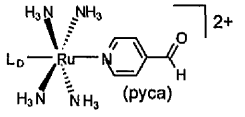

L_D = dmap (**128**)

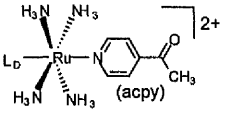

L_D = dmap (**129**), mim (**130**), dmabn (**131**),

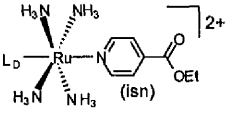

L_D = dmap (**132**)

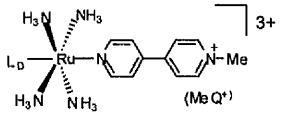

L_D = dmap (**133**), mim (**134**), dmabn (**135**), 4-acpy (**136**) PTZ (**137**), NH_3 (**138**)

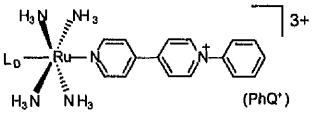

L_D = dmap (**139**), mim (**140**), dmabn (**141**), PTZ (**142**), NH_3 (**143**)

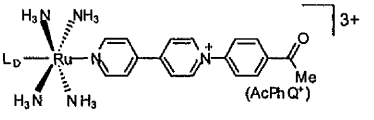

L_D = dmap (**144**), mim (**145**), dmabn (**146**), PTZ (**147**), NH_3 (**148**)

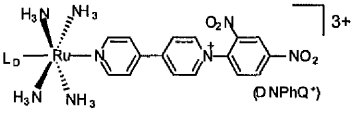

L_D = NH_3 (**149**)

Table 4. NLO data for complexes 128–149 recorded by HRS.

No.	L_A	L_D	λ_{max}[MLCT]/nm	β_{1064} (10^{-30} esu)	β_0 (10^{-30} esu)
128	pyca	dmap	544	362	12
129	acpy	dmap	520	284	12
130	acpy	mim	510	232	14
131	acpy	dmabn	472	310	53
132	isn	dmap	500	302	27
133	MeQ^+	dmap	614	587	130
134	MeQ^+	mim	602	523	100
135	MeQ^+	dmabn	540	621	14
136	MeQ^+	4-acpy	562	550	46
137	MeQ^+	PTZ	498	419	40
138	MeQ^+	NH_3	590	750	123
139	PhQ^+	dmap	658	794	260
140	PhQ^+	mim	648	874	266
141	PhQ^+	dmabn	572	1273	141
142	PhQ^+	PTZ	526	698	12
143	PhQ^+	NH_3	628	858	220
144	$AcPhQ^+$	dmap	688	1048	410
145	$AcPhQ^+$	mim	666	962	332
146	$AcPhQ^+$	dmabn	586	1214	180
147	$AcPhQ^+$	PTZ	538	727	12
148	$AcPhQ^+$	NH_3	654	1112	354
149	$DNPhQ^+$	NH_3	660	871	289

λ_{max} and HRS data recorded in acetonitrile.

The acceptor strength of L_A, increases in the order $MeQ^+ < PhQ^+ < AcPhQ^+ < DNPhQ^+$. However, **149** has a smaller β_0 than its $AcPhQ^+$ analogue. This phenomenon is attributed to ring twisting (caused by the steric hindrance of the *ortho*-nitro group) which reduces the overall D-A π-delocalisation. For a given L_A, the β_0 values are similar for L_D = NH_3, dmap or mim, which indicates that a trans *N*-heterocyclic ligand is not essential for large first hyperpolarizabilities.

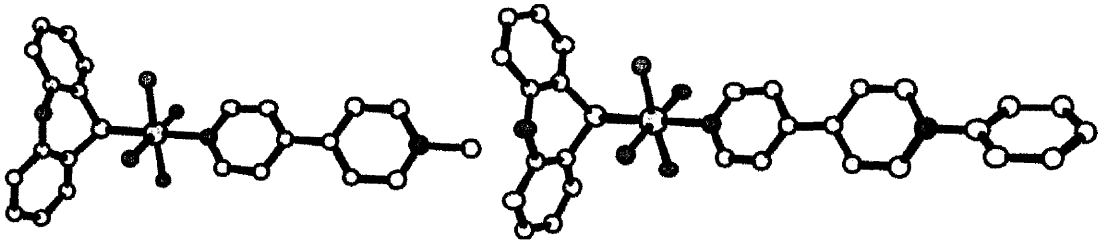

Figure 8. Structural representations of the cations *trans*-$[Ru^{II}(NH_3)_4PTZ(MeQ^+)]^{3+}$ and *trans*-$[Ru^{II}(NH_3)_4PTZ(PhQ^+)]^{3+}$.

Crystallographic studies of PF_6^- salts of **137** and **142** reveal twisting between the pyridyl rings, with torsion angles of 9.6° and 2.6°, respectively (Figure 8). A corresponding angle of 19.8° was found in the free $[PhQ^+]Cl^- \bullet 2H_2O$ ligand salt. It was originally suggested that the smaller torsion angle in **142** may reflect greater electronic delocalisation between the two pyridyl rings, compared to **137**. In order to test this hypothesis, a series of complex salts *trans*-$[Ru^{II}Cl(pdma)_2L_A](PF_6)_2$ [pdma = 1,2-phenylenebis(dimethylarsine), L_A = MeQ^+, PhQ^+, $AcPhQ^+$, $DNPhQ^+$ or $PymQ^+$ (**150–154**)] were prepared and crystallographically characterized.[93] The torsion angles between the two pyridyl rings show no correlation with the L_A acceptor strength. Hence, it can be concluded that the different torsion angles in the related tetraammine complexes are not due to electronic effects but are simply caused by crystal packing factors.

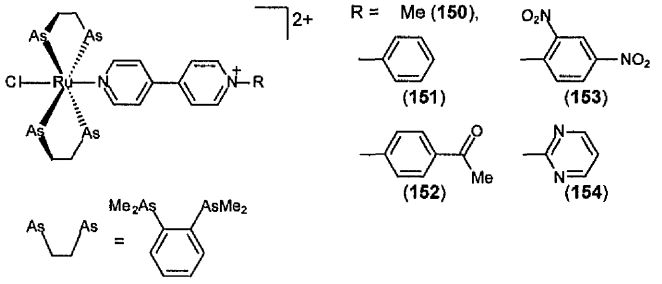

$[Ru^{II}(NH_3)_5]^{n+}$ (n = 2 or 3) centres exhibit reversible redox waves at readily accessible potentials (*ca.* 0.46 V *vs.* SCE), and hence are of interest for switching of NLO responses.[50] Addition of an excess of 1:1 aqueous H_2O_2/2M HCl solution to **138**, **143** or **148** (as their Cl^- salts) in water results in complete bleaching of the MLCT absorptions because of Ru(II)→Ru(III) oxidation; the oxidised complexes contain two opposing electron acceptors. The reverse processes are readily accomplished by adding a slight excess of hydrazine hydrate which restores the MLCT absorptions.

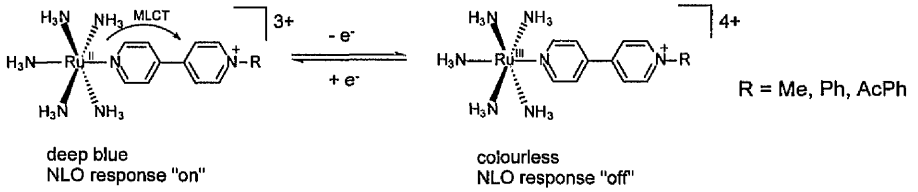

Figure 9. Redox switching of NLO properties.

HRS studies show that the loss of the MLCT absorptions is accompanied by marked decreases in the quadratic NLO responses, corresponding to effective redox-switching (Figure 9). The MLCT bleaching and the β switching processes are both fully-reversible and in the case of **148**, a decrease in β of approximately 10–20 fold was observed upon oxidation.

In summary, ruthenium(II) penta/tetraammines show great potential for second-order NLO applications. The β_0 values for the PhQ^+ and $AcPhQ^+$-based complexes are larger than those of most other organo-transition metal complexes previously studied, *e.g.* **144**. However, the properties of such complexes have not yet been optimised and a number of issues remain to be addressed, *e.g.* maximization of β, comparison of Ru(II) ammine donors with more traditional organic donor groups, stability, *etc.*

Chapter 2. Tuning of Charge-Transfer Absorption and Molecular Quadratic Nonlinear Optical Properties in Ruthenium(II) Ammine Complexes

2.1 Introduction

The work presented in this chapter concentrates on extending the previous studies by Coe *et al.* on the second order NLO properties of ruthenium(II) ammine complexes (see section 1.8.5) by using different ligand bridges with similar *N*-alkyl/aryl substituents. In these dipolar molecules the d^6-Ru^{II} metal centre acts as a powerful π-electron donor whilst the pyridinium ring is an electron acceptor. Hence, intense low energy MLCT absorptions are observed which are associated with the large hyperpolarizabilities.

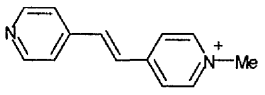

(Mebpe$^+$)

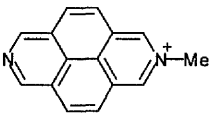

(Medap$^+$)

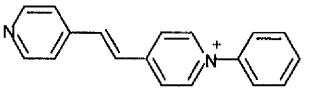

(Phbpe$^+$)

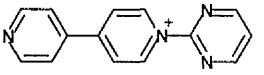

(PymQ$^+$)

The ligand *N*-methyl-4-[*trans*-2-(4-pyridyl)-ethenyl]pyridinium (Mebpe$^+$) was chosen because of its increased conjugation length compared to MeQ^+. It has been shown previously that increased conjugation length can lead to substantial gains in β (see section 1.5.4). *N*-Methyl-2,7-diazapyrenium (Medap$^+$) was chosen because initial studies on **137** showed a slight twisting between the pyridyl rings (9.6°) in the solid state. It appears likely that in solution free-rotation of the rings will serve to lower the electronic coupling across the 4,4′-bipyridinium bridge, so fixing of these rings may be beneficial. *N*-Phenyl-4-[*trans*-2-(4-pyridyl)-ethenyl]pyridinium (Phbpe$^+$) was used for similar reasons to Mebpe$^+$ *i.e.* extended conjugation length, and also because previous studies had shown that *N*-aryl pyridinium complexes have larger β values than their *N*-methyl counterparts. *N*-(2-Pyrimidyl)-4,4′-bipyridinium (PymQ$^+$) was chosen because the presence of the electronegative nitrogen atoms ortho to the quarternised nitrogen results in an increase in acceptor strength compared to PhQ^+.

2.2 *Experimental*

2.2.1 Materials and procedures

The compound $RuCl_3 \cdot 2H_2O$ was supplied by Johnson Matthey plc. The salts $[Ru^{II}(NH_3)_5(H_2O)][PF_6]_2$,[94] *trans*-$[Ru^{II}Cl(NH_3)_4(SO_2)]Cl$,[94] *trans*-$[Ru^{III}(SO_4)(NH_3)_4py]Cl$,[94] *N*-methyl-2,7-diazapyrenium chloride ($[Medap^+]Cl$)[95] and *N*-methyl-4-[*trans*-2-(4-pyridyl)-ethenyl]pyridinium iodide ($[Mebpe^+]I$)[96] were prepared according to published procedures. The latter two salts were metathesized to $[Medap^+]PF_6$ and $[Mebpe^+]PF_6$, respectively, by precipitation from water/aqueous NH_4PF_6. All other reagents were obtained commercially and used as supplied. Products were dried overnight at room temperature in a vacuum desiccator ($CaSO_4$) prior to characterization.

2.2.2 Physical measurements

Proton NMR spectra were recorded on a Varian Gemini 200 spectrometer and all shifts are referenced to $SiMe_4$. The fine splitting of pyridyl or phenyl ring AA′BB′ patterns is ignored and the signals are reported as simple doublets, with *J* values referring to the two most intense peaks. Elemental analyses were performed by the Microanalytical Laboratory, University of Manchester and UV/VIS spectra were obtained by using a Varian Cary 1E spectrophotometer.

Cyclic voltammetric measurements were carried out by using an EG&G PAR model 173 potentiostat/galvanostat with a model 175 universal programmer. A single-compartment cell was used with the saturated calomel reference electrode (SCE) separated by a salt bridge from the platinum-bead working electrode and platinum-wire auxiliary electrode. Acetonitrile (HPLC grade) was used as received and tetra-*n*-butyl ammonium hexafluorophosphate, twice recrystallized from ethanol and dried *in vacuo*, as supporting

electrolyte. Solutions containing *ca.* 10^{-3} M analyte (0.1 M electrolyte) were deaerated by purging with N_2. All $E_{1/2}$ values were calculated from $(E_{pa} + E_{pc})/2$ at a scan rate of 200 mV s^{-1}.

2.2.3 Syntheses

***N*-(2,4-Dinitrophenyl)-4-picolinium hexafluorophosphate, [dnppic$^+$]PF_6.** A solution of 4-picoline (2.4 mL, 24.7 mmol) and 2,4-dinitrochlorobenzene (5.00 g, 24.7 mmol) in ethanol (25 mL) was heated under reflux for 2 h. After cooling to room temperature, diethyl ether was added and the black precipitate was filtered off, washed with diethyl ether and dried. The crude product was purified by precipitation from boiling ethanol/diethyl ether. The resulting grey solid was filtered off, washed with diethyl ether and dried: [yield 5.18 g. $\delta_H(D_2O)$ 9.31 (d, 1 H, *J* 2.5 Hz, H^3), 8.89–8.83 (m, 3 H, H^5 + C_5H_4N), 8.19–8.06 (m, 3 H, H^6 + C_5H_4N), 2.79 (s, 3 H, Me)]. This material is unstable in air and was hence not further purified, but was dissolved in a minimum volume of water and aqueous NH_4PF_6 was added. The precipitate was filtered off, washed with water and dried. Further purification was effected by precipitation from acetone/diethyl ether: yield 5.38 g (53%). $\delta_H(CD_3COCD_3)$ 9.27–9.24 (m, 3 H, C_5H_4N + H^3), 9.01 (dd, 1 H, *J* 8.7, 2.5 Hz, H^5), 8.54 (d, 1 H, *J* 8.8 Hz, H^6), 8.39 (d, 2 H, *J* 6.5 Hz, C_5H_4N), 2.94 (s, 3 H, Me) (Found: C, 35.72; H, 2.51; N, 10.24. Calc for $C_{12}H_{10}F_6N_3O_4P$: C, 35.57; H, 2.49; N, 10.37%).

***N*-Phenyl-4-picolinium chloride, [ppic$^+$]Cl.** A sample of [dnppic$^+$]Cl, prepared as described above, was dissolved in boiling ethanol (30 mL), aniline (5.6 mL, 61 mmol) was added and the resulting solution was heated under reflux for 3 h. The solution was cooled to room temperature and reduced to half volume *in vacuo*. The addition of water caused the formation of a green precipitate which was filtered off, washed with water and discarded. The filtrate was reduced to dryness and dissolved in ethanol. The addition of diethyl ether afforded a golden-brown precipitate which was filtered off, washed with

diethyl ether and dried: yield 2.24 g (39%). $\delta_H(D_2O)$ 8.85 (d, 2 H, *J* 6.6 Hz, C_5H_4N), 7.99 (d, 2 H, *J* 6.9 Hz, C_5H_4N), 7.67 (s, 5 H, Ph), 2.71 (s, 3 H, Me) (Found: C, 63.30; H, 6.06; N, 6.23. Calc for $C_{12}H_{12}ClN \cdot 1.25H_2O$: C, 63.16; H, 6.40; N, 6.14%).

***N*-Phenyl-4-[*trans*-2-(4-pyridyl)ethenyl]pyridinium chloride, [Phbpe$^+$]Cl.** A mixture of [ppic$^+$]Cl•1.25H_2O (3.08 g, 13.5 mmol), pyridine-4-carboxaldehyde (1.5 mL, 15.8 mmol) and piperidine (0.4 mL) in ethanol (3 mL) was heated at reflux for 15 min. The resulting solution was cooled in an ice bath, causing formation of a solid mass. A black liquid was decanted off and the residue was dissolved in ethanol and precipitated by addition of diethyl ether. The pink solid was filtered off, washed with diethyl ether and dried: yield 1.04 g (23%). $\delta_H(D_2O)$ 8.94 (2 H, d, *J* 6.8 Hz, C_5H_4N), 8.48 (2 H, d, *J* 5.9 Hz, C_5H_4N), 8.19 (2 H, d, *J* 6.7 Hz, C_5H_4N), 7.71 (1 H, d, *J* 16.4 Hz, CH), 7.69 (5 H, s, Ph), 7.59 (2 H, d, *J* 6.2 Hz, C_5H_4N), 7.51 (1 H, d, *J* 16.4 Hz, CH) (Found: C, 64.19; H, 5.38; N, 8.06. Calc. for $C_{18}H_{15}ClN_2 \cdot 2.25H_2O$: C, 64.48; H, 5.86; N, 8.35%).

***N*-Phenyl-4-[*trans*-2-(4-pyridyl)ethenyl]pyridinium hexafluorophosphate, [Phbpe$^+$]PF_6.** [Phbpe$^+$]Cl•2.25H_2O (200 mg, 0.596 mmol) was dissolved in a minimum volume of water and aqueous NH_4PF_6 was added dropwise. The white precipitate was filtered off, washed with water and dried: yield 210 mg (87%). $\delta_H(CD_3COCD_3)$ 9.31 (2 H, d, *J* 6.8 Hz, C_5H_4N), 8.71 (2 H, d, *J* 6.1 Hz, C_5H_4N), 8.57 (2 H, d, *J* 6.8 Hz, C_5H_4N), 8.16 (1 H, d, *J* 16.4 Hz, CH), 8.00–7.95 (2 H, m, Ph), 7.94 (1 H, d, *J* 16.4 Hz, CH), 7.82–7.78 (3 H, m, Ph), 7.72 (2 H, d, *J* 6.0 Hz, C_5H_4N) (Found: C, 53.56; H, 3.77; N, 6.72. Calc. for $C_{18}H_{15}F_6N_2P$: C, 53.48; H, 3.74; N, 6.93%).

***N*-(2-Pyrimidyl)-4,4′-bipyridinium chloride, [PymQ$^+$]Cl.** A mixture of 4,4′-bipyridine (2.06 g, 13.2 mmol) and 2-chloropyrimidine (1.00 g, 8.73 mmol) were heated quickly to *ca.* 70 °C. Upon solidification, the green material was dissolved in ethanol (5 mL) and heated at reflux for 6 h. Addition of diethyl ether afforded a green precipitate which was filtered off, washed with diethyl ether and dried: yield 1.30 g (55%). $\delta_H(D_2O)$ 10.08 (2 H, d, *J* 7.3 Hz, C_5H_4N), 9.10 (2 H, d, *J* 4.9 Hz, $C_4H_3N_2$), 8.74 (2 H, d, *J* 6.1 Hz, C_5H_4N), 8.61 (2 H,

d, *J* 7.3 Hz, C_5H_4N), 7.96 (2 H, d, *J* 6.3 Hz, C_5H_4N), 7.85 (1 H, t, *J* 5.0 Hz, $C_4H_3N_2$) (Found: C, 61.94; H, 4.42; N, 20.39. Calc for $C_{14}H_{11}ClN_4$: C, 62.11; H, 4.10; N, 20.70%).

***N*-(2-Pyrimidyl)-4,4′-bipyridinium hexafluorophosphate, [PymQ$^+$]PF$_6$.** [PymQ$^+$]Cl (500 mg, 1.85 mmol) was dissolved in a minimum volume of water and aqueous NH_4PF_6 was added dropwise. The white precipitate was filtered off, washed with water and dried: yield 665 mg (95%). $\delta_H(CD_3COCD_3)$ 10.36 (2 H, d, *J* 7.4 Hz, C_5H_4N), 9.29 (2 H, d, *J* 4.8 Hz, $C_4H_3N_2$), 8.96–8.91 (4 H, m, C_5H_4N), 8.14 (2 H, d, *J* 6.3 Hz, C_5H_4N), 8.04 (1 H, t, *J* 4.8 Hz, $C_4H_3N_2$) (Found: C, 44.36; H, 2.93; N, 14.88. Calc. for $C_{14}H_{11}F_6N_4P$: C, 44.22; H, 2.92; N, 14.73%).

[Ru^{II}(NH$_3$)$_5$(Medap$^+$)][PF$_6$]$_3$ 155. A solution of [Ru^{II}(NH$_3$)$_5$(H$_2$O)][PF$_6$]$_2$ (250 mg, 0.505 mmol) and [Medap$^+$]PF$_6$ (188 mg, 0.516 mmol) in Ar-degassed acetone (5 mL) was stirred at room temperature under Ar for 2 h. The addition of diethyl ether afforded a dark precipitate which was filtered off, washed with diethyl ether and dried. Purification was effected by precipitations from acetone/aqueous NH_4PF_6 and then from acetone/diethyl ether to afford a dark purple solid: yield 137 mg (32%). $\delta_H(CD_3COCD_3)$ 10.05 (2 H, s, $C_{14}H_8N_2$), 9.83 (2 H, s, $C_{14}H_8N_2$), 8.54 (2 H, d, *J* 9.2 Hz, $C_{14}H_8N_2$), 8.48 (2 H, d, *J* 9.2 Hz, $C_{14}H_8N_2$), 4.89 (3 H, s, Me), 3.59 (3 H, s, *trans*-NH_3), 2.81 (12 H, s, 4 × *cis*-NH_3) (Found C, 21.10; H, 3.08; N, 11.49. Calc. for $C_{15}H_{26}F_{18}N_7P_3Ru$: C, 21.44; H, 3.12; N, 11.67%).

[Ru^{II}(NH$_3$)$_5$(PymQ$^+$)][PF$_6$]$_3$ 156. This was prepared in identical manner to **155** by using [Ru^{II}(NH$_3$)$_5$(H$_2$O)][PF$_6$]$_2$ (100 mg, 0.202 mmol) and [PymQ$^+$]PF$_6$ (77 mg, 0.203 mmol) in place of [Medap$^+$]PF$_6$. Purification was effected by several precipitations from acetone/diethyl ether to afford a dark blue solid: yield 75 mg (42%). $\delta_H(CD_3COCD_3)$ 10.17 (2 H, d, *J* 7.5 Hz, C_5H_4N), 9.28–9.22 (4 H, m, C_5H_4N + $C_4H_3N_2$), 8.94 (2 H, d, *J* 7.5 Hz, C_5H_4N), 8.03–7.96 (3 H, m, C_5H_4N + $C_4H_3N_2$), 3.75 (3 H, s, *trans*-NH_3), 2.74 (12 H, s, 4 × *cis*-NH_3) (Found: C, 19.15; H, 3.14; N, 13.76. Calc. for $C_{14}H_{26}F_{18}N_9P_3Ru{\bullet}2H_2O$: C, 18.84; H, 3.39; N, 14.13%).

$[Ru^{II}(NH_3)_5(Mebpe^+)][PF_6]_3$ 157. This was prepared in similar manner to **156** by using $[Mebpe^+]I$ (79 mg, 0.244 mmol) in place of $[PymQ^+]PF_6$ and 1:1 water/acetone (5 mL) in place of acetone. The addition of aqueous NH_4PF_6 afforded a dark precipitate which was filtered off, washed with water and dried. Purification was effected by precipitations from acetone/diethyl ether, acetone/NBu^n_4Cl and finally water/aqueous NH_4PF_6 to afford a dark purple solid: yield 58 mg (35%). $\delta_H(CD_3COCD_3)$ 8.94 (4 H, d, *J* 6.9 Hz, C_5H_4N), 8.33 (2 H, d, *J* 7.0 Hz, C_5H_4N), 8.02 (1 H, d, *J* 16.4 Hz, CH), 7.89 (1 H, d, *J* 16.4 Hz, CH), 7.54 (2 H, d, *J* 6.8 Hz, C_5H_4N), 4.49 (3 H, s, Me), 3.41 (3 H, s, *trans*-NH_3), 2.65 (12 H, s, 4 × *cis*-NH_3). (Found: C, 19.28; H, 3.18; N, 11.68. Calc. for $C_{13}H_{28}F_{18}N_7P_3Ru$: C, 19.08; H, 3.45; N, 11.98%).

$[Ru^{II}(NH_3)_5(Phbpe^+)][PF_6]_3$ 158. This was prepared in identical manner to **156** by using $[Phbpe^+]PF_6$ (83 mg, 0.205 mmol) in place of $[PymQ^+]PF_6$. The product was purified as for **157** with one further precipitation from acetone/diethyl ether to afford a dark blue solid: yield 113 mg (62%). $\delta_H(CD_3COCD_3)$ 9.25 (2 H, d, *J* 7.0 Hz, C_5H_4N), 8.97 (2 H, d, *J* 6.3 Hz, C_5H_4N), 8.51 (2 H, d, *J* 6.9 Hz, C_5H_4N), 8.18 (1 H, d, *J* 16.2 Hz, CH), 8.04 (1 H, d, *J* 16.2 Hz, CH), 7.99–7.94 (2 H, m, Ph), 7.81–7.77 (3 H, m, Ph), 7.58 (2 H, d, *J* 6.9 Hz, C_5H_4N), 3.44 (3 H, s, *trans*-NH_3), 2.65 (12 H, s, 4 × *cis*-NH_3) (Found: C, 25.28; H, 3.52; N, 10.51. Calc for $C_{18}H_{30}F_{18}N_7P_3Ru{\bullet}0.3C_3H_6O$: C, 25.28; H, 3.57; N, 10.92%).

***trans*-$[Ru^{III}(SO_4)(NH_3)_4mim]Cl$ 159.** A mixture of *trans*-$[Ru^{II}Cl(NH_3)_4(SO_2)]Cl$ (100 mg, 0.329 mmol) and 1-methylimidazole (mim, 0.2 mL, 2.51 mmol) was dissolved in water (5 mL) and heated at *ca.* 45 °C under Ar for 30 min. Acetone (100 mL) was added to the brown solution and a white precipitate was filtered off, washed with acetone and dried to afford crude *trans*-$[Ru^{II}(NH_3)_4mim(SO_2)]Cl_2$ (124 mg, 98%). This material was dissolved in water (5 mL) and oxidised by the addition of a 1/1 mixture of 30% aqueous H_2O_2/2 M HCl (2 mL). After 5 min at room temperature, acetone (200 mL) was added and the golden precipitate was filtered off, washed with acetone and dried: yield 111 mg (88%).

***trans*-[$Ru^{III}(SO_4)(NH_3)_4(Medap^+)$]$Cl_2$ 160.** This was prepared in identical manner to **159** by using [$Medap^+$]Cl (167 mg, 0.656 mmol) in place of mim. The addition of acetone (30 mL) to the brown solution afforded a mauve precipitate which was filtered off, washed with acetone and dried to yield crude *trans*-[$Ru^{II}(NH_3)_4(Medap^+)(SO_2)$]$Cl_3$ (151 mg, 82%). The oxidation was carried out by using water (10 mL) to dissolve the SO_2 complex and acetone (100 mL) to precipitate the golden product: yield 108 mg (59%).

***trans*-[$Ru^{III}(SO_4)(NH_3)_4(Mebpe^+)$]$Cl_2$ 161.** This was prepared in identical manner to **160** by using [$Mebpe^+$]I (214 mg, 0.660 mmol) in place of [$Medap^+$]Cl to afford a golden solid: yield 135 mg (77%).

***trans*-[$Ru^{II}(NH_3)_4py(Medap^+)$][$PF_6$]$_3$ 162.** A solution of *trans*-[$Ru^{III}(SO_4)(NH_3)_4py$]Cl (108 mg, 0.284 mmol) in water (5 mL) was reduced over zinc amalgam (5 lumps) with Ar agitation for 15 min. This was filtered under Ar into a flask containing [$Medap^+$]Cl (360 mg, 1.41 mmol) and the solution was stirred at room temperature in the dark under Ar for 6 h. The addition of acetone (100 mL) to the deep blue solution gave a dark precipitate which was filtered off, washed with acetone and dried (crude *trans*-[$Ru^{II}(NH_3)_4py(Medap^+)$]$Cl_3$). This material was purified by precipitation from water/acetone and then metathesised to its PF_6^- salt by precipitation from water/aqueous NH_4PF_6. Further purification was effected by several precipitations from acetone/diethyl ether to afford a dark blue solid: yield 99 mg (39%). $\delta_H(CD_3COCD_3)$ 10.15 (2 H, s, $C_{14}H_8N_2$), 9.99 (2 H, s, $C_{14}H_8N_2$), 9.00 (2 H, d, $H^{2,6}$), 9.12 (2 H, d, *J* 9.1 Hz, $C_{14}H_8N_2$), 8.63 (2 H, d, *J* 9.2 Hz, $C_{14}H_8N_2$), 8.03 (1 H, t, H^4), 7.65 (2 H, t, $H^{3,5}$), 5.01 (3 H, s, Me), 2.83 (12 H, s, $4NH_3$) (Found: C, 26.78; H, 3.09; N, 10.61. Calc for $C_{20}H_{28}F_{18}N_7P_3Ru$: C, 26.62; H, 3.13; N, 10.86%).

***trans*-[$Ru^{II}(NH_3)_4py(PymQ^+)$][$PF_6$]$_3$ 163.** This was prepared in identical manner to **162** by using *trans*-[$Ru^{III}(SO_4)(NH_3)_4py$]Cl (103 mg, 0.271 mmol) and [$PymQ^+$]Cl (367 mg, 1.36 mmol) in place of [$Medap^+$]Cl. Purification was effected by precipitation from acetone/diethyl ether to afford a dark blue solid: yield 172 mg (69%). $\delta_H(CD_3COCD_3)$

10.28 (2 H, d, *J* 7.4 Hz, C_5H_4N), 9.27 (2 H, d, *J* 4.9 Hz, $C_4H_3N_2$), 9.26 (2 H, d, *J* 7.0 Hz, C_5H_4N), 8.99–8.93 (4 H, m, $C_5H_4N + H^{2,6}$), 8.19 (2 H, d, *J* 7.0 Hz, C_5H_4N), 8.06–7.98 (2 H, m, $H^4 + C_4H_3N_2$), 7.63 (2 H, t, $H^{3,5}$), 2.88 (12 H, s, $4NH_3$) (Found: C, 25.16; H, 3.10; N, 13.32. Calc. for $C_{19}H_{28}F_{18}N_9P_3Ru$: C, 24.85; H, 3.07; N, 13.73%).

***trans*-[$Ru^{II}(NH_3)_4$py(Mebpe$^+$)][PF_6]$_3$ 164.** This was prepared in similar manner to **162** by using **161** (135 mg, 0.253 mmol) in place of *trans*-[$Ru^{III}(SO_4)(NH_3)_4$py]Cl and pyridine (0.1 mL, 1.24 mmol) in place of [Medap$^+$]Cl. The solution was stirred for 3 h in the dark and addition of aqueous NH_4PF_6 gave a dark precipitate which was filtered off, washed with water and dried. Purification was effected by precipitation from acetone/diethyl ether to afford a dark blue solid: yield 81 mg (36%). $\delta_H(CD_3COCD_3)$ 8.98–8.92 (4 H, m, $C_5H_4N + H^{2,6}$), 8.88 (2 H, d, *J* 6.5 Hz, C_5H_4N), 8.36 (2 H, d, *J* 6.9 Hz, C_5H_4N), 8.09 (1 H, d, *J* 16.5 Hz, CH), 7.95 (1 H, t, H^4), 7.93 (1 H, d, *J* 16.4 Hz, CH), 7.74 (2 H, d, *J* 6.8 Hz, C_5H_4N), 7.56 (2 H, t, $H^{3,5}$), 4.53 (3 H, s, Me), 2.78 (12 H, s, $4NH_3$) (Found: C, 24.72; H, 3.50; N, 10.85. Calc for $C_{18}H_{30}F_{18}N_7P_3Ru$: C, 24.56; H, 3.43; N, 11.14%).

***trans*-[$Ru^{II}(NH_3)_4$py(Phbpe$^+$)][PF_6]$_3$ 165.** This was prepared in identical manner to **162** by using *trans*-[$Ru^{III}(SO_4)(NH_3)_4$py]Cl (109 mg, 0.287 mmol) and [Phbpe$^+$]Cl•$2.25H_2O$ (424 mg, 1.26 mmol) instead of [Medap$^+$]Cl. Purification was effected by precipitation from acetone/diethyl ether to afford a dark blue solid: yield 163 mg (58%). $\delta_H(CD_3COCD_3)$ 9.30 (2 H, d, *J* 6.9 Hz, C_5H_4N), 8.98 (2 H, d, *J* 6.6 Hz, C_5H_4N), 8.90 (2 H, d, $H^{2,6}$), 8.55 (2 H, d, *J* 7.0 Hz, C_5H_4N), 8.25 (1 H, d, *J* 16.2 Hz, CH), 8.07 (1 H, d, *J* 16.2 Hz, CH), 8.00–7.93 (3 H, m, Ph + H^4), 7.82–7.78 (5 H, m, Ph + C_5H_4N), 6.90 (2 H, t, $H^{3,5}$), 2.81 (12 H, s, $4NH_3$) (Found: C, 30.18; H, 3.39; N, 9.64. Calc for $C_{23}H_{32}F_{18}N_7P_3Ru$•$0.5C_3H_6O$: C, 30.29; H, 3.63; N, 10.09%).

***trans*-[$Ru^{II}(NH_3)_4$mim(Medap$^+$)][PF_6]$_3$ 166.** This was prepared in similar manner to **162** by using **160** (108 mg, 0.194 mmol) in place of *trans*-[$Ru^{III}(SO_4)(NH_3)_4$py]Cl and mim (0.2 mL, 2.51 mmol) in place of [Medap$^+$]Cl. The solution was stirred for 3 h in the dark and addition of aqueous NH_4PF_6 afforded a dark precipitate which was filtered off, washed

with water and dried. Purification was effected by sequential precipitations from acetone/$^{n}Bu_4NCl$, water/aqueous NH_4PF_6 and finally from acetone/diethyl ether: yield 69 mg (39%). $\delta_H(CD_3COCD_3)$ 10.10 (2 H, s, $C_{14}H_8N_2$), 9.88 (2 H, s, $C_{14}H_8N_2$), 8.59 (2 H, d, *J* 8.8 Hz, $C_{14}H_8N_2$), 8.53 (2 H, d, *J* 9.2 Hz, $C_{14}H_8N_2$), 8.31 (1 H, s, $C_3N_2H_3$), 7.51 (1 H, s, $C_3N_2H_3$), 7.47 (1 H, s, $C_3N_2H_3$), 4.93 (3 H, s, $C_{14}H_8N_2$–*Me*), 3.95 (3 H, s, $C_3N_2H_3$–*Me*), 2.85 (s, 12 H, $4NH_3$) (Found: C, 26.02; H, 3.20; N, 11.98. Calc for $C_{19}H_{29}F_{18}N_8P_3Ru \cdot 0.3C_3H_6O$: C, 25.90; H, 3.36; N, 12.14%).

***trans*-[$Ru^{II}(NH_3)_4$mim(PymQ$^+$)][PF_6]$_3$ 167.** This was prepared and purified in identical manner to **166** by using **159** (109 mg, 0.285 mmol) in place of **160** and [PymQ$^+$]Cl (385 mg, 1.42 mmol) in place of mim. A dark blue solid was obtained: yield 76 mg (28%). $\delta_H(CD_3COCD_3)$ 10.22 (2 H, d, *J* 7.5 Hz, C_5H_4N), 9.27–9.24 (4 H, m, C_5H_4N + $C_4H_3N_2$), 8.95 (2 H, d, *J* 7.4 Hz, C_5H_4N), 8.28 (1 H, s, $C_3N_2H_3$), 8.08 (2 H, d, *J* 6.6 Hz, C_5H_4N), 8.03 (1 H, t, *J* 4.1 Hz, $C_4H_3N_2$), 7.50 (1 H, s, $C_3N_2H_3$), 7.44 (1 H, s, $C_3N_2H_3$), 3.95 (3 H, s, Me), 2.78 (12 H, s, $4NH_3$) (Found: C, 24.03; H, 3.46; N, 14.68. Calc. for $C_{18}H_{29}F_{18}N_{10}P_3Ru \cdot 0.3C_3H_6O$: C, 24.18; H, 3.31; N, 14.92%).

***trans*-[$Ru^{II}(NH_3)_4$mim(Mebpe$^+$)][PF_6]$_3$ 168.** This was prepared and purified in identical manner to **166** by using **161** (104 mg, 0.195 mmol) in place of **160**. A dark purple solid was obtained: yield 64 mg (37%). $\delta_H(CD_3COCD_3)$ 8.94 (4 H, d, *J* 5.1 Hz, C_5H_4N), 8.35 (2 H, d, *J* 6.5 Hz, C_5H_4N), 8.18 (1 H, s, $C_3N_2H_3$), 8.06 (1 H, d, *J* 16.4 Hz, CH), 7.91 (1 H, d, *J* 16.5 Hz, CH), 7.62 (2 H, d, *J* 6.6 Hz, C_5H_4N), 7.45 (1 H, s, $C_3N_2H_3$), 7.37 (1 H, s, $C_3N_2H_3$), 4.51 (3 H, s, C_5H_4N–*Me*), 3.91 (3 H, s, $C_3N_2H_3$–*Me*), 2.65 (12 H, s, $4NH_3$) (Found: C, 23.44; H, 3.56; N, 12.41. Calc for $C_{17}H_{31}F_{18}N_8P_3Ru$: C, 23.11; H, 3.54; N, 12.68%).

***trans*-[$Ru^{II}(NH_3)_4$mim(Phbpe$^+$)][PF_6]$_3$ 169.** This was prepared in identical manner to **166** by using **159** (115 mg, 0.300 mmol) in place of **160** and [Phbpe$^+$]Cl•2.25H_2O (445 mg, 1.33 mmol) in place of mim. Purification was effected by precipitation from acetone/diethyl ether to give a dark blue solid: yield 97 mg (34%). $\delta_H(CD_3COCD_3)$ 9.26 (2 H, d, *J* 6.9 Hz,

C_5H_4N), 8.96 (2 H, d, *J* 5.6 Hz, C_5H_4N), 8.52 (2 H, d, *J* 6.9 Hz, C_5H_4N), 8.23 (1 H, d, *J* 16.2 Hz, CH), 8.18 (1 H, s, $C_3N_2H_3$), 8.04 (1 H, d, *J* 16.2 Hz, CH), 8.00–7.96 (2 H, m, Ph), 7.81-7.78 (3 H, m, Ph), 7.68 (2 H, d, *J* 5.9 Hz, C_5H_4N), 7.45 (1 H, s, $C_3N_2H_3$), 7.39 (1 H, s, $C_3N_2H_3$), 3.94 (3 H, s, Me), 2.67 (12 H, s, $4NH_3$) (Found: C, 28.51; H, 3.94; N, 11.08. Calc for $C_{22}H_{33}F_{18}N_8P_3Ru \cdot 0.3C_3H_6O$: C, 28.56; H, 3.64; N, 11.64%).

2.2.4 Hyper-Rayleigh scattering

Details of the hyper-Rayleigh scattering (HRS) experiment have been discussed elsewhere,[12,97] and the experimental procedure used was as described previously.[98] β values were determined by using the electric-field-induced second harmonic generation β_{1064} for *p*-nitroaniline (29.2×10^{-30} esu in acetonitrile)[99] as an external reference. All measurements were performed using the 1064 nm fundamental wavelength of an injection-seeded, Q-switched Nd-YAG laser (Quanta-Ray GCR-5, 8 ns pulses, 7 mJ, 10 Hz). The use of dilute acetonitrile solutions (10^{-5}–10^{-6} mol dm^{-3}) ensured a linear dependence of $I_{2\omega}/I_{\omega}^2$ upon solute concentration, precluding the need for Lambert-Beer correction factors. Samples were passed through a 0.45 μm filter (Millipore), and were checked for fluorescence.[81a,100] One-dimensional hyperpolarizability is assumed, *i.e.* $\beta_{1064} = \beta_{zzz}$, and a relative error of ±15% is estimated.

2.2.5 X-ray structural determination

Crystals of **162**•4MeCN were obtained by slow diffusion of diethyl ether vapour into acetonitrile solutions. A red-brown crystal of approximate dimensions 0.1 × 0.1 × 0.15 mm was chosen for diffraction studies.

Data were collected on a Nonius Kappa CCD area-detector diffractometer at the window of a rotating anode FR591 generator (50 kV, 20 mA) and controlled by the Collect software package.[101] Images of 1.6° thickness and 15 s exposure were taken (360° ϕ scan

and ω scans to fill Ewald sphere) with a detector to crystal distance of 40 mm and processed by Denzo[102] to give 99.9% coverage of the unique dataset. Data were corrected for absorption by using the empirical method employed in Sortav[103] from within the MaXus suite of programs.[104] The structure was solved by direct methods and refined by full-matrix least-squares on all F_o^2 data using SHELXS-97[105] and SHELXL-97.[106] All non-hydrogen atoms, including those of the PF_6^- anions and the acetonitrile molecules of crystallization, were refined anisotropically with hydrogen atoms included in idealised positions and thermal parameters riding on those of the parent atom.

A representation of the complex cation is given in Figure 12. Crystallographic data and refinement details are presented in Table 7, and selected bond distances and angles in Table 8. Cambridge Crystallographic Data Centre reference number 186/1638. See http://www.rsc.org/suppdata/dt/1999/3617/ for crystallographic file in .cif format.

2.3 Results and Discussion

2.3.1 Molecular Design and Synthesis

The new complexes in the salts **155–158** and **162–169** (Figure 10) were designed to probe the effects of several molecular structural changes on the electronic absorption and quadratic NLO properties. The structural changes are as follows:

1. The complexes of $Medap^+$ in **155**, **162**, and **166** feature fixed coplanar rings and an additional four π-electrons compared to their MeQ^+ analogues.
2. The complexes of $Mebpe^+$ and $Phbpe^+$ in **157**, **164**, **168** and **158**, **165**, **169**, respectively, have planar conjugated systems featuring extended conjugation compared to their MeQ^+ and PhQ^+ analogues.
3. The 2-pyrimidyl ring in the complexes of $PymQ^+$ in **156**, **163** and **167** is more electron deficient compared to the *N*-aryl substituents used previously.

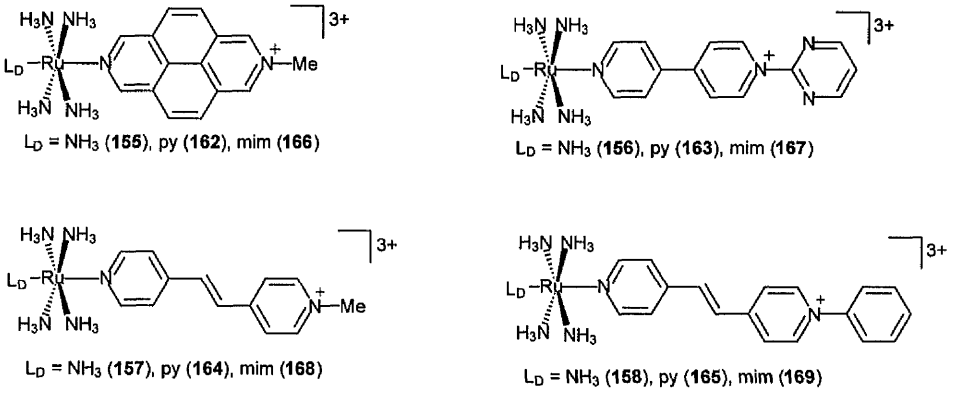

Figure 10. Structures of new complexes of the form *trans*-$[Ru^{II}(NH_3)_4(L_A)(L_D)]^{3+}$.

The salt [PymQ$^+$]Cl has been reported previously, but without details.[107] It was prepared by nucleophilic attack of 4,4′-bipyridine on 2-chloropyrimidine and we have found that initial melt reactions improve the yields of subsequent reactions in refluxing ethanol.

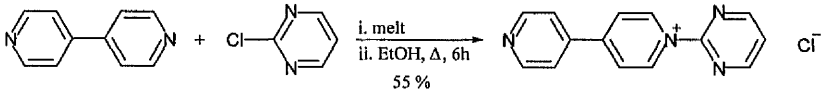

N-phenyl-4-picolinium chloride was prepared by nucleophilic attack of 4-picoline on 2,4-dinitrochlorobenzene, followed by reaction with aniline in an analogous fashion to the synthesis of PhQ$^+$.

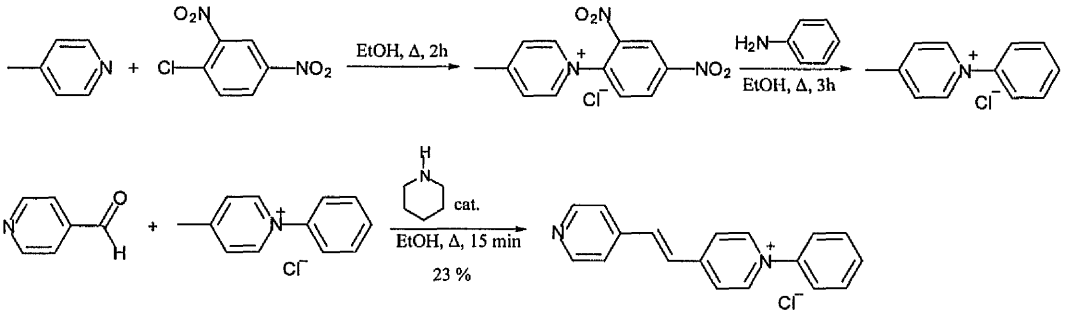

For the synthesis of [Phbpe$^+$]Cl, an analogous method to the preparation of PhQ$^+$ was explored, but the second aniline step was unsuccessful. Hence, [Phbpe$^+$]Cl was obtained from the condensation of *N*-phenyl-4-picolinium chloride with pyridine-4-carboxaldehyde using piperidine as a catalyst. The yield of this base catalysed reaction diminishes with increasing reflux times, in a similar fashion to the related, published preparation of Mebpe$^+$.[108]

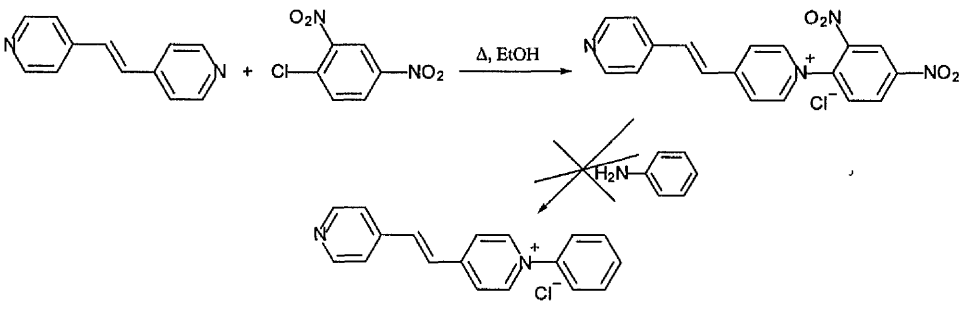

2,7-Diazapyrene used in the synthesis of the Medap^{+} ligand was prepared by a combination of published procedures,[109] with one simple modification. In the literature the intermediate 1,3,6,8-tetrahydro-2,7-dimethyldiazapyrene was extracted into THF. However, we found that this approach is inefficient and does not yield a pure product. Extraction with boiling methanol gives a higher yield of a purer product, although the yield is still lower than that published.

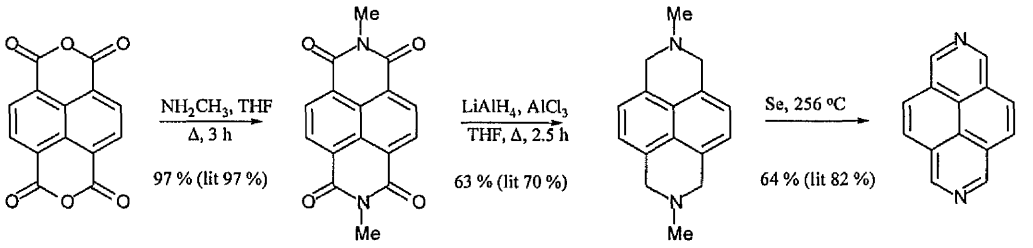

The new complex salts were prepared and purified using previously described procedures,[90,91] with some minor modifications. Complex salts **155–158** were synthesised from $[Ru^{II}(NH_3)_5(H_2O)][PF_6]_2$ which was prepared by the reduction of $[Ru^{II}(NH_3)_5Cl]Cl$ with zinc amalgam in the presence of trifluoroacetic acid (TFA). The aquo ligand in $[Ru^{II}(NH_3)_5(H_2O)]^{2+}$ is easily substituted by L_A ligands.

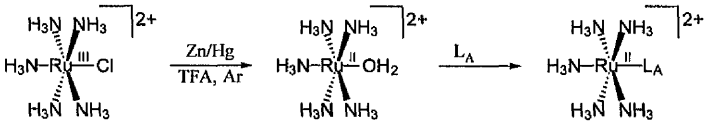

Complex salts **162–169** were synthesised from *trans*-$[Ru^{II}Cl(NH_3)_4(SO_2)]Cl$ in a step-wise fashion. The SO_2 ligand labilizes the trans chloride ligand, allowing the introduction of the first ligand, L_A, under mild conditions. The resulting complex is then

oxidised to produce a *trans*-Ru^{III}-SO_4 complex. A subsequent two-step process facilitates the introduction of the second ligand, L_D. Firstly, the Ru^{III} complex is reduced to give a Ru^{II}-SO_4 complex which loses sulfate to produce an aquo complex. Secondly, the aquo ligand is substituted by the incoming ligand, L_D, to produce the final asymmetrically substituted product.

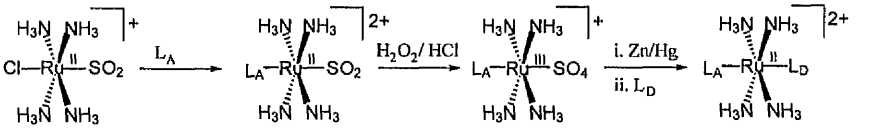

2.3.2 Electronic Spectroscopy Studies

The electronic spectra of all the new complex salts, except for the Ru^{III} sulfato intermediates, **159–161**, were recorded in acetonitrile and the results are presented in Table 5. Complexes **155–158** and **162–169** show intense, broad $d\pi(Ru^{II})\rightarrow\pi^*(L_A)$ (L_A = pyridinium-substituted ligand) MLCT bands in the region 560–700 nm. The energies of these MLCT bands depend on the relative energies of the Ru-based HOMO and the L_A-based LUMO.[110] A representative spectrum of *trans*-$[Ru^{II}(NH_3)_4(py)(PymQ^+)][PF_6]_3$, **163**, can be found in Figure 11.

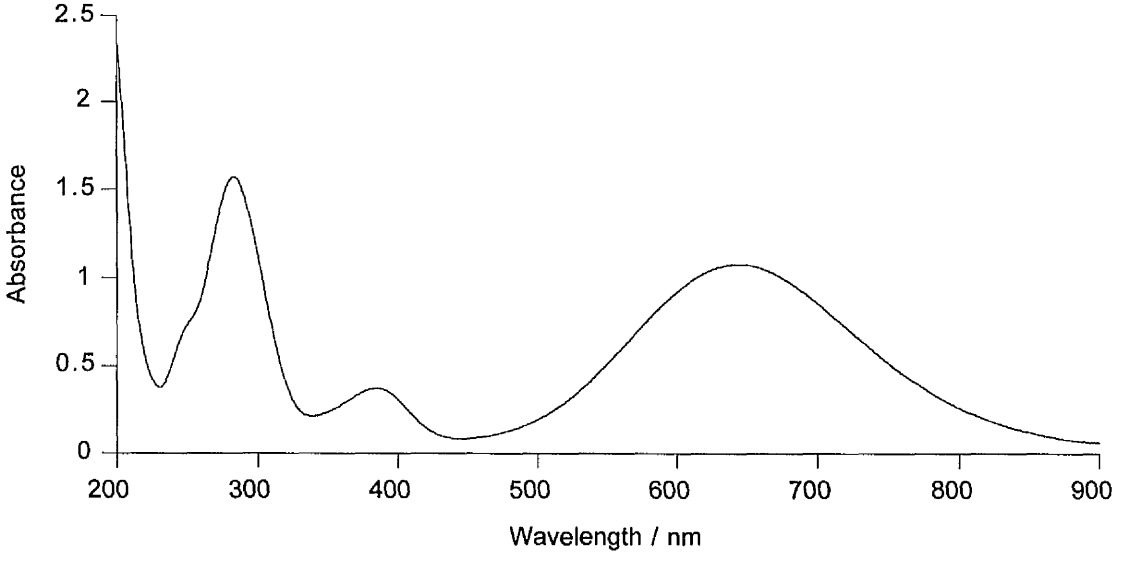

Figure 11. UV/Visible/NIR absorption spectrum of *trans*-$[Ru^{II}(NH_3)_4(py)(PymQ^+)][PF_6]_3$, 163, in acetonitrile.

Table 5. UV/Visible/NIR data for complex salts 155–169 in acetonitrile.

Salt	L_D	L_A	λ_{max}/nm (ε/M^{-1} cm^{-1})[a]	Assignment
155	NH_3	$Medap^+$	581 (14 800)	$d_\pi \rightarrow \pi^*(Medap^+)$
			397 (10 900)	$\pi \rightarrow \pi^*$
			376 (7800)	$\pi \rightarrow \pi^*$
			335 (24 900)	$\pi \rightarrow \pi^*$
			241 (37 200)	$\pi \rightarrow \pi^*$
156	NH_3	$PymQ^+$	673 (18 000)	$d_\pi \rightarrow \pi^*(PymQ^+)$
			285 (21 500)	$\pi \rightarrow \pi^*$
157	NH_3	$Mebpe^+$	595 (16 100)	$d_\pi \rightarrow \pi^*(Mebpe^+)$
			312 (23 800)	$\pi \rightarrow \pi^*$
158	NH_3	$Phbpe^+$	628 (17 200)	$d_\pi \rightarrow \pi^*(Phbpe^+)$
			329 (25 800)	$\pi \rightarrow \pi^*$
162	py	$Medap^+$	564 (12 300)	$d_\pi \rightarrow \pi^*(Medap^+)$
			397 (11 300)	$\pi \rightarrow \pi^*$
			378 (10 900)	$\pi \rightarrow \pi^*$
			334 (19 100)	$\pi \rightarrow \pi^*$
			242 (33 100)	$\pi \rightarrow \pi^*$
163	py	$PymQ^+$	644 (16 800)	$d_\pi \rightarrow \pi^*(PymQ^+)$
			385 (5800)	$d_\pi \rightarrow \pi^*(py^+)$
			283 (24 500)	$\pi \rightarrow \pi^*$
164	py	$Mebpe^+$	563 (14 800)	$d_\pi \rightarrow \pi^*(Mebpe^+)$
			386 (5900)	$d_\pi \rightarrow \pi^*(py^+)$
			311 (23 800)	$\pi \rightarrow \pi^*$
165	py	$Phbpe^+$	591 (17 100)	$d_\pi \rightarrow \pi^*(Mebpe^+)$
			387 (sh) (6900)	$d_\pi \rightarrow \pi^*(py^+)$
			328 (30 000)	$\pi \rightarrow \pi^*$
166	mim	$Medap^+$	593 (16 700)	$d_\pi \rightarrow \pi^*(Medap^+)$
			398 (12 000)	$\pi \rightarrow \pi^*$
			377 (9300)	$\pi \rightarrow \pi^*$
			337 (27 600)	$\pi \rightarrow \pi^*$
			242 (33 100)	$\pi \rightarrow \pi^*$
167	mim	$PymQ^+$	698 (18 700)	$d_\pi \rightarrow \pi^*(PymQ^+)$
			285 (24 300)	$\pi \rightarrow \pi^*$
168	mim	$Mebpe^+$	604 (16 200)	$d_\pi \rightarrow \pi^*(Mebpe^+)$
			310 (23 000)	$\pi \rightarrow \pi^*$
169	mim	$Phbpe^+$	638 (17 600)	$d_\pi \rightarrow \pi^*(Phbpe^+)$
			329 (28 400)	$\pi \rightarrow \pi^*$

[a] Solutions (5–7) × 10^{-5} M.

The trans-py complexes in **162–165** also show less intense, high energy $d\pi(Ru^{II}) \rightarrow \pi^*(py)$ MLCT bands at *ca.* 385 nm, although this absorption is obscured by a more intense UV band in **162**. All of the complexes show one or more intense UV absorptions due to $\pi \rightarrow \pi^*$ excitations. Data for the visible bands of **155–159** and **162–169** are collected in Table 6 as well as additional data for related salts of the ligands MeQ^+, PhQ^+, $AcPhQ^+$ and $DNPhQ^+$ for the purpose of comparison.[90,91]

The MLCT band maxima of the $Medap^+$ complexes in **155** and **166** are higher in energy by 0.03 eV compared to those of their MeQ^+ analogues.[90,91] The MLCT maxima of

the $PymQ^+$ complexes in **156** and **167** are lower in energy by *ca.* 0.06–0.08 eV compared to their $AcPhQ^+$ analogues.[91] Electrochemical studies (see section 2.3.3) show that these complexes have an almost constant HOMO energy, thus $PymQ^+$ has the lowest LUMO energy of the 4,4′-bipyridinium ligands studied. This is as expected considering the electron deficient nature of the 2-pyrimidyl ring. Hence, the acceptor strength of L_A increases in the order $MeQ^+ < PhQ^+ < AcPhQ^+ < DNPhQ^+ < PymQ^+$. The MLCT energies of the complexes of $Mebpe^+$ (**157** and **168**) and $Phbpe^+$ (**158** and **169**) are very similar to those of their MeQ^+ and PhQ^+ analogues.

Comparison of the MLCT energies of the *N*-methyl *vs. N*-phenyl analogues, *i.e.* the pairs **157/158**, **164/165** and **168/169** shows a difference of about –0.1 eV on replacing *N*-methyl with *N*-phenyl. This shows that $Phbpe^+$ is a stronger electron acceptor than $Mebpe^+$ and is in agreement with the previously observed differences between PhQ^+ and MeQ^+. With a given L_A, the MLCT energy decreases as the net donor strength of L_D increases, *i.e.* in the order py < NH_3 < mim, which reflects a progressive destabilization of the ruthenium-based HOMO.

2.3.3 Electrochemical Studies

The new complex salts **155–158** and **162–169** were studied by cyclic voltammetry in acetonitrile and the results are presented in Table 6. All show reversible or quasi-reversible $Ru^{III/II}$ oxidation waves as well as generally irreversible ligand-based reduction processes. The related complexes of MeQ^+, PhQ^+ and $AcPhQ^+$ each show two reversible or quasi-reversible ligand reduction waves,[90,91] and data for these complex salts as well as data for **155–158** and **162–169** are included in Table 6 for comparison purposes.

The $Ru^{III/II}$ $E_{1/2}$ values for **155** and **166** are shifted by *ca.* +40 mV compared to those of their MeQ^+ analogues.[90] This is due to the lower basicity of $Medap^+$ caused by an increase in delocalisation. The blue shift in the MLCT energy (see section 2.3.2) can hence be attributed largely to stabilisation of the Ru-based HOMOs in the $Medap^+$ complexes.

An ethylene unit is slightly electron donating and increases the basicity of the Mebpe$^+$ and Phbpe$^+$ ligands compared with MeQ$^+$ or PhQ$^+$, respectively. Thus the $Ru^{III/II}$ $E_{1/2}$ values for **157**, **158**, **168** and **169** are shifted by *ca.* –40 mV compared to those of their MeQ$^+$ and PhQ$^+$ analogues.[90,91] Comparing the $Ru^{III/II}$ $E_{1/2}$ values for the Mebpe$^+$/Phbpe$^+$ complex pairs **157/158**, **164/165** and **168/169** shows negligible shifts on replacing *N*-methyl with *N*-phenyl. The ligand E_{pc} values however, show large positive shifts and thus the red shifting of the MLCT bands (see section 2.3.2) in these complex pairs is a result of stabilisation of the ligand based LUMOs.

For a given acceptor-substituted ligand, L_A, the $Ru^{III/II}$ $E_{1/2}$ values become less positive as the donor strength of L_D increases, *i.e.* in the order py < mim < NH_3. This trend reflects the HOMO destabilisation as indicated by the MLCT data.

Table 6. Electrochemical data for the salts *trans*-$[Ru^{II}(NH_3)_4(L_D)(L_A)][PF_6]_3$ in acetonitrile.

			$E_{1/2}$/V vs. SCE (ΔE_p/m V)	
Salt	L_D	L_A	$Ru^{III/II}$	Ligand Waves
155	NH_3	Medap$^+$	0.50 (70)	–0.98[b]
156	NH_3	PymQ$^+$	0.49 (100)	–0.45 (200)[c]
157	NH_3	Mebpe$^+$	0.41 (70)	–0.85[b]
158	NH_3	Phbpe$^+$	0.42 (90)	–0.66[b]
[e]	NH_3	MeQ$^+$	0.46 (75)	–0.91 (70), –1.52 (70)
[e]	NH_3	PhQ$^+$	0.46 (75)	–0.75 (70), –1.35 (70)
[e]	NH_3	AcPhQ$^+$	0.47 (80)	–0.64 (75), –1.17 (155)[c]
[e]	NH_3	DNPhQ$^+$	0.46[d]	–0.40[b]
162	py	Medap$^+$	0.65 (75)	–0.95[b]
163	py	PymQ$^+$	0.67 (80)	–0.41 (90),[c] –1.10 (100)[c]
164	py	Mebpe$^+$	0.60 (70)	–0.75 (150)[c]
165	py	Phbpe$^+$	0.61 (90)	–0.64[b]
166	mim	Medap$^+$	0.51 (70)	–0.97[b]
167	mim	PymQ$^+$	0.52 (90)	–0.41 (120)[c]
168	mim	Mebpe$^+$	0.42 (80)	–0.86[b]
169	mim	Phbpe$^+$	0.43 (70)	–0.66[c]
[f]	mim	MeQ$^+$	0.47 (75)	–0.88 (70), –1.48 (65)
[e]	mim	PhQ$^+$	0.46 (70)	–0.73 (70), –1.34 (70)
[e]	mim	AcPhQ$^+$	0.48 (75)	–0.63 (70), –1.16 (120)[c]

[a] Measured in solutions *ca.* 10^{-3} M in analyte and 0.1 M in $NBu^n_4PF_6$ at a platinum-bead working electrode with a scan rate of 200 mV s^{-1}. Ferrocene internal reference $E_{1/2}$ = 0.41 V. ΔE_p = 90 mV. [b] E_{pc} for an irreversible reduction process. [c] Irreversible process as evidenced by $i_{pc} \neq i_{pa}$. [d] E_{pa} for an irreversible oxidation process. [e] Ref. 91. [f] Ref. 90.

Comparison of the ligand reduction potentials for the complexes with 4,4′-bipyridinium ligands shows that the $E_{1/2}$ values for **156** and **167** are more positive than those of their MeQ$^+$, PhQ$^+$ and AcPhQ$^+$ analogues. This confirms that the PymQ$^+$ ligand

is the strongest electron acceptor, in agreement with the MLCT data. By contrast, the $Ru^{III/II}$ $E_{1/2}$ values only vary by a small extent, indicating that the HOMO energy is relatively insensitive to changes in the *N*-substituent.

2.3.4 Crystallographic Studies

A single crystal X-ray structure for **162**•4MeCN was obtained and a representation of the molecular structure of the complex cation is shown in Figure 12. The torsion angle C(1)–N(1)–N(2)–C(6) between the py ligand and the coordinated pyridyl ring of the $Medap^+$ ligand is 9.8°, with the planes of the coordinated rings approximately bisecting the H_3N–Ru–NH_3 angles. The Ru(1)–N(2) distance is *ca.* 0.05 Å shorter than the Ru(1)–N(1) distance, indicative of stronger π-back bonding to $Medap^+$ than to pyridine, in keeping with the fact that $Medap^+$ is a considerably stronger π-acceptor than pyridine. The structure of **162**•4MeCN is extensively hydrogen bonded. Each cation forms two H-bonds to one PF_6^- anion and six H-bonds to four acetonitrile molecules of crystallization via the NH_3 ligands. **162**•4MeCN adopts the noncentrosymmetric space group $Pna2_1$ and hence, owing to its large molecular hyperpolarizability, it might be anticipated that crystals of **162**•4MeCN will exhibit macroscopic NLO effects. However, crystal packing diagrams (Figure 13) reveal that the complex dipoles are aligned almost completely antiparallel thus precluding the observation of significant bulk optical nonlinearities.

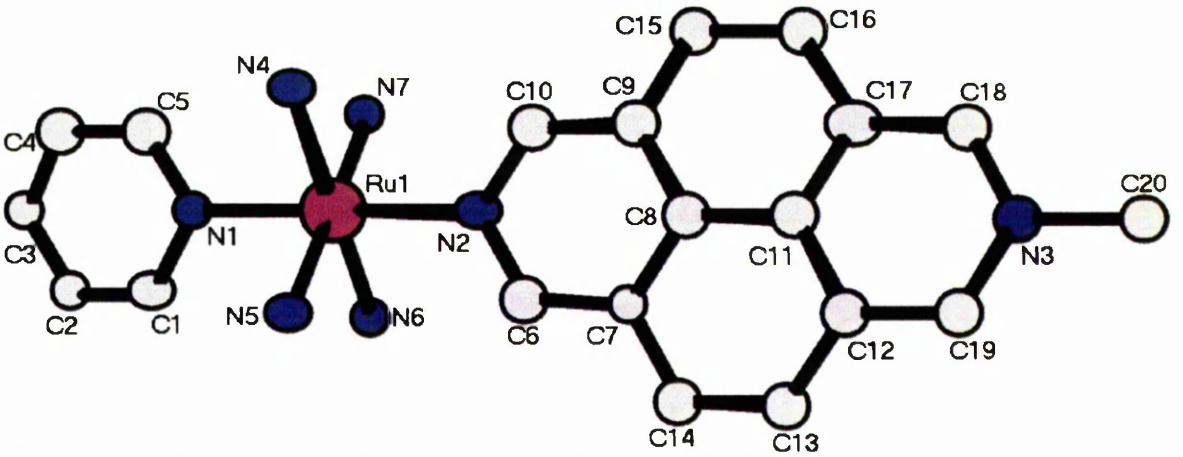

Figure 12. Structural representation of the complex cation in the salt 162•4MeCN.

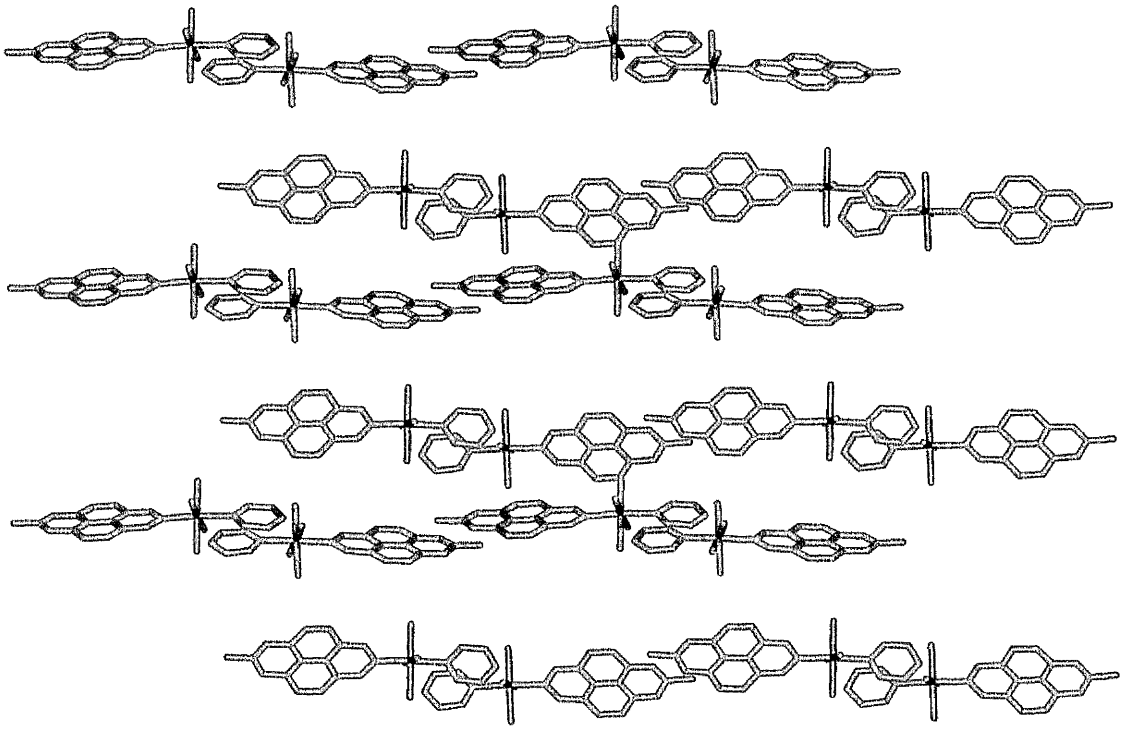

Figure 13. Packing diagram for 162•4MeCN viewed approximately along the *a* axis (PF_6^- anions and MeCN solvent of crystalization removed for clarity).

Table 7. Crystallographic data and refinement details for 162•4MeCN

Formula	$C_{28}H_{40}F_{18}N_{11}P_3Ru$
M	1066.69
Crystal system	Orthorhombic
Space group	$Pna2_1$
a/Å	12.8413(3)
b/Å	23.9689(3)
c/Å	14.0305(5)
β°	90
U/Å^3	4318.47(19)
Z	4
T/K	150(2)
μ/ mm^{-1}	0.589
Reflections collected	45910
Independent reflections (R_{int})	8434 (0.1226)
Final *R*1, *w R*2 [$I > 2\sigma(I)$][a]	0.0482, 0.0867
(all data)	0.0972, 0.0979

[a] Structure was refined on F_o^2 using all data; the value of R1 is given for comparison with older refinements based on F_o with a typical threshold of $F_o > 4\sigma(F_o)$

Table 8. Selected interatomic distances (Å) and angles (°) for 162•4MeCN.

Ru1–N2	2.046(3)	Ru1–N5	2.138(5)
Ru1–N1	2.083(3)	Ru1–N7	2.147(5)
Ru1–N4	2.127(4)	Ru1–N6	2.154(4)
N2–Ru1–N1	177.2(2)	N4–Ru1–N7	90.72(19)
N2–Ru1–N4	91.18(16)	N5–Ru1–N7	179.4(2)
N1–Ru1–N4	87.37(16)	N2–Ru1–N6	90.85(15)
N2–Ru1–N5	87.9(2)	N1–Ru1–N6	90.68(16)
N1–Ru1–N5	89.7(2)	N4–Ru1–N6	177.21(19)
N4–Ru1–N5	88.8(2)	N5–Ru1–N6	93.18(19)
N2–Ru1–N7	91.7(2)	N7–Ru1–N6	87.30(19)
N1–Ru1–N7	90.6(2)		

2.3.5 ^{1}H NMR Studies

The ^{1}H NMR spectra of all the new Ru^{II} complex salts are well defined and therefore allow unambiguous identification and assessment of purity. A singlet in the region of 2.65–2.85 ppm for the four cis-ammine ligands confirms the trans geometry in each case. A coupling constant of *ca.* 16 Hz for the ethylene bridge protons in $Mebpe^+$ and $Phbpe^+$ confirms the trans geometry of the ethylene units. Coordination of the free ligands results in upfield shifts of the ligand proton signals, the magnitude of which is dependent on the donor strength of the Ru^{II} centre. Selected ^{1}H NMR data for various signals of the complexes **155–158**, **162** and **164–169**, as well as data for related complexes, are presented in Table 9.

The chemical shift of the signals for the protons ortho to the quarternised nitrogen is dependent on the acceptor strength of the *N*-substituent. In the case of complexes with 4,4′-bipyridinium ligands, replacing an *N*-methyl with an *N*-phenyl substituent results in a shift of this signal by *ca.* 0.2 ppm downfield. In general, the magnitude of this shift increases as the acceptor strength of L_A increases. In the $PymQ^+$ complexes **156** and **167** the signal is shifted downfield by *ca.* 1.0 ppm compared to that in their MeQ^+ analogues, confirming the strongly electron-withdrawing nature of the 2-pyrimidyl ring.

A similar shift downfield of *ca.* 0.3 ppm is observed for the *ortho* proton signals when comparing the $Mebpe^+$/$Phbpe^+$ complex pairs. Similarly, the signals for the ethylene

bridge protons shift by *ca.* 0.15 ppm downfield on replacing an *N*-methyl by an *N*-phenyl substituent.

The location of the signals for the donor ligand, L_D, is affected by the acceptor strength of L_A to a small extent. For example, the signals for the mim ring protons shift downfield by 0.04–0.07 ppm, and the signals of the trans NH_3 ligand by *ca.* 0.25 ppm, on replacing an *N*-methyl by an *N*-pyrimidyl substituent.

The signals for L_A in the complexes **162**, **164** and **165** are shifted slightly downfield compared to those in their mim/NH_3 analogues, reflecting the decreased electron density at the ruthenium due to the lower basicity of the py ligand.

Table 9. Selected ^{1}H NMR data for new and previously studied $[Ru^{II}(NH_3)_4(L_A)(L_D)][PF_6]_3$ complexes.[a]

Salt	L_D	L_A	Pyridinium ortho-H	mim	ethylene bridge	trans-NH_3	cis-NH_3
134 [c]	mim	MeQ^+	9.15	8.21, 7.46, 7.38	–	–	2.69
140 [b]	mim	PhQ^+	9.38	8.24, 7.48, 7.41	–	–	2.73
145 [b]	mim	$AcPhQ^+$	9.45	8.26, 7.50, 7.43	–	–	2.75
167	mim	$PymQ^+$	10.22	8.28, 7.50, 7.44,	–	–	2.78
138 [b]	NH_3	MeQ^+	9.15	–	–	3.50	2.66
143 [b]	NH_3	PhQ^+	9.33	–	–	3.60	2.70
148 [b]	NH_3	$AcPhQ^+$	9.40	–	–	3.64	2.72
149 [b]	NH_3	$DNPhQ^+$	9.37	–	–	3.74	2.75
156	NH_3	$PymQ^+$	10.17	–	–	3.75	2.74
157	NH_3	$Mebpe^+$	8.94	–	8.02, 7.89	3.41	2.65
158	NH_3	$Phbpe^+$	9.25	–	8.18, 8.04	3.44	2.65
164	py	$Mebpe^+$	8.98-8.92	–	8.09, 7.93	–	2.78
165	py	$Phbpe^+$	9.30	–	8.25, 8.07	–	2.81
168	mim	$Mebpe^+$	8.94	8.18, 7.45, 7.37	8.06, 7.91	–	2.65
169	mim	$Phbpe^+$	9.26	8.18, 7.45, 7.39	8.23, 8.04	–	2.67
155	NH_3	$Medap^+$	10.05	–	–	3.59	2.81
162	py	$Medap^+$	10.15	–	–	–	2.83
166	mim	$Medap^+$	10.10	9.31, 7.51, 7.47	–	–	2.85

[a] Recorded in d_6-acetone on a Varian Gemini 200 spectrometer; all shifts referenced to $SiMe_4$. [b] Ref. 91. [c] Ref 90.

2.3.6 Nonlinear Optical Studies

The first hyperpolarizabilities, β, of the new complex salts **155–158** and **162–169** were measured in acetonitrile using the HRS technique[12,97,98] (see section 1.4.3) with a 1064 nm Nd:YAG laser fundamental. Static hyperpolarizabilities, β_0, were estimated using the two-level model (see section 1.5.1) and the results are collected in Table 6 along with data for a selection of previously reported complexes. The relatively large errors in the HRS β values (±15 %) mean that scope for comparison of the data is limited.

Table 10.Visible MLCT absorption and HRS data for the salts *trans*-$[Ru^{II}(NH_3)_4(L_A)(L_D)][PF_6]_3$ in acetonitrile.

Salt	L_D	L_A	λ_{max}[MLCT] (ε/M^{-1} cm^{-1})	E_{max}[MLCT]/eV	β_{1064}[a] (10^{-30} esu)	β_0[a] (10^{-30} esu)
155	NH_3	$Medap^+$	581 (14 800)	2.13	660	89
156	NH_3	$PymQ^+$	673 (18 000)	1.84	640	230
157	NH_3	$Mebpe^+$	595 (16 100)	2.08	828	142
158	NH_3	$Phbpe^+$	628 (17 200)	1.97	751	192
[b]	NH_3	MeQ^+	590 (15 800)	2.10	750	123
[b]	NH_3	PhQ^+	628 (19 300)	1.97	858	220
[b]	NH_3	$AcPhQ^+$	654 (18 000)	1.90	1112	354
[b]	NH_3	$DNPhQ^+$	660 (16 900)	1.88	871	289
162	py	$Medap^+$	564 (12 300)	2.20	579	51
163	py	$PymQ^+$	644 (16 800)	1.93	774	228
164	py	$Mebpe^+$	563 (14 800)	2.20	904	78
165	py	$Phbpe^+$	591 (17 100)	2.10	936	151
166	mim	$Medap^+$	593 (16 700)	2.09	756	126
167	mim	$PymQ^+$	698 (18 700)	1.78	818	336
168	mim	$Mebpe^+$	604 (16 200)	2.05	857	168
169	mim	$Phbpe^+$	638 (17 600)	1.93	1068	310
[c]	mim	MeQ^+	602 (16 200)	2.06	523	100
[b]	mim	PhQ^+	642 (21 500)[d]	1.93	874	254
[b]	mim	$AcPhQ^+$	666 (19 500)	1.86	962	332

[a] The value of β_{1064} ($\times$ 10^{-30} esu) is the uncorrected first hyperpolarizability measured using a 1064 nm Nd-YAG laser fundamental (15 % error); β_0 is the static hyperpolarizability estimated by using the two-level model.[19] The quoted cgs units (esu) can be converted into SI units (C^3 m^3 J^{-2}) by dividing by a factor of 2.693×10^{20}. [b] Ref. 91. [c] Ref 90. [d] λ_{max} slightly altered from the value quoted in ref. 91.

The new complexes show very large β and β_0 values which are comparable to those of related complexes.[90,91] Comparison of the data for the $Medap^+$ complexes in **155** and **166** with their MeQ^+ analogues shows that for $L_D = NH_3$ the $Medap^+$ complex has a marginally smaller β_0, whilst when L_D = mim the reverse is true. This means that fixing the planarity of the 4,4′-bipyridinium rings does not have a great effect on β_0. Previous

crystallographic studies have shown that the MeQ^+ ligand is slightly twisted in the solid state, but in solution the pyridyl rings can be expected to rotate freely. Comparison of the β_0 data for the $Medap^+/MeQ^+$ pairs suggests that MeQ^+ adopts a predominantly planar conformation in solution, likely due to strong donor-acceptor electronic coupling.

Visible absorption and electrochemical data clearly show that $PymQ^+$ is the strongest electron acceptor of the 4,4′-bipyridinium ligands studied (see sections 2.3.2 and 2.3.3), but this does not result in the expected increases in β_0 for the complexes in **156** or **167**. Indeed, the β_0 values of **156** and **167** are similar or approximately equal to those of their $AcPhQ^+$ analogues. We have no clear explanation for this result, but the β_0 values of the $AcPhQ^+$ complexes may be boosted to some degree by the acetyl groups which increase the overall conjugation length of the complexes and also increase the total number of π electrons.

The $Mebpe^+$ and $Phbpe^+$ complexes, with the exception of **168,** have β_0 values which are similar to those of their 4,4′-bipyridinium analogues. Hence, the *trans*-ethylene unit does not seem to provide any enhancement of the NLO properties. This is in contrast to DπA organics where extension of conjugation length always results in increased hyperpolarizabilities (see section 1.5.4 and below).

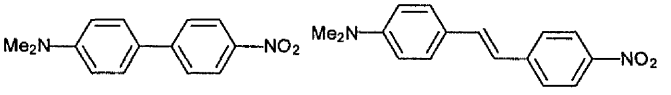

$CHCl_3$; λ_{max} = 390 nm; $\beta_{1907} = 50 \times 10^{-30}$ esu; $\beta_0 = 40 \times 10^{-30}$ esu;

$CHCl_3$; λ_{max} = 430 nm; $\beta_{1907} = 73 \times 10^{-30}$ esu; $\beta_0 = 55 \times 10^{-30}$ esu;[11d]

The significant lowering of the MLCT energy due to the increased acceptor strength of $Phbpe^+$ compared to $Mebpe^+$ results in an increase in β_0 between the pairs **157/158**, **164/165** and **168/169**. This is in accord with previously observed differences between the complexes of PhQ^+ and MeQ^+.[91] For a given L_A, the β_0 values increase in the order L_D = py < NH_3 < mim.

From the two-level model, the dominant component of β is inversely proportional to E_{CT}^2 (square of the energy gap between the ground state and the first charge-transfer

excited state). A good correlation between β_0 and $1/E_{max}[MLCT]^2$ has been previously demonstrated[91] and Figure 14 shows that the data for the new complexes fit reasonably well with this trend.

Decreasing the MLCT energy of these Ru^{II} chromophores generally corresponds to an increase in the first hyperpolarizability. The fact that this correlation is only partial may be explained by the fact that β_0 is also dependent upon a number of other factors such as the oscillator strength of the MLCT transition (see section 1.5.1).

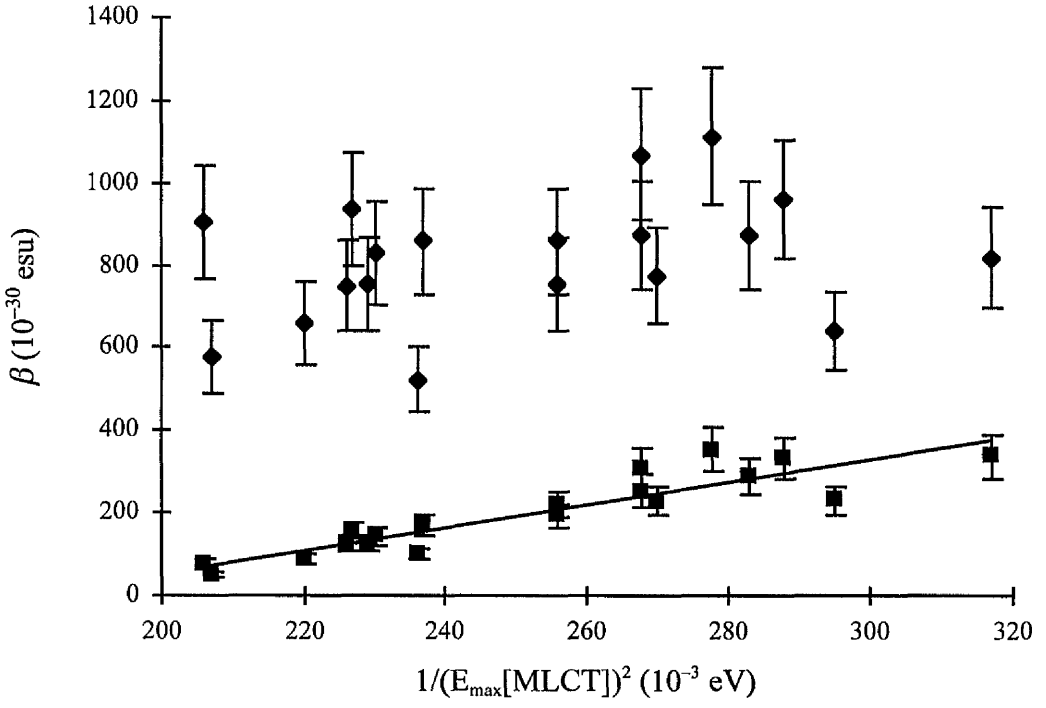

Figure 14. Plot of the first hyperpolarizability against the inverse square of the MLCT energy for the salts 155–158, 162–169 and other salts included in Table 6 [90,91] (◆= β_{1064}; ■ = β_0).

2.4 Conclusion

The MLCT absorption energies of Ru^{II} complexes, *trans*-$[Ru^{II}(NH_3)_4(L_D)(L_A)]^{3+}$, where L_D = an electon-rich ligand such as pyridine, 1-methylimidazole or NH_3 and L_A = a pyridinium-substituted ligand, show a fine degree of tunability. The large molecular hyperpolarizabilities, β, associated with these MLCT absorptions are also tunable,

although to a lesser extent. In general, the β_0 values increase as the MLCT energy decreases, in agreement with the two-level model. Extension of the conjugated bridge by an ethylene unit neither significantly alters the MLCT energies nor leads to increases in β_0.

2.5 *Future Work*

Although very large β_0 values have been observed, these have by no means been maximised and it is anticipated that increases in acceptor strength will increase β_0 further. Another strategy for increasing β_0 is to increase the donor strength of the ruthenium metal centre and perhaps using these strategies in conjunction (as in **170** below) may lead to substantial increases in molecular quadratic NLO responses.

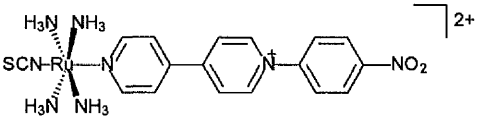

170

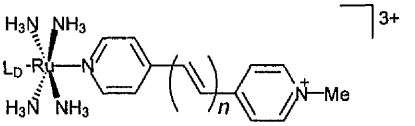

$L_D = NH_3$, py, mim

171

The fact that increasing the conjugation length of the bridge in L_A appears to have no significant effect on β_0 also requires further investigation. A study of β_0 *vs.* n (as in **171** above) may be of value in this context.

Chapter 3. Electroabsorption Spectroscopic Studies of Dipolar Ruthenium(II) Complexes Possessing Large Quadratic Nonlinear Optical Responses

3.1 Introduction

We have previously investigated the second-order NLO behaviour of ruthenium ammine complexes, the redox and spectroscopic properties of which have been thoroughly characterised over the years,[111] using the HRS technique. Electroabsorption (Stark) spectroscopy[112] has recently been used to study mono- and binuclear $[Ru^{II}(NH_3)_5]^{2+}$ complexes of pyrazine or 4,4′-bpy[113] and also a variety of other mononuclear $[Ru^{II}(NH_3)_5]^{2+}$ and $[Ru^{II}(NH_3)_5]^{3+}$ complexes.[114] We are interested in using electroabsorption spectroscopy as a tool to improve our understanding of the observed large molecular quadratic NLO responses in Ru^{II} ammine complexes.[90,91,115] Of particular relevance to this work are the very recent electroabsorption studies involving cyanide bridged $[Ru^{III}(NH_3)_n]^{3+}$ (n = 4 or 5) mixed valence complexes[116] and the tris-chelate $[Ru^{II}(trans\text{-}4,4'\text{-diethylaminostyryl-}2,2'\text{-bipyridine})_3]^{2+}$ which exhibit pronounced quadratic NLO properties.[87] Other NLO-active organic molecules such as donor-acceptor polyenes,[117] porphyrins[118] and metallocenyl derivatives[59] have also been investigated by using electroabsorption measurements.

3.2 Experimental

3.2.1 Materials and Procedures

All of the complex salts were synthesized according to previously published procedures.[90,91,115b] The identity and purity of the samples used for electroabsorption studies were confirmed by using ^1H NMR spectroscopy and elemental analyses.

3.2.2 Instrumentation and Measurements

The electroabsorption apparatus and experimental procedures were as previously reported,[114b] but incorporating the minor modifications described below. Butyronitrile

(Aldrich) was used as the glassing medium. The electroabsorption signal was always found to be quadratic in the field and the fit parameters presented are the average values.

Sample Cell. Two strips of Kapton film (50 μm, Dupont) were arranged so that they lay flush with the two long edges of the ITO glass (Figure 15). The cell was held vertically and a drop of sample was placed onto the top horizontal edge of the lower plate where it could run into the cavity produced by the Kapton film spacers.

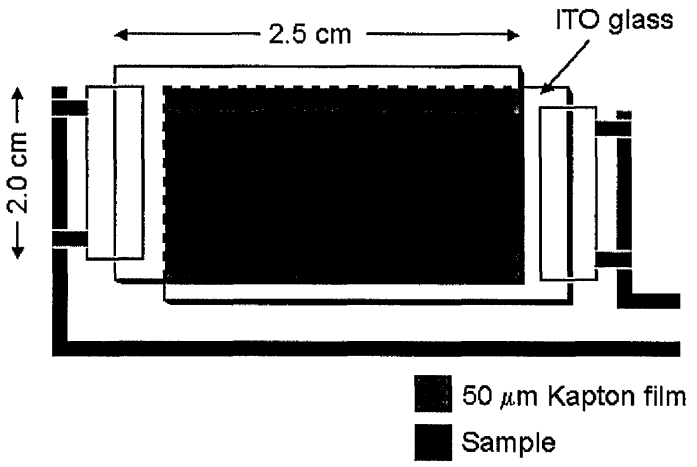

Figure 15. Sample cell assembly for the electroabsorption experiments.

Glass Characterization. Absorption spectra on the sample cell taken in the near IR region (800–1700 nm at 298 K) show oscillations due to the interference between the light reflected from the two glass surfaces that are 50 μm apart. The absorbance data were analysed as follows: a smoothed baseline was subtracted from the data, the Fourier transform (FT) of this data was then obtained and the power spectrum calculated. The maximum in the power spectrum was then taken as the product of the refractive index and the cell spacing, $n \times d$. The FT analysis of the oscillations on cells charged with air (n_1 = 1.00) and butyronitrile (n_1 = 1.38) at room temperature and 77 K allowed the determination of the distance between the electrodes (52.2 μm) and the refractive index of the frozen samples. The measured density of butyronitrile between 298 and 193 K was linear with temperature, and the density is estimated to be 15% higher at 77 K than at 298 K. A static dielectric constant D_s of the glass of 4.01 was determined from capacitance measurements

made with a BK Precision 878 capacitance meter at 1 kHz. The method was calibrated with 9 materials of known dielectric constant.

3.2.3 Data Treatment

The data analysis was carried out as previously described,[114b] by using the first and second derivatives of the absorption spectrum for analysis of the electroabsorption $\Delta\varepsilon(\nu)$ spectrum in terms of the Liptay treatment:[119]

$$\Delta\varepsilon(\nu)/\nu = \left[A_x \varepsilon(\nu)/\nu + \frac{B_x}{15h}\frac{\partial(\varepsilon(\nu)/\nu)}{\partial\nu} + \frac{C_x}{30h^2}\frac{\partial^2(\varepsilon(\nu)/\nu)}{\partial\nu^2} \right] F_{\text{int}}^2 \tag{12}$$

where ν is the frequency of the light in Hz. For a randomly oriented, fixed sample, the following relationships hold:

$$A_x = A_1 + (3\cos^2(\chi) - 1)A_2 \tag{13}$$

$$B_x = B_1 + (3\cos^2(\chi) - 1)B_2 \tag{14}$$

$$C_x = C_1 + (3\cos^2(\chi) - 1)C_2 \tag{15}$$

where χ is the angle between the direction of the applied electric field and the polarization direction of the incident light. The dipole moment change for the MLCT excitation is obtained from the coefficient of the second derivative term:

$$|\Delta\mu_{12}| = \sqrt{C_1/5} \tag{16}$$

$$|\mathrm{m} \bullet \Delta\mu_{12}| = \sqrt{C_2/3 + C_1/15} \tag{17}$$

where m is the unit transition dipole moment, $\mu_{12}/|\mu_{12}|$. The internal electric field is related to the applied external field by $\mathbf{F}_{int} = f_{int}\mathbf{F}_{ext}$. For the butyronitrile medium used here the local field correction f_{int} is estimated as 1.33.[114b]

A two-level model (ground and excited) can be used to analyse the charge-transfer transitions. If ψ_a and ψ_b denote the wave functions of the zero-order diabatic states (*i.e.* the metal-centred and ligand-centred localised states), then their interaction gives two adiabatic wavefunctions $\psi_1 = c_a\psi_a + c_b\psi_b$ (ground) and $\psi_2 = c_a\psi_b - c_b\psi_a$ (excited), where the overlap integral is neglected and the mixing coefficients are normalised. This model gives:

$$\Delta\mu_{ab}^2 = \Delta\mu_{12}^2 + 4\mu_{12}^2 \tag{18}$$

where $\Delta\mu_{ab}$ is the dipole moment difference between the diabatic states, $\Delta\mu_{12}$ is the observed (adiabatic) dipole moment difference, and μ_{12} is the transition dipole moment. The latter can be determined from the oscillator strength f_{os} of the transition by

$$|\mu_{12}| = \left[f_{os}/\left(1.08\times10^{-5}(E_{max})\right)\right]^{1/2} \tag{19}$$

where E_{max} is the energy of the MLCT maximum (in wavenumbers). The degree of delocalization c_b^2 and electronic coupling matrix element H_{ab} for the diabatic states are given by

$$c_b^2 = \frac{1}{2}\left[1-\left(\frac{\Delta\mu_{12}^2}{\Delta\mu_{12}^2 + 4(\mu_{12})^2}\right)^{1/2}\right] \tag{20}$$

$$|H_{ab}| = \left|\frac{E_{max}\mu_{12}}{\Delta\mu_{ab}}\right| \tag{21}$$

If the polarizability change $\Delta\alpha$ and hyperpolarizability β_0 tensors have only nonzero elements along the direction of the charge-transfer, then these quantities are given by

$$\Delta\alpha = -4\frac{(\mu_{12})^2}{E_{max}} \tag{22}$$

$$\beta_0 = \frac{3\Delta\mu_{12}(\mu_{12})^2}{(E_{max})^2} \tag{23}$$

3.3 Results and Discussion

1.1.1 Electroabsorption Studies.

The structures of the 20 complexes in the salts studied are shown in Figure 16. As found previously with related Ru^{II} ammine complexes[114b] the electroabsorption spectra of these salts were successfully modelled in terms of a large second derivative term, a small first derivative component and a negligible zeroth derivative contribution. Spectra were also recorded for 5 other salts, *trans*-$[Ru^{II}(NH_3)_4(L_D)(L_A)][PF_6]_3$ [L_D = NH_3 and L_A = $PymQ^+$;[115b] L_D = mim and L_A = $Medap^+$;[115b] L_D = py and L_A = $Medap^+$;[115b] L_D = dmabn and L_A = PhQ^+ or $AcPhQ^+$ [91]], but satisfactory data fits could not be obtained. Representative absorption spectra, electroabsorption spectra and the spectral components for the salts **143**, **144** and **145** are presented in Figure 17.

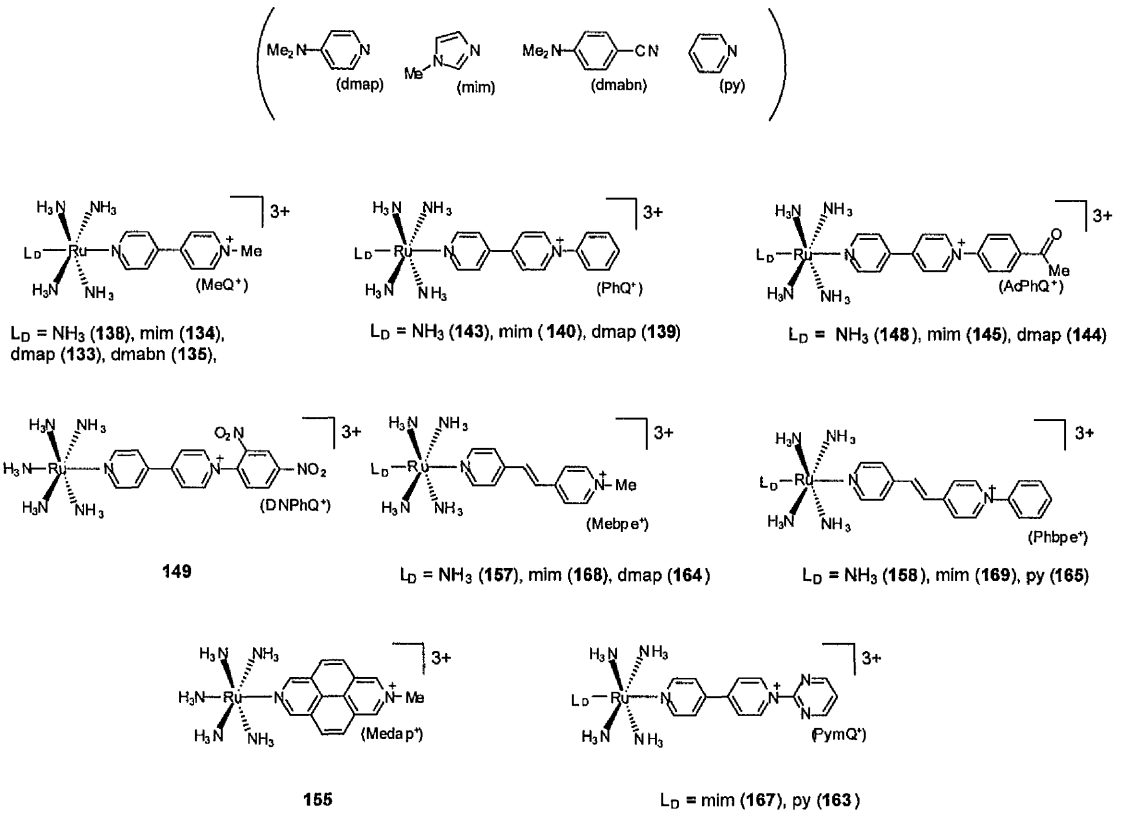

Figure 16. Structures of the 20 complex cations studied.

The parameters derived from fitting the electroabsorption spectra to Liptay's equation[119] are given in Table 11, together with the oscillator strengths f_{os}, MLCT absorption maxima λ_{max}, at 298 and 77 K, and the values inferred from equations 16 and 17 for $|\Delta\mu_{12}|$ and $|\mathbf{m}\bullet\Delta\mu_{12}|$ in multiples of f_{int}. Deviations are of the order of 10^{-58} C^2 m^2 (5–10%), 10^{-38} C m^2 V^{-1} (*ca.* 50%) and *ca.* 10^{-20} m^2 V^{-2} for the second, first and zeroth derivative terms, respectively. The $f_{int}|\Delta\mu_{12}|$ values cover a range of 16–28 D which includes those found previously for $[Ru^{II}(NH_3)_5(L^A)]Cl_3$ (L^A = *N*-protonated 4,4′-bipyridine) (20 and 23.1 D).[113b,114b] In almost all cases, $f_{int}|\Delta\mu_{12}|$ and $f_{int}|\mathbf{m}\bullet\Delta\mu_{12}|$ agree within experimental error, confirming that the transition dipole moment and the dipole moment change lie along the same axis.

In all cases the MLCT bands undergo marked red-shifts in the 77 K glass, in agreement with previous studies.[114b] The changes in ΔE_{max} are larger for the $Mebpe^+/Phbpe^+$ complexes than for the MeQ^+/PhQ^+ complexes [the average shifts in

eV(L_A) are: –0.13 (MeQ^+), –0.22 ($Mebpe^+$), –0.15 (PhQ^+), –0.21 ($Phbpe^+$)]. The f_{os} values were determined directly by numerical integration of the digitized absorption spectra, and do not differ significantly (± 5%) from those obtained by using the band maxima and half widths and assuming Gaussian absorption profiles. Although the band maxima and half widths change between 298 and 77 K, the f_{os} values show very little temperature dependence (≤ 5%).

The dipole moment changes $\Delta\mu_{12}$ and the transition dipole moments μ_{12} for the MLCT excitations are of direct relevance to the second-order NLO responses of the salts studied. Both $\Delta\mu_{12}$ and μ_{12} lie along the Ru–L_A bond in all cases and values of these quantities, calculated from the electroabsorption results in Table 11 by using $f_{int} = 1.33$ and eq 18 and 19, are given in Table 12. The nominal metal-to-centre-of-ligand distances r^0 (obtained from measurements on Cerius^2 models)[120] and $\Delta\mu_{ab}$ (diabatic dipole moment change), c_b^2 (degree of delocalization), H_{ab} (electronic coupling matrix element), $\Delta\alpha$ (polarizability change on MLCT excitation) and β_0 (static first hyperpolarizability) values calculated from the two-level model according to eqs 18 and 20–23 are included in Table 12 as well as data for a number of previously measured complexes for purposes of comparison.[114b]

The μ_{12} values cover a fairly narrow range (*ca.* 4–7 D) and generally increase with the electron accepting strength of L_A. For the monoaryl complexes $[Ru^{II}(NH_3)_5L_A]^{n+}$ (n = 2 or 3), μ_{12} increases in the order L_A = py-4-NH_2 = py < pz ≈ py-4-COOH < pzH^+ < $pzMe^+$. The pentaammine complexes of the 4,4′-bipyridine-based L_A ligands exhibit a similar trend. μ_{12} increases in the order L_A = 4,4′-bpy ≈ $Medap^+$ < MeQ^+ ≈ 4,4′-$bpyH^+$ < PhQ^+ ≈ $AcPhQ^+$ = $DNPhQ^+$. Data for the complexes of the other L_D ligands reveals that μ_{12} invariably increases on replacing an *N*-methyl with an *N*-phenyl substituent, but the differences are smaller in the bpe-based complexes than in their 4,4′-bpy counterparts. Furthermore, μ_{12} is not greatly increased when a more electron deficient 4-acetylphenyl, 2,4-dinitrophenyl or 2-pyrimidyl ring replaces an *N*-phenyl group. The extension of the conjugated system by the addition of a *trans*-ethylene bridge causes μ_{12} to change by between 0 (**143**→**158**) and +0.8 D (**134**→**168**).

Table 11. Spectral Data and Fitting Results (Eq 12[a]) For The Complex Salts Studied.[b]

No	L_D	L_A	λ_{max} (nm)		ΔE_{max}[c]	f_{os}	$f_{int}^2 A_1$	$f_{int}^2 A_2$	$f_{int}^2 B_1$	$f_{int}^2 B_2$	$f_{int}^2 C_1$	$f_{int}^2 C_2$	$f_{int}\lvert\Delta\mu_{12}\rvert$	$f_{int}\lvert m\cdot\Delta\mu_{12}\rvert$
			298 K	77 K	(eV)		(10^{-20} m^2 V^{-2})		(10^{-38} C m^2 V^{-1})		(10^{-57} C^2 m^2)		(D)	(D)
138	NH_3	MeQ^+	597	645	–0.15	0.20	16.4	0.005	16.8	4.7	18.7	4.8	18.3	15.9
143	NH_3	PhQ^+	634	696	–0.17	0.22	19.3	–4.9	22.2	9.0	23.2	8.0	20.4	19.5
148	NH_3	$AcPhQ^+$	651	718	–0.18	0.20	44.3	13.7	24.6	9.2	28.5	10.7	22.6	22.1
149	NH_3	$DNPhQ^+$	672	731	–0.15	0.22	55.5	37.7	17.2	5.4	26.1	7.6	21.7	19.6
157	NH_3	$Mebpe^+$	604	681	–0.23	0.23	-3.4	–11.7	26.5	11.9	25.6	8.6	21.5	20.3
158	NH_3	$Phbpe^+$	641	714	–0.19	0.21	18.3	2.57	35.2	13.2	37.4	12.1	25.9	24.3
155	NH_3	$Medap^+$	590	632	–0.14	0.17	31.7	0.8	6.9	1.1	19.5	6.2	18.7	17.3
134	mim	MeQ^+	610	658	–0.15	0.22	-2.1	6.1	28.8	9.5	29.0	8.0	22.8	20.4
140	mim	PhQ^+	651	708	–0.15	0.27	8.4	–9.2	27.8	9.6	29.9	10.2	23.2	22.0
145	mim	$AcPhQ^+$	668	721	–0.14	0.26	15.7	14.1	27.5	10.9	27.9	10.1	22.4	21.7
167	mim	$PymQ^+$	715	784	–0.15	0.24	12.8	10.9	24.5	5.7	27.7	9.4	22.3	21.2
168	mim	$Mebpe^+$	616	687	–0.21	0.26	-8.7	–1.1	26.5	9.0	31.6	10.4	23.9	22.4
169	mim	$Phbpe^+$	651	741	–0.23	0.26	-5.3	–5.5	37.6	12.1	39.9	14.2	26.8	25.8
133	dmap	MeQ^+	624	667	–0.13	0.25	0.7	2.3	16.8	5.4	22.9	7.7	20.3	19.2
139	dmap	PhQ^+	663	714	–0.13	0.31	-2.8	2.4	21.5	6.5	24.8	7.6	21.1	19.4
144	dmap	$AcPhQ^+$	680	734	–0.13	0.30	-1.3	–5.6	34.2	11.2	40.5	14.2	27.0	25.8
163	py	$PymQ^+$	655	711	–0.15	0.29	-9.4	–7.8	13.8	4.4	15.2	4.2	16.5	14.7
164	py	$Mebpe^+$	577	638	–0.21	0.25	-1.82	–3.2	20.7	6.9	36.8	12.3	25.7	24.3
165	py	$Phbpe^+$	607	672	–0.20	0.26	-12.7	–9.7	27.9	9.2	41.8	13.6	27.4	25.6
135	dmabn	MeQ^+	547	571	–0.10	0.26	1.51	0.3	17.9	6.8	3.69	12.8	25.7	24.5

[a] Relationships between the parameters in eq 12 and the terms *D–I* defined in ref 111b are $A_1 = D/3$, $A_2 = E/30$, $B_1 = 5F$, $B_2 = G$, $C_1 = 5H$ and $C_2 = I$.
[b] In butyronitrile at 77 K. [c] Shift in the MLCT band maximum energy on moving from 298 to 77 K.

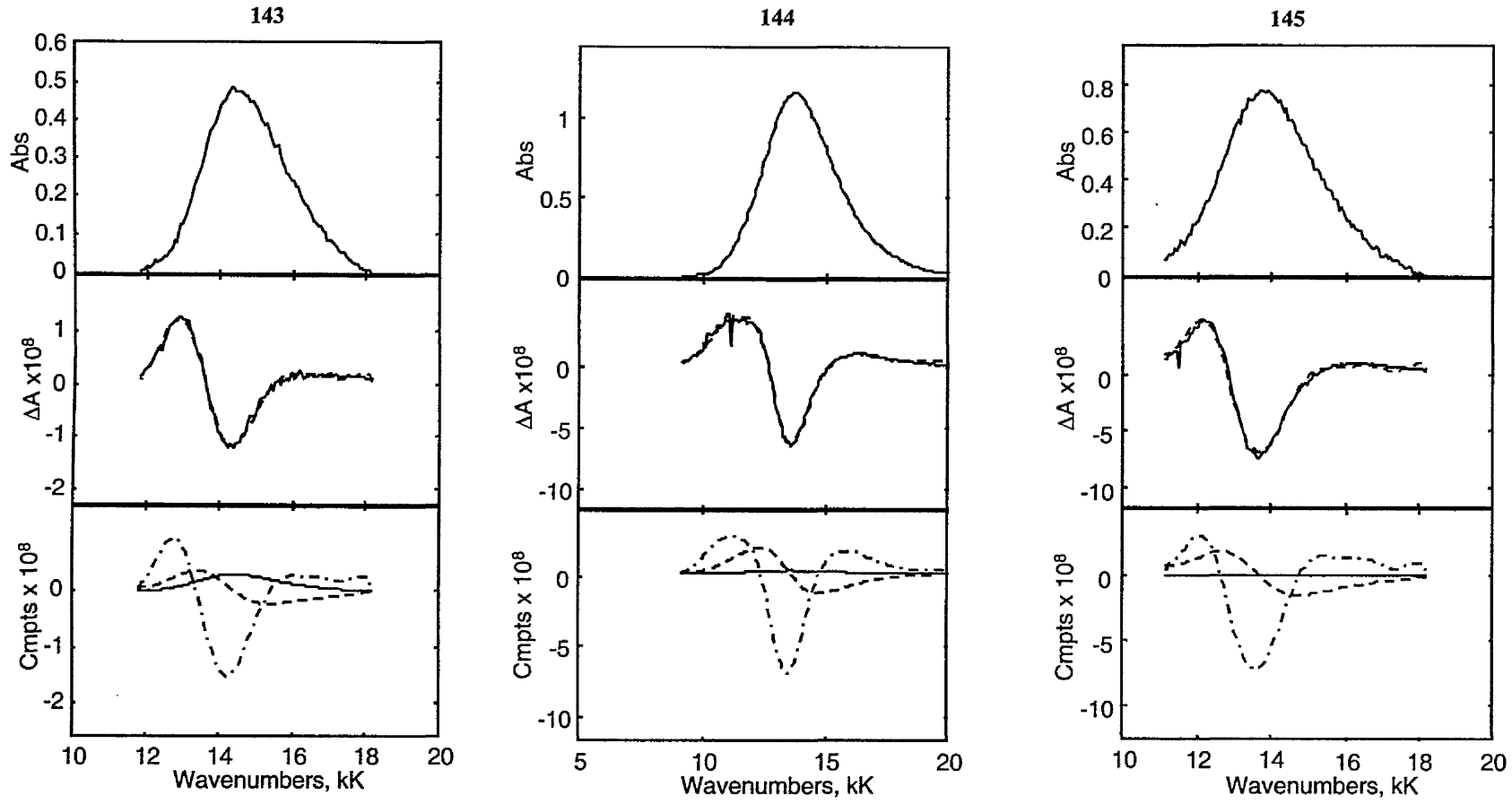

Figure 17. Electroabsorption spectra and calculated fits for 143, 144 and 145 in an external electric fields of 1.92, 2.39 and 3.84 × 10^7 V m^{-1} respectively. Top panel: absorption spectrum; middle panel: electroabsorption spectrum, experimental (—) and fits (- - -) according to the Liptay equation; bottom panel: contribution of 0th (——), 1st (– – –) and 2nd (- - -) derivatives of the absorption spectrum to the calculated fit.

Table 12. Values of Metal-to-Ligand Distance, Transition Dipole Moment, Dipole Moment Change, Diabatic Dipole Moment Change, Electron-Transfer Distances, Degree of Delocalization, Electronic Coupling Matrix Element, Polarizability Change and First Hyperpolarizability

No.	L^D	L^A	λ_{max} 77 K (nm)	E_{max} 77 K (10^{-19} J)	r^0 (Å)	$\lvert\mu_{12}\rvert$[a] (D)	$\lvert\Delta\mu_{12}\rvert$[b] (D)	$\Delta\mu_{ab}$[c] (D)	r_{12}[d] (Å)	r_{ab}[e] (Å)	c_b^2[f]	H_{ab}[g] (10^3 cm^{-1})	$\Delta\alpha$[h] (10^{-39} C m^2 V^{-1})	β_0[i] (10^{-49} C m^3 V^{-2})
[j]	NH_3	Py	432	4.60	3.3	3.8	3.4	8.3	0.7	1.7	0.30	10.5	1.4	0.3
[j]	NH_3	Pz	497	4.00	3.4	4.6	3.5	9.8	0.7	2.0	0.32	9.4	2.4	0.6
[j]	NH_3	pzH^+	532	3.73	3.4	5.0	≤ 2	≤ 10.2	0.2	2.1	≥ 0.40	≥ 9.2	3.0	0.2
[j]	NH_3	$PzMe^+$	536	3.71	3.9	5.5	≤ 2	≤ 11.2	0.2	2.3	≥ 0.41	≥ 9.2	3.7	0.2
[j]	NH_3	py-4-NH_2	389	5.11	3.8	3.8	5.9	9.6	1.2	2.0	0.19	10.1	1.2	0.4
[j]	NH_3	py-4-COOH	528	3.76	4.6	4.7	5.9	11.1	1.2	2.3	0.24	8.0	2.6	1.1
[j]	NH_3	4,4′-bpy	530	3.75	5.5	4.7	13	16.0	2.7	3.3	0.09	5.5	2.6	2.4
[j]	NH_3	4,4′-$bpyH^+$	624	3.18	5.5	5.3	17	20.0	3.5	4.2	0.07	4.2	3.9	5.5
138[k]	NH_3	MeQ^+	645	3.08	5.5	5.2	13.8	17.3	2.9	3.6	0.10	4.7	37.8	4.5
143[k]	NH_3	PhQ^+	696	2.85	7.7	5.7	15.3	19.1	3.2	4.0	0.10	4.3	50.2	6.9
148[k]	NH_3	$AcPhQ^+$	718	2.76	8.7	5.8	17.0	20.6	3.5	4.3	0.09	3.9	55.7	8.5
149[k]	NH_3	$DNPhQ^+$	731	2.72	8.7	5.8	16.3	20.0	3.4	4.2	0.09	4.0	39.1	8.4
157[k]	NH_3	$Mebpe^+$	681	2.92	6.7	5.5	16.2	19.6	3.4	4.1	0.09	4.1	59.9	6.5
158[k]	NH_3	$Phbpe^+$	714	2.79	8.8	5.7	19.5	22.6	4.1	4.7	0.07	3.5	79.9	9.2
155[k]	NH_3	$Medap^+$	632	3.14	5.5	4.8	14.1	17.1	2.9	3.6	0.09	4.4	15.6	3.7
134[k]	mim	MeQ^+	658	3.01	5.5	5.5	17.1	20.3	3.6	4.2	0.08	4.1	65.3	6.3
140[k]	mim	PhQ^+	708	2.80	7.7	6.2	17.4	21.4	3.6	4.5	0.09	4.1	62.9	9.6
145[k]	mim	$AcPhQ^+$	721	2.74	8.7	6.4	16.8	21.1	3.5	4.4	0.10	4.2	62.2	10.4
167[k]	mim	$PymQ^+$	784	2.53	7.7	6.4	16.8	21.1	3.5	4.4	0.10	3.9	55.5	12.0
168[k]	mim	$Mebpe^+$	687	2.88	6.7	6.3	18.0	22.0	3.7	4.6	0.09	4.2	60.0	9.5
169[k]	mim	$Phbpe^+$	741	2.68	8.8	6.5	20.2	24.0	4.2	5.0	0.08	3.6	84.9	13.1
133[k]	dmap	MeQ^+	667	2.96	5.5	6.1	15.3	19.6	3.2	4.1	0.11	4.6	38.1	7.1
139[k]	dmap	PhQ^+	714	2.77	7.7	7.1	15.9	21.3	3.3	4.4	0.13	4.6	48.5	11.6
144[k]	dmap	$AcPhQ^+$	734	2.71	8.7	6.8	20.3	24.4	4.2	5.1	0.08	3.8	77.4	14.4
163[k]	py	$PymQ^+$	711	2.79	7.7	6.5	12.4	18.0	2.6	3.7	0.15	5.1	31.3	7.5
164[k]	py	$Mebpe^+$	638	3.11	6.7	6.0	19.3	22.7	4.0	4.7	0.08	4.1	46.9	8.1
165[k]	py	$Phbpe^+$	672	2.96	8.8	6.2	20.6	24.0	4.3	5.0	0.07	3.8	62.9	10.0
135[k]	dmabn	MeQ^+	571	3.48	5.5	5.7	19.3	22.4	4.0	4.7	0.07	4.5	40.6	5.8

[a] Transition dipole moment calculated from eq 19. [b] Dipole moment change calculated from $f_{int}\Delta\mu_{12}$ using $f_{int} = 1.33$. [c] Diabatic dipole moment change calculated from eq 18. [d] Delocalized electron-transfer distance calculated from $\Delta\mu_{12}/e$. [e] Effective (localized) electron-transfer distance calculated from $\Delta\mu_{ab}/e$. [f] Degree of delocalization calculated from eq 20. [g] Electronic coupling matrix element calculated from eq 21. [h] Polarizability change calculated from eq 11. [i] First hyperpolarizability calculated from eq 23. [j] In 1:1 glycerol-water (pz = pyrazine, pzH^+ = *N*-protonated pyrazine, $pzMe^+$ = *N*-methylated pyrazine, 4,4′-$bpyH^+$ = *N*-protonated 4,4′-bipyridine).[9b] [k] In butyronitrile.

Patterns in the variation of μ_{12} with the nature of L_D are observed, but the origins of these effects are unclear. For L_A = MeQ^+ (in **133**, **134**, **135** and **138**), μ_{12} increases in the order L_D = NH_3 < mim < dmabn < dmap, and a similar trend is found for L_A = PhQ^+ (in **139**, **140** and **143**) or $AcPhQ^+$ (in **144**, **145** and **148**). The difference in μ_{12} between the two extremes is 1.4 D for the PhQ^+ series. For L_A = $Mebpe^+$ (in **157**, **164** and **168**) or $Phbpe^+$ (in **158**, **165** and **169**), μ_{12} increases in the order L_D = NH_3 < py < mim.

The values of $\Delta\mu_{12}$ for the pentaammine complexes generally increase as the size of L_A increases due to the addition of aryl rings and/or *trans*-ethylene units. Generally, similar effects are observed in the complexes where L_D = mim or dmap. For L_D = NH_3 (in **138**, **143** and **148**) or dmap (in **133**, **139** and **144**), $\Delta\mu_{12}$ increases with L_A length in the order MeQ^+ < PhQ^+ < $AcPhQ^+$. However, when L_D = mim, the $\Delta\mu_{12}$ values are very similar for L_A = MeQ^+, PhQ^+, $AcPhQ^+$ or $PymQ^+$ (in **134**, **140**, **145** and **167**). The insertion of a *trans*-CH=CH bridge between the two 4,4′-bipyridinium rings in **134**, **138**, **140** or **143** causes $\Delta\mu_{12}$ to increase by *ca.* 1–4 D. The parallel between the r^0 and $\Delta\mu_{12}$ values suggests that the ligand π^* orbital is partially delocalized over multiple aryl rings. The same result is suggested by ZINDO calculations on the complexes.[121] The close similarity between the $\Delta\mu_{12}$ and $\Delta\mu_{ab}$ values of **138** and of its $Medap^+$ analogue (**155**) suggests that any torsion between the 4,4′-bipyridinium rings does not significantly reduce the delocalization of the L_A π^* orbital.

The dependence of $\Delta\mu_{12}$ on L_D is less readily explained. For L_A = MeQ^+ (in **133**, **134**, **135** and **138**), $\Delta\mu_{12}$ increases in the order L_D = NH_3 < dmap < mim < dmabn, with a difference of 5.5 D between the two extremes. A parallel trend is found for L_A = PhQ^+ (in **139**, **140** and **143**). However, when L_A = $AcPhQ^+$, the $\Delta\mu_{12}$ values are very similar for L_D = NH_3 (in **148**) and mim (in **145**), but larger for L_D = dmap (in **144**). For L_A = $Mebpe^+$ (in **157**, **164** and **168**) or $Phbpe^+$ (in **158**, **165** and **169**), $\Delta\mu_{12}$ increases in the order L_D = NH_3 < mim < py, although the differences are only small for the $Phbpe^+$ complexes. The fact that the pentaammine complexes generally have the smallest $\Delta\mu_{12}$ values may be due to the difference in back-bonding between the metal and the L_D ligand for NH_3 compared to the

JOHN RYLANDS
UNIVERSITY
LIBRARY OF
MANCHESTER

other ligands. Decreases in this back-bonding allow more electron density to move toward L_A.

The diabatic dipole moment changes, $\Delta\mu_{ab}$ for the complexes studied are on average 23% larger than their adiabatic counterparts. This close parallel between $\Delta\mu_{12}$ and $\Delta\mu_{ab}$ arises from the relatively modest and fairly constant μ_{12} values. The dipole moment changes can be used to calculate charge-transfer distances if it is assumed that one electronic charge is transferred in an MLCT transition ($r_{12} = \Delta\mu_{12}/e$ or $r_{ab} = \Delta\mu_{ab}/e$). Values of r_{12} (the delocalized electron-transfer distance) and r_{ab} (the effective (localized) electron-transfer distance) are also included in Table 12. It can be seen that r^0 is generally about twice r_{12} and *ca.* 60–70% larger than r_{ab}.

The mixing between the diabatic states is reflected in c_b^2. The maximum possible value of c_b^2 is 0.5, corresponding to essentially complete delocalization of the orbitals involved in the electronic excitation. Such a situation has been observed for the visible absorption band (λ_{max} = 538 nm at 298 K in 1:1 glycerol-water) of $[Ru^{II}(NH_3)_5(L_A)][BF_4]_3$ (L_A = *N*-methylpyrazinium), which is accordingly best described as a bonding-to-antibonding transition (this complex salt exhibits a true MLCT band at λ_{max} = 880 nm at 298 K in 1:1 glycerol-water).[114b] By contrast, the c_b^2 values for the complexes studied are all close to 0.1 and similar to that found for $[Ru^{II}(NH_3)_5(L_A)]Cl_3$ (L_A = *N*-protonated 4,4′-bipyridine).[114b] Such a limited degree of delocalization is clearly consistent with the description of the low energy absorption bands in the complexes studied as MLCT in character. Comparison of the present values of c_b^2 and H_{ab} with those for the pentaammine complexes studied previously shows that c_b^2 tends to decrease as the L_A length increases, as would be expected. For a ligand of the size of pyridine H_{ab} is *ca.* 10×10^3 cm^{-1}, while for the L_A ligands studied here H_{ab} is only *ca.* 4×10^3 cm^{-1}, similar to that observed for protonated 4,4′-bpy. This decrease in c_b^2 and H_{ab} is not observed for the ligands studied here, hence the decrease with length reaches a minimum when L_A is longer than 4,4′-bpy. The $\Delta\alpha$ values are relatively large and generally increase in size as the length of L_A increases.

For the ruthenium ammine complexes studied previously, the difference between r_{ab} and r^0 was attributed to polarization of the ligand by the increased charge on the metal

centre in the excited state.[114b] This increase in charge polarizes the electrons of the ligand toward the metal and decreases the dipole moment change observed. The same effect would be expected to operate in **1–20**. For the largest L_A ligands, the difference between r^0 and r_{ab} is approximately 4 Å which corresponds to a difference of almost 20 D. ZINDO calculations examining the polarization effect in the complexes studied have been carried out and show that the calculated and observed diabatic dipole moment changes are in reasonable agreement.[121] These calculations also suggest that the orbital(s) that receive the MLCT electron are delocalized only over the first two aromatic rings.

3.3.2 First Hyperpolarizabities: Trends and Comparisons between Electroabsorption and HRS Results.

The electroabsorption-derived static first hyperpolarizabilities, β_0[Stark], (converted into esu) are presented in Table 13, together with the λ_{max} and β_0[HRS] values for acetonitrile solutions of the complexes studied at 298 K.[90,91,115b] The latter were derived from the application of eq 24 (E is the fundamental laser energy) to the β_{1064} values obtained from HRS measurements.[90,91,115b]

Other two-level descriptions are available (see section 1.5.1), which would change the β_0[Stark] values quoted here by a constant factor of either 0.5 or 2.[20] However, it is noteworthy that when using eq 23, the extent of agreement between β_0[Stark], and β_0[HRS] is generally good, and in 4 cases excellent ($\leq \pm 5\%$). When considering only complexes that do not absorb near the second harmonic, the complexes with the smallest and the largest β_0 values are the same in both series (in salts **144** and **155**, respectively).

$$\beta_{1064} = \beta_0 \frac{E_{max}}{[1-(2E)^2(E_{max}^2)^{-1}][E_{max}^2 - E^2]} \qquad (24)$$

The poor correlations observed for **135** and **164** can be traced to the fact that the β_0[HRS] values of these compounds are underestimated due to the close proximity of their MLCT maxima to the second harmonic wavelength at 532 nm.[90,115b] Hence, the β_0[Stark]

values for **135** and **164** are more reliable estimates of their actual static first hyperpolarizabilities. Importantly, the present studies confirm the large magnitudes of β_0 in Ru^{II} penta/tetraammine complexes with pyridinium ligands. Furthermore, they also provide support for our earlier conclusion that the quadratic NLO responses of the *N*-arylpyridinium Ru^{II} chromophores are larger than those of their *N*-methyl analogues.[91,115b]

Table 13. First Hyperpolarizabilities Derived from Electroabsorption Spectra and Hyper-Rayleigh Scattering for the 20 Complex Salts Studied.

No.	L_D	L_A	λ_{max}[a]/nm	β_0[Stark][b] (10^{-30} esu)	β_0[HRS][c] (10^{-30} esu)
138	NH_3	MeQ^+	590[d]	120	123[d]
143	NH_3	PhQ^+	628[d]	186	220[d]
148	NH_3	$AcPhQ^+$	654[d]	229	354[d]
149	NH_3	$DNPhQ^+$	660[d]	225	289[d]
157	NH_3	$Mebpe^+$	595[e]	175	142[e]
158	NH_3	$Phbpe^+$	628[e]	249	192[e]
155	NH_3	$Medap^+$	581[e]	98	89[e]
134	mim	MeQ^+	602[f]	170	100[f]
140	mim	PhQ^+	648[d]	258	254[d]
145	mim	$AcPhQ^+$	666[d]	279	332[d]
167	mim	$PymQ^+$	698[e]	323	336[e]
168	mim	$Mebpe^+$	604[e]	256	168[e]
169	mim	$Phbpe^+$	638[e]	352	310[e]
133	dmap	MeQ^+	614[f]	191	130[f]
139	dmap	PhQ^+	658[d]	313	260[d]
144	dmap	$AcPhQ^+$	688[d]	388	410[d]
163	py	$PymQ^+$	644[e]	200	228[e]
164	py	$Mebpe^+$	563[e]	218	78[e]
165	py	$Phbpe^+$	591[e]	269	151[e]
135	dmabn	MeQ^+	540[f]	157	14[f]

[a] Measured in acetonitrile at 298 K. [b] Static first hyperpolarizability calculated by using $\Delta\mu_{12}$ and μ_{12} values and eq 23. [c] Static first hyperpolarizability derived from 1064 nm HRS measurements and corrected by using the two-level model according to eq 24 (±15%). [d] Ref. 91. [e] Ref. 115b. [f] Ref. 90.

Comparison of the data in Table 12 and Table 13 is informative regarding the factors responsible for the observed differences and trends in β_0. Within the three triads with a given L_D [(**138**, **143** and **148**), (**134**, **140** and **145**) and (**133**, **139** and **144**)], the MLCT λ_{max} red-shifts as the electron accepting strength of L_A increases in the order $MeQ^+ < PhQ^+ < AcPhQ^+$, as confirmed by electrochemical studies.[91,115a] β_0 increases in the same order, in keeping with principles well-established in dipolar organic chromophores. As

noted previously, for $L_D = NH_3$ (in **138**, **143** and **148**) or dmap (in **133**, **139** and **144**), $\Delta\mu_{12}$ clearly increases in the order $MeQ^+ < PhQ^+ < AcPhQ^+$, but when L_D = mim (in **134**, **140** and **145**), no trend is found. By contrast, μ_{12} also increases on replacement of MeQ^+ with PhQ^+, but the values for the $AcPhQ^+$ complexes are similar to those of their PhQ^+ counterparts. Hence, the observed increases in β_0 are generally associated with increases in both μ_{12} and $\Delta\mu_{12}$.

The $DNPhQ^+$ and $PymQ^+$ complexes in **149** and **167** possess essentially identical values of μ_{12} and $\Delta\mu_{12}$ and also similar β_0 values when compared with their $AcPhQ^+$ analogues. As discussed previously,[91] β_0 in **149** is smaller than would be expected, based on the very strongly electron-withdrawing nature of a 2,4-DNPh ring. This observation is attributed to an attenuation of mesomeric coupling, arising from twisting about the $N_{pyridyl}$–C_{phenyl} bond due to the steric effect of the ortho-NO_2 substituent.[91] Also, it is clear that replacement of $AcPhQ^+$ by the considerably more strongly electron-accepting ligand $PymQ^+$ (cyclic voltammetric data show that coordinated $PymQ^+$ is easier to reduce than $AcPhQ^+$ by ca. 0.2 eV)[93,115b] is not an especially effective means to increase β_0, despite the significant red-shifting of the MLCT absorption in moving from **145** to **167**.

The β_0 values for the $Medap^+$ complex in **155** are slightly smaller than those of the analogous MeQ^+ complex in **138**. Hence, it appears that fixing the coplanarity of the 4,4′-bipyridinium rings actually has a deleterious effect on β_0 (the original expectation was the reverse),[115b] which can be traced to a small blue shift in λ_{max}, together with a slight decrease in μ_{12} in moving from **138** to **155**. With a given L_A (MeQ^+, PhQ^+ or $AcPhQ^+$), the λ_{max}, μ_{12} and β_0[Stark] (but not always β_0[HRS]) values all increase in the order $L_D = NH_3$ < mim < dmap, but no accompanying trend in $\Delta\mu_{12}$ is observed (see section 3.3.1).

In purely organic dipolar chromophores, the extension of conjugated bridges leads to red-shifting of charge-transfer bands and increases in $\Delta\mu_{12}$, and is hence a well-established strategy for enhancing β_0 (see section 1.5.4). Given the relatively large experimental errors, our previous HRS studies failed to provide compelling evidence that insertion of a *trans*-CH=CH bond into the 4,4′-bipyridinium unit serves to enhance β_0 in Ru^{II} ammines.[115b] However, comparison of the β_0[Stark] values for the pairs **138/157**,

143/158, 134/168 and **140/169** does reveal increases of *ca.* 35–50% in each case, generally accompanied by small increases in μ_{12} and larger increases in $\Delta\mu_{12}$, as noted earlier.

Although the trends are the same, the *differences* in μ_{12} and β_0 between the pairs of $Mebpe^+/Phbpe^+$ complexes (in **157/158, 168/169** and **164/165**) are consistently smaller than those observed within the MeQ^+/PhQ^+ pairs. However, the reverse is true of the $\Delta\mu_{12}$ values, *i.e.* these show larger increases on moving from *N*-Me to *N*-Ph in the bpe-based complexes than in their 4,4′-bpy-based counterparts. Both the HRS and electroabsorption studies clearly demonstrate that the enhancement of β_0 by pyridyl *N*-phenylation is most significant in the 4,4′-bpy-based complexes.

3.4 Conclusion

The electroabsorption spectra of the salts *trans*-$[Ru^{II}(NH_3)_4(L_D)(L_A)][PF_6]_3$ (L_D = electron-rich ligand; L_A = electron-deficient pyridinium ligand) in butyronitrile at 77 K were successfully modelled to afford transition dipole moments μ_{12} and dipole moment changes $\Delta\mu_{12}$ for their MLCT excitations. The μ_{12} values cover a fairly narrow range (*ca.* 4–7 D) and generally increase with the electron accepting strength of L_A, most notably on replacing an *N*-methyl with a *N*-phenyl substituent. The $\Delta\mu_{12}$ values are large (*ca.* 14–21 D) and generally increase as the size of L_A increases due to the addition of aryl rings and/or *trans*-ethylene units, suggesting that the L_A π^* orbital is partially delocalized over multiple rings. For a given L_A, the pentaammine complexes typically have the smallest μ_{12} and $\Delta\mu_{12}$ values.

A consideration of charge-transfer distances provides estimated diabatic dipole moment changes $\Delta\mu_{ab}$ which are in reasonable agreement with their experimentally observed counterparts, except for the complexes of the longest L_A ligands. This result suggests that the orbital(s) that receive the MLCT electron are delocalized only over the first two aryl rings.

The β_0 values calculated by using μ_{12} and $\Delta\mu_{12}$ are generally in good agreement with those derived from HRS measurements on acetonitrile solutions of the complexes studied at

298 K. HRS severely underestimates β_0 values where the MLCT maximum is close to the second harmonic wavelength (532 nm), and the electroabsorption-derived β_0 values are hence the first meaningful estimates available for salts **135** and **164**. This study confirms the unusually large magnitudes of β_0 in Ru^{II} penta/tetraammine complexes and also reinforces the conclusion that *N*-arylation is an effective means to enhance β_0. Both the HRS and electroabsorption data show that the latter effect is most significant in the 4,4′-bpy-based complexes. The observed increases in β_0 are generally associated with decreases in the MLCT energy and increases in both μ_{12} and $\Delta\mu_{12}$. Although the HRS results are less conclusive, the electroabsorption studies show that insertion of a *trans*-ethylene bridge into the 4,4′-bipyridinium unit of L_A enhances β_0 by *ca.* 35–50%.

Chapter 4. Quadratic NLO Properties of Purely Organic *N*-Aryl Pyridinium Chromophores

4.1 Introduction

Most organic molecules which exhibit second-order NLO effects are neutral and are therefore studied using the EFISHG technique (see section 1.4.2). Various charged organic compounds also display NLO effects and have been studied using the Kurtz powder test, and more recently using HRS (see section 1.4.3). An aspect of particular interest in organic salts is the use of counter-ion variation to tailor the crystal packing and potentially produce noncentrosymmetric bulk structures, suitable for bulk second-order NLO effects.

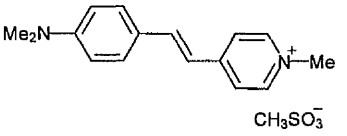

172. $SHG_{1907} = 220 \times$ urea

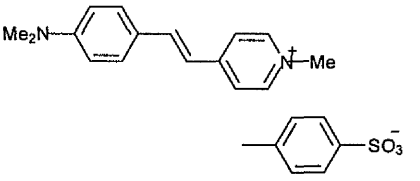

173. $SHG_{1907} = 1000 \times$ urea; methanol; $\lambda_{max} = 474$ nm; $\beta_{1064} = 2200 \times 10^{-30}$ esu; $\beta_0 = 363 \times 10^{-30}$ esu

Meredith *et al.* first demonstrated large SHG efficiencies in stilbazolium salts,[17a] for example **172**. The author suggested that coulombic interactions could override the dipolar interactions that provide a strong driving force for centrosymmetric crystallization in DπA covalent compounds. The argument is that the counter-ions can separate and screen the dipolar chromophores from one another, therefore reducing the undesirable dipole-dipole interactions.

After observing a sensitivity of $\chi^{(2)}$ to the nature of the counter-ion in ferrocenyl pyridinium salts,[52] Marder *et al.*[122] studied a series of 4-*N*-methylstilbazolium salts with various donor groups and counter-ions. Compound **173**, 4-dimethylamino-*N*-methylstilbazolium tosylate (DAST) has a very large powder SHG efficiency and crystallizes in the noncentrosymmetric monoclinic space group *Cc*. The tosylate anion is situated close to the pyridinium moiety and serves to line up adjacent rows of chromophores in a parallel manner, giving a 20° angle between the molecular long axis and the polar *a* axis of the crystal. This angle is not the optimum for SHG even though the

observed efficiency is very large. In the space group *Cc* the optimal angle between the charge-transfer axis of the chromophores and the crystal *b* axis for phase matching of SHG is 35°.[40] The corresponding angle in DAST is *ca.* 68°.

Work has also been carried out on analogous 2-*N*-methylstilbazolium salts.[123] The largest SHG efficiency of such compounds is for 3′-methoxy-2-*N*-methylstilbazolium triflate, **174**. In contrast to neutral dipolar systems where geometric asymmetry appears to increase the probability of noncentrosymmetric crystallization, Marder *et al.* found that the probability of obtaining noncentrosymmetric space groups with stilbazolium salts is higher when the chromophore is approximately linear.

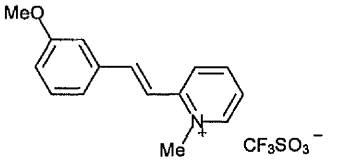

174. $SHG_{1064} = 24 \times$ urea;

Matsuda *et al.*[124] measured the β values of DAST and of a longer conjugated homologue (**176**) using HRS at 1064 nm. DAST and **176** were found to have β_0 values of *ca.* 363 and 625×10^{-30} esu, respectively, which are strongly enhanced due to two-photon fluorescence. The β_0 value of sodium *p*-toluenesulfonate, **175,** was also measured and found to be *ca.* 17×10^{-30} esu. Thus Matsuda *et al.* concluded that the stilbazolium cation is primarily responsible for the large NLO response of DAST.

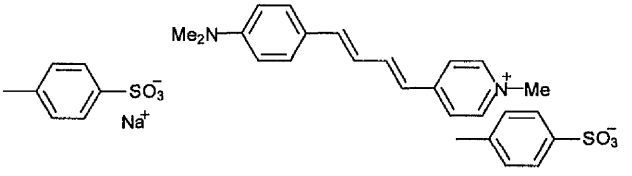

175. methanol; $\lambda_{max} = 222$ nm;
$\beta_{1064} = 22 \times 10^{-30}$ esu;
$\beta_0 = 17 \times 10^{-30}$ esu

176. methanol; $\lambda_{max} = 492$ nm;
$\beta_{1064} = 5500 \times 10^{-30}$ esu;
$\beta_0 = 625 \times 10^{-30}$ esu

Because of their attractive second-order NLO properties, *N*-alkylstilbazolium salts have received a great deal of attention. Research has been carried out to establish molecular structure-property relationships and to incorporate the chromophores into bulk structures,

such as intercalates,[125] polymers[126] and LB films.[127] Chiral stilbazolium cations have also been incorporated into materials combining NLO properties with semiconducting behaviour.[128] Furthermore, crystal growth methods for DAST have been refined to allow the growth of large, fault-free crystals.[129]

4.1.1 DAST Crystal Growth[129]

Sohma *et al.*[129d] have developed a method for growing large, high quality crystals quickly and reproducibly using seed fixing. The optical nonlinearity of DAST is based on a large molecular β value which leads to large electro-optical (E-O) and bulk second-order NLO coefficients. DAST also has a low dielectric constant and thus is applicable to high speed E-O devices, *e.g.* involving E-O modulation and detection in the high frequency region. Sohma *et al.* were able to grow crystals of DAST large enough for device applications. It was found that the crystals grew differently depending on the solution saturation (Figure 18); the crystals grew along the crystallographic *a* axis under low saturation, but along the *c* axis under high saturation. Using this method, large crack-free crystals of dimensions *ca.* 15 × 15 × 1 mm with a typical growth term of 6–7 days can be grown reproducibly. The second-order NLO coefficient was evaluated using optical rectification experiments and a value *ca.* 72 times larger than that of $LiNbO_3$ was obtained.

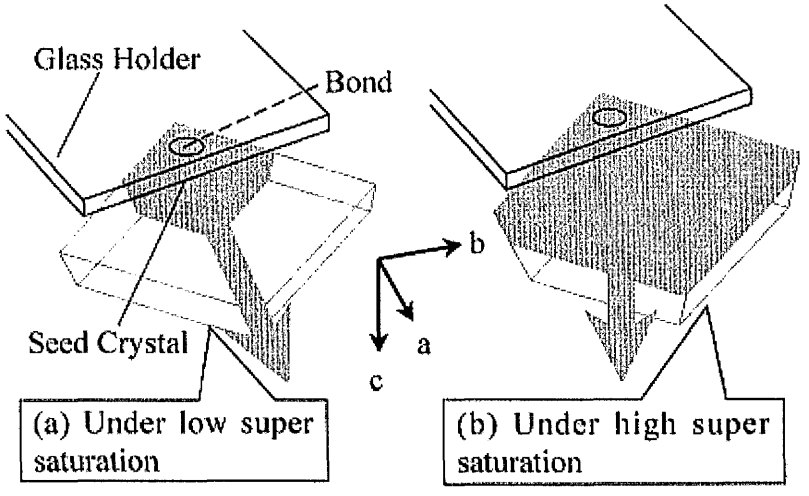

Figure 18. A diagram illustrating DAST crystal growth directions.[129d]

Blanchard-Desce *et al.*[130] performed a study on the influence of conjugation length on the second-order NLO properties of amphiphilic stilbazolium-like salts. As the compounds are ionic they would normally be studied by HRS, but in this case the quadratic NLO properties were measured using EFISHG. This was made possible by using a solvent of low polarity ($CHCl_3$) which promotes the formation of close ion pairs.

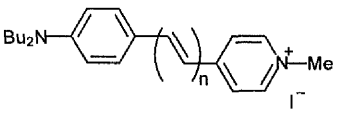

177–181.

	n	λ_{max}[$CHCl_3$] /nm	$\mu\beta_{1907}$ $\times 10^{-48}$ esu	$\mu\beta_0$ $\times 10^{-48}$ esu
177	1	517	840	550
178	2	558	2230	1340
179	3	581	2700	1540
180	4	589	3380	1890
181	5	598	3690	2020

Increasing the polyene chain length (*i.e.* from **177** to **181**) results in a bathochromic shift of the charge-transfer band and thus increases in $\mu\beta_0$, as large as 2020 $\times 10^{-48}$ esu for **181**, are observed. This is in agreement with previous studies on the effect of conjugation length on β_0, although there are diminishing returns as the number of double bonds increases. The quinolinium compound, **182**, has a $\mu\beta_0$ approximately 50% larger than that of its stilbazolium analogue, although the charge-transfer absorption is significantly red-shifted, reducing the transparency window. Hence, elongation of the polyene chain is a preferable method for increasing β with respect to the transparency-efficiency trade off (see section 1.5.1).

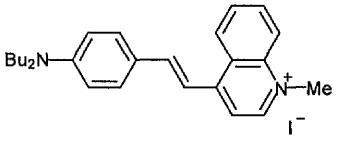

182. $CHCl_3$; λ_{max} = 603 nm;
$\mu\beta_{1907}$= 1380 × 10^{-48} esu;
$\mu\beta_0$ = 745 × 10^{-48} esu

Clays *et al.*[131] studied a similar series of compounds using HRS. Because of the fluorescent nature of the compounds it was necessary to use high frequency, amplitude modulated femtosecond HRS. The observed values initially increase with additional ethylene bonds, but then decrease as the conjugation length exceeds three double bonds.

The authors attribute this trend to laser-induced trans-cis isomerisation during the HRS measurements.

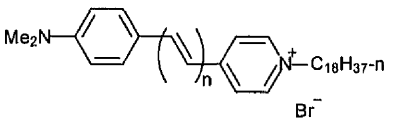

183–187.

	n	λ_{max}[$CHCl_3$] /nm	β_{1300} × 10^{-30} esu	β_0 × 10^{-30} esu
183	1	496	100	36
184	2	524	1640	481
185	3	546	2045	496
186	4	556	780	171
187	5	570	1200	224

4.1.2 Intercalation of Stilbazolium Cations

Clément *et al.*[125] have prepared intercalated materials comprising of a stilbazolium dye and inorganic MPS_3 (M = Mn^{2+} and Cd^{2+}) phases. The intercalation process induces a spontaneous poling of the chromophores, resulting in materials with very large SHG efficiencies. The chromophores undergo strong intramolecular interactions, forming J-type aggregates along the inorganic channels in the material (Figure 19). It was found that only materials with such aggregates show SHG activity.

This type of intercalation does not significantly dilute the concentration of the chromophores. For example, in DAST there is one chromophore per 525 $Å^3$, compared to one in 740 $Å^3$ in the intercalate. These intercalated materials are also very stable; Clément *et al.* recorded no significant decay in the SHG signal over the course of several months. However, most of the materials studied had SHG efficiencies lower than that of urea and thus it would appear that intercalation in MPS_3 layered phases is not a general method for obtaining SHG active materials.

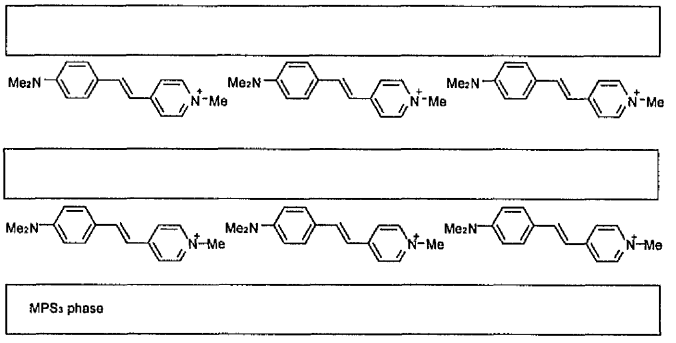

M = Mn^{2+}; SHG_{1340} = 300 × urea;
M = Cd^{2+}; SHG_{1340} = 750 × urea;

Figure 19. Schematic diagram of the J-type aggregates within the channels of an MPS_3 intercalated material.

4.1.3 Amylose-Dye Inclusion Complexes

Kim *et al.*[132] have developed a strategy for the spontaneous alignment of chromophores by employing a supramolecular architecture. This approach increases the thermal and mechanical stability by uniaxially including a chromophore in the helical cavity of amylose to form a rigid-rod, supramolecular complex (Figure 20).

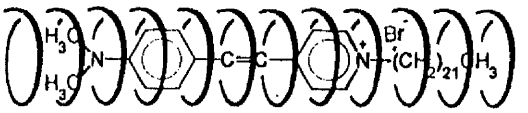

Figure 20. Amylose-stilbazolium dye inclusion complex.[132,133]

In such an inclusion complex the chromophores are completely screened from each other and mechanically and thermally shielded by the host amylose molecule. Amylose is a rod-like polymer consisting of α-1,4-glycosidic units. The helical cavity is large enough to include hydrophobic organic molecules, forming a six-fold helix. Kim *et al.* included the stilbazolium dye 4-[4-(dimethylaminostyryl]-1-docosyl-pyridinium bromide ($DASPC_{22}$, **188**). **188** is particularly suitable because of its strong hydrophobicity, large β and because only one molecule can fit into the host cavity to form a 1:1 complex. The solid inclusion complex exhibited a significant increase in thermal stability (*ca.* 30°) of the chromophores and has excellent long-term stability (no decay in $\chi^{(2)}$ at room temperature after 5600 h or at 90° C for 100 h). Unfortunately, the SHG at 1064 nm was found to be lower than that of other material systems comprising similar chromophores,[134b] with $\chi_{33} = 9 \times 10^{-9}$ esu. The authors attribute this to low chromophore number density due to the large volume of the supramolecular complexes compared to the free chromophore.

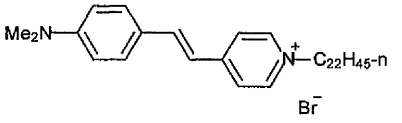

188.

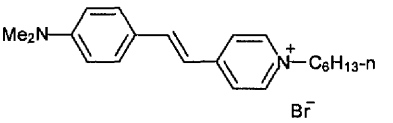

189.

Clays *et al.*[133] measured the β values of a shorter homologue dye ($DASPC_6$, **189**) and of the corresponding amylose inclusion complex using HRS. The amylose inclusion complex is fluorescent, so high-frequency demodulation of the time-delayed multi-photon fluorescence was used to obtain a fluorescence-free β_0. The β_0 value for this inclusion complex (200×10^{-30} esu) is *ca.* twice that of the free dye.

4.1.4 SHG from LB Films of Stilbazolium Dyes

4-*N*-alkylstilbazolium chromophores possessing long hydrophobic alkyl chains are ideal candidates for the production of LB films (see section 1.6.2). Ashwell *et al.*[127] have prepared LB films of the amphiphilic $DASPC_{18}$ cation, **190**, with various counter-ions. The SHG response increases significantly with octadecylsulfate as the counter-ion, compared to the bromide or iodide salts. This increase was attributed to suppression of molecular aggregation by dilution of the chromophore layers.[127]

Hodge *et al.*[126a] prepared alternating LB multilayers from a non-polymeric stilbazolium salt, **192**, and a poly(4-vinylpyridine) quarternised with docosyl bromide, **191**. The intensity of the SHG signal was found to increase as the square of the number of bi-layers, up to *ca.* 60 bi-layers. However, the thermal stability of the films was found to be inferior to that of similar all-polymeric LB films.[126b]

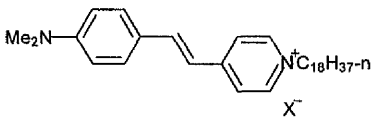

190.

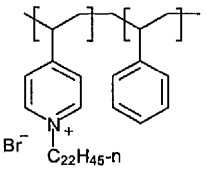

191.

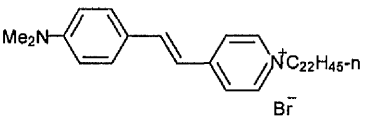

192.

4.1.5 Self-Assembled Superlattices

Marks *et al.*[134] have studied self-assembled superlattice materials containing stilbazolium chromophores. The chromophoric multilayers are assembled on clean glass or

single-crystal substrates by following an iterative reaction process. These materials (Figure 21) are photochemically and thermally stable, with very high structural regularities and large optical nonlinearities.

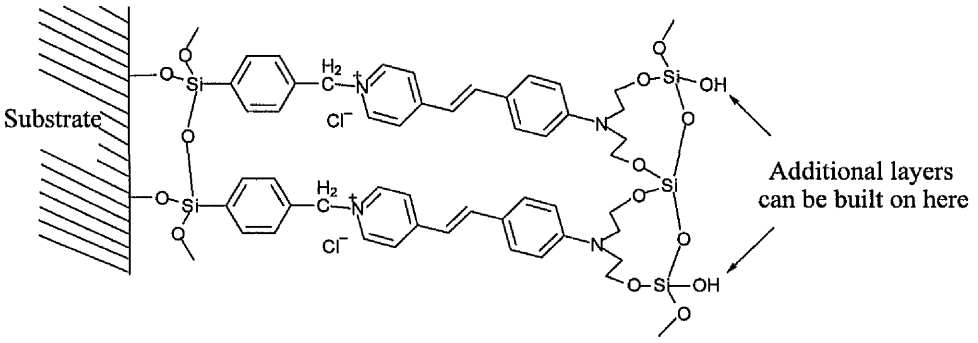

Figure 21. The first layer of a self-assembled superlattice containing stilbazolium chromophores.[134a]

4.1.6 Multi-property Materials

Lacroix *et al.*[128a] have studied multi-property materials which combine NLO effects with semiconducting behaviour. They prepared a number of chiral stilbazolium salts of anions including reduced 7,7′,8,8′-tetracyanoquinodimethane (TCNQ, **194**). The salt **193**, crystallizes in the noncentrosymmetric space group $P2_1$ and exhibits a sizeable SHG response which is phase matchable. Of the salts of TCNQ, only **195** exhibits an observable NLO response and semiconducting behaviour. Similar work has been done using $[Ni(dmit)_2]^-$ (dmit = 2-thioxo-1,3-dithiole-4,5-dithiolato) anions instead of TCNQ. The resulting materials exhibit semiconductivity, but no bulk second-order NLO properties due to crystal centrosymmetry.[128b]

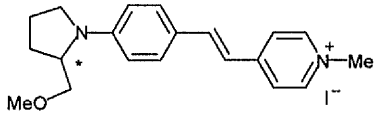

193. Ethanol; λ_{max} = 484 nm; SHG_{1907} = 40–80 × urea

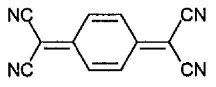

194. TCNQ

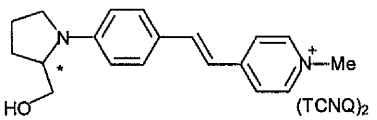

195. SHG_{1907} = 45 × urea[135]

Although stilbazolium salts show great promise for quadratic NLO applications, only *N*-alkyl derivatives have been studied to date. It has been demonstrated that dipolar ruthenium(II) ammine complexes of *N*-aryl-4,4′-bipyridinium or *N*-aryl-4-[*trans*-2-(4-pyridyl)ethenyl]pyridinium ligands possess β_0 values which are 2–3 times larger than those of their *N*-methyl analogues.[90,91,115b] Hence, a similar strategy is expected to lead to enhanced quadratic NLO properties in organic pyridinium dyes such as stilbazolium salts.

4.2 *Experimental*

4.2.1 Materials and procedures

The compounds *N*-methyl-4-picolinium iodide ([mepic$^+$]I),[136] *N*-(2,4-dinitrophenyl)-4-picolinium hexafluorophosphate ([dnppic$^+$]PF_6),[115b] 4-(dimethylaminophenyl)pyridine•0.15H_2O,[137] 4-(4-dimethylaminophenyl)-*N*-methyl-pyridinium iodide ([**196**]I),[138] 4-(4-dimethylaminophenyl)-*N*-phenylpyridinium chloride ([**197**]Cl),[138] 4-(4-dimethylamino-phenyl)-*N*-(2,4-dinitrophenyl)-pyridinium chloride•0.8H_2O ([**198**]Cl•0.8H_2O),[138] *trans*-4′-dimethylamino-*N*-methyl-4-stilbazolium iodide ([**200**]I),[139] *trans*-4′-methoxy-4-stilbazole,[140] *trans*-4′-methoxy-*N*-methyl-4-stilbazolium iodide ([**208**]I),[139] 4-[(4-dimethylaminophenyl)iminomethyl]-*N*-methyl-pyridinium iodide ([**212**]I)[141] and 4-picolyltriphenylphosphonium chloride[142] were prepared according to published procedures. [mepic$^+$]I, [**196**]I, [**197**]Cl, [**198**]Cl•0.8H_2O, [**200**]I, [**208**]I and [**212**]I were metathesised to their corresponding hexafluorophosphate salts by precipitation from water/aqueous NH_4PF_6. All other reagents were obtained commercially and used as supplied. Products were dried overnight at room temperature in a vacuum desiccator ($CaSO_4$) prior to characterization.

4.2.2 Physical measurements

These details were as for Chapter 2, except that the cyclic voltammetric measurements were carried out by using an EG&G PAR model 173

potentiostat/galvanostat with a model 175 universal programmer. A single-compartment cell was used with a Ag/ 3M NaCl/saturated AgCl reference electrode separated by a salt bridge from the platinum-bead working electrode and platinum-wire auxiliary electrode. Acetonitrile (HPLC grade) was used as received and tetra-*n*-butyl ammonium hexafluorophosphate, twice recrystallized from ethanol and dried *in vacuo*, as supporting electrolyte. Solutions containing *ca.* 10^{-3} M analyte (0.1 M electrolyte) were deaerated by purging with N_2. All $E_{1/2}$ values were calculated from $(E_{pa} + E_{pc})/2$ at a scan rate of 200 mV s^{-1}. Electrospray mass spectra were recorded on a Micromass Platform II spectrometer.

4.2.3 Syntheses

***N*-Methyl-4-picolinium hexafluorophosphate, [mepic$^+$]PF_6.** $\delta_H(CD_3COCD_3)$ 8.87 (d, 2 H, J 6.5 Hz, C_5H_4N), 8.04 (d, 2 H, J 5.9 Hz, C_5H_4N), 4.51 (s, 3 H, N^+–Me), 2.72 (s, 3 H, Me) (Found: C, 33.37; H, 3.95; N 5.32. Calc. for $C_7H_{10}F_6NP$: C, 33.22; H, 3.98; N 5.53%).

***N*-Phenyl-4-picolinium hexafluorophosphate, [ppic$^+$]PF_6.** [ppic$^+$]Cl•1.25H_2O (See chapter 2; 500 mg, 2.20 mmol) was metathesised to [ppic$^+$]PF_6 by precipitation from water/aqueous NH_4PF_6: yield 547 mg (79%). $\delta_H(CD_3COCD_3)$ 9.21 (d, 2 H, J 6.8 Hz, C_5H_4N), 8.27 (d, 2 H, J 6.3 Hz, C_5H_4N), 7.96–7.91 (m, 2 H, Ph), 7.80–7.77 (m, 3 H, Ph), 2.86 (s, 3 H, Me) (Found: C, 45.88; H, 3.88; N, 4.45. Calc. for $C_{12}H_{12}F_6NP$: C, 45.73; H, 3.84; N, 4.44%).

***N*-(2-Pyrimidyl)-4-picolinium hexafluorophosphate, [pympic$^+$]PF_6.** A mixture of 2-chloropyrimidine (2.86 g, 25.0 mmol) and 4-picoline (1.2 mL, 12.3 mmol) was heated to produce a dark green solution. Ethanol (5 mL) was added and the resulting solution was heated under reflux for 8 h. After cooling to room temperature, the addition of diethyl ether afforded a grey/green precipitate which was filtered off, washed with diethyl ether and dried [1.16 g. $\delta_H(D_2O)$ 9.76 (d, 2 H, J 6.6 Hz, C_5H_4N), 9.04 (d, 2 H, J 4.9 Hz, $H^{4,6}$), 8.07 (d, 2 H, J 6.6 Hz, C_5H_4N), 7.79 (t, 1 H, J 4.9 Hz, H^5), 2.75 (s, 3 H, Me)]. This material was dissolved in a minimum volume of water and aqueous NH_4PF_6 was added. A

black precipitate was filtered off and discarded. Further addition of aqueous NH_4PF_6 yielded a yellow precipitate which was filtered off, washed with water and dried. Purification was effected by precipitation from acetone/diethyl ether: yield 1.64 g (41%). $\delta_H(CD_3COCD_3)$ 10.08 (d, 2 H, J 7.0 Hz, C_5H_4N), 9.23 (d, 2 H, J 4.8 Hz, $H^{4,6}$), 8.35 (d, 2 H, J 6.9 Hz, C_5H_4N), 7.98 (t, 1 H, J 4.9 Hz, H^5), 2.92 (s, 3 H, Me) (Found: C, 38.33; H, 3.24; N, 13.07. Calc. for $C_{10}H_{10}F_6N_3P$: C, 37.87; H, 3.18; N, 13.25%).

4-(4-Dimethylaminophenyl)-*N*-methylpyridinium hexafluorophosphate, [196]PF_6. $\delta_H(CD_3COCD_3)$ 8.76 (d, 2 H, J 7.0 Hz, C_5H_4N), 8.33 (d, 2 H, J 7.3 Hz, C_5H_4N), 8.01 (d, 2 H, J 9.2 Hz, C_6H_4), 6.92 (d, 2 H, J 9.2 Hz, C_6H_4), 4.43 (s, 3 H, N^+–Me), 3.14 (s, 6 H, NMe_2) (Found: C, 46.88; H, 4.57; N, 7.88. Calc. for $C_{14}H_{17}F_6N_2P$: C, 46.94; H, 4.78; N, 7.82%). m/z: 213 ($[M - PF_6^-]^+$).

4-(4-Dimethylaminophenyl)-*N*-phenylpyridinium hexafluorophosphate, [197]PF_6. A mixture of [**198**]Cl•0.8H_2O (200 mg, 0.482 mmol) and aniline (0.44 mL, 4.80 mmol) in DMF (5 mL) was heated at 60 °C for 24 h. The resulting solution was added to diethyl ether (300 mL) and a yellow material was filtered off. This crude chloride salt was metathesised to [**197**]PF_6 by precipitation from water/aqueous NH_4PF_6 and purified by precipitation from acetone/diethyl ether: yield 88 mg (44%). $\delta_H(CD_3COCD_3)$ 9.01 (d, 2 H, J 7.3 Hz, C_5H_4N), 8.49 (d, 2 H, J 7.3 Hz, C_5H_4N), 8.15 (d, 2 H, J 9.2 Hz, C_6H_4), 7.95–7.90 (m, 2 H, Ph), 7.76 (m, 3 H, Ph), 6.98 (d, 2 H, J 9.2 Hz, C_6H_4), 3.19 (s, 6 H, NMe_2) (Found: C, 54.57; H, 4.74; N, 6.53. Calc. for $C_{19}H_{19}F_6N_2P$: C, 54.29; H, 4.56; N, 6.66%). m/z: 275 ($[M - PF_6^-]^+$).

4-(4-Dimethylaminophenyl)-*N*-(2,4-dinitrophenyl)pyridinium hexafluorophosphate, [198]PF_6. $\delta_H(CD_3COCD_3)$ 9.23 (d, 1 H, J 2.6 Hz, H^3), 9.02–8.95 (m, 3 H, $C_5H_4N + H^5$), 8.55 (d, 2 H, J 7.4 Hz, C_5H_4N), 8.55 (d, 1 H, J 7.4 Hz, H^6), 8.21 (d, 2 H, J 9.2 Hz, C_6H_4), 7.00 (d, 2 H, J 9.2 Hz, C_6H_4), 3.23 (s, 6 H, NMe_2) (Found: C, 45.03; H, 3.27; N, 10.68. Calc. for $C_{19}H_{17}F_6N_4O_4P$: C, 44.72; H, 3.36; N, 10.98%). m/z: 365 ($[M - PF_6^-]^+$). **[198]OTs.** [**198**]Cl•0.8H_2O was dissolved in a minimum amount of water and sodium p-

toluenesulphonate was added producing a red precipitate which was filtered, washed with water and dried.

4-(4-Dimethylaminophenyl)-*N*-(2-pyrimidyl)pyridinium hexafluorophosphate, [199]PF_6. A mixture of 4-(dimethylaminophenyl)pyridine•0.15H_2O (201 mg, 1.01 mmol) and 2-chloropyrimidine (573 mg, 5.00 mmol) was heated quickly to 80 °C, forming a red melt. After 15 min, DMF (5 mL) was added and the reaction was maintained at 80 °C for a further 30 min. $AgCF_3CO_2$ (220 mg, 1.00 mmol) was added and the temperature was maintained at 80 °C for 20 h. The resulting solution was added to diethyl ether (300 mL) to produce an orange precipitate which was filtered off, washed with diethyl ether and dried. This crude CF_3CO_2- salt was metathesised to **[199]**PF_6 by precipitation from water/aqueous NH_4PF_6. Purification was effected by filtration through celite 545 in acetone, followed by sequential precipitations from water/aqueous NH_4PF_6, acetone/[N^nBu_4]Cl, water/aqueous NH_4PF_6 and acetone/diethyl ether: yield 201 mg (48%). $\delta_H(CD_3COCD_3)$ 9.78 (d, 2 H, J 7.7 Hz, C_5H_4N), 9.18 (d, 2 H, J 4.9 Hz, $H^{4,6}$), 8.51 (d, 2 H, J 7.7 Hz, C_5H_4N), 8.22 (d, 2 H, J 9.3 Hz, C_6H_4), 7.90 (t, 1 H, J 4.9 Hz, H^5), 7.02 (d, 2 H, J 9.3 Hz, C_6H_4), 3.24 (s, 6 H, NMe_2) (Found: C, 48.35; H, 4.06; N, 13.27. Calc. for $C_{17}H_{17}F_6N_4P$: C, 48.21; H, 4.25; N, 13.18%). m/z: 277 ([M – PF_6^-]$^+$).

Trans-4′-(dimethylamino)-*N*-methyl-4-stilbazolium hexafluorophosphate, [200]PF_6. $\delta_H(CD_3CN)$ 8.29 (d, 2 H, J 6.9 Hz, C_5H_4N), 7.84 (d, 2 H, J 6.8 Hz, C_5H_4N), 7.86 (d, 1 H, J 15.9 Hz, CH), 7.59 (d, 2 H, J 8.9 Hz, C_6H_4), 7.06 (d, 1 H, J 15.8 Hz, CH), 6.80 (d, 2 H, J 8.9 Hz, C_6H_4), 4.12 (s, 3 H, N^+–Me), 3.08 (s, 6 H, NMe_2) (Found: C, 50.10; H, 4.92; N, 7.29. Calc. for $C_{16}H_{19}F_6N_2P$: C, 50.01; H, 4.98; N, 7.29%). m/z: 239 ([M – PF_6^-]$^+$).

Trans-4′-(dimethylamino)-*N*-phenyl-4-stilbazolium hexafluorophosphate, [201]PF_6. A solution of [ppic$^+$]Cl•1.25H_2O (250 mg, 1.10 mmol), 4-(dimethylamino)benzaldehyde (363 mg, 2.43 mmol) and piperidine (4 drops) in methanol (20 mL) was heated under reflux for 4 h. The addition of diethyl ether to the deep red solution afforded a dark precipitate which was filtered off, washed with diethyl ether and dried (390 mg). This crude chloride salt was metathesised to **[201]**PF_6 by precipitation from water/aqueous NH_4PF_6: yield 468

mg (96%). $\delta_H(CD_3CN)$ 8.57 (d, 2 H, J 7.0 Hz, C_5H_4N), 7.98 (d, 2 H, J 7.0 Hz, C_5H_4N), 7.91 (d, 1 H, J 15.9 Hz, CH), 7.70 (s, 5 H, Ph), 7.65 (d, 2 H, J 9.1 Hz, C_6H_4), 7.15 (d, 1 H, J 15.8 Hz, CH), 6.82 (d, 2 H, J 8.9 Hz, C_6H_4), 3.08 (s, 6 H, NMe_2) (Found: C, 56.35; H, 5.04; N, 6.11. Calc. for $C_{21}H_{21}F_6N_2P$: C, 56.51; H, 4.74; N, 6.28%). m/z: 301 ([M – PF_6^-]$^+$). **[201]OTs.** [**201**]Cl was dissolved in a minimum amount of water and sodium p-toluenesulphonate was added producing a dark red precipitate which was filtered, washed with water and dried.

Trans-4′-(dimethylamino)-*N*-(2,4-dinitrophenyl)-4-stilbazolium hexafluorophosphate, [202]PF_6. This was prepared in identical fashion to [**201**]PF_6 by using [dnppic$^+$]PF_6 (196 mg, 0.484 mmol) and 4-(dimethylamino)benzaldehyde (149 mg, 0.999 mmol). A dark green solid was obtained: yield 127 mg (50%). $\delta_H(CD_3CN)$ 9.11 (d, 1 H, J 2.5 Hz, H^3), 8.79 (dd, 1 H, J 8.7, 2.5 Hz, H^5), 8.39 (d, 2 H, J 7.1 Hz, C_5H_4N), 8.08 (d, 1 H, J 8.7 Hz, H^6), 7.99 (d, 1 H, J 15.8 Hz, CH), 7.98 (d, 2 H, J 7.2 Hz, C_5H_4N), 7.68 (d, 2 H, J 9.1 Hz, C_6H_4), 7.17 (d, 1 H, J 15.8 Hz, CH), 6.83 (d, 2 H, J 9.0 Hz, C_6H_4), 3.11 (s, 6 H, NMe_2) (Found: C, 47.02; H, 3.71; N, 10.40. Calc. for $C_{21}H_{19}F_6N_4O_4P$: C, 47.03; H, 3.57; N, 10.45%). m/z: 391 ([M – PF_6^-]$^+$).

Trans-4′-(dimethylamino)-*N*-(2-pyrimidyl)-4-stilbazolium hexafluorophosphate, [203]PF_6. This was prepared in identical fashion to [**201**]PF_6 by using [pympic$^+$]PF_6 (161 mg, 0.508 mmol) and 4-(dimethylamino)benzaldehyde (149 mg, 0.999 mmol). A purple solid was obtained: yield 72 mg (32%). $\delta_H(CD_3CN)$ 9.53 (d, 2 H, J 7.4 Hz, C_5H_4N), 9.01 (d, 2 H, J 4.8 Hz, $H^{4,6}$), 8.00 (d, 1 H, J 16.0 Hz, CH), 7.97 (d, 2 H, J 7.5 Hz, C_5H_4N), 7.71 (t, 1 H, J 4.8 Hz, H^5), 7.68 (d, 2 H, J 9.0 Hz, C_6H_4), 7.19 (d, 1 H, J 15.8 Hz, CH), 6.82 (d, 2 H, J 9.1 Hz, C_6H_4), 3.10 (s, 6 H, NMe_2) (Found: C, 51.15; H, 4.29; N, 12.78. Calc. for $C_{19}H_{19}F_6N_4P$: C, 50.90; H, 4.27; N, 12.50%). m/z: 303 ([M – PF_6^-]$^+$). **[203]BPh_4.** [**203**]Cl was dissolved in a minimum amount of water and sodium tetraphenylborate was added producing a dark blue precipitate which was filtered, washed with water and dried.

Trans-*N*-methyl-4-(4-dimethylaminophenyl-4-buta-1,3-dienyl)pyridinium hexafluorophosphate, [204]PF_6. This was prepared in similar fashion to [**201**]PF_6 by using [mepic$^+$]PF_6 (380 mg, 1.50 mmol), 4-(dimethylamino)cinnamaldehyde (263 mg, 1.50 mmol) in place of 4-(dimethylamino)benzaldehyde and the reaction was heated in the dark. The crude product was purified by sequential precipitations from acetone/[N^nBu_4]Cl, water/aqueous NH_4PF_6 and acetone/diethyl ether to afford an orange/red crystalline material: yield 301 mg (49%). $\delta_H(CD_3CN)$ 8.29 (d, 2 H, J 6.7 Hz, C_5H_4N), 7.88 (d, 2 H, J 6.9 Hz, C_5H_4N), 7.63 (dd, 1 H, J 15.7, 8.4 Hz, CH), 7.47 (d, 2 H, J 8.9 Hz, C_6H_4), 7.08–6.89 (m, 2 H, 2CH), 6.75 (d, 2 H, J 8.9 Hz, C_6H_4), 6.66 (d, 1 H, J 15.4 Hz, CH), 4.12 (s, 3 H, N^+–Me), 3.02 (s, 6 H, NMe_2) (Found: C, 52.69; H, 5.19; N, 6.76. Calc. for $C_{18}H_{21}F_6N_2P$: C, 52.69; H, 5.16; N, 6.83%). m/z: 265 ([M – PF_6^-]$^+$).

Trans-4-(4-dimethylaminophenyl-4-buta-1,3-dienyl)pyridine. Sodium ethoxide (4.04 g, 57.1 mmol) in ethanol (100 mL) was added drop-wise to a suspension of 4-(dimethylamino)cinnamaldehyde (2.00 g, 11.4 mmol) and 4-picolyltriphenyl-phosphonium chloride (4.45 g, 11.4 mmol) in ethanol (150 mL). A fine golden precipitate was produced immediately, and the reaction was stirred at room temperature for 23 h before heating under reflux for 1 h. The reaction mixture was reduced in volume and a golden precipitate was filtered off. This material was dissolved in $CHCl_3$, filtered, dried ($MgSO_4$), filtered, and the filtrate reduced to dryness to produce the pure product (crop 1). The initial filtrate from crop 1 was reduced to dryness, washed with acetone and dissolved in 4 M HCl. This solution was extracted with $CHCl_3$ (3 × 100 mL) and the aqueous layer was then basified with 50% aqueous NaOH. The resulting brown precipitate was filtered off and purified as for crop 1 to afford further product (crop 2): total yield 982 mg (34%). $\delta_H(CD_2Cl_2)$ 8.50 (d, 2 H, J 6.1 Hz, C_5H_4N), 7.38 (d, 2 H, J 8.7 Hz, C_6H_4), 7.30 (d, 2 H, J 6.1 Hz, C_5H_4N), 7.19 (dd, 1 H, J 15.4, 9.8 Hz, CH), 6.90–6.76 (m, 2 H, 2CH), 6.71 (d, 2 H, J 9.0 Hz, C_6H_4), 6.51 (d, 1 H, J 15.3 Hz, CH), 3.01 (s, 6 H, NMe_2) (Found: C, 81.49; H, 7.57; N, 11.29. Calcd for $C_{17}H_{18}N_2$: C, 81.56; H, 7.25; N, 11.19%).

Trans-*N*-phenyl-4-(4-dimethylaminophenyl-4-buta-1,3-dienyl)pyridinium hexafluorophosphate, [205]PF_6. A solution of trans-4-(4-dimethylaminophenyl-4-buta-1,3-dienyl)pyridine (100 mg, 0.399 mmol) and 2,4-dinitrochlorobenzene (808 mg, 3.99 mmol) in DMF (5 mL) was heated at 80 °C for 5 h in the dark. The resulting dark purple solution was added to diethyl ether (400 mL) and the black precipitate was collected by filtration. This solid (crude [**206**]Cl) was redissolved in DMF (5 mL), aniline (0.5 mL, 5.48 mmol) was added and the reaction was heated at 60 °C for 21 h in the dark. The resulting red/purple solution was added to diethyl ether (300 mL) and a green precipitate was filtered off. The crude chloride salt was dissolved in a minimum volume of water and the solution was filtered. Addition of aqueous NH_4PF_6 to the filtrate afforded a green precipitate which was filtered off, washed with water and dried. Purification was achieved by sequential precipitations from acetone/$[N^nBu_4]Cl$, water/aqueous NH_4PF_6 and acetone/diethyl ether to afford a dark green crystalline material: yield 67 mg (35%). $\delta_H(CD_3CN)$ 8.58 (d, 2 H, J 7.2 Hz, C_5H_4N) 7.95 (d, 2 H, J 7.1 Hz, C_5H_4N), 7.79 (dd, 1 H, J 15.2, 9.0 Hz, CH), 7.73–7.62 (m, 5 H, Ph), 7.50 (d, 2 H, J 9.0 Hz, C_6H_4), 7.17–7.07 (m, 2 H, 2CH), 6.79–6.71 (m, 3 H, C_6H_4 + CH), 3.03 (s, 6 H, NMe_2) (Found: C, 58.53; H, 4.56; N, 5.78. Calc. for $C_{23}H_{23}F_6N_2P$: C, 58.48; H, 4.91; N, 5.93%). m/z: 327 ($[M - PF_6^-]^+$).

Trans-*N*-(2,4-dinitrophenyl)-4-(4-dimethylaminophenyl-4-buta-1,3-dienyl)pyridinium hexafluorophosphate, [205]PF_6. [**206**]Cl was prepared as described above and metathesised to [**206**]PF_6 by precipitation from water/aqueous NH_4PF_6. Purification was effected by precipitation from acetone/diethyl ether to give a dark green crystalline material: yield 202 mg (90%). $\delta_H(CD_3CN)$ 9.12 (d, 1 H, J 2.5 Hz, H^3), 8.79 (dd, 1 H, J 8.7, 2.5 Hz, H^5), 8.42 (d, 2 H, J 7.2 Hz, C_5H_4N), 8.07 (d, 1 H, J 8.7 Hz, H^6), 7.97 (d, 2 H, J 7.1 Hz, C_5H_4N), 7.89 (dd, 1 H, J 15.1, 10.1 Hz, CH), 7.54 (d, 2 H, J 7.7 Hz, C_6H_4), 7.25–7.01 (m, 2 H, 2CH), 6.81–6.74 (m, 3 H, C_6H_4 + CH), 3.06 (s, 6 H, NMe_2) (Found: C, 49.19; H, 3.83; N, 9.68. Calcd for $C_{23}H_{21}F_6N_4O_4P$: C, 49.12; H, 3.76; N, 9.96%). m/z: 417 ($[M - PF_6^-]^+$).

Trans-*N*-(2-pyrimidyl)-4-(4-dimethylaminophenyl-4-buta-1,3-dienyl)pyridinium hexafluorophosphate, [207]PF_6. This was prepared and purified in similar fashion to [**199**]PF_6 by using trans-4-(4-dimethylaminophenyl-4-buta-1,3-dienyl)pyridine (100 mg, 0.399 mmol) and 2-chloropyrimidine (458 mg, 3.99 mmol). The DMF was added after 5 min, and no final precipitation from acetone/diethyl ether was necessary: yield 111 mg (59%). $\delta_H(CD_3CN)$ 9.51 (d, 2 H, J 7.4 Hz, C_5H_4N), 9.00 (d, 2 H, J 4.9 Hz, $H^{4,6}$), 7.92 (d, 2 H, J 7.4 Hz, C_5H_4N), 7.86 (dd, 1 H, J 15.1, 10.2 Hz, CH), 7.71 (t, 1 H, J 4.8 Hz, H^5), 7.49 (d, 2 H, J 9.0 Hz, C_6H_4), 7.21–6.96 (m, 2 H, 2CH), 6.76 (d, 1 H, J 15.1 Hz, CH), 6.73 (d, 2 H, J 9.0 Hz, C_6H_4), 3.03 (s, 6 H, NMe_2) (Found: C, 53.43; H, 4.14; N, 11.70. Calc. for $C_{21}H_{21}F_6N_4P$: C, 53.17; H, 4.46; N, 11.81%). m/z: 329 ($[M - PF_6^-]^+$).

Trans-4′-methoxy-*N*-methyl-4-stilbazolium hexafluorophosphate, [208]PF_6. $\delta_H(CD_3COCD_3)$ 8.86 (d, 2 H, J 7.0 Hz, C_5H_4N), 8.24 (d, 2 H, J 6.9 Hz, C_5H_4N), 8.01 (d, 1 H, J 16.3 Hz, CH), 7.75 (d, 2 H, J 6.9 Hz, C_6H_4), 7.40 (d, 1 H, J 16.4 Hz, CH), 7.05 (d, 2 H, J 6.9 Hz, C_6H_4), 4.48 (s, 3 H, N^+–Me), 3.88 (s, 3 H, OMe) (Found: C, 48.57; H, 4.50; N, 3.74. Calc. for $C_{15}H_{16}F_6NOP$: C 48.53, H 4.34, N 3.77%). m/z: 226 ($[M - PF_6^-]^+$).

Trans-4′-methoxy-*N*-phenyl-4-stilbazolium hexafluorophosphate, [209]PF_6. This was prepared in an identical fashion to [**201**]PF_6 by using $[ppic^+]Cl{\bullet}1.25H_2O$ (150 mg, 0.657 mmol) and 4-methoxybenzaldehyde (0.156 mL, 1.29 mmol) in place of 4-(dimethylamino)benzaldehyde. Purification was effected by sequential precipitations from acetone/diethyl ether: yield 184 mg (66%). $\delta_H(CD_3COCD_3)$ 9.14 (d, 2 H, J 6.9 Hz, C_5H_4N), 8.41 (d, 2 H, J 6.9 Hz, C_5H_4N), 8.18 (d, 1 H, J 16.4 Hz, CH), 7.97–7.92 (m, 2 H, Ph), 7.84–7.76 (m, 5 H, C_6H_4 + Ph), 7.54 (d, 1 H, J 16.2 Hz, CH), 7.09 (d, 2 H, J 8.8 Hz, C_6H_4), 3.90 (s, 3 H, Me) (Found: C, 55.25; H, 4.23; N, 3.18. Calc. for $C_{20}H_{18}F_6NOP$: C, 55.44; H, 4.19; N, 3.23%). m/z: 288 ($[M - PF_6^-]^+$).

Trans-4′-methoxy-*N*-(2,4-dinitrophenyl)-4-stilbazolium hexafluorophosphate, [210]PF_6. A mixture of trans-4′-methoxy-4-stilbazole (100 mg, 0.473 mmol) and 2,4-dinitrochlorobenzene (959 mg, 4.73 mmol) in DMF (5 mL) was heated at 80 °C for 5 h.

The resulting yellow solution was added to diethyl ether (300 mL) to produce an orange precipitate which was filtered off, washed with diethyl ether and dried. This crude chloride salt was metathesised to [**210**]PF_6 by precipitation from water/aqueous NH_4PF_6, and purified by precipitation from acetone/aqueous NH_4PF_6: yield 202 mg (81%). $\delta_H(CD_3COCD_3)$ 9.25 (d, 1 H, J 2.5 Hz, H^3), 9.17 (d, 2 H, J 7.1 Hz, C_5H_4N), 9.02 (dd, 1 H, J 8.7, 2.5 Hz, H^5), 8.57 (d, 1 H, J 8.7 Hz, H^6), 8.51 (d, 2 H, J 7.2 Hz, C_5H_4N), 8.28 (d, 1 H, J 16.1 Hz, CH), 7.85 (d, 2 H, J 8.8 Hz, C_6H_4), 7.60 (d, 1 H, J 16.3 Hz, CH), 7.11 (d, 2 H, J 8.7 Hz, C_6H_4), 3.91 (s, 3 H, Me) (Found: C, 45.75; H, 3.23; N, 7.77. Calc. for $C_{20}H_{16}F_6N_3O_5P$: C, 45.90; H, 3.08; N, 8.03%). m/z: 378 ($[M - PF_6^-]^+$).

Trans-4′-methoxy-*N*-(2-pyrimidyl)-4-stilbazolium hexafluorophosphate, [211]PF_6. This was prepared and purified in identical fashion to [**207**]PF_6 by using trans-4′-methoxy-4-stilbazole (100 mg, 0.473 mmol) in place of trans-4-(4-dimethylaminophenyl-4-buta-1,3-dienyl)pyridine and 2-chloropyrimidine (542 mg, 4.73 mmol). An orange solid was obtained: yield 97 mg (47%). $\delta_H(CD_3COCD_3)$ 9.98 (d, 2 H, J 7.3 Hz, C_5H_4N), 9.21 (d, 2 H, J 4.8 Hz, $H^{4,6}$), 8.47 (d, 2 H, J 7.3 Hz, C_5H_4N), 8.29 (d, 1 H, J 16.4 Hz, CH), 7.95 (t, 1 H, J 4.9 Hz, H^5), 7.86 (d, 2 H, J 8.9 Hz, C_6H_4), 7.61 (d, 1 H, J 16.3 Hz, CH), 7.10 (d, 2 H, J 8.9 Hz, C_6H_4), 3.91 (s, 3 H, Me) (Found: C, 49.33; H, 3.60; N, 9.48. Calc. for $C_{18}H_{16}F_6N_3OP$: C, 49.67; H, 3.70; N, 9.65%). m/z: 290 ($[M - PF_6^-]^+$).

Trans-4-[(4-dimethylaminophenyl)iminomethyl]-*N*-methylpyridinium hexafluorophosphate [212]PF_6. $\delta_H(CD_3CN)$ 9.04 (d, 2 H, J 6.8 Hz, C_5H_4N), 8.96 (s, 1 H, CH), 8.50 (d, 2 H, J 6.8 Hz, C_5H_4N), 7.55 (d, 2 H, J 9.2 Hz, C_6H_4), 6.84 (d, 2 H, J 9.2 Hz, C_6H_4), 4.59 (s, 3 H, Me), 3.08 (s, 6 H, NMe_2) (Found: C, 46.80; H, 4.53; N, 10.37. Calc. for $C_{15}H_{18}F_6N_3P{\bullet}0.15C_4H_{10}O$: C, 47.10; H, 4.83; N, 10.67%). m/z : 240 ($[M - PF_6^-]^+$).

Trans-4-[(4-dimethylaminophenyl)iminomethyl]-*N*-phenylpyridinium hexafluorophosphate [213]PF_6. This was prepared in a similar manner to [**201**]PF_6 using [ppic$^+$]Cl·1.25H_2O (220 mg, 0.878 mmol), N,N-dimethyl-4-nitrosoaniline (219 mg, 1.458

mmol) and piperidine (2 drops) in methanol (15 mL), heated under reflux for 1.5 h. The resulting purple solution was reduced to dryness on a rotary evaporator. The crude chloride salt was metathesized to the PF_6^- salt by precipitation from water/aqueous NH_4PF_6 and purified by column chromatography [silica gel, 70–230 mesh acetone/dichloromethane 1:10] followed by precipitation from acetone/diethyl ether: yield 59 mg (14%). $\delta_H(CD_3CN)$ 9.31 (d, 2 H, J 7.0 Hz, C_5H_4N), 9.07 (s, 1 H, CH), 8.66 (d, 2 H, J 7.0 Hz, C_5H_4N), 8.01–7.96 (m, 2 H, Ph), 7.84–7.79 (m, 3 H, Ph), 7.61 (d, 2 H, J 9.1 Hz, C_6H_4), 6.87 (d, 2 H, J 9.2 Hz, C_6H_4), 3.11 (s, 6 H, NMe_2) (Found: C, 53.99; H, 4.57; N, 9.21. Calc. for $C_{20}H_{20}F_6N_3P$: C, 53.69; H, 4.51; N, 9.39%). m/z : 302 ($[M - PF_6^-]^+$).

4.2.4 Hyper-Rayleigh scattering

Details of the HRS experiment incorporating high frequency fluorescence demodulation have been discussed elsewhere,[143] and the experimental procedures used for measurements at 1300 nm[143,144,131] and 800 nm[133] were as described previously. β values were determined by using β_{1300} for disperse red 1 (86×10^{-30} esu in acetonitrile: obtained from the value of 54×10^{-30} esu in $CHCl_3$ and taking into account local field correction factors at optical frequencies) and β_{800} for crystalviolet (500×10^{-30} esu in acetonitrile: obtained from the value of 340×10^{-30} esu in methanol and taking into account local field correction factors at optical frequencies) as external references. Measurements were performed using a femtosecond Ti:Sapphire laser (Spectra-Physics "Tsunami", 100 fs pulses, 500 mW, 80 MHz) with 800 or 1300 nm fundamental wavelengths. The use of dilute acetonitrile solutions (10^{-5}–10^{-6} M) ensured a linear dependence of $I_{2\omega}/I_{\omega}^2$ upon solute concentration, precluding the need for Lambert-Beer correction factors. One-dimensional hyperpolarizability is assumed, *i.e.* $\beta_{800/1300} = \beta_{zzz}$.

4.2.5 X-ray crystallography

Crystals were grown as follows: [**198**]OTs•MeOH and [**201**]OTs by slow diffusion of diethyl ether vapour into methanol solutions; [**202**]PF_6 by slow diffusion of diethyl ether vapour into a DMF solution; [**201**]PF_6 and [**213**]PF_6 by slow evaporation of an acetonitrile solution; [**201**]Cl•1.5H_2O by slow evaporation of a methanol-diethyl ether solution; [**203**]BPh_4 by slow evaporation of an acetone-water solution. The approximate dimensions (mm) of the crystals chosen for diffraction studies were: [**198**]OTs•MeOH (0.275 × 0.175 × 0.04); [**201**]PF_6 (0.55 × 0.175 × 0.04); [**201**]Cl•1.5H_2O (0.60 × 0.50 × 0.32); [**201**]OTs (0.35 × 0.30 × 0.02); [**202**]PF_6 (0.30 × 0.015 × 0.15); [**203**]BPh_4 (0.80 × 0.20 × 0.02); [**213**]PF_6 (0.10 × 0.10 × 0.10).

Data collection details are as follows: for [**201**]Cl•1.5H_2O data were collected on a Siemens SMART CCD area-detector diffractometer. An empirical absorption correction was applied by using multiple measurements of equivalent reflections, and the data were integrated by using SAINT.[145] For [**198**]OTs•MeOH, [**201**]PF_6, [**201**]OTs, [**202**]PF_6, [**203**]BPh_4 and [**213**]PF_6 data were collected on a Nonius Kappa CCD area-detector diffractometer controlled by the Collect software package.[146] The data were processed by Denzo[147] and corrected for absorption by using the empirical method employed in Sortav[103] from within the MaXus suite of programs.[148]

The structure of [**201**]Cl•1.5H_2O was solved by direct methods and refined by full-matrix least-squares on all F_0^2 data using Siemens SHELXTL 5.03.[145] The same approach was used for [**198**]OTs•MeOH, [**201**]PF_6, [**201**]OTs, [**202**]PF_6 , [**203**]BPh_4 and [**213**]PF_6, but using SHELXS-97[105] and SHELXL-97.[106] In all cases, all non-hydrogen atoms were refined anisotropically with hydrogen atoms included in idealised positions with thermal parameters riding on those of the parent atom. In [**201**]Cl•1.5H_2O and [**201**]OTs the asymmetric units contain one ordered cation and one disordered cation in which the ethylene bridge shows equal occupancy over two positions.

Representations of the cations in [**198**]OTs•MeOH, [**201**]PF_6, [**201**]Cl•1.5H_2O, [**201**]OTs, [**202**]PF_6 , [**203**]BPh_4 and [**213**]PF_6 are given in Figure 25. Crystallographic

data and refinement details are presented in Tables 17–18, and selected bond distances and angles in Tables 19–22.

4.3 Results and Discussion

4.3.1 Molecular Design and Synthesis

We have synthesised a total of 18 DπA pyridinium salts (Figure 22) in order to elucidate structure-property relationships for such ionic organic NLO chromophores. In particular, comparison of the series **[196–199]**PF_6, **[200–203]**PF_6 and **[204–207]**PF_6 will provide information on the effects of conjugation length and acceptor strength. Comparison of **[200–203]**PF_6 and **[208–211]**PF_6 will provide information on the effects of donor strength. Also, the properties of **[200]**PF_6, **[201]**PF_6, **[208]**PF_6 and **[209]**PF_6 can be compared to those of the Ru^{II} complexes of $Mebpe^+$ and $Phbpe^+$ ligands in salts **157**, **168**, **158** and **169** (see Chapter 2). Furthermore, the series **[196–199]**PF_6 can be compared to the Ru^{II} complexes of 4,4′-bipyridinium ligands, *e.g.* **133–143**, **149**, **156**, **163** and **167**. Such comparisons will allow an evaluation of the electron donating abilities of the $[Ru^{II}(NH_3)_4L_D]^{2+}$ (L_D = NH_3 or mim) moieties, as an alternative to the commonly used $-NMe_2$ or –OMe groups.

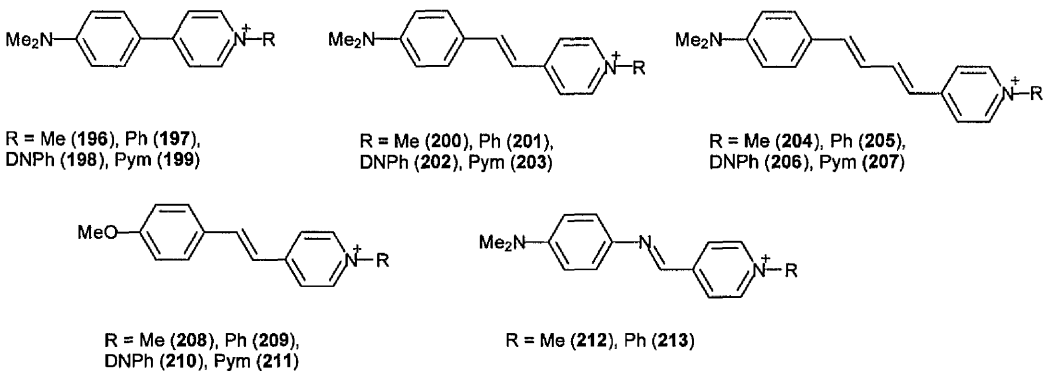

Figure 22. Structures of the organic chromophores in salts [196–213]PF_6.

The ions **196**, **197**, **198**, **200**, **204**, **208** and **212** are known compounds and were synthesised following literature methods or slight modifications thereof. Compounds [**197–199**]PF_6, [**205–207**]PF_6, [**210**]PF_6 and [**211**]PF_6 were synthesised by direct reaction of the appropriate pyridyl derivative with 2,4-dinitrochlorobenzene (followed by reaction with aniline) or 2-chloropyrimidine. The precursor to [**205–207**]PF_6, *trans*-4-(4-dimethylaminophenyl-4-buta-1,3-dienyl)pyridine, was synthesized using standard Wittig chemistry. For the synthesis of the *N*-(2-pyrimidyl)- derivatives it was found that yields are greatly improved if silver trifluoroacetate is added to the reactions.

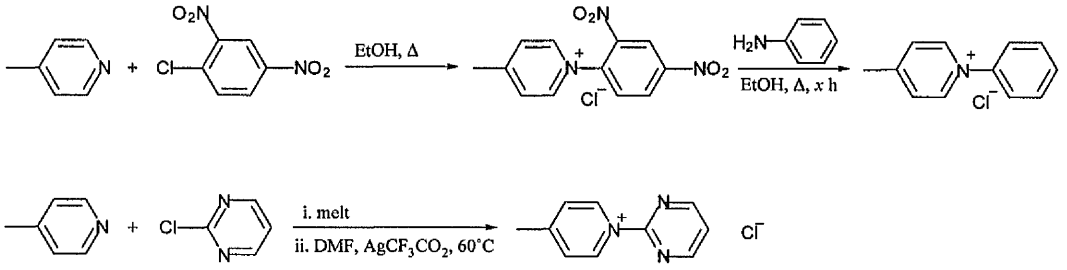

Compounds [**200–204**]PF_6, [**208**]PF_6 and [**209**]PF_6 were synthesised by base-catalyzed condensations of appropriate picolinium salts with suitable aldehydes.

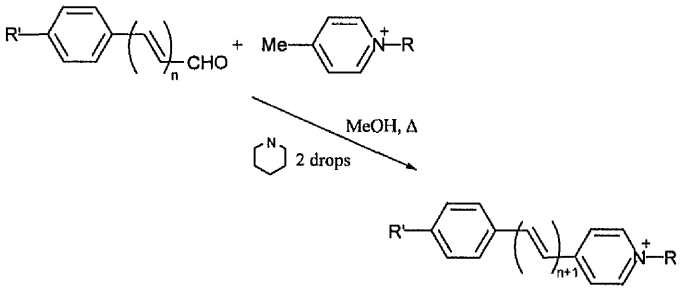

R′	R	n
NMe_2	Me	0
NMe_2	Ph	0
NMe_2	DNPh	0
NMe_2	Pym	0
NMe_2	Me	1
OMe	Me	0
OMe	Ph	0

A similar strategy was originally attempted for the syntheses of [**205–207**]PF_6, but only the stilbazolium salts [**201–203**]PF_6 were isolated from these reactions (Figure 23). Clearly, an *N*-aryl substituent will decrease the basicity of the carbanion formed from deprotonation of a 4-picolinium ion. In such cases, nucleophilic attack on 4-(dimethylamino)cinnamaldehyde occurs at the β-vinyl carbon, rather than at the carbonyl group. However, exactly how the position of attack is related to the carbanion basicity is unclear.

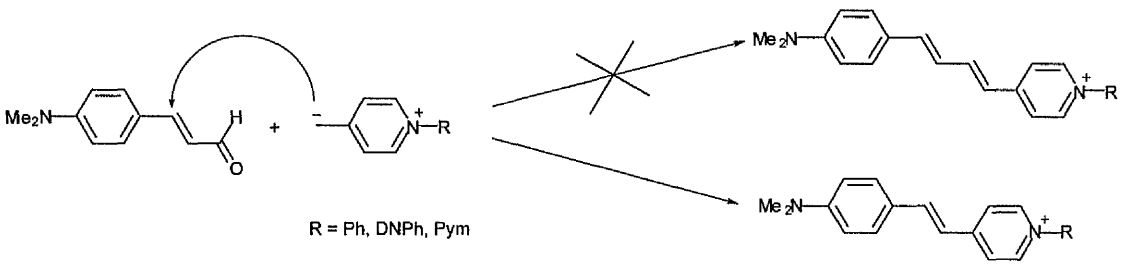

Figure 23. Attempted synthesis of butadienyl compounds by base-catalysed condensation reactions.

Compounds [**212**]PF_6 and [**213**]PF_6 were synthesised by base-catalysed condensations of picolinium salts with *N*,*N*-dimethyl-4-nitrosoaniline. The yields of these reactions were lower than those of the analogous reactions with 4-(dimethylamino)benzaldehyde and purification of the products was more laborious, requiring column chromatography. Significant quantities of the unwanted cis isomers of [**212**]PF_6 and [**213**]PF_6 were also isolated.

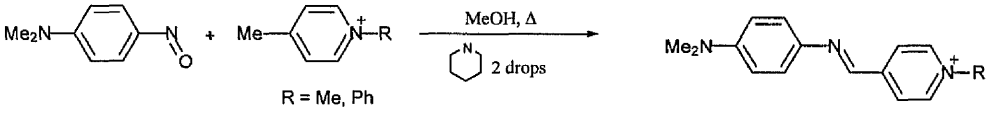

4.3.2 Electronic Spectroscopy Studies

The electronic absorption spectra of the new salts [**196–213**]PF_6 were recorded in acetonitrile and the results are presented in Table 14. The cations in [**196–213**]PF_6 exhibit intense absorptions with λ_{max} values in the region 375–580 nm corresponding to $\pi \rightarrow \pi^*$ intramolecular charge-transfer (ICT) excitations from the NMe_2/OMe electron donor groups to the pyridinium acceptors. A representative spectrum of [**203**]PF_6 can be found in Figure 24. The energies of these ICT absorptions depend on the relative energies of the NMe_2/OMe-based HOMOs and of the pyridinium-based LUMOs. All of the salts show one or more less intense absorptions to higher energy due to non-directional $\pi \rightarrow \pi^*$ excitations.

Table 14. UV/Visible/NIR data for salts [196-213]PF_6 in acetonitrile.

Compound	λ_{max}/ nm (ε_{max} /M^{-1} cm^{-1})[a]	E_{max} /eV	Assignment
[196]PF_6	420 (40 200)	2.95	ICT ($\pi \rightarrow \pi^*$)
	252 (16 300)	4.92	$\pi \rightarrow \pi^*$
[197]PF_6	448 (50 100)	2.77	ICT ($\pi \rightarrow \pi^*$)
	258 (13 000)	4.81	$\pi \rightarrow \pi^*$
[198]PF_6	469 (45 250)	2.64	ICT ($\pi \rightarrow \pi^*$)
	227 (25 500)	5.46	$\pi \rightarrow \pi^*$
[199]PF_6	485 (55 600)	2.56	ICT ($\pi \rightarrow \pi^*$)
	266 (12 900)	4.66	$\pi \rightarrow \pi^*$
[200]PF_6	470 (42 800)	2.64	ICT ($\pi \rightarrow \pi^*$)
	270 (11 100)	4.59	$\pi \rightarrow \pi^*$
[201]PF_6	504 (51 400)	2.47	ICT ($\pi \rightarrow \pi^*$)
	309 (11 100)	4.04	$\pi \rightarrow \pi^*$
	276 (10 400)	4.52	$\pi \rightarrow \pi^*$
[202]PF_6	537 (47 500)	2.32	ICT ($\pi \rightarrow \pi^*$)
	319 (9 800)	3.91	$\pi \rightarrow \pi^*$
	224 (23 000)	5.57	$\pi \rightarrow \pi^*$
[203]PF_6	553 (57 200)	2.25	ICT ($\pi \rightarrow \pi^*$)
	324 (10 300)	3.85	$\pi \rightarrow \pi^*$
	282 (9 200)	4.42	$\pi \rightarrow \pi^*$
	243 (8 900)	5.13	$\pi \rightarrow \pi^*$
[204]PF_6	487 (38 700)	2.56	ICT ($\pi \rightarrow \pi^*$)
	316 (10 800)	3.95	$\pi \rightarrow \pi^*$
	264 (9 900)	4.72	$\pi \rightarrow \pi^*$
[205]PF_6	525 (52 300)	2.38	ICT ($\pi \rightarrow \pi^*$)
	333 (13 900)	3.74	$\pi \rightarrow \pi^*$
	270 (10 300)	4.62	$\pi \rightarrow \pi^*$
[206]PF_6	565 (45 500)	2.21	ICT ($\pi \rightarrow \pi^*$)
	353 (12 600)	3.53	$\pi \rightarrow \pi^*$
	225 (24 400)	5.54	$\pi \rightarrow \pi^*$
[207]PF_6	579 (46 600)	2.15	ICT ($\pi \rightarrow \pi^*$)
	345 (11 300)	3.61	$\pi \rightarrow \pi^*$
	261 (10 300)	4.78	$\pi \rightarrow \pi^*$
[208]PF_6	376 (16 000)	3.32	ICT ($\pi \rightarrow \pi^*$)
	251 (17 500)	4.97	$\pi \rightarrow \pi^*$
[209]PF_6	397 (22 200)	3.14	ICT ($\pi \rightarrow \pi^*$)
	258 (17 700)	4.83	$\pi \rightarrow \pi^*$
[210]PF_6	418 (41 800)	2.98	ICT ($\pi \rightarrow \pi^*$)
	231 (20 600)	5.39	$\pi \rightarrow \pi^*$
[211]PF_6	426 (42 600)	2.93	ICT ($\pi \rightarrow \pi^*$)
	264 (11 600)	4.72	$\pi \rightarrow \pi^*$
[212]PF_6	501 (27 800)	2.49	ICT ($\pi \rightarrow \pi^*$)
	273 (17 400)	4.57	$\pi \rightarrow \pi^*$
[213]PF_6	534 (32 900)	2.34	ICT ($\pi \rightarrow \pi^*$)
	284 (16 500)	4.39	$\pi \rightarrow \pi^*$

[a] Solutions *ca.* 10^{-5} M.

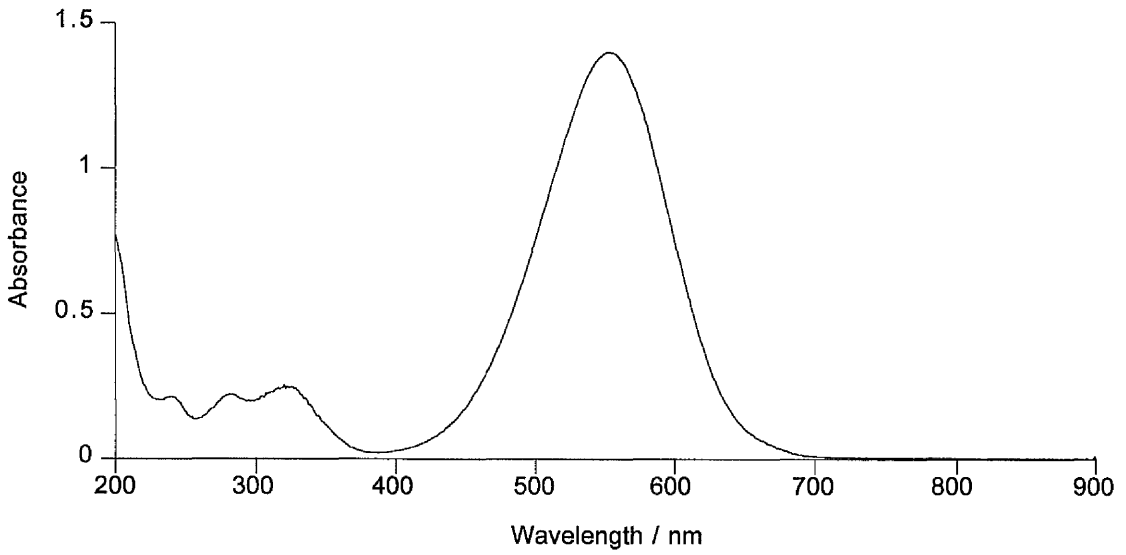

Figure 24. UV/Visible/NIR absorption spectrum of [203]PF_6 in acetonitrile.

Within each of the series [**196–199**]PF_6, [**200–203**]PF_6, [**204–207**]PF_6 and [**208–211**]PF_6 the ICT absorption energy decreases as the *N*-substituent changes in the order methyl > phenyl > 2,4-dinitrophenyl > pyrimidyl, reflecting the increasing electron acceptor strength of the quarternised pyridinium nitrogen due to increasing electron deficiency. Within all four series, the difference in the ICT energy between the *N*-methyl and the *N*-2-pyrimidyl derivatives is *ca.* –0.40 eV. This trend is consistent with results previously reported for Ru^{II} ammine complexes of *N*-aryl/alkyl pyridinium ligands,[90,91] and also with studies carried out by Hutchings.[138] The latter author found that substitution in the 4-position of the *N*-phenyl ring in [**197**]$^+$ influences the absorption spectra such that more electron-withdrawing substituents lead to larger bathochromic shifts. Interestingly, Hutchings also found a negligible shift in the ICT energy between [**198**]$^+$ and its 4-nitrophenyl analogue. This observation indicates that the steric effect of the *ortho*-NO_2 group offsets the increased electron deficiency of the 2,4-dinitrophenyl ring in [**198**]$^+$.

The Schiff base salts [**212–213**]PF_6 also follow this trend, the ICT band in [**213**]PF_6 being *ca.* 0.15 eV lower in energy than that of [**212**]PF_6. Although the molar extinction coefficients do not follow a consistent trend, that of the *N*-Me chromophore is invariably the lowest within each series.

As would be expected, elongation of the conjugation length between the electron donor/acceptor groups (*i.e.* [**196–199**]PF_6 → [**200–203**]PF_6 → [**204–205**]PF_6) results in bathochromic shifts of the ICT bands. Addition of one trans C=C bond decreases the ICT energy on average by 0.32 eV, whilst addition of a second trans C=C bond results in a further, smaller average shift of 0.10 eV. With the exception of [**207**]PF_6, the molar extinction coefficients remain relatively constant on chain extension.

Replacing the $-NMe_2$ donor group by the less electron rich –OMe donor results, as expected, in hypsochromic shifts in the ICT absorptions. Hence the ICT bands for the salts [**208–211**]PF_6 are blue-shifted on average by *ca.* 0.66 eV compared to those of [**200–203**]PF_6. These blue-shifts are accompanied by a loss of intensity in every case.

The introduction of a nitrogen atom into the conjugated bridge results in bathochromic shifts and intensity decreases for the ICT absorptions. The ICT bands for the salts [**212, 213**]PF_6 are red-shifted on average by *ca.* 0.15 eV compared to those of [**200, 201**]PF_6.

4.3.3 Electrochemical Studies

The picolinium salt precursors and the new salts [**196–203**]PF_6 were studied by cyclic voltammetry in acetonitrile and the results are presented in Table 15. These compounds all exhibit largely irreversible redox processes, although in some cases reverse waves were observed. In all cases, the first oxidation process is assigned to removal of an electron from the HOMO localized on the $-NMe_2$ group, whilst the first reduction process is assigned to the addition of an electron to the pyridinium-localized LUMO.

A similar trend is observed in the picolinium salts and in the two series [**196–199**]PF_6 and [**200–203**]PF_6; the LUMO energy decreases as the *N*-substituent is changed in the order methyl > phenyl > pyrimidyl > 2,4-dinitrophenyl. The potential for oxidation of the $-NMe_2$ group only changes slightly across the series and consequently has little influence on the red-shifting of the ICT absorptions. Hence, the stabilization of the pyridinium-centred LUMOs is responsible for the red-shifting of the ICT absorptions (see section 4.3.2). The presence of the 2,4-dinitrophenyl group gives rise to the most positive

potential for NMe_2 oxidation in each series. **[198]**PF_6 and **[202]**PF_6 also have the least negative pyridinium reduction potentials, and hence appear to have the smallest HOMO-LUMO energy gaps within each series. However, the ICT bands of **[198]**PF_6 and **[202]**PF_6 are higher in energy than those of their *N*-pyrimidyl analogues. This apparent discrepancy probably arises from the use of E_{pa}/E_{pc} rather than $E_{1/2}$ values.

Table 15. Electrochemical and ICT absorption data for selected organic salts in acetonitrile.

Compound	$E_{1/2}$/V *vs.* Ag–AgCl (ΔE_p/mV)[a] E_{pa}[b]	E_{pc}[c]	λ_{max}[ICT]/ nm (ε_{max} /M^{-1} cm^{-1})[d]
[mepic$^+$]PF_6	–	–1.43	–
[ppic$^+$]PF_6	–	–1.13	–
[dnppic$^+$]PF_6	–	–0.50	–
[pympic$^+$]PF_6	–	–0.82	–
[196]PF_6	1.14	–1.35	420 (40 200)
[197]PF_6	1.18	–1.11	448 (50 100)
[198]PF_6	1.27	–0.55	469 (45 250)
[199]PF_6	1.12	–0.81	485 (55 600)
[200]PF_6	0.94	–1.11	470 (42 800)
[201]PF_6	0.93	–0.88	504 (51 400)
[202]PF_6	0.96	–0.52	537 (47 500)
[203]PF_6	0.95	–0.66	553 (57 200)

[a] Measured in solutions *ca.* 10^{-3} M in analyte and 0.1 M in $NBu^n_4PF_6$ at a platinum bead/disc working electrode with a scan rate of 200 mV s^{-1}. Ferrocene internal reference $E_{1/2}$ = 0.45 V. [b] Peak potential for first irreversible oxidation (of HOMO, localized on $-NMe_2$ group); return wave also observed in some cases. [c] Peak potential for first irreversible reduction (of LUMO, localized on pyridinium group); return wave also observed in some cases. [d] Solutions ca. 10^{-5} M.

Elongation of the conjugated bridge between the electron donor/acceptor groups (*i.e.* **[196–199]**PF_6 → **[200–203]**PF_6) results in negative shifts of 170–310 mV for oxidation of the $-NMe_2$ groups and positive shifts of 30–240 mV for reduction of the pyridinium units. Therefore, the $-NMe_2$ groups are harder to oxidise and the pyridinium groups are harder to reduce in **[196–199]**PF_6 than in their stilbazolium analogues. Both of these effects are consistent with the red-shifts of the ICT bands evident in the UV/Visible/NIR absorption spectra.

4.3.4 Crystallographic Studies

Single crystal X-ray structures were determined for [**198**]OTs, [**201**]Cl, [**201**]OTs, [**201**]PF_6, [**202**]PF_6, [**203**]BPh_4 and [**213**]PF_6 and representations of the molecular structures of the cations are shown in Figure 25. Selected interatomic distances and angles are collected in Table 16 for comparison purposes.

The structures of the cations in salts [**198**]OTs, [**201**]Cl, [**201**]OTs, [**201**]PF_6, [**202**]PF_6, [**203**]BPh_4 and [**213**]PF_6 show evidence of ground state polarization to varying degrees; both the pyridyl and phenyl rings are partially quinoidal in all cases except for [**201**]OTs in which only the pyridyl ring is quinoidal. For example, in [**201**]Cl the average of the bond distances C142–C143 and C145–C146 is *ca.* 0.03 Å shorter than the average of the other phenylene bond distances. Similar differences are found in all the quinoidal rings, ranging from 0.03–0.04 Å. The ground state polarization also results in a shortening of the NMe_2–C(Ph) bond distance; in all cases the NMe_2–C(Ph) bond exhibits significant double bond character, being *ca.* 0.08 Å shorter than the N–Me bond distances.

Table 16. Comparison of selected interatomic distances (Å) and angles (°) for the salts [198]OTs, [201]Cl, [201]OTs, [201]PF_6, [202]PF_6, [203]BPh_4 and [213]PF_6.

	[**198**]OTs	[**201**]Cl	[**201**]OTs	[**201**]PF_6	[**202**]PF_6	[**203**]BPh_4	[**213**]PF_6
C–NMe_2	1.360(3)	1.373(2)	1.372(3)	1.360(3)	1.366(4)	1.371(4)	1.363(3)
C(Ph)–C(Ph)1[a]	1.410(6)	1.404(5)	1.392(9)	1.409(8)	1.406(8)	1.392(12)	1.408(4)
C(Ph)–C(Ph)2[b]	1.373(4)	1.372(4)	1.387(6)	1.377(6)	1.376(6)	1.359(7)	1.373(4)
C(Ph)–C(Py)	1.455(3)	–	–	–	–	–	–
C(Ph)–C/N(Eth)	–	1.438(2)	1.568(15)	1.433(4)	1.464(4)	1.653(9)	–
C/N(Eth)–C(Eth)	–	1.356(3)	1.277(18)	1.363(4)	1.336(4)	1.098(8)	–
C(Ph)–N(Im)	–	–	–	–	–	–	1.392(3)
N(Im)–C(Im)	–	–	–	–	–	–	1.288(3)
C(Im)–C(Py)	–	–	–	–	–	–	1.454(3)
C(Eth)–C(Py)	–	1.439(3)	1.639(18)	1.435(4)	1.431(4)	1.665(8)	
C(Py)–C(Py)1[c]	1.412(4)	1.405(4)	1.396(7)	1.406(5)	1.413(6)	1.382(8)	1.395(4)
C(Py)–C(Py)2[d]	1.360(4)	1.364(4)	1.353(6)	1.357(6)	1.350(6)	1.348(7)	1.368(4)
N(Py)–C(Ar)	1.440(3)	1.452(2)	1.451(3)	1.436(3)	1.448(4)	1.453(4)	1.443(3)
Dihedral angle 1[e]	14.44(11)	10.28(4)	12.38(14)	10.75(19)	14.46(8)	8.37(17)	7.5(2)
Dihedral angle 2[f]	61.55(6)	21.97(4)	28.20(11)	55.79(11)	84.42(11)	12.17(18)	56.6(1)
BLA	–	+0.082	+0.103[g]	+0.071	+0.113[g]	+0.561[g]	–

Abbreviations: Ph = phenyl; Eth = ethenyl; Py = pyridyl; Im = iminomethyl. [a] Average CH–C(N/C) distance in 4-(dimethylamino)phenyl ring. [b] Average CH–CH distance in 4-(dimethylamino)phenyl ring. [c] Average C(C)–CH distance in pyridyl ring. [d] Average CH–CH distance in pyridyl ring. [e] Angle between planes of 4-(dimethylamino)phenyl and pyridyl rings. [f] Angle between planes of pyridyl and aryl rings. [g] BLA overestimated due to disorder in crystal structure.

In the salts [**201**]Cl and [**201**]PF_6 the ethylene bridge C–C bond distances also show evidence of polarization, as shown by BLA values of +0.082 and +0.071 respectively. The structures of [**201**]OTs, [**202**]PF_6 and [**203**]BPh_4, however, do not show similar evidence of polarization, with BLA values of +0.103, +0.113 and +0.561 respectively. As noted earlier, polyenes have a typical BLA of *ca.* +0.11 (see section 1.5.2), thus these three large BLA values arise from disorder in the crystal structure.

The degree of twisting between the 4-(dimethylamino)phenyl and pyridyl rings is small for all of the cations, indicating substantial coupling through the DπA framework in each case. The dihedral angles between these two rings lie in the range 7.5(2)–14.46(8)°.

In all cases, the *N*-aryl ring is twisted with respect to the pyridyl ring. The relevant dihedral angles lie in the range 12.17(18)–84.42(11)° and depend largely on steric factors as well as crystal packing factors. For example, in the cations of [**201**]PF_6, [**201**]Cl and [**201**]OTs these dihedral angles lie in the range 21.97(4)–55.79(11)°, although the amount of steric hindrance between the phenylene H atoms and the pyridyl H atoms remains the same. The particularly large dihedral angle between the pyridyl and 2,4-dinitrophenyl rings of [**202**]PF_6 can be attributed in part to the steric effect of the ortho-NO_2 group.

Figure 25 Structural representations of the cations in [198]OTs, [201]Cl, [201]OTs, [201]PF_6, [202]PF_6, [203]BPh_4 and [213]PF_6.

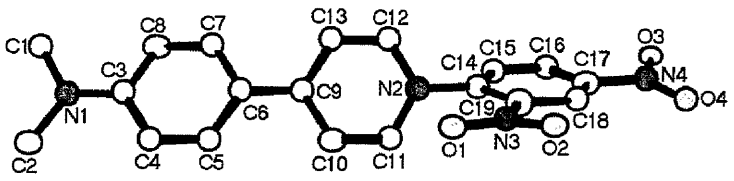

[198]OTs

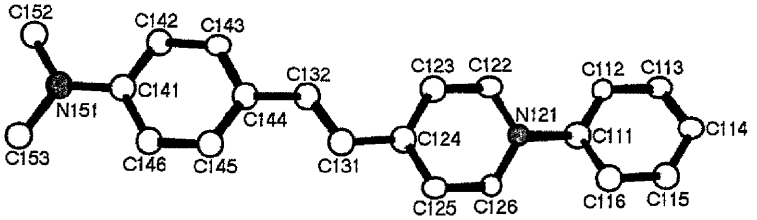

[201]Cl

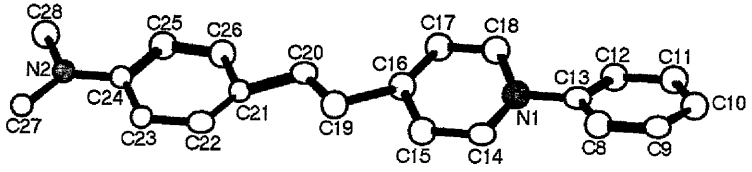

[201]OTs

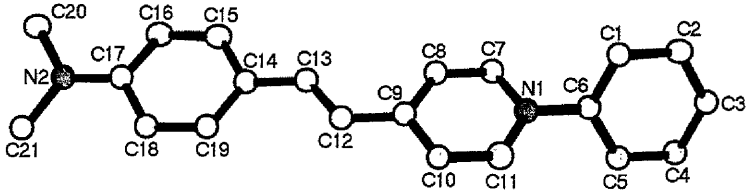

[201]PF_6

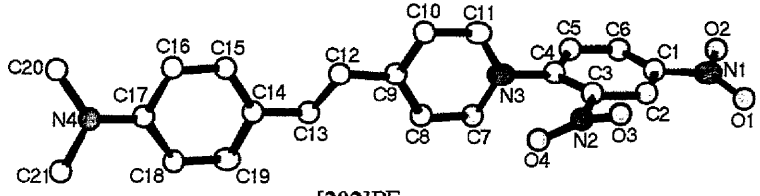

[202]PF_6

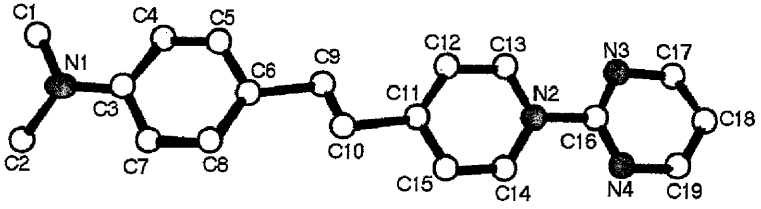

[203]BPh_4

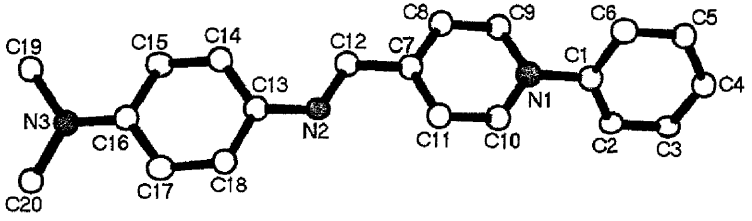

[213]PF_6

Table 17. Crystal data and structure refinement details for [198]OTs, [201]Cl, [201]OTs and [201]PF_6.

	[198]OTs	[201]Cl	[201]OTs	[201]PF_6
Empirical Formula	$C_{27}H_{28}N_4O_8S$	$C_{21}H_{24}ClN_2O_{1.5}$	$C_{28}H_{28}N_2O_3S$	$C_{21}H_{21}F_6N_2P$
Formula Weight	568.59	363.87	472.58	446.37
Temperature	150(2) K	173(2) K	150(2) K	150(2) K
Wavelength	0.71073 Å	0.71073 Å	0.71073 Å	0.71073 Å
Crystal System	Triclinic	Triclinic P	Monoclinic	Monoclinic
Space Group	$P\bar{1}$	$P\bar{1}$	$P2_1/c$	Cc
Unit Cell Dimensions	a = 7.9975(16) Å α = 103.62(3)°	a = 9.678(5) Å α = 97.51(3)°	a = 8.051(2) Å α = 90°	a = 19.384(4) Å α = 90°
	b = 11.315(2) Å β = 92.08(3)°	b = 13.668(3) Å β = 107.3(3)°	b = 19.225(4) Å β = 93.85(3)°	b = 10.636(2) Å β = 125.93(3)°
	c = 16.063(3) Å γ = 107.40(3)°	c = 15.706(7) Å γ = 104.98(2)°	c = 15.161(3) Å γ = 90°	c = 11.784(2) Å γ = 90°
Volume	1339.1(5) $Å^3$	1867.1 $Å^3$	2341.3(9) $Å^3$	1967.3(7) $Å^3$
Z	2	4	4	4
Density (Calculated)	1.410 Mg /m^3	1.294 Mg /m^3	1.341 Mg /m^3	1.507 Mg /m^3
Absorption Coefficient	0.179 mm^{-1}	0.219 mm^{-1}	0.172 mm^{-1}	0.206 mm^{-1}
F(000)	596	772	1000	920
Crystal Size	0.275 × 0.177 × 0.04 mm^3	0.6 × 0.5 × 0.32 mm^3	0.35 × 0.3 × 0.02 mm^3	0.55 × 0.17 × 0.04 mm^3
θ Range For Data Collection	2.99–27.50°	1.58–27.52°	2.12–26.00°	2.31–27.48°
Index Ranges	$-9 \le h \le 10$, $-14 \le k \le 12$, $-20 \le l \le 20$	$-12 \le h \le 12$, $-17 \le k \le 17$, $-20 \le l \le 20$	$-9 \le h \le 9$, $-23 \le k \le 23$, $-18 \le l \le 18$	$-23 \le h \le 25$, $-13 \le k \le 13$, $-15 \le l \le 15$
Reflections Collected	21282	19230	33550	8007
Independent Reflections	6014 [R_{int} = 0.0634]	8422 [R_{int} = 0.0313]	4594 [R_{int} = 0.1331]	3783 [R_{int} = 0.0573]
Refinement Method	Full-matrix least-squares on F^2	Full-matrix least-squares on F^2	Full-matrix least-squares on F^2	Full-matrix least-squares on F^2
Data / Restraints / Parameters	6014 / 0 / 365	8422 / 2 / 491	4594 / 0 / 328	3783 / 2 / 275
Goodness-of-Fit on F^2	0.952	0.906	0.966	1.027
Final R Indices [$F^2 > 2\sigma(F^2)$]	$R1$ = 0.0521, $wR2$ = 0.1303	$R1$ = 0.0470, $wR2$ = 0.1161	$R1$ = 0.0590, $wR2$ = 0.1365	$R1$ = 0.0420, $wR2$ = 0.1009
R Indices (all data)	$R1$ = 0.0885, $wR2$ = 0.1526	$R1$ = 0.0753, $wR2$ = 0.1274	$R1$ = 0.1301, $wR2$ = 0.1738	$R1$ = 0.0519, $wR2$ = 0.1074
Largest Diff. Peak and Hole	0.429 and –0.415 e $Å^{-3}$	0.508 and –0.385 e $Å^{-3}$	0.242 and –0.499 e $Å^{-3}$	0.263 and –0.268 e $Å^{-3}$

Table 18.Crystal data and structure refinement details for [202]PF_6, [203]BPh_4, and [213]PF_6.

	[202]PF_6	[203]BPh_4	[213]PF_6
Empirical Formula	$C_{21}H_{19}F_6N_4O_4P$	$C_{43}H_{39}BN_4$	$C_{20}H_{20}F_6N_3P$
Formula Weight	536.37	622.59	447.36
Temperature	150(2) K	293(2) K	150(2) K
Wavelength	0.71073 Å	0.71073 Å	0.71073 Å
Crystal System	Monoclinic	Triclinic	Monoclinic
Space Group	$P2_1/c$	$P\bar{1}$	Cc
Unit Cell Dimensions	a = 17.365(3) Å α = 90°	a = 11.481(2) Å α = 93.74(3)°	a = 19.3044(4) Å α = 90°
	b = 11.091(2) Å β = 109.19(3)°	b = 12.580(3) Å β = 105.59(3)°	b = 10.6009(2) Å β = 125.527(3)°
	c = 12.635(3) Å γ = 90°	c = 13.029(7) Å γ = 106.68(2)°	c = 11.6549(2) Å γ = 90°
Volume	2298.2(8) Å^3	1715.5 Å^3	1941.10(8) Å^3
Z	4	2	4
Density (Calculated)	1.550 Mg /m^3	1.205 Mg /m^3	1.531 Mg /m^3
Absorption Coefficient	0.206 mm^{-1}	0.070 mm^{-1}	0.210 mm^{-1}
F(000)	1096	660	920
Crystal Size	0.3 × 0.015 × 0.15 mm^3	0.8 × 0.2 × 0.02 mm^3	0.10 × 0.10 × 0.10 mm^3
θ Range For Data Collection	2.22–26.00°	2.50–22.50°	3.64–25.98°
Index Ranges	$-21 \le h \le 21$, $-13 \le k \le 13$, $-15 \le l \le 15$	$-12 \le h \le 12$, $-13 \le k \le 13$, $-14 \le l \le 14$	$-23 \le h \le 23$, $-12 \le k \le 13$, $-13 \le l \le 12$
Reflections Collected	35191	24399	6150
Independent Reflections	4517 [R_{int} = 0.0922]	4471 [R_{int} = 0.1529]	3240 [R_{int} = 0.0267]
Refinement Method	Full-matrix least-squares on F^2	Full-matrix least-squares on F^2	Full-matrix least-squares on F^2
Data / Restraints / Parameters	4496 / 6 / 372	4471 / 0 / 444	3240 / 2 / 292
Goodness-of-Fit on F^2	1.167	1.105	0.998
Final R Indices [$F^2 > 2\sigma(F^2)$]	$R1$ = 0.0660, $wR2$ = 0.1695	$R1$ = 0.0633, $wR2$ = 0.1710	$R1$ = 0.0359, $wR2$ = 0.0877
R Indices (all data)	$R1$ = 0.1141, $wR2$ = 0.1975	$R1$ = 0.1120, $wR2$ = 0.2018	$R1$ = 0.0418, $wR2$ = 0.0920
Largest Diff. Peak and Hole	0.362 and –0.542 e Å^{-3}	0.385 and –0.227 e Å^{-3}	0.219 and –0.214 e Å^{-3}

Table 19. Selected interatomic distances (Å) and angles (°) for the salts [198]OTs and [201]Cl.

[198]OTs				[201]Cl			
O1-N3	1.215(2)	C3-N1-C2	120.71(17)	C111-C112	1.383(3)	C112-C111-C116	120.1(2)
O2-N3	1.219(2)	C3-N1-C1	120.49(17)	C111-C116	1.388(3)	C112-C111-N121	120.6(2)
O3-N4	1.223(3)	C2-N1-C1	118.63(17)	C111-N121	1.452(2)	C116-C111-N121	119.2(2)
O4-N4	1.228(3)	C11-N2-C12	120.03(17)	C112-C113	1.388(3)	C111-C112-C113	119.6(2)
N1-C3	1.360(3)	C11-N2-C14	119.00(16)	C113-C114	1.376(3)	C114-C113-C112	120.6(2)
N1-C2	1.453(3)	C12-N2-C14	120.74(16)	C114-C115	1.378(3)	C113-C114-C115	119.5(2)
N1-C1	1.457(3)	O1-N3-O2	124.15(18)	C115-C116	1.386(3)	C114-C115-C116	120.8(2)
N2-C11	1.357(3)	O1-N3-C19	119.39(17)	N121-C126	1.355(2)	C115-C116-C111	119.3(2)
N2-C12	1.357(3)	O2-N3-C19	116.44(18)	N121-C122	1.374(2)	C126-N121-C122	118.4(2)
N2-C14	1.440(3)	O3-N4-O4	124.3(2)	C122-C123	1.357(3)	C126-N121-C111	120.8(2)
N3-C19	1.477(3)	O3-N4-C17	118.0(2)	C123-C124	1.403(3)	C122-N121-C111	120.7(2)
N4-C17	1.468(3)	O4-N4-C17	117.75(19)	C124-C125	1.407(3)	C123-C122-N121	121.4(2)
C3-C8	1.409(3)	N1-C3-C8	121.48(18)	C124-C131	1.439(3)	C122-C123-C124	121.7(2)
C3-C4	1.415(3)	N1-C3-C4	121.53(18)	C125-C126	1.371(3)	C123-C124-C125	115.6(2)
C4-C5	1.372(3)	C8-C3-C4	116.98(18)	C131-C132	1.356(3)	C123-C124-C131	124.3(2)
C5-C6	1.405(3)	C5-C4-C3	121.38(19)	C132-C144	1.438(2)	C125-C124-C131	120.1(2)
C6-C7	1.410(3)	C4-C5-C6	121.94(19)	C141-N151	1.373(2)	C126-C125-C124	121.3(2)
C6-C9	1.455(3)	C5-C6-C7	116.44(18)	C141-C142	1.406(3)	N121-C126-C125	121.5(2)
C7-C8	1.373(3)	C5-C6-C9	121.91(18)	C141-C146	1.410(2)	C132-C131-C124	124.2(2)
C9-C13	1.407(3)	C7-C6-C9	121.64(18)	C142-C143	1.370(3)	C131-C132-C144	127.3(2)
C9-C10	1.416(3)	C8-C7-C6	122.19(19)	C143-C144	1.397(2)	N151-C141-C142	121.7(2)
C10-C11	1.364(3)	C7-C8-C3	121.03(18)	C144-C145	1.401(3)	N151-C141-C146	121.0(2)
C12-C13	1.356(3)	C13-C9-C10	115.65(18)	C145-C146	1.374(3)	C142-C141-C146	117.3(2)
C14-C15	1.387(3)	C13-C9-C6	122.53(18)	N151-C152	1.446(2)	C143-C142-C141	120.6(2)
C14-C19	1.397(3)	C10-C9-C6	121.82(18)	N151-C153	1.452(2)	C142-C143-C144	122.7(2)
C15-C16	1.381(3)	C11-C10-C9	120.84(19)			C143-C144-C145	116.5(2)
C16-C17	1.382(3)	N2-C11-C10	120.99(18)			C143-C144-C132	119.2(2)
C17-C18	1.373(3)	C13-C12-N2	120.58(18)			C145-C144-C132	124.3(2)
C18-C19	1.384(3)	C12-C13-C9	121.86(18)			C146-C145-C132	121.8(2)
		C15-C14-C19	119.23(18)			C145-C146-C141	121.0(2)
		C15-C14-N2	116.57(17)			C141-N151-C152	119.6(2)
		C19-C14-N2	124.20(17)			C141-N151-C153	120.8(2)
		C16-C15-C14	120.86(19)			C152-N151-C153	118.4(2)
		C17-C16-C15	118.37(18)				
		C18-C17-C16	122.45(19)				
		C18-C17-N4	118.80(19)				
		C16-C17-N4	118.74(19)				
		C17-C18-C19	118.62(19)				
		C18-C19-C14	120.46(18)				
		C18-C19-N3	116.09(18)				
		C14-C19-N3	123.32(18)				

Table 20. Selected interatomic distances (Å) and angles (°) for the salts [201]OTs and [201]PF_6.

[201]OTs				[201]PF_6			
N1-C18	1.355(4)	C18-N1-C14	118.8(2)	N1-C7	1.363(3)	C7-N1-C11	119.2(2)
N1-C14	1.358(4)	C18-N1-C13	121.2(2)	N1-C11	1.370(3)	C7-N1-C6	121.6(2)
N1-C13	1.451(3)	C14-N1-C13	120.0(2)	N1-C6	1.436(3)	C11-N1-C6	119.2(2)
N2-C24	1.372(3)	C24-N2-C27	120.7(3)	N2-C17	1.360(3)	C17-N2-C21	119.9(3)
N2-C27	1.447(4)	C24-N2-C28	120.9(3)	N2-C21	1.444(4)	C17-N2-C20	121.2(2)
N2-C28	1.453(4)	C27-N2-C28	118.4(3)	N2-C20	1.449(4)	C21-N2-C20	118.9(2)
C8-C13	1.381(4)	C13-C8-C9	118.5(3)	C1-C2	1.384(4)	C2-C1-C6	118.7(3)
C8-C9	1.392(4)	C10-C9-C8	121.3(3)	C1-C6	1.395(4)	C3-C2-C1	120.5(3)
C9-C10	1.371(5)	C9-C10-C11	119.1(3)	C2-C3	1.384(4)	C2-C3-C4	120.2(3)
C10-C11	1.373(5)	C10-C11-C12	121.1(3)	C3-C4	1.388(4)	C5-C4-C3	119.9(3)
C11-C12	1.391(4)	C13-C12-C11	118.9(3)	C4-C5	1.383(4)	C6-C5-C4	119.6(3)
C12-C13	1.375(4)	C12-C13-C8	121.2(3)	C5-C6	1.382(4)	C5-C6-C1	121.1(3)
C14-C15	1.340(4)	C12-C13-N1	119.7(3)	C7-C8	1.360(4)	C5-C6-N1	119.6(2)
C15-C16	1.378(5)	C8-C13-N1	119.0(3)	C8-C9	1.407(4)	C1-C6-N1	119.3(2)
C16-C17	1.413(5)	C15-C14-N1	121.6(3)	C9-C10	1.405(3)	C8-C7-N1	120.8(2)
C16-C19	1.456(7)	C14-C15-C16	121.9(3)	C9-C12	1.435(4)	C7-C8-C9	121.4(2)
C17-C18	1.365(4)	C15-C16-C17	116.3(3)	C10-C11	1.353(4)	C10-C9-C8	116.2(2)
C19-C20	1.360(7)	C15-C16-C19	112.6(4)	C12-C13	1.363(4)	C10-C9-C12	123.4(2)
C20-C21	1.469(7)	C17-C16-C19	131.1(4)	C13-C14	1.433(4)	C8-C9-C12	120.4(2)
C21-C26	1.359(5)	C18-C17-C16	120.3(3)	C14-C19	1.400(4)	C11-C10-C9	121.1(3)
C21-C22	1.396(5)	N1-C18-C17	121.1(3)	C14-C15	1.406(4)	C10-C11-N1	121.3(2)
C22-C23	1.399(4)	C20-C19-C16	121.4(7)	C15-C16	1.370(4)	C13-C12-C9	124.5(2)
C23-C24	1.412(4)	C19-C20-C21	121.6(7)	C16-C17	1.427(4)	C12-C13-C14	126.9(3)
C24-C25	1.400(4)	C26-C21-C22	116.5(3)	C17-C18	1.402(4)	C19-C14-C15	116.5(3)
C25-C26	1.374(4)	C26-C21-C20	114.8(4)	C18-C19	1.384(4)	C19-C14-C13	119.8(3)
		C22-C21-C20	128.8(4)			C15-C14-C13	123.7(3)
		C21-C22-C23	122.2(3)			C16-C15-C14	122.3(3)
		C22-C23-C24	119.8(3)			C15-C16-C17	121.0(3)
		N2-C24-C25	121.4(3)			N2-C17-C18	122.7(2)
		N2-C24-C23	121.5(3)			N2-C17-C16	120.4(3)
		C25-C24-C23	117.0(3)			C18-C17-C16	116.9(2)
		C26-C25-C24	120.9(3)			C19-C18-C17	121.1(3)
		C21-C26-C25	123.6(4)			C18-C19-C14	122.2(3)

Table 21. Selected interatomic distances (Å) and angles (°) for the salts [202]PF_6 and [203]BPh_4.

[202]PF_6				[203]BPh_4			
N1-O1	1.214(4)	O1-N1-O2	124.0(3)	N1-C3	1.371(4)	C3-N1-C1	121.7(3)
N1-O2	1.220(4)	O1-N1-C1	118.3(3)	N1-C1	1.439(5)	C3-N1-C2	119.4(3)
N1-C1	1.480(4)	O2-N1-C1	117.7(3)	N1-C2	1.451(5)	C1-N1-C2	116.9(3)
N2-O4	1.195(4)	O4-N2-O3	124.7(3)	N2-C13	1.347(4)	C13-N2-C14	119.6(3)
N2-O3	1.240(4)	O4-N2-C3	119.2(3)	N2-C14	1.353(4)	C13-N2-C16	120.6(3)
N2-C3	1.476(4)	O3-N2-C3	116.0(3)	N2-C16	1.453(4)	C14-N2-C16	119.8(3)
N3-C7	1.357(4)	C7-N3-C11	120.3(3)	N3-C16	1.311(4)	C16-N3-C17	113.6(4)
N3-C11	1.361(4)	C7-N3-C4	119.3(2)	N3-C17	1.343(5)	C16-N4-C19	113.8(3)
N3-C4	1.448(4)	C11-N3-C4	120.3(2)	N4-C16	1.311(4)	N1-C3-C4	121.0(3)
N4-C17	1.366(4)	C17-N4-C21	120.7(3)	N4-C19	1.338(5)	N1-C3-C8	121.2(3)
N4-C21	1.445(4)	C17-N4-C20	120.9(3)	C3-C4	1.399(5)	C4-C3-C8	117.8(3)
N4-C20	1.458(4)	C21-N4-C20	117.8(3)	C3-C8	1.403(5)	C5-C4-C3	121.5(4)
C1-C6	1.361(5)	C6-C1-C2	122.8(3)	C4-C5	1.332(5)	C4-C5-C6	122.6(4)
C1-C2	1.387(4)	C6-C1-N1	119.1(3)	C5-C6	1.374(7)	C5-C6-C7	117.1(4)
C2-C3	1.382(4)	C2-C1-N1	118.1(3)	C6-C7	1.392(7)	C5-C6-C9	113.5(5)
C3-C4	1.379(4)	C3-C2-C1	116.9(3)	C6-C9	1.653(9)	C7-C6-C9	129.4(6)
C4-C5	1.379(4)	C4-C3-C2	121.4(3)	C7-C8	1.385(5)	C8-C7-C6	121.9(4)
C5-C6	1.380(4)	C4-C3-N2	122.2(3)	C9-C10	1.098(8)	C7-C8-C3	119.1(4)
C7-C8	1.342(4)	C2-C3-N2	116.4(3)	C10-C11	1.665(8)	C10-C9-C6	110.7(7)
C8-C9	1.397(4)	C5-C4-C3	119.8(3)	C11-C15	1.372(6)	C9-C10-C11	108.6(7)
C9-C10	1.429(4)	C5-C4-N3	117.7(3)	C11-C12	1.392(6)	C15-C11-C12	116.3(3)
C9-C12	1.431(4)	C3-C4-N3	122.5(3)	C12-C13	1.360(5)	C15-C11-C10	114.2(4)
C10-C11	1.358(4)	C4-C5-C6	119.8(3)	C14-C15	1.335(5)	C12-C11-C10	129.5(5)
C12-C13	1.336(4)	C1-C6-C5	119.2(3)	C17-C18	1.362(6)	C13-C12-C11	121.4(4)
C13-C14	1.464(4)	C8-C7-N3	120.9(3)	C18-C19	1.358(6)	N2-C13-C12	119.8(3)
C14-C15	1.399(4)	C7-C8-C9	121.7(3)			C15-C14-N2	121.2(4)
C14-C19	1.402(4)	C8-C9-C10	116.1(3)			C14-C15-C11	121.6(4)
C15-C16	1.383(4)	C8-C9-C12	119.5(3)			N4-C16-N3	130.0(3)
C16-C17	1.415(4)	C10-C9-C12	124.4(3)			N4-C16-N2	114.8(3)
C17-C18	1.407(4)	C11-C10-C9	120.6(3)			N3-C16-N2	115.2(3)
C18-C19	1.369(4)	C10-C11-N3	120.4(3)			N3-C17-C18	122.8(4)
		C13-C12-C9	125.6(3)			C19-C18-C17	116.7(4)
		C12-C13-C14	125.7(3)			N4-C19-C18	123.1(4)
		C15-C14-C19	117.2(3)				
		C15-C14-C13	123.4(3)				
		C19-C14-C13	119.4(3)				
		C16-C15-C14	122.0(3)				
		C15-C16-C17	120.4(3)				
		N4-C17-C18	122.1(3)				
		N4-C17-C16	120.8(3)				
		C18-C17-C16	117.1(3)				
		C19-C18-C17	121.6(3)				
		C18-C19-C14	121.5(3)				

Table 22. Selected interatomic distances (Å) and angles (°) for the salt [213]PF_6.

[213]PF_6			
N1-C9	1.353(3)	C9-N1-C10	119.8(2)
N1-C10	1.361(3)	C9-N1-C1	120.8(2)
N1-C1	1.443(3)	C10-N1-C1	119.3(2)
N2-C12	1.288(3)	C12-N2-C13	121.9(2)
N2-C13	1.392(3)	C16-N3-C20	120.3(2)
N3-C16	1.363(3)	C16-N3-C19	121.1(2)
N3-C20	1.445(4)	C20-N3-C19	118.6(2)
N3-C19	1.459(3)	C2-C1-C6	121.8(2)
C1-C2	1.383(4)	C2-C1-N1	119.1(2)
C1-C6	1.388(3)	C6-C1-N1	119.1(2)
C2-C3	1.392(4)	C1-C2-C3	119.3(2)
C3-C4	1.392(4)	C4-C3-C2	119.2(3)
C4-C5	1.380(4)	C5-C4-C3	120.7(2)
C5-C6	1.384(3)	C4-C5-C6	120.6(2)
C7-C8	1.391(4)	C5-C6-C1	118.4(2)
C7-C11	1.399(3)	C8-C7-C11	118.0(2)
C7-C12	1.454(3)	C8-C7-C12	121.4(2)
C8-C9	1.368(4)	C11-C7-C12	120.7(2)
C10-C11	1.362(3)	C9-C8-C7	120.4(2)
C13-C18	1.403(4)	N1-C9-C8	120.7(2)
C13-C14	1.406(3)	N1-C10-C11	121.1(2)
C14-C15	1.362(3)	C10-C11-C7	119.8(2)
C15-C16	1.428(4)	N2-C12-C7	119.5(2)
C16-C17	1.395(4)	N2-C13-C18	116.7(2)
C17-C18	1.384(4)	N2-C13-C14	126.2(2)
		C18-C13-C14	117.1(2)
		C15-C14-C13	121.6(2)
		C14-C15-C16	121.4(2)
		N3-C16-C17	122.4(2)
		N3-C16-C15	120.4(2)
		C17-C16-C15	117.1(2)
		C18-C17-C16	121.0(2)
		C17-C18-C13	121.9(2)

The salts [**198**]OTs, [**201**]Cl, [**201**]OTs, [**202**]PF_6 and [**203**]BPh_4 all adopt centrosymmetric space groups and thus will not exhibit macroscopic NLO effects. However, the salts [**201**]PF_6 and [**213**]PF_6 adopt the noncentrosymmetric space group *Cc* and thus are expected to exhibit bulk NLO properties.

The well-studied compound DAST (*i.e.* [**200**]OTs) also crystallizes in the space group *Cc* and is very SHG active due to a favourable arrangement of the chromophores (Figure 26). The *p*-toluenesulfonate anions form sheets, separating the dipolar cations and allowing them to align in a parallel manner.

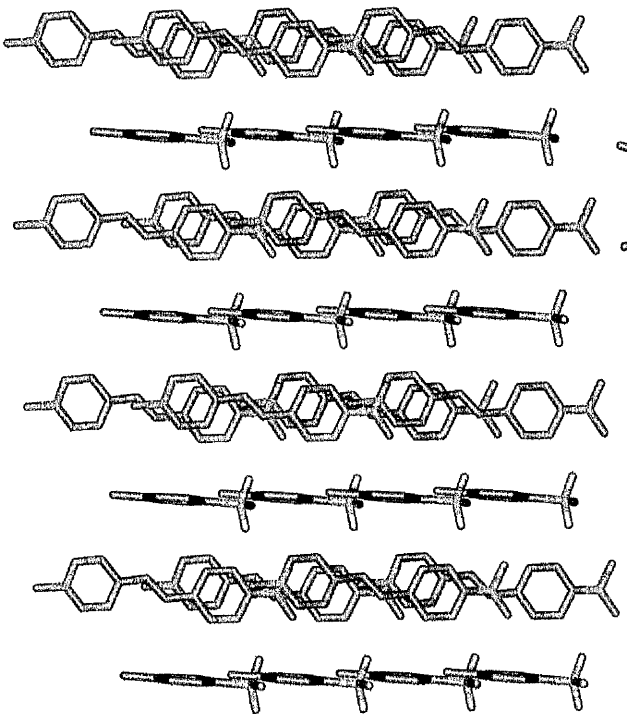

Viewed approximately along the crystallographic *b* axis

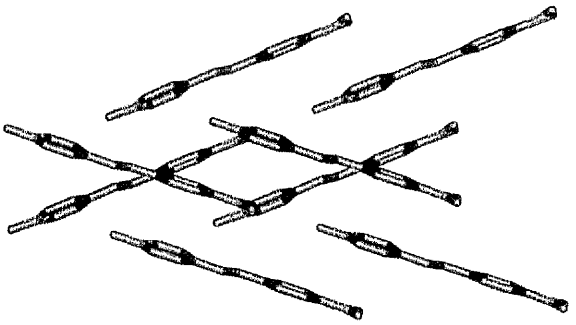

Viewed approximately along the crystallographic *c* axis (*p*-toluenesulfonate anions removed for clarity)

Figure 26. Crystal packing diagrams for DAST ([200]OTs).

The use of *p*-toluenesulfonate anions generally appears to encourage the formation of favourable packing arrangements in stilbazolium salts,[123b] but in [**201**]OTs the chromophores align antiparallel, precluding any bulk second-order NLO activity. However, [**201**]PF_6 crystallizes in *Cc*, with the chromophores aligned in a parallel arrangement (Figure 27), giving a 20° angle between the dipolar axis (approximated as the N1-N2 vector) and the polar *a* axis of the crystal. When viewed down the crystallographic *c* axis, the chromophores form a herring-bone pattern similar to DAST. In [**201**]PF_6, the angle θ_m between the dipolar axis and the crystallographic *b* axis is 74.51(11)°, whilst the optimal θ_m value for SHG phase-matching in the *m* symmetry point group is 35.26°.[40] The structure of [**201**]PF_6 is hence not optimised for SHG, but is better suited to electro-optic behaviour. Given the larger β_0 value for [**201**]PF_6 (see section 4.3.6.1) with respect to [**200**]PF_6, it can hence be anticipated that crystals of [**201**]PF_6 may exhibit larger electro-optical coefficients than those of DAST.

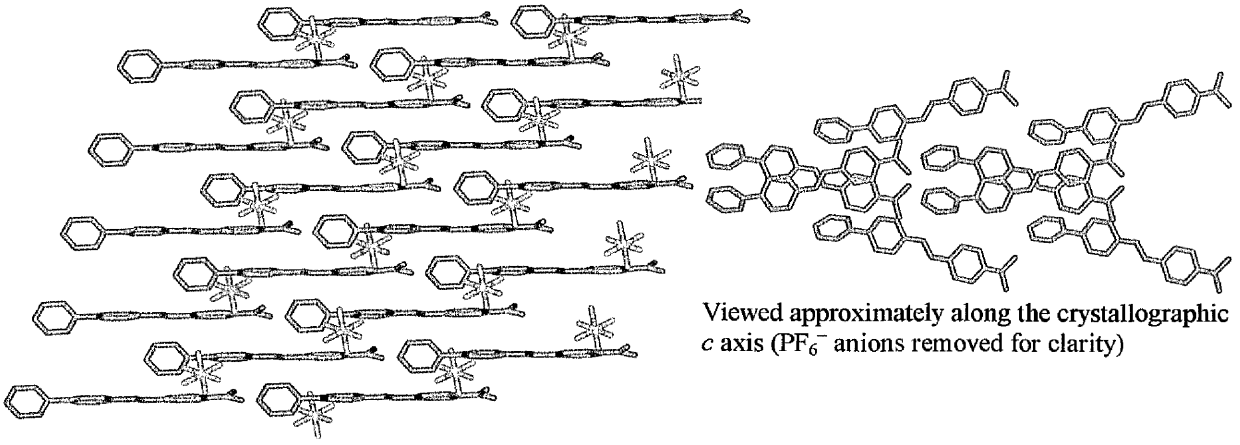

Viewed approximately along the crystallographic *c* axis (PF_6^- anions removed for clarity)

Viewed approximately along the crystallographic *b* axis

Figure 27. Crystal packing diagrams for [201]PF_6.

[**213**]PF_6 also crystallizes in *Cc*, is almost isostructural with [**201**]PF_6 (Figure 28), having similar angles between the dipolar axis (approximated as the N1-N3 vector) and the crystallographic *a* (25.3°) and *b* (θ_m = 74.33°) axes, and forms a herring bone structure as seen in DAST. Hence, it is anticipated that both [**201**]PF_6 and [**213**]PF_6 will exhibit substantial bulk second-order NLO effects (see section 4.3.6.2).

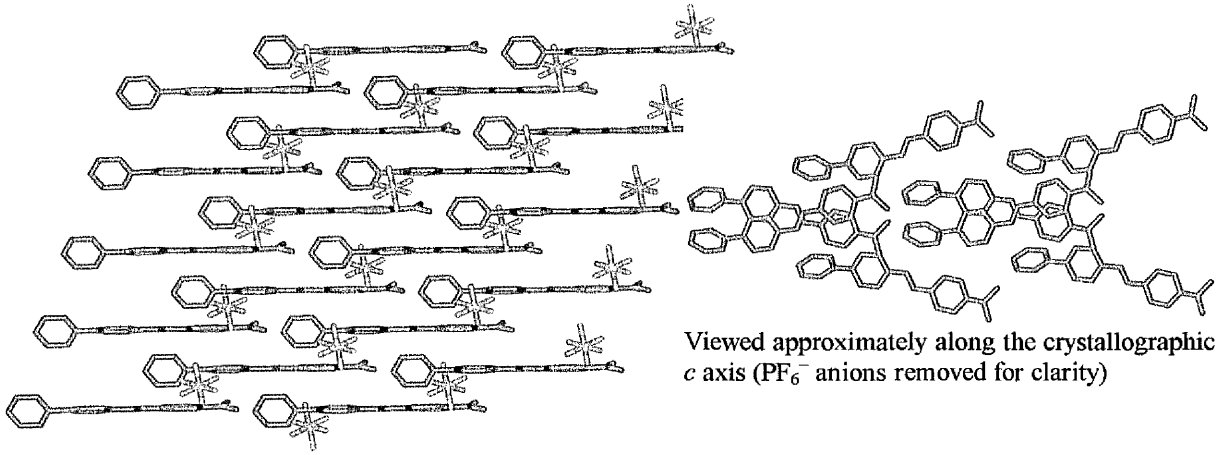

Viewed approximately along the crystallographic *c* axis (PF_6^- anions removed for clarity)

Viewed approximately along the crystallographic *b* axis

Figure 28. Crystal packing diagrams for [213]PF_6.

4.3.5 ^{1}H NMR Studies

The ^{1}H NMR spectra of the new organic salts [**196–213**]PF_6 are well defined and hence allow unambiguous identification and assessment of purity. Coupling constants of *ca.* 15–16 Hz for the ethylene bridge protons in the salts [**200–211**]PF_6 confirm the trans geometries. Selected ^{1}H NMR data for the precursors [mepic$^+$]PF_6, [ppic$^+$]PF_6, [dnppic$^+$]PF_6, [pympic$^+$]PF_6 and for the salts [**196–211**]PF_6 are presented in Table 23.

Table 23. Selected ^{1}H NMR data for precursor salts [mepic$^+$]PF_6, [ppic$^+$]PF_6, [dnppic$^+$]PF_6, [pympic$^+$]PF_6, and salts [196–211]PF_6.[a]

Salt	Pyridinium ortho-H	Ethylene bridge	NMe_2/OMe
[mepic$^+$]PF_6[b]	8.87	–	–
[ppic$^+$]PF_6[b]	9.21	–	–
[dnppic$^+$]PF_6[b]	9.27–9.24	–	–
[pympic$^+$]PF_6[b]	10.08	–	–
[**196**]PF_6[b]	8.76	–	3.14
[**197**]PF_6[b]	9.01	–	3.19
[**198**]PF_6[b]	9.02–8.95	–	3.23
[**199**]PF_6[b]	9.78	–	3.24
[**200**]PF_6[c]	8.29	7.86, 7.06	3.08
[**201**]PF_6[c]	8.57	7.91, 7.15	3.08
[**202**]PF_6[c]	8.39	7.99, 7.17	3.11
[**203**]PF_6[c]	9.53	8.00, 7.19	3.10
[**204**]PF_6[c]	8.29	7.63, 7.08–6.89, 6.66	3.02
[**205**]PF_6[c]	8.58	7.79, 7.17–7.07, 6.79–6.71	3.03
[**206**]PF_6[c]	8.42	7.89, 7.25–7.01, 6.81–6.74	3.06
[**207**]PF_6[c]	9.51	7.86, 7.21–6.96, 6.76	3.03
[**208**]PF_6[b]	8.86	8.01, 7.40	3.88
[**209**]PF_6[b]	9.14	8.18, 7.54	3.90
[**210**]PF_6[b]	9.17	8.28, 7.60	3.91
[**211**]PF_6[b]	9.98	8.29, 7.61	3.91

[a] Recorded on a Varian Gemini 200 spectrometer; all shifts referenced to $SiMe_4$. [b] d_6-acetone. [c] d_3-acetonitrile

The chemical shifts of the signals for the protons ortho to the quarternised nitrogen are dependent on the acceptor strength of the *N*-substituent. In the picolinium precursor salts, these signals shift downfield in the substituent order *N*-Me > *N*-Ph > *N*-DNPh > *N*-Pym. This trend is repeated in the series [**196–199**]PF_6 and [**208–211**]PF_6, but not in the series [**200–203**]PF_6 and [**204–207**]PF_6 where the observed trend is *N*-Me > *N*-DNPh > *N*-

Ph > *N*-Pym. In each of the series, replacing an *N*-methyl with an *N*-phenyl substituent results in a downfield shift of the ortho-H signal of *ca.* 0.25 ppm. Similarly, replacing an *N*-methyl with an *N*-pyrimidyl substituent results in downfield shifts of *ca.* 1.0 ppm, confirming the strongly electron-withdrawing nature of the 2-pyrimidyl ring. Within each of the series [**200–203**]PF_6, [**204–207**]PF_6 and [**208–211**]PF_6, the chemical shifts of the signals for the $-NMe_2$ or –OMe protons remain approximately constant as the electron-withdrawing nature of the *N*-substituent increases. However the signal for the $-NMe_2$ protons in the series [**196–199**]PF_6 shifts downfield by a total of *ca.* 0.1 ppm in the substituent order *N*-Me > *N*-Ph > *N*-DNPh > *N*-Pym. Clearly, the NMe_2 group 'feels' the electron-withdrawing influence of the pyridinium unit more strongly through the shortest π-bridge system. Similar downfield shifts for the ethylene bridge signals are observed in the salts [**200–211**]PF_6, with a difference of *ca.* 0.2 ppm on going from an *N*-methyl to an *N*-pyrimidyl group.

4.3.6 Nonlinear Optical Studies

4.3.6.1 HRS Results

The first hyperpolarizabilities, β, of the new salts [**196–211**]PF_6 were measured in acetonitrile using femtosecond HRS experiments with a 1300 nm laser fundamental,[144] incorporating high-frequency demodulation of multi-photon fluorescence contributions.[143] β values were determined by using β_{1300} for disperse red 1 (86×10^{-30} esu in acetonitrile: obtained from the value of 54×10^{-30} esu in chloroform and taking into account local field correction factors at optical frequencies) as an external reference. Additionally, the β values of [**204–207**]PF_6 were measured using femtosecond HRS experiments with an 800 nm laser fundamental,[133] incorporating high-frequency demodulation of multi-photon fluorescence contributions.[143] In this case β values were determined by using β_{800} for crystalviolet (500×10^{-30} esu in acetonitrile: obtained from the value of 340×10^{-30} esu in methanol and taking into account local field correction factors at optical frequencies) as an

external reference. Estimated static hyperpolarizabilities, β_0, were derived using the two-level model (see section 1.5.1) and the results are presented in Table 24.

The primary objective of this study is to establish whether *N*-arylation is an effective strategy for increasing β_0 in stilbazolium (and related) chromophores. However, since HRS data are unfortunately not yet available for [**196**]PF_6, [**208**]PF_6 or [**209**]PF_6, only limited conclusions can be drawn at present.

Table 24. Visible absorption and HRS data for the salts [196–211]PF_6 in acetonitrile.

Salt	λ_{max}/ nm (ε_{max} /M^{-1} cm^{-1})	E_{max}/ eV	β_{1300} [a] / β_{800} [b] (10^{-30} esu)	β_0 [c] (10^{-30} esu)
[**196**]PF_6	420 (40 200)	2.952	–/–	–/–
[**197**]PF_6	448 (50 100)	2.768	50/–	23/–
[**198**]PF_6	469 (45 250)	2.644	70/–	29/–
[**199**]PF_6	485 (55 600)	2.556	75/–	28/–
[**200**]PF_6	470 (42 800)	2.638	60/–	25/–
[**201**]PF_6	504 (51 400)	2.460	355/–	120/–
[**202**]PF_6	537 (47 500)	2.309	380/–	100/–
[**203**]PF_6	553 (57 200)	2.242	1017/–	230/–
[**204**]PF_6	487 (38 700)	2.546	770/166	290/51
[**205**]PF_6	525 (52 300)	2.362	1536/301	446/123
[**206**]PF_6	565 (45 500)	2.194	1155/304	228/152
[**207**]PF_6	579 (46 600)	2.141	1396/435	231/227
[**208**]PF_6	376 (16 000)	3.297	–/–	–/–
[**209**]PF_6	397 (22 200)	3.123	–/–	–/–
[**210**]PF_6	418 (41 800)	2.966	50/–	26/–
[**211**]PF_6	426 (42 600)	2.910	90/–	46/–

[a] β_{1300} is the dynamic first hyperpolarizability measured using a 1300 nm laser fundamental. [a] β_{800} is the dynamic first hyperpolarizability measured using an 800 nm laser fundamental. [c] β_0 is the static hyperpolarizability estimated by using the two-level model.[19] The quoted cgs units (esu) can be converted into SI units ($C^3m^3J^{-2}$) by dividing by a factor of 2.693×10^{20}.

The β_0 values for the series [**200–203**]PF_6 do show a large increase between [**200**]PF_6 and its *N*-aryl analogues. However, it seems unlikely that this enhancement effect is actually as great as it would appear. The β_0 value for [**200**]PF_6 is lower than expected; for example values of 100 and 46×10^{-30} esu, respectively, have been obtained previously for related *N*-alkyl chromophores [**217**]Br[144] and [**218**]Br.[133]

In the series [**204–207**]PF_6, there is an increase in β_0 going from an *N*-Me to an *N*-Ph substituent. However, the observation that the β_0 values (derived from β_{1300}) for [**206**]PF_6 and [**207**]PF_6 appear lower than that for [**204**]PF_6 is counter-intuitive.

Conversely, the β_0 values derived from measurements with an 800 nm fundamental follow a similar trend to the series **[200–203]**PF_6, although a direct comparison cannot be made. The anomalies in the present 1300 nm HRS data are likely due to problems with the femtosecond frequency-demodulation experiments, which are in their developmental stages.

Nevertheless, the β_0 values derived from measurements with an 1300 nm fundamental for **[197–199]**PF_6, **[210]**PF_6 and **[211]**PF_6 do seem reasonable, both compared with the values for **[201–205]** and also other existing literature data. For example, comparison of **214** and **215** shows a 38% enhancement of β_0 on elongation of the conjugation length. Large increases in β_0 are also observed when comparing **[197–199]**PF_6 with the series **[201–203]**PF_6. On comparison of **215** and **216** or **219** and **220** a large increase in β_0 is observed on going from an –OMe to an $-NMe_2$ electron donor group. Similar increases in β_0 are also observed when comparing **[210–211]**PF_6 with **[202–203]**PF_6.

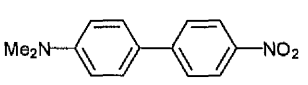

214. λ_{max} = 390 nm; $CHCl_3$;
$\beta_{1907} = 50 \times 10^{-30}$ esu;
$\beta_0 = 40 \times 10^{-30}$ esu[11d]

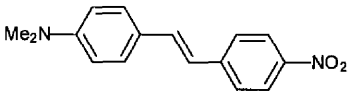

215. λ_{max} = 430 nm; $CHCl_3$;
$\beta_{1907} = 73 \times 10^{-30}$ esu;
$\beta_0 = 55 \times 10^{-30}$ esu[11d]

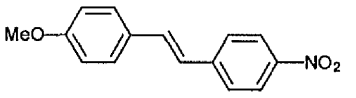

216. λ_{max} = 376; $CHCl_3$;
$\beta_{1907} = 34 \times 10^{-30}$ esu;
$\beta_0 = 28 \times 10^{-30}$ esu[11d]

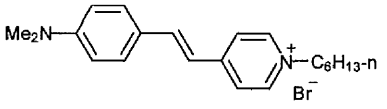

217. λ_{max} = 477 nm; DMSO;
$\beta_{800} = 360 \times 10^{-30}$ esu;
$\beta_0 = 100 \times 10^{-30}$ esu[144]

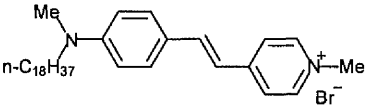

218. λ_{max} = 508 nm; $CHCl_3$;
$\beta_{1300} = 140 \times 10^{-30}$ esu;
$\beta_0 = 46 \times 10^{-30}$ esu[133]

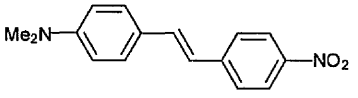

219. λ_{max} = 437 nm; $CHCl_3$;
$\beta_{1300} = 110 \times 10^{-30}$ esu;
$\beta_0 = 53 \times 10^{-30}$ esu[133]

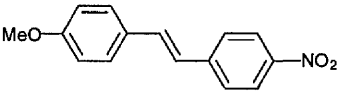

220. λ_{max} = 377 nm; $CHCl_3$;
$\beta_{1300} = 16 \times 10^{-30}$ esu;
$\beta_0 = 10 \times 10^{-30}$ esu[133]

4.3.6.2 Kurtz Powder Test Results

The salts [**201**]PF_6 and [**213**]PF_6 crystallize in the noncentrosymmetric space group *Cc* and can therefore exhibit bulk quadratic NLO effects (see section 4.3.4). Their SHG efficiencies have been measured using the Kurtz powder test[5] (see section 1.4.1) with a fundamental wavelength of 1907 nm and the results are presented in Table 25. Particle size differentiation was carried out using precision sieves, resulting in powders containing particles of 53–63 μm in diameter. Powdered samples of urea and DAST were prepared in the same way for purposes of comparison.

Table 25. Powder SHG efficiencies of [201]PF_6 and [213]PF_6.

Salt	SHG_{1907}[a]	SHG_{1907}[b]
Urea	1	1
DAST	--	550
[**201**]PF_6	600	470
[**213**]PF_6	400	240

[a] No particle size differentiation. [b] 53–63 μm particle size.

The validity of the comparison between [**201**]PF_6 and [**213**]PF_6 and DAST is questionable because powder SHG results can be particle size dependent (see section 1.4.1). For example, in our measurements DAST exhibits approximately half the SHG efficiency at 1907 nm that Marder *et al.*[122] observed. Nevertheless, there is no doubt that the SHG efficiencies measured at 1907 nm of [**201**]PF_6 and [**213**]PF_6 are very large. Since [**201**]PF_6 and [**213**]PF_6 are approximately isostructural (see section 4.3.4) the reduced SHG efficiency of the latter indicates that [**213**]PF_6 has a smaller β_0 value than [**201**]PF_6.

4.3.7 Comparison of the $[Ru^{II}(NH_3)_4L_D]^{2+}$ (L_D = NH_3 or mim) moieties with the $-NMe_2$ group as electron donors.[149]

The data presented in this chapter together with those in Chapter 2 and previous studies[90,91] allows quantitative and systematic comparison of the electronic properties of the $[Ru^{II}(NH_3)_4L_D]^{2+}$ (L_D = NH_3 or mim) metal centres with the traditional organic $-NMe_2$ group.

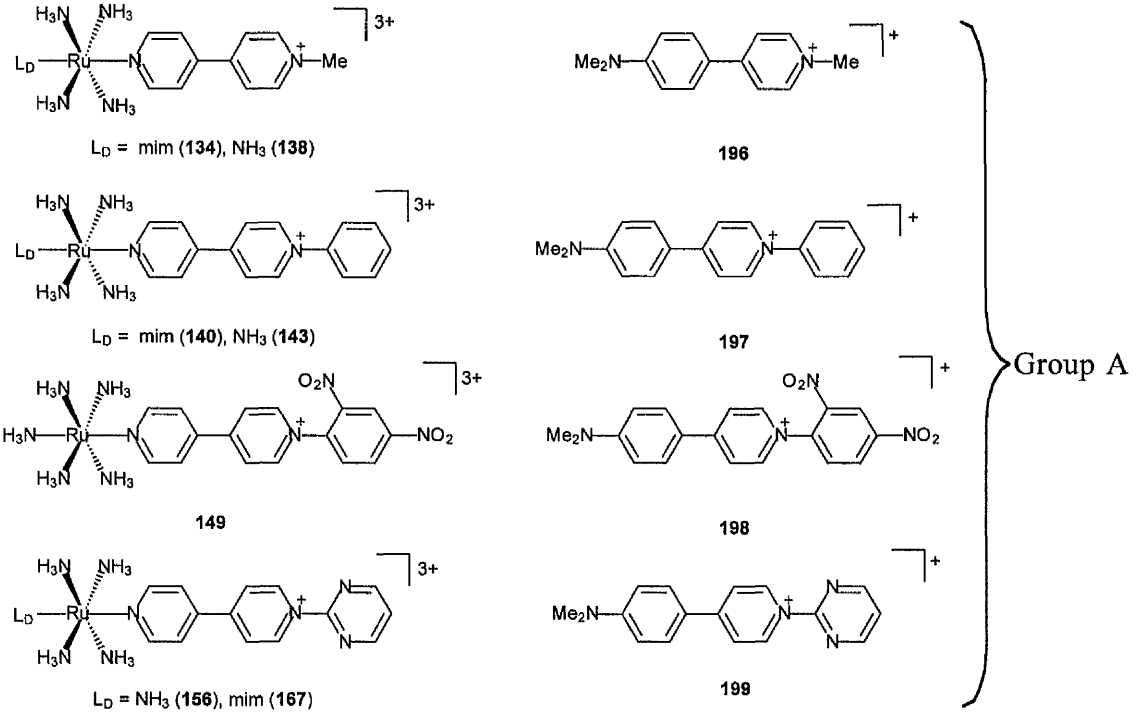

Series 1 = **138, 143, 149, 156;** Series 2 = **134, 140, 167;** Series 3 = **[196–199]**PF_6.

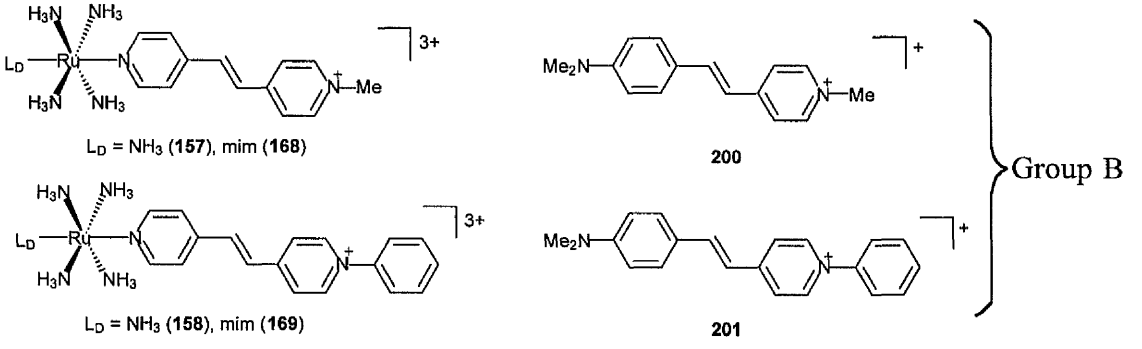

Selected visible absorption data for the compounds under comparison are presented in Table 26 and representative electronic spectra of the *N*-pym substituted salts **156** and [**199**]PF_6 are shown in Figure 29. The intense, broad visible absorptions of the ruthenium complex salts are due to $d\pi(Ru^{II}) \rightarrow p\pi^*$(pyridinium) CT excitations (see section 2.3.2), whilst those of the organic salts arise from $p\pi$ (NMe_2)$\rightarrow p\pi^*$(pyridinium) CT processes. The CT energies E_{max}[CT] are determined by the difference between the energies of the $[Ru^{II}(NH_3)_4L_D]^{2+}$/$NMe_2$-localised HOMOs and the pyridinium-localised LUMOs. The E_{max}[CT] values of the organic salts are considerably higher than those of the related complex salts. When L_D = NH_3, the organic *vs.* Ru complex CT energy difference in the biaryl systems (*i.e.* Group A) steadily decreases from 0.85 to 0.72 eV as the pyridinium *N*-substituent changes in the order Me > Ph > DNPh > Pym. A similar trend and differences are observed when L_D = mim. The organic *vs.* complex CT energy differences between related ethenyl bridged salts (Group B) are smaller. For example, comparison of [**200**]PF_6 and [**201**]PF_6 with the corresponding complexes where L_D = NH_3 reveals energy differences of 0.56 and 0.49 eV.

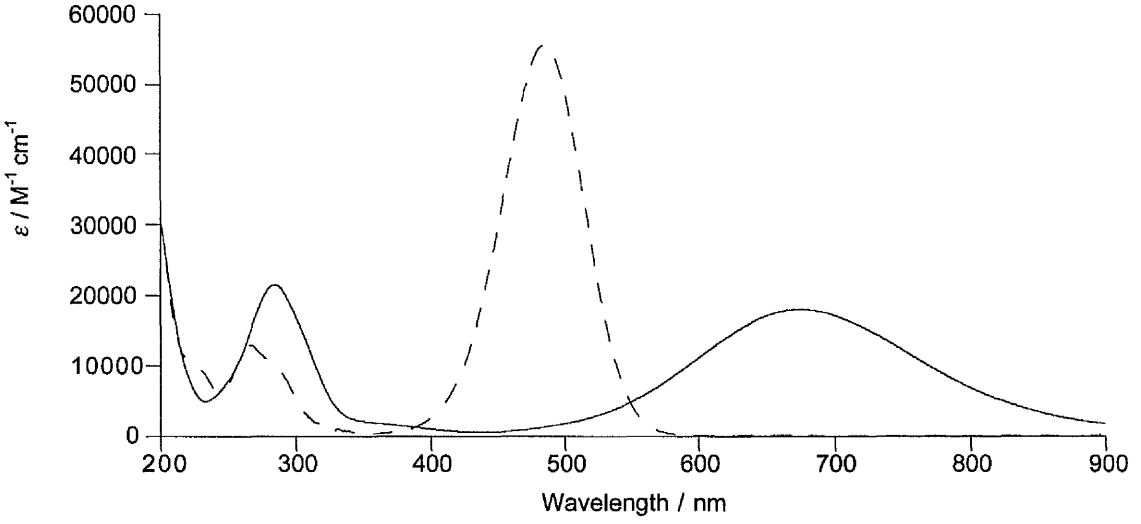

Figure 29. UV/Visible/NIR absorption spectra of 156 (——) and [199]PF_6 (- - -).

Within the three different series in group A E_{max}[CT] decreases as the pyridinium *N*-substituent changes in the order Me > Ph > DNPh > Pym, the differences between the extremes being 0.26, 0.28 and 0.39 eV for series 1, 2 and 3 respectively. The differences in CT energy between the *N*-Me/*N*-Ph pairs in groups A and B are larger for the organics (0.18 eV) than for the corresponding complex salts (0.10–0.14 eV). The molar extinction coefficients of the CT bands of the organics are *ca.* 2–3 times larger than those of their complex counterparts.

Table 26. Visible absorption, cyclic voltammetric, proton NMR and HRS data for the salts in Groups A and B.

Salt	λ_{max}[CT]/nm (ε/M^{-1} cm^{-1})	E_{max}[CT] [a] eV	*E*/V *vs.* Ag–AgCl [b] E_{ox} [d]	E_{red} [e]	δ/ppm [c] *ortho*–H [f]	NH_3/NMe_2 [g]	β (10^{-30} esu) [h]	β_0 (10^{-30} esu) [i]
138 [k]	590 (15 800)	2.10	0.52	–0.86	9.15	3.50	750	123
143 [k]	628 (19 300)	1.97	0.52	–0.70	9.33	3.60	858	220
149 [k]	660 (16 900)	1.88	0.48	–0.30	9.37	3.74	871	289
156 [k]	673 (18 000)	1.84	0.56	–0.33	10.17	3.75	640	230
134 [j]	602 (16 200)	2.06	0.53	–0.83	9.15	–	523	100
140 [k]	642 (21 500)	1.93	0.52	–0.68	9.38	–	874	254
167 [k]	698 (18 700)	1.78	0.59	–0.33	10.22	–	818	336
[**196**]PF_6	420 (40 200)	2.95	1.14	–1.35	8.76	3.14	–	–
[**197**]PF_6	448 (50 100)	2.77	1.18	–1.11	9.01	3.19	50	23
[**198**]PF_6	469 (45 300)	2.64	1.27	–0.55	9.23	3.23	70	29
[**199**]PF_6	485 (55 600)	2.56	1.22	–0.81	9.78	3.24	75	28
[**200**]PF_6	470 (42 800)	2.64	0.94	–1.11	8.29 [l]	3.08 [l]	60	25
[**201**]PF_6	504 (51 400)	2.46	0.93	–0.88	8.57 [l]	3.08 [l]	355	120
157 [m]	595 (16 100)	2.08	0.47	–0.83	8.94	3.41	828	142
158 [m]	628 (17 200)	1.97	0.49	–0.64	9.25	3.44	751	192
168 [m]	563 (14 800)	2.05	0.48	–0.84	8.94	–	857	168
169 [m]	591 (17 100)	1.93	0.49	–0.64	9.26	–	1068	310

[a] Using acetonitrile solutions with concentrations *ca.* 10^{-5} M. [b] Measured in acetonitrile solutions *ca.* 10^{-3} M in analyte and 0.1 M in $NBu^n_4PF_6$ at a platinum-bead/disk working electrode with a scan rate of 200 mV s^{-1}. [c] Chemical shift at 200 MHz with respect to $SiMe_4$ in CD_3COCD_3. [d] Peak potential, E_{pa}, for first oxidation of HOMO. [e] Peak potential, E_{pc}, for first reduction of LUMO. [f] Doublet signal for protons *ortho* to pyridinum N atom. [g] Singlet signal for protons of trans NH_3, or $-NMe_2$ group. [h] Dynamic first hyperpolarizability measured using a nanosecond 1064 nm laser for Ru complex salts and a femtosecond 1300 nm laser for the organics. [i] Static first hyperpolarizability estimated from β by application of the two-level model.[19] [j] 90. [k] 91. [l] Chemical shift at 200 MHz with respect to $SiMe_4$ in CD_3CN. [m] 115b.

Cyclic voltammetric data for the complex salts and organic salts are also compiled in Table 26. Although the majority of the complex salts exhibit reversible redox processes, only the peak potentials (E_{pa} or E_{pc}) for these processes are presented for purposes of comparison. The data clearly show that the $[Ru^{II}(NH_3)_4L_D]^{2+}$ (L_D = NH_3 or mim) moieties are much easier to oxidise than is the $-NMe_2$ group (*i.e.* the potentials are less positive). Also, the pyridinium groups in the Ru complexes are easier to reduce than those in the

organics (*i.e.* the potentials are less negative). These two observations are consistent with the observed lower E_{max}[CT] values, arising from the smaller HOMO-LUMO gaps for the Ru complexes compared with their organic counterparts.

Within the different series in group A E_{ox} does not change greatly, but E_{red} steadily becomes less negative, and therefore reduction becomes easier, as the *N*-substituent changes in the order Me > Ph > Pym > DNPh, the differences between the extremes being *ca.* 0.5 V in each case.

Within group A, the E_{red} values for the organics are generally more negative than those of the analogous complexes, indicating that the pyridinum acceptor groups are more electron rich in the latter. The organic *vs.* complex difference in E_{red} lies between –0.41 and –0.53 V, with the exception of the *N*-DNPh substituent (**149** *vs.* [**198**]PF_6) where the difference is only –0.25 V. The E_{red} values for [**200**]PF_6 and [**201**]PF_6 are also more negative compared to those of the corresponding complexes, but the differences are smaller (between –0.24 and –0.30 V). The observation of such large E_{red} differences shows that the $-NMe_2$ group exerts a greater electron-donating influence on the acceptors than do the $[Ru^{II}(NH_3)_4L_D]^{2+}$ (L_D = NH_3 or mim) moieties, despite the fact that the latter are actually the more electron rich entities.

Selected ^1H NMR data for the protons ortho to the pyridinium nitrogen and the trans NH_3/NMe_2 groups are also presented in Table 26. Within group A, the *ortho*-H signals are at higher fields in the organics than in the corresponding Ru complexes. These protons are hence more shielded in [**196–199**]PF_6, consistent with the greater electron-donating effect of the $-NMe_2$ group compared with the $[Ru^{II}(NH_3)_4L_D]^{2+}$ (L_D = NH_3 or mim) moieties shown by the electrochemical data. Within group A, the donor group protons are increasingly deshielded as the *N*-substituent becomes more electron-withdrawing in the order Me < Ph < DNPh ≈ Pym. The difference between the extreme chemical shifts is larger for the trans NH_3 protons of the complexes (0.25 ppm) than for the $-NMe_2$ protons of [**196–199**]PF_6 (0.10 ppm).

The greater overall electron-donating influence of an $-NMe_2$ group compared with pyridyl-coordinated $[Ru^{II}(NH_3)_4L_D]^{2+}$ (L_D = NH_3 or mim) centres can be traced to two factors. Firstly, the $[Ru^{II}(NH_3)_4L_D]^{2+}$ (L_D = NH_3 or mim) moieties behaves as σ-electron

JOHN RYLANDS
UNIVERSITY
LIBRARY OF
MANCHESTER

acceptors, as well as π-donors. Therefore, complexation also removes electron density from the L_A ligands (note also that an uncoordinated pyridyl ring is itself mildly electron withdrawing), whilst an $-NMe_2$ group acts solely as a π-donor. Secondly, and perhaps more importantly, is more effective p(N)–p(C) compared with p(N)–d(Ru) π-orbital overlap. Such an effect has been invoked to rationalise marked differences between ions such as $[\mathbf{221}]^+$ and $[\mathbf{222}]^{5+}$; $[\mathbf{221}]^+$ is a fully delocalised system, whilst $[\mathbf{222}]^{5+}$ is a valence-localised mixed-valence complex.[150]

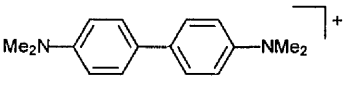

$[\mathbf{221}]^+$

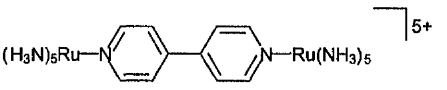

$[\mathbf{222}]^{5+}$

The molecular quadratic NLO properties of the salts in groups A and B have been studied using HRS (see section 1.8.5, 2.2.4 and 4.3.6.1) and the data is presented in Table 26. The previously reported β_0 values of the Ru complex salts were derived from standard nanosecond HRS with a 1064 nm laser,[90,91,115b] whilst the organic salts were studied using femtosecond HRS with a 1300 nm laser. Two conclusions can be drawn from the HRS data. Firstly, the β_0 values of the Ru complex chromophores appear to be considerably larger than those of their organic counterparts. However, comparison of HRS β_0 values obtained under different experimental conditions may be of limited validity.[151] Secondly, the red-shifting of the CT bands generally corresponds with increasing β_0 in all of the series.

In conclusion, pyridyl-coordinated $[Ru^{II}(NH_3)_4L_D]^{2+}$ (L_D = NH_3 or mim) centres are much more electron rich than an $-NMe_2$ group, but the latter exerts a greater net electron donating effect due in part to more effective π-orbital overlap. HRS data indicate that Ru complexes have considerably larger β_0 values than their purely organic counterparts.

4.4 Conclusion

We have shown that the salts [**196–211**]PF_6 exhibit large β_0 values and a significant enhancement in β_0 on going from an *N*-methyl to a *N*-pyrimidyl substituent is found in the series [**200–203**]PF_6. Furthermore, both [**201**]PF_6 and [**213**]PF_6 crystallize in the noncentrosymmetric space group *Cc* and exhibit substantial bulk SHG efficiencies at 1907 nm.

Comparison of data from electronic absorption spectroscopy, electrochemistry, proton NMR spectroscopy and HRS for the organic chromophores [**196–199**, **200**, and **201**,]PF_6 with related Ru ammine complexes indicates that although the Ru ammine metal centres are more electron rich, the $-NMe_2$ group exerts a greater electron donating effect due in part to more effective π-orbital overlap.

4.5 Further Work

Although large β_0 values have been observed, these have not been maximised. Hence, further structural changes such as increasing the acceptor strength or increasing the polyene chain length are anticipated to lead to additional increases in β_0. Different quarternised *N*-heterocyclic systems may also provide further enhancements to β_0, for example, quinolinium analogues of stilbazolium chromophores have been shown to possess $\mu\beta$ values some 50% larger than those of their stilbazolium analogues (*e.g.* **177** *vs.* **182**).[130]

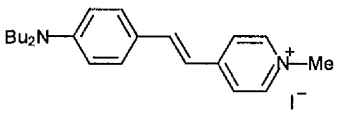

182. $CHCl_3$; λ_{max} = 517 nm;
$\mu\beta_{1907}$= 840 × 10^{-48} esu;
$\mu\beta_0$ = 550 × 10^{-48} esu

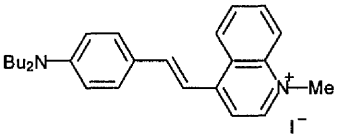

182. $CHCl_3$; λ_{max} = 603 nm;
$\mu\beta_{1907}$= 1380 × 10^{-48} esu;
$\mu\beta_0$ = 745 × 10^{-48} esu

In the longer term, the *N*-aryl substituents in the chromophores studied could be readily derivatized so as to produce compounds (*e.g.* **223**) suitable for incorporation into macroscopic structures such as LB films.

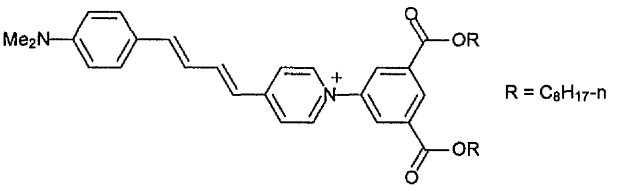

223.

More detailed comparative SHG studies of DAST, [**201**]PF_6 and [**213**]PF_6 may also prove fruitful. In particular, a particle size dependence study may be of interest. A larger range of particle sizes will allow a more thorough examination of bulk SHG efficiencies and may facilitate comparison with DAST. Furthermore, the possibility of growing larger crystals of [**201**]PF_6 and [**213**]PF_6 using other crystal growing techniques is of interest. Large, high-quality crystals are necessary if the E-O properties of these materials are to be studied.

Chapter 5. Ruthenium(II) Ammine Complexes Containing Two Pyridinium Acceptor Groups

5.1 Introduction

Most molecules proposed for second-order NLO effects are linear with a donor/acceptor pair separated by some kind of conjugated aromatic bridge. Such molecules show intense CT bands in the visible region, due to excitations which occur parallel to the long molecular axis. Hence, the two-level model predicts that the dominant contribution to β is also parallel to the long molecular axis (z-axis).

Introducing more than one donor and/or acceptor group into a conjugated aromatic system increases the number of significant components of β, which then acquires a two-dimensional (2D) character. It has been shown that off-diagonal tensor components of β can become significant in dipolar molecules with C_{2v} symmetry where the direction of the transition dipole moment is perpendicular to the C_2 axis.[152] These molecules offer new design possibilities to circumvent the efficiency-transparency trade-off and to achieve phase-matched second harmonic generation in organic materials.[153]

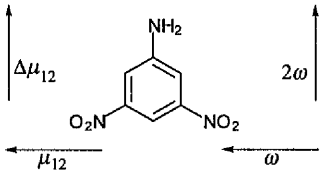

224. dioxane; λ_{max} = 389 nm

Wortmann *et al.*[152] investigated 3,5-dinitroaniline, **224**, and found that μ_{12} (the transition dipole moment) is perpendicular to $\Delta\mu_{12}$ (the change in dipole moment) upon electronic excitation. Therefore, irradiation with light polarized perpendicular to the C_2 axis will produce frequency-doubled light polarized parallel to this axis (perpendicular to the transition dipole moment). This is significant because it means that in a perfectly ordered system the second harmonic light can not be reabsorbed and thus the efficiency-transparency trade-off can be circumvented.

Subsequently,[153] a number of organic molecules possessing C_{2v} symmetry have been investigated. Using a combination of EFISHG and HRS experiments allows the determination of three independent tensor components of β; β_{zzz}, β_{zyy} and $\beta_{yzy} = \beta_{yyz}$.

Compound **225** was found to be a dipolar one-dimensional chromophore having only one significant component of β, β_{zzz}. However, the first hyperpolarizabilities of chromophores **226–228** have two-dimensional character with significant enhancement of the off-diagonal components β_{zyy} and β_{yzy}.

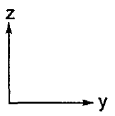

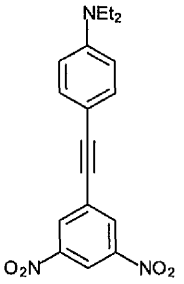

225. dioxane; λ_{max} = 383, 327 nm
$\beta_{zzz} = 331 \times 10^{-30}$ esu;
$\beta_{zyy} = 16 \times 10^{-30}$ esu;
$\beta_{yzy} = \beta_{yyz} = 11 \times 10^{-30}$ esu

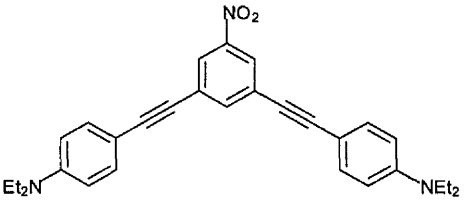

226. dioxane; λ_{max} = 361 nm;
$\beta_{zzz} = 43 \times 10^{-30}$ esu;
$\beta_{zyy} = 180 \times 10^{-30}$ esu;
$\beta_{yzy} = \beta_{yyz} = 194 \times 10^{-30}$ esu

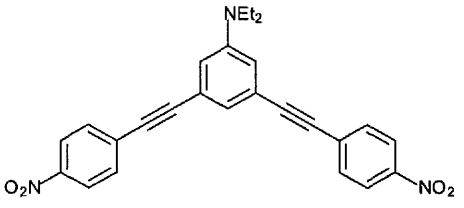

227. dioxane; λ_{max} = 393, 322 nm
$\beta_{zzz} = 46 \times 10^{-30}$ esu;
$\beta_{zyy} = 92 \times 10^{-30}$ esu;
$\beta_{yzy} = \beta_{yyz} = 84 \times 10^{-30}$ esu

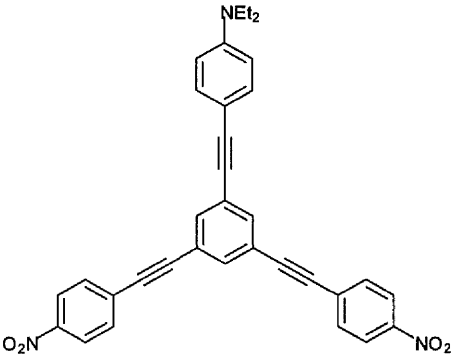

228. dioxane; λ_{max} = 340 nm;
$\beta_{zzz} = 197 \times 10^{-30}$ esu;
$\beta_{zyy} = 135 \times 10^{-30}$ esu;
$\beta_{yzy} = \beta_{yyz} = 135 \times 10^{-30}$ esu

Ruthenium complexes have been studied extensively for second-order NLO properties (see section 1.8) and large β values have been reported. The work presented in this chapter concentrates on extending our studies on ruthenium ammine complexes by moving to three-component chromophores which combine a Ru^{II} electron donor centre with two pyridinium acceptor groups. A series of symmetrical complexes *cis*-$[Ru^{II}(NH_3)_4(L_A)_2]^{4+}$ (L_A = MeQ^+, PhQ^+, $AcPhQ^+$ or $PymQ^+$) have been investigated. These complexes have C_{2v} symmetry and hence may be expected to exhibit two-dimensional β responses. A series of symmetrical and asymmetrical complexes *trans*-

$[Ru^{II}(NH_3)_4(L_A)_2]^{4+}$ and *trans*-$[Ru^{II}(NH_3)_4(L_{A1})(L_{A2})]^{4+}$ have also been prepared. The symmetrical trans complexes will not exhibit second-order molecular NLO effects, but their asymmetrical counterparts may to some extent.

5.2 *Experimental*

5.2.1 Materials and procedures

The compound $RuCl_3 \cdot 2H_2O$ was supplied by Johnson Matthey plc. The salts *cis*-$[Ru^{III}(NH_3)_4Cl_2]Cl$,[154] $[MeQ^+]I$,[90] $[PhQ^+]Cl \cdot 2H_2O$,[91] $[AcPhQ^+]Cl \cdot 2H_2O$,[91] $[PymQ^+]Cl$,[115b] and *trans*-$[Ru^{II}Cl(NH_3)_4(SO_2)]Cl$[94] were prepared as described in the literature. All other reagents were obtained commercially and used as supplied. Products were dried overnight at room temperature in a vacuum desiccator ($CaSO_4$) prior to characterization.

5.2.2 Physical measurements

These details were as for Chapter 2 except the cyclic voltammetric measurements were carried out by using an EG&G PAR model 173 potentiostat/galvanostat with a model 175 universal programmer. A single-compartment cell was used with a Ag/3M NaCl/saturated AgCl reference electrode separated by a salt bridge from the platinum-bead working electrode and platinum-wire auxiliary electrode. Acetonitrile (HPLC grade) was used as received and tetra-*n*-butyl ammonium hexafluorophosphate, twice recrystallized from ethanol and dried *in vacuo*, as supporting electrolyte. Solutions containing *ca.* 10^{-3} M analyte (0.1 M electrolyte) were deaerated by purging with N_2. All $E_{1/2}$ values were calculated from $(E_{pa} + E_{pc})/2$ at a scan rate of 200 mV s^{-1}.

5.2.3 Syntheses

***cis*-[$Ru^{II}(NH_3)_4(MeQ^+)_2$][PF_6]$_4$ 229.** A solution of *cis*-[$Ru^{III}(NH_3)_4Cl_2$]Cl (55 mg, 0.200 mmol) in degassed water (5 mL) acidified with TFA (3 drops) was reduced over zinc amalgam (5 lumps) for 15 min with Ar agitation. The solution was filtered under Ar into a flask containing [MeQ^+]I (298 mg, 1.00 mmol) and the reaction was stirred in the dark under Ar for 5 h. Acetone (850 mL) was added and a crude halide product was collected by filtration, washed with acetone and dried. This material was metathesised using water/aqueous NH_4PF_6 to yield a dark blue solid. Purification was achieved by precipitation from acetone/aqueous NH_4PF_6: yield 109 mg (49%). $\delta_H(CD_3COCD_3)$ 9.12 (d, 4 H, *J* 6.9 Hz, $2C_5H_4N$), 8.88 (d, 4 H, *J* 6.9 Hz, $2C_5H_4N$), 8.66 (d, 4 H, *J* 7.0 Hz, $2C_5H_4N$), 7.95 (d, 4 H, *J* 6.9 Hz, $2C_5H_4N$), 4.61 (s, 6 H, 2Me), 3.39 (s, 6 H, $2NH_3$), 2.99 (s, 6 H, $2NH_3$) (Found: C, 23.69; H, 3.19; N, 9.63. Calc. for $C_{22}H_{34}N_8RuP_4F_{24}$•$1.5H_2O$: C, 23.62; H, 3.33; N, 10.02%).

***cis*-[$Ru^{II}(NH_3)_4(PhQ^+)_2$][PF_6]$_4$ 230.** This was prepared in an identical fashion to **229** using [PhQ^+]Cl•$2H_2O$ (305 mg, 1.00 mmol) instead of [MeQ^+]I. Acetone (150 mL) was added to precipitate the crude chloride product. Purification was achieved by sequential precipitations from acetone/diethyl ether: yield 120 mg (49%). $\delta_H(CD_3COCD_3)$ 9.42 (d, 4 H, *J* 7.2 Hz, $2C_5H_4N$), 8.95 (d, 4 H, *J* 6.9 Hz, $2C_5H_4N$), 8.84 (d, 4 H, *J* 7.2 Hz, $2C_5H_4N$), 8.05 (d, 4 H, *J* 7.0 Hz, $2C_5H_4N$), 8.01–7.96 (m, 4 H, 2Ph), 7.85–7.79 (m, 6 H, 2Ph), 3.45 (s, 6 H, $2NH_3$), 3.04 (s, 6 H, $2NH_3$) (Found: C, 31.34; H, 3.24; N, 9.01. Calc. for $C_{32}H_{38}N_8RuP_4F_{24}$•$0.5H_2O$: C, 31.38; H, 3.21; N, 9.15%).

***cis*-[$Ru^{II}(NH_3)_4(AcPhQ^+)_2$][$PF_6$]$_4$ 231.** This was prepared and purified in an identical fashion to **229** using [$AcPhQ^+$]Cl•$2H_2O$ (347 mg, 1 mmol) instead of [MeQ^+]I. Acetone (100 mL) was added to precipitate the crude chloride product: yield 121 mg (46%). $\delta_H(CD_3COCD_3)$ 9.47 (d, 4 H, *J* 6.9 Hz, $2C_5H_4N$), 8.95 (d, 4 H, *J* 6.8 Hz, $2C_5H_4N$), 8.87 (d, 4 H, *J* 6.8 Hz, $2C_5H_4N$), 8.36 (d, 4 H, *J* 8.8 Hz, $2C_6H_4$), 8.15 (d, 4 H, *J* 8.8 Hz, $2C_6H_4$),

8.05 (d, 4 H, *J* 6.8 Hz, $2C_5H_4N$), 3.46 (s, 6 H, $2NH_3$), 3.05 (s, 6 H, $2NH_3$), 2.72 (s, 6 H, 2Me) (Found: C, 32.92; H, 2.87; N, 8.26. Calc. for $C_{36}H_{42}N_8O_2RuP_4F_{24}\cdot H_2O$: C, 32.81; H, 3.37; N, 8.50%).

***cis*-$[Ru^{II}(NH_3)_4(PymQ^+)_2][PF_6]_4$ 232.** This was prepared and purified in an identical fashion to **231** using $[PymQ^+]Cl$ (271 mg, 1 mmol) instead of $[AcPhQ^+]Cl\cdot 2H_2O$. Further purification was achieved by precipitation from acetone/aqueous NH_4PF_6: yield 64 mg (26%). $\delta_H(CD_3COCD_3)$ 10.26 (d, 4 H, *J* 7.3 Hz, $2C_5H_4N$), 9.27 (d, 4 H, *J* 4.8 Hz, $2C_4H_3N_2$), 9.01–8.92 (m, 8 H, $4C_5H_4N$), 8.11 (d, 4 H, *J* 7.0 Hz, $2C_5H_4N$), 8.04 (t, 2 H, *J* 4.9 Hz, $2C_4H_3N_2$), 3.53 (s, 6 H, $2NH_3$), 3.09 (s, 6 H, $2NH_3$) (Found: C, 27.13; H, 2.64; N, 13.13. Calc. for $C_{28}H_{34}N_{12}RuP_4F_{24}\cdot H_2O$: C, 27.17; H, 2.93; N, 13.58%).

***trans*-$[Ru^{II}(NH_3)_4(MeQ^+)_2][PF_6]_4$ 233.** A mixture of *trans*-$[Ru^{II}Cl(NH_3)_4(SO_2)]Cl$ (100 mg, 0.329 mmol) and $[MeQ^+]I$ (196 mg, 0.658 mmol) was dissolved in water (5 mL) and heated at *ca.* 50 °C under Ar for 30 min. Acetone (30 mL) was added to the brown solution and a brown precipitate was filtered off, washed with acetone and dried. This material (a mixture of chloride or iodide salts of *trans*-$[Ru^{II}(MeQ^+)(NH_3)_4(SO_2)]^{3+}$ and unreacted $[MeQ^+]I$) was dissolved in water (5 mL) and oxidized by the addition of a 1:1 mixture of 30% aqueous H_2O_2/2M HCl (3 mL). After 5 min at room temperature, a brown precipitate was filtered off, washed with water and discarded. Acetone (200 mL) was added to the filtrate and a golden yellow precipitate was filtered off, washed with acetone and dried to afford *trans*-$[Ru^{III}(NH_3)_4(SO_4)(MeQ^+)]Cl_2$. This product was dissolved in water (5 mL) and reduced over zinc amalgam (5 lumps) with Ar agitation for 15 min. The deep blue solution was then filtered under Ar into a flask containing $[MeQ^+]I$ (196 mg, 0.658 mmol) and the solution was stirred at room temperature in the dark under Ar for 24 h. The addition of acetone (100 mL) to the deep blue solution gave a dark precipitate which was filtered off, washed with acetone dried. This crude material was metathesized by precipitation from water/aqueous NH_4PF_6. Further purification was effected by precipitation from acetone/aqueous NH_4PF_6, then from acetone/diethyl ether: yield 188 mg (36%). $\delta_H(CD_3COCD_3)$ 9.21 (d, 4 H, *J* 6.9 Hz, $2C_5H_4N$), 9.19 (d, 4 H, *J* 7.2 Hz, $2C_5H_4N$),

8.73 (d, 4 H, *J* 7.0 Hz, $2C_5H_4N$), 8.16 (d, 4 H, *J* 6.9 Hz, $2C_5H_4N$), 4.65 (s, 6 H, 2Me), 2.90 (s, 12 H, $4NH_3$) (Found: C, 24.34; H, 3.27; N, 10.11. Calc. for $C_{22}H_{34}N_8RuP_4F_{24}$: C, 24.21; H, 3.14; N, 10.27%).

***trans*-$[Ru^{II}(NH_3)_4(PhQ^+)_2][PF_6]_4$ 234.** This was prepared and purified in a similar fashion to **233**, using $[PhQ^+]Cl{\bullet}2H_2O$ (200 mg, 0.658 mmol) instead of $[MeQ^+]I$. Following the oxidation step no brown precipitate was produced and the *trans*-$[Ru^{III}(PhQ^+)(NH_3)_4(SO_4)]Cl_2$ product was precipitated with acetone (100 mL): yield 159 mg (39%). $\delta_H(CD_3COCD_3)$ 9.49 (d, 4 H, *J* 7.1 Hz, $2C_5H_4N$), 9.27 (d, 4 H, *J* 6.8 Hz, $2C_5H_4N$), 8.92 (d, 4 H, *J* 7.1 Hz, $2C_5H_4N$), 8.26 (d, 4 H, *J* 6.8 Hz, $2C_5H_4N$), 8.04–7.98 (m, 4 H, 2Ph), 7.84–7.81 (m, 6 H, 2Ph), 2.94 (s, 12 H, $4NH_3$) (Found: C, 31.05; H, 3.25; N, 8.76. Calc. for $C_{32}H_{38}N_8RuP_4F_{24}{\bullet}H_2O$: C, 31.16; H, 3.27; N, 9.08%).

***trans*-$[Ru^{II}(NH_3)_4(AcPhQ^+)_2][PF_6]_4$ 235.** This was prepared and purified in a similar fashion to **234**, using $[AcPhQ^+]Cl{\bullet}2H_2O$ (228 mg, 0.658 mmol) instead of $[PhQ^+]Cl{\bullet}2H_2O$: yield 123 mg (29%). $\delta_H(CD_3COCD_3)$ 9.54 (d, 4 H, *J* 7.0 Hz, $2C_5H_4N$), 9.27 (d, 4 H, *J* 6.7 Hz, $2C_5H_4N$), 8.94 (d, 4 H, *J* 7.0 Hz, $2C_5H_4N$), 8.38 (d, 4 H, *J* 8.8 Hz, $2C_6H_4$), 8.27 (d, 4 H, *J* 6.7 Hz, $2C_5H_4N$), 8.17 (d, 4 H, *J* 8.7 Hz, $2C_6H_4$), 2.95 (s, 12 H, $4NH_3$), 2.86 (s, 6 H, 2Me) (Found: C, 33.27; H, 3.36; N, 8.25. Calc. for $C_{36}H_{42}N_8O_2RuP_4F_{24}$: C, 33.27; H, 3.21; N, 8.62%).

***trans*-$[Ru^{II}(NH_3)_4(PymQ^+)_2][PF_6]_4$ 236.** This was prepared and purified in a similar fashion to **234**, using $[PymQ^+]Cl$ (178 mg, 0.658 mmol) instead of $[PhQ^+]Cl{\bullet}2H_2O$: yield 176 mg (43%). $\delta_H(CD_3COCD_3)$ 10.32 (d, 4 H, *J* 7.3 Hz, $2C_5H_4N$), 9.32 (d, 4 H, *J* 6.9 Hz, $2C_5H_4N$), 9.29 (d, 4 H, *J* 4.9 Hz, $2C_4H_3N_2$), 9.00 (d, 4 H, *J* 7.3 Hz, $2C_5H_4N$), 8.30 (d, 4 H, *J* 6.9 Hz, $2C_5H_4N$), 8.04 (t, 2 H, *J* 4.9 Hz, $2C_4H_3N_2$), 2.97 (s, 12 H, $4NH_3$) (Found: C, 26.82; H, 2.79; N, 13.27. Calc. for $C_{28}H_{34}N_{12}RuP_4F_{24}{\bullet}2H_2O$: C, 26.78; H, 3.05; N, 13.38%).

***trans*-[$Ru^{II}(NH_3)_4(MeQ^+)(PhQ^+)][PF_6]_4$ 237.** This was prepared and purified in a similar fashion to **233**. The second portion of [MeQ^+]I was replaced by [PhQ^+]Cl•$2H_2O$ (200 mg, 0.658 mmol): yield 130 mg (34%). $\delta_H(CD_3COCD_3)$ 9.49 (d, 2 H, *J* 7.1 Hz, C_5H_4N), 9.27–9.18 (m, 6 H, $3C_5H_4N$), 8.91 (d, 2 H, *J* 7.2 Hz, C_5H_4N), 8.74 (d, 2 H, *J* 7.0 Hz, C_5H_4N), 8.24 (d, 2 H, *J* 6.9 Hz, C_5H_4N), 8.18 (d, 2 H, *J* 6.8 Hz, C_5H_4N), 8.04–7.99 (m, 2 H, Ph), 7.84–7.81 (m, 3 H, Ph), 4.66 (s, 3 H, Me), 2.92 (s, 12 H, $4NH_3$) (Found: C, 28.09; H, 3.10; N, 9.50. Calc. for $C_{27}H_{36}N_8RuP_4F_{24}$: C, 28.17; H, 3.15; N, 9.71%).

***trans*-[$Ru^{II}(NH_3)_4(MeQ^+)(AcPhQ^+)][PF_6]_4$ 238.** This was prepared and purified in a similar fashion to **233**. The second portion of [MeQ^+]I was replaced by [$AcPhQ^+$]Cl•$2H_2O$ (228 mg, 0.658 mmol): yield 124 mg (32%). $\delta_H(CD_3COCD_3)$ 9.53 (d, 2 H, *J* 7.2 Hz, C_5H_4N), 9.27–9.17 (m, 6 H, $3C_5H_4N$), 8.93 (d, 2 H, *J* 7.1 Hz, C_5H_4N), 8.74 (d, 2 H, *J* 7.0 Hz, C_5H_4N), 8.38 (d, 2 H, *J* 8.1 Hz, C_6H_4), 8.24 (d, 2 H, *J* 7.0 Hz, C_5H_4N), 8.18–8.14 (m, 4 H, C_5H_4N + C_6H_4), 4.65 (s, 3 H, Me), 2.92 (s, 12 H, $4NH_3$), 2.73 (s, 3 H, Me) (Found: C, 28.84; H, 3.32; N, 9.23. Calc. for $C_{29}H_{38}N_8ORuP_4F_{24}$: C, 29.13; H, 3.20; N, 9.37%).

***trans*-[$Ru^{II}(NH_3)_4(MeQ^+)(PymQ^+)][PF_6]_4$ 239.** This was prepared in a similar fashion to **233**. The second portion of [MeQ^+]I was replaced by [$PymQ^+$]Cl (178 mg, 0.658 mmol): yield 104 mg (27%). $\delta_H(CD_3COCD_3)$ 10.31 (d, 2 H, *J* 7.1 Hz, C_5H_4N), 9.31–9.18 (m, 8 H, $3C_5H_4N$ + $C_4H_3N_2$), 9.00 (d, 2 H, *J* 7.3 Hz, C_5H_4N), 8.74 (d, 2 H, *J* 6.9 Hz, C_5H_4N), 8.27 (d, 2 H, *J* 7.0 Hz, C_5H_4N), 8.19 (d, 2 H, *J* 6.8 Hz, C_5H_4N), 8.05 (t, 1 H, *J* 4.7 Hz, $C_4H_3N_2$), 4.66 (s, 3 H, Me), 2.94 (s, 12 H, $4NH_3$) (Found: C, 26.25; H, 2.79; N, 11.82. Calc. for $C_{25}H_{34}N_{10}RuP_4F_{24}$: C, 25.99; H, 2.97; N, 12.12%).

5.3 Results and Discussion

5.3.1 Molecular Design and Synthesis

The new three-component complexes in the salts **229–239** (Figure 30) were designed to probe the effects of the cis/trans arrangement of the acceptor substituted ligands on the electrochemical, electronic absorption and quadratic NLO properties.

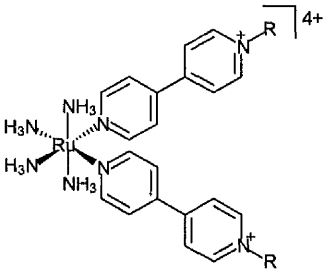

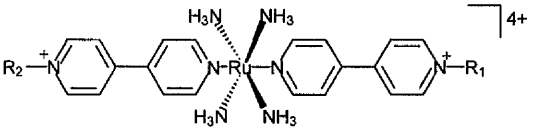

229. R = Me
230. R = Ph
231. R = AcPh
232. R = Pym

233. $R_1 = R_2$ = Me
234. $R_1 = R_2$ = Ph
235. $R_1 = R_2$ = AcPh
236. $R_1 = R_2$ = Pym

237. R_1 = Me, R_2 = Ph
238. R_1 = Me, R_2 = AcPh
239. R_1 = Me, R_2 = Pym

Figure 30. Structures of new complexes of the form *cis*-$[Ru^{II}(NH_3)_4(L_A)_2]^{4+}$, *trans*-$[Ru^{II}(NH_3)_4(L_A)_2]^{4+}$ and *trans*-$[Ru^{II}(NH_3)_4(L_{A1})(L_{A2})]^{4+}$.

Complex salts **229–232** were prepared using established synthetic ruthenium chemistry.[155] The Ru^{III} tetraammine dichloro species is reduced with zinc amalgam in the presence of trifluoroacetic acid (TFA), to produce the Ru^{II} tetraammine diaquo complex. Both aquo ligands can then be easily substituted by the incoming ligand L_A, to form the final product.

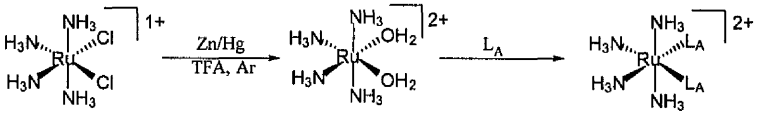

Complex salts **233–239** were prepared and purified using the methods outlined in Chapter 2, involving step-wise substitutions on the precursor *trans*-$[Ru^{II}Cl(NH_3)_4(SO_2)]Cl$.

5.3.2 Electronic Spectroscopy Studies

The electronic spectra of all the new complex salts were recorded in acetonitrile and the results are presented in Table 27. All of the complexes in **229–239** exhibit intense $\pi \rightarrow \pi^*$ intraligand absorptions in the UV region, together with intense, broad $d_\pi(Ru^{II}) \rightarrow \pi^*(L_A)$ (L_A = pyridinium-substituted ligand) visible MLCT bands. Complexes **229–232** show two MLCT bands with maxima in the region 497–644 nm, and in each case the lower energy band is more intense by *ca.* 20–32%. A representative spectrum of *cis*-$[Ru^{II}(NH_3)_4(PhQ^+)_2][PF_6]_4$, **230**, can be found in Figure 31.

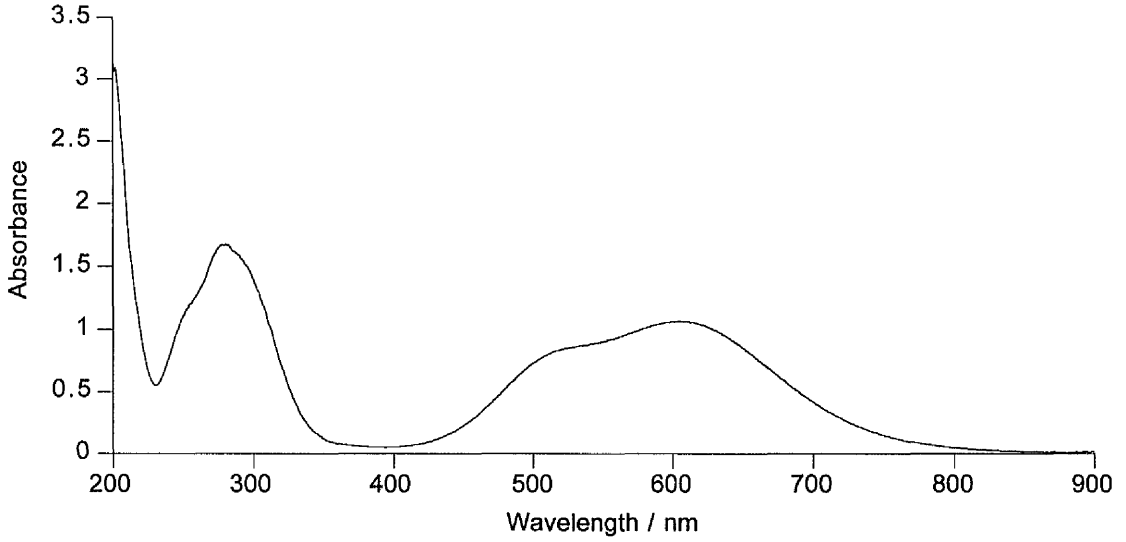

Figure 31. UV/Visible/NIR absorption spectrum of *cis*-$[Ru^{II}(NH_3)_4(PhQ^+)_2][PF_6]_4$, 230, in acetonitrile.

The energies of the MLCT bands depend on the relative energies of the Ru-based HOMO and the L_A-based LUMOs.[110] Two MLCT bands have been previously observed in *cis*-$[Ru^{II}(NH_3)_4(L)_2]^{2+}$ (L = pyridine, isonicotinamide, methyl isonicotinamide or pyrazine) complexes, as predicted by group theory.[156] Zwickel and Creutz[156] have carried out a MO treatment of complexes of the form $[Ru^{II}(NH_3)_5L]^{2+}$, *cis*-$[Ru^{II}(NH_3)_4L_2]^{2+}$ and *trans*-$[Ru^{II}(NH_3)_4L_2]^{2+}$ (L = pyridine based ligand) and made the following predictions: (i) *trans*-$[Ru^{II}(NH_3)_4L_2]^{2+}$ complexes should exhibit two MLCT transitions, but the higher energy transition is parity forbidden, (ii) *cis*-$[Ru^{II}(NH_3)_4L_2]^{2+}$ complexes should exhibit two orthogonal allowed MLCT transitions and (iii) $[Ru^{II}(NH_3)_5L]^{2+}$ complexes should

exhibit only one MLCT transition. The differences in energy between the two MLCT bands in **229–232** are *ca.* 0.31–0.34 eV and show no trend across the series. As with the complexes in **138**, **143**, **148** and **156**, electrochemical studies (see section 2.3.3) show that these complexes have an almost constant HOMO energy. Thus, as previously observed (see Chapter 2), $PymQ^+$ has the lowest LUMO energy of the 4,4′-bipyridinium ligands studied. The energies of both MLCT bands decrease in the order $L_A = MeQ^+ > PhQ^+ > AcPhQ^+ > PymQ^+$ with differences of *ca.* 0.25 and 0.26 eV between the lower energy and the higher energy bands, respectively, of **229** and **232** reflecting the increased acceptor strength of the pyridinium groups in **232**.

Table 27. UV/Visible/NIR data for complex salts 229–239.

Salt	λ_{max}/ nm (ε_{max} /M^{-1} cm^{-1})[a]	Energy/eV	Assignment
229 *cis*-$[Ru^{II}(NH_3)_4(MeQ^+)_2][PF_6]_4$	570 (19000)	2.18	$d\pi \rightarrow \pi^*$
	497 (15900)	2.50	$d\pi \rightarrow \pi^*$
	262 (37000)	4.73	$\pi \rightarrow \pi^*$
230 *cis*-$[Ru^{II}(NH_3)_4(PhQ^+)_2][PF_6]_4$	605 (20700)	2.05	$d\pi \rightarrow \pi^*$
	521 (16300)	2.38	$d\pi \rightarrow \pi^*$
	280 (32600)	4.43	$\pi \rightarrow \pi^*$
231 *cis*-$[Ru^{II}(NH_3)_4(AcPhQ^+)_2][PF_6]_4$	621 (23000)	2.00	$d\pi \rightarrow \pi^*$
	531 (17400)	2.34	$d\pi \rightarrow \pi^*$
	284 (46000)	4.37	$\pi \rightarrow \pi^*$
232 *cis*-$[Ru^{II}(NH_3)_4(PymQ^+)_2][PF_6]_4$	644 (22000)	1.93	$d\pi \rightarrow \pi^*$
	555 (17250)	2.23	$d\pi \rightarrow \pi^*$
	281 (49500)	4.41	$\pi \rightarrow \pi^*$
233 *trans*-$[Ru^{II}(NH_3)_4(MeQ^+)_2][PF_6]_4$	595 (27700)	2.08	$d\pi \rightarrow \pi^*$
	259 (35200)	4.79	$\pi \rightarrow \pi^*$
234 *trans*-$[Ru^{II}(NH_3)_4(PhQ^+)_2][PF_6]_4$	628 (29400)	1.97	$d\pi \rightarrow \pi^*$
	277 (31700)	4.48	$\pi \rightarrow \pi^*$
235 *trans*-$[Ru^{II}(NH_3)_4(AcPhQ^+)_2][PF_6]_4$	641 (31100)	1.93	$d\pi \rightarrow \pi^*$
	283 (43600)	4.38	$\pi \rightarrow \pi^*$
236 *trans*-$[Ru^{II}(NH_3)_4(PymQ^+)_2][PF_6]_4$	673 (33700)	1.84	$d\pi \rightarrow \pi^*$
	282 (53500)	4.40	$\pi \rightarrow \pi^*$
237 *trans*-$[Ru^{II}(NH_3)_4(MeQ^+)(PhQ^+)][PF_6]_4$	611 (29600)	2.03	$d\pi \rightarrow \pi^*$
	268 (31700)	4.63	$\pi \rightarrow \pi^*$
238 *trans*-$[Ru^{II}(NH_3)_4(MeQ^+)(AcPhQ^+)][PF_6]_4$	620 (30700)	2.00	$d\pi \rightarrow \pi^*$
	269 (35800)	4.61	$\pi \rightarrow \pi^*$
239 *trans*-$[Ru^{II}(NH_3)_4(MeQ^+)(PymQ^+)_2][PF_6]_4$	639 (28400)	1.94	$d\pi \rightarrow \pi^*$
	272 (38900)	4.56	$\pi \rightarrow \pi^*$

[a] Solutions (3–5) × 10^{-5} M.

In agreement with previous studies on related trans complexes,[156] **233–235** show one intense, broad MLCT band with maxima in the region 595–639 nm. A representative spectrum of *trans*-$[Ru^{II}(NH_3)_4(PhQ^+)_2][PF_6]_4$, **234**, can be found in Figure 32. The observation that this MLCT band is lower in energy than that of $[Ru^{II}(NH_3)_5(PhQ^+][PF_6]_3$, **143**, is attributed to π-coupling between the two PhQ^+ ligands.[156] As with **229–232** and other related complexes (see section 1.8.5 and Chapter 2), the MLCT band energy decreases in the order $L_A = MeQ^+ > PhQ^+ > AcPhQ^+ > PymQ^+$, with a difference of *ca.* 0.24 eV between **233** and **236** (and *ca.* 0.09 eV between **237** and **239**).

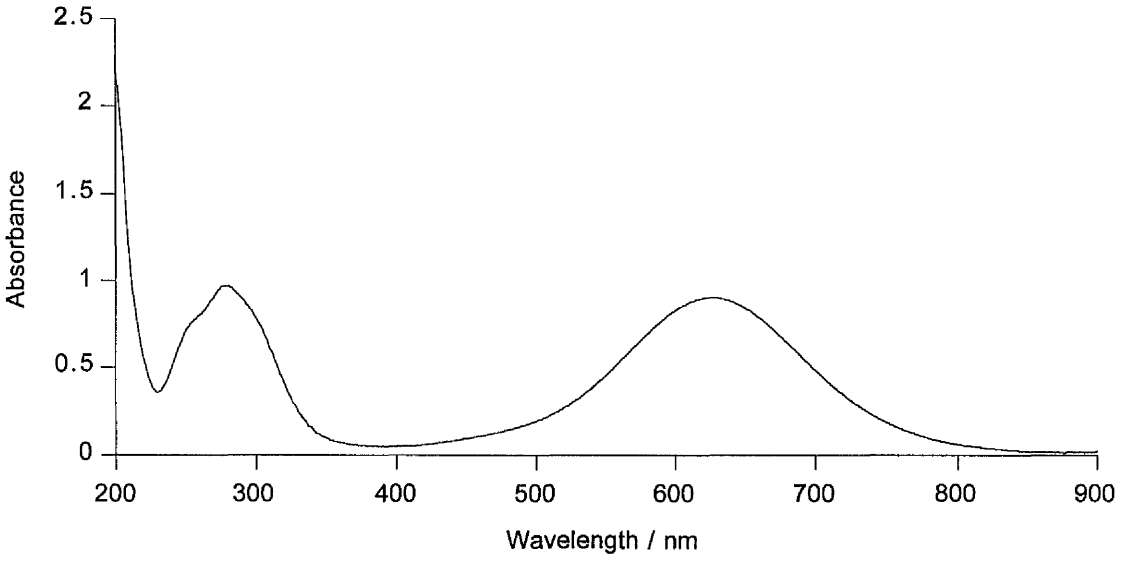

Figure 32. UV/Visible/NIR absorption spectrum of *trans*-$[Ru^{II}(NH_3)_4(PhQ^+)_2][PF_6]_4$, 234, in acetonitrile.

MLCT absorption data for **229–239** are collected in Table 28, with additional data for related complex salts of the ligands MeQ^+, PhQ^+, $AcPhQ^+$ and $PymQ^+$ for purposes of comparison.[90,91,115b] For a given L_A ligand, the MLCT energies of **229–232** are higher than those of the pentaammine complexes. This result seems logical, since substitution of NH_3 by a L_A ligand would be expected to deplete the electron density at the Ru^{II} centre. However, the MLCT energies of the trans isomers in **233–236** are similar to those of their pentaammine counterparts, an observation which is not readily explained.

Table 28. MLCT absorption data for complex salts 229–239 and previously studied $[Ru^{II}(NH_3)_5L_A][PF_6]_3$ complex salts.

Complex	λ_{max}/ nm (ε_{max} /M^{-1} cm^{-1})[a]	Energy/ eV
229 *cis*-$[Ru^{II}(NH_3)_4(MeQ^+)_2][PF_6]_4$	570 (19 000)	2.18
	497 (15 900)	2.50
230 *cis*-$[Ru^{II}(NH_3)_4(PhQ^+)_2][PF_6]_4$	605 (20 700)	2.05
	521 (16 300)	2.38
231 *cis*-$[Ru^{II}(NH_3)_4(AcPhQ^+)_2][PF_6]_4$	621 (23 000)	2.00
	531 (17 400)	2.34
232 *cis*-$[Ru^{II}(NH_3)_4(PymQ^+)_2][PF_6]_4$	644 (22 000)	1.93
	555 (17 250)	2.23
233 *trans*-$[Ru^{II}(NH_3)_4(MeQ^+)_2][PF_6]_4$	595 (27 700)	2.08
234 *trans*-$[Ru^{II}(NH_3)_4(PhQ^+)_2][PF_6]_4$	628 (29 400)	1.97
235 *trans*-$[Ru^{II}(NH_3)_4(AcPhQ^+)_2][PF_6]_4$	641 (31 100)	1.93
236 *trans*-$[Ru^{II}(NH_3)_4(PymQ^+)_2][PF_6]_4$	673 (33 700)	1.84
237 *trans*-$[Ru^{II}(NH_3)_4(MeQ^+)(PhQ^+)][PF_6]_4$	611 (29 600)	2.03
238 *trans*-$[Ru^{II}(NH_3)_4(MeQ^+)(AcPhQ^+)][PF_6]_4$	620 (30 700)	2.00
239 *trans*-$[Ru^{II}(NH_3)_4(MeQ^+)(PymQ^+)_2][PF_6]_4$	639 (28 400)	1.94
138 [c] $[Ru^{II}(NH_3)_5(MeQ^+)][PF_6]_3$	590 (15 800)	2.10
143 [c] $[Ru^{II}(NH_3)_5(PhQ^+)][PF_6]_3$	628 (19 300)	1.97
148 [c] $[Ru^{II}(NH_3)_5(AcPhQ^+)][PF_6]_3$	654 (18 000)	1.90
156 [d] $[Ru^{II}(NH_3)_5(PymQ^+)][PF_6]_3$	673 (18 000)	1.84

[b] Solutions (3–7) × 10^{-5} M. [c] Ref 91. [d] Ref 115b.

5.3.3 Electrochemical Studies

The new complex salts **229–239** were studied by cyclic voltammetry in acetonitrile and the results are presented in Table 29. All of the complexes show reversible or quasi-reversible $Ru^{III/II}$ oxidation waves as well as reversible and/or irreversible ligand-based reduction processes. Representative cyclic voltammograms of **230, 233** and **237** can be found in Figure 33. The related pentaammine complexes of MeQ^+, PhQ^+, $AcPhQ^+$ and $PymQ^+$ also show reversible/quasi-reversible/irreversible ligand reduction waves and the data for these complex salts are included in Table 29.

The $Ru^{III/II}$ $E_{1/2}$ values for **229–239** are all shifted by *ca.* 300 mV to more positive potentials compared with those of the related pentaammine complexes. These shifts reflect the decreased electron density at the metal center as a consequence of replacing one ammine with a L_A ligand. Within each series (**229–232, 233–236** and **237–239**) the $Ru^{III/II}$ $E_{1/2}$ value remains essentially constant, showing that the HOMO energy is not sensitive to the pyridinium substituent.

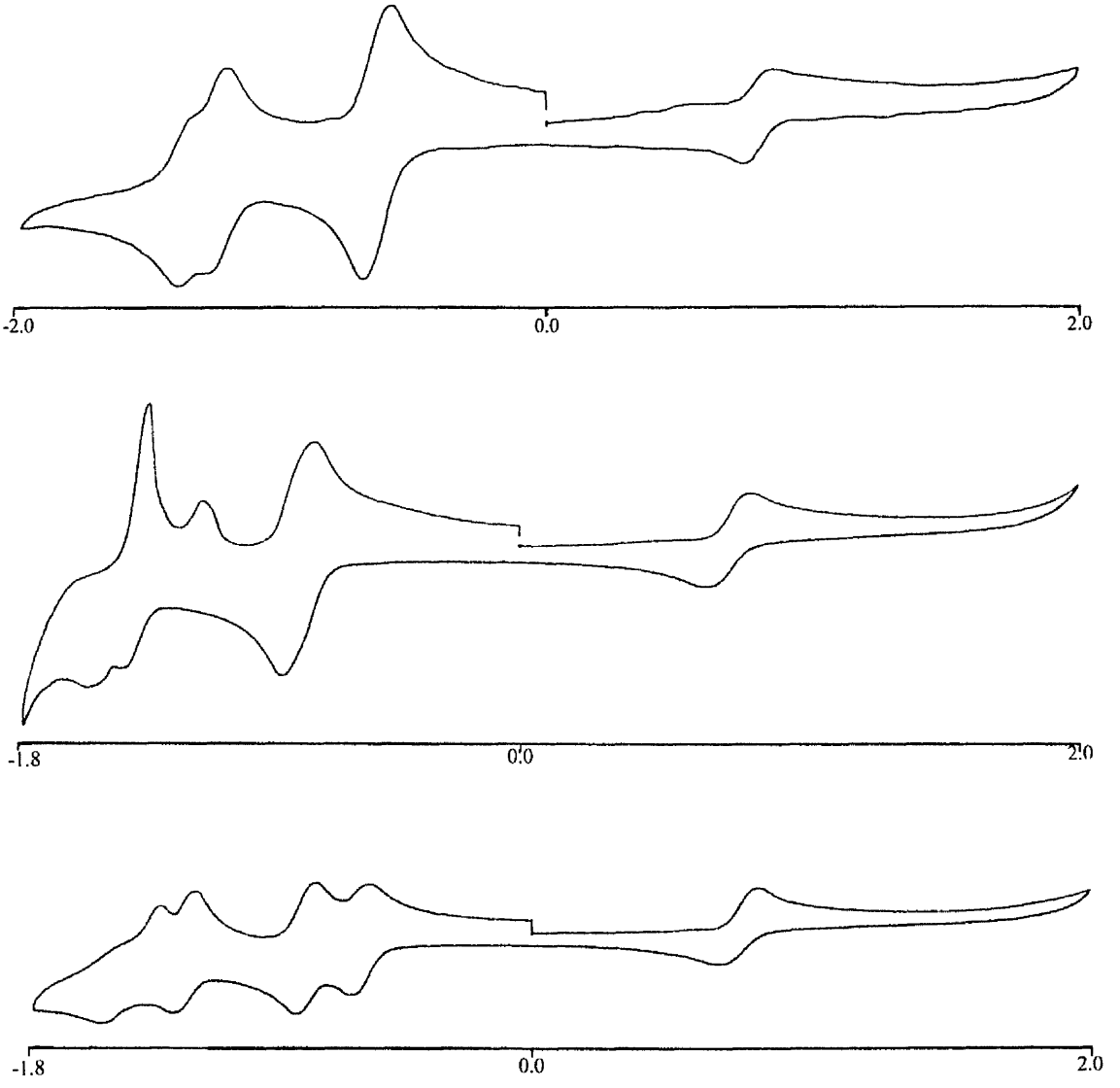

Figure 33 Cyclic voltammograms of 230 (top), 233 (middle) and 237 (bottom).

Salts **229–231** show especially interesting ligand-based electrochemistry. They all exhibit a reversible (presumably) two-electron $L_A^{+/0}$ ligand reduction process, the potential of which becomes less negative in the order L_A = MeQ^+ < PhQ^+ <$AcPhQ^+$, with a difference of *ca.* 280 mV between the extremes. This trend reflects the increasing acceptor strength of the L_A ligands and is mirrored in the red-shifting of the MLCT bands (see section 5.3.2). **232** however, does not show similar behaviour, exhibiting only one irreversible ligand reduction. **229** and **230** also each show two separate, reversible $L_A^{0/-}$ reduction processes. The differences between the two $E_{1/2}$ values for these processes are

ca. 120 and 150 mV, for **229** and **230** respectively, indicating that the neutral ligands communicate to some extent. By contrast, only one $L_A^{0/-}$ wave is observed for **231**.

The salts **233–235** all show one broad, ligand reduction wave comprising of two one-electron processes, as well as other irreversible processes. As with **229–232** the reduction waves shift to less negative potentials as the L_A acceptor strength increases. **235** shows just one irreversible ligand reduction process similar to that of **232**. **237–239** all show 3 reversible, one-electron ligand reduction waves, the least negative of which corresponds to the $L_A^{+/0}$ process of the *N*-aryl substituted ligand in each case. The second reduction wave represents $MeQ^{+/0}$ and remains constant across the series. The $L_A^{+/0}$ waves of **229–231**, **233–235** and **237–239** are *ca.* 10–80 mV less negative than those of the corresponding pentaammine complexes, reflecting the effect of the decreased donor strength of the Ru^{II} centres on the ligand-based waves.

Table 29. Electrochemical data for complex salts 229–239.

Complex	$E_{1/2}$/ V (ΔE_p/ mV) vs. Ag/AgCl[a]	
	$Ru^{III/II}$	Ligand Waves
229 *cis*-$[Ru^{II}(NH_3)_4(MeQ^+)_2][PF_6]_4$	0.78 (80)	–0.83 (100), –1.44 (75), –1.56 (80)
230 *cis*-$[Ru^{II}(NH_3)_4(PhQ^+)_2][PF_6]_4$	0.79 (80)	–0.65 (100), –1.25 (70), –1.40 (60)
231 *cis*-$[Ru^{II}(NH_3)_4(AcPhQ^+)_2][PF_6]_4$	0.80 (120)	–0.55 (120), –1.11 (260)
232 *cis*-$[Ru^{II}(NH_3)_4(PymQ^+)_2][PF_6]_4$	0.81 (110)	–0.42[b]
233 *trans*-$[Ru^{II}(NH_3)_4(MeQ^+)_2][PF_6]_4$	0.73 (100)	–0.84 (130), –1.39[d], –1.46[c]
234 *trans*-$[Ru^{II}(NH_3)_4(PhQ^+)_2][PF_6]_4$	0.75 (90)	–0.67 (100), –1.22[d], –1.26[c], –1.37[c]
235 *trans*-$[Ru^{II}(NH_3)_4(AcPhQ^+)_2][PF_6]_4$	0.76 (90)	–0.57 (100), –1.10[c]
236 *trans*-$[Ru^{II}(NH_3)_4(PymQ^+)_2][PF_6]_4$	0.75 (80)	–0.45[b]
237 *trans*-$[Ru^{II}(NH_3)_4(MeQ^+)(PhQ^+)][PF_6]_4$	0.71 (100)	–0.67 (70), –0.87 (70), –1.28 (80)
238 *trans*-$[Ru^{II}(NH_3)_4(MeQ^+)(AcPhQ^+)][PF_6]_4$	0.73 (90)	–0.59 (80), –0.85 (80), –1.12 (150)
239 *trans*-$[Ru^{II}(NH_3)_4(MeQ^+)(PymQ^+)_2][PF_6]_4$	0.73 (90)	–0.42 (90), –0.86 (70), –1.17 (100)
138 [e] $[Ru^{II}(NH_3)_5(MeQ^+)][PF_6]_3$	0.48	–0.89 (70), –1.50 (70)
143 [e] $[Ru^{II}(NH_3)_5(PhQ^+)][PF_6]_3$	0.48	–0.73(70), –1.33 (70)
148 [e] $[Ru^{II}(NH_3)_5(AcPhQ^+)][PF_6]_3$	0.49	–0.62(70), –1.15 (155)[c]
156 [f] $[Ru^{II}(NH_3)_5(PymQ^+)][PF_6]_3$	0.51	–0.43(200)[c]

[a] Measured in solutions *ca.* 10^{-3} M in analyte and 0.1 M in $NBu^n_4PF_6$ at a platinum-bead working electrode with a scan rate of 200 mV s^{-1}. Ferrocene internal reference $E_{1/2}$ = 0.43 V. ΔE_p = 100 mV. [b] E_{pc} for an irreversible reduction process. [c] Irreversible process as evidenced by $i_{pc} \neq i_{pa}$. [d] E_{pa} for an irreversible oxidation process. [e] Ref 91. [f] Ref 115b.

5.3.4 ^{1}H NMR Studies

The ^{1}H NMR spectra of the new Ru^{II} complex salts are well defined and therefore allow unambiguous identification and assessment of purity. The presence of two singlets in the region 3.39–3.53 and 2.99–3.09 ppm for the ammine ligands confirms the cis geometry in salts **229–232**. Similarly, a singlet in the region 2.90–2.97 ppm confirms the trans geometry in salts **233–239**. Selected ^{1}H NMR data for various signals of the complex salts **229–239**, as well as data for related compounds are presented in Table 30.

Table 30. Selected ^{1}H NMR data for 229–239 and related compounds.[a]

Salt	Pyridinium *ortho*-H	NH_3 trans to L_A	NH_3 cis to L_A
229 *cis*-$[Ru^{II}(NH_3)_4(MeQ^+)_2][PF_6]_4$	9.12	3.39	2.99
230 *cis*-$[Ru^{II}(NH_3)_4(PhQ^+)_2][PF_6]_4$	9.42	3.45	3.04
231 *cis*-$[Ru^{II}(NH_3)_4(AcPhQ^+)_2][PF_6]_4$	9.47	3.46	3.05
232 *cis*-$[Ru^{II}(NH_3)_4(PymQ^+)_2][PF_6]_4$	10.26	3.53	3.09
233 *trans*-$[Ru^{II}(NH_3)_4(MeQ^+)_2][PF_6]_4$	9.21	–	2.90
234 *trans*-$[Ru^{II}(NH_3)_4(PhQ^+)_2][PF_6]_4$	9.49	–	2.94
235 *trans*-$[Ru^{II}(NH_3)_4(AcPhQ^+)_2][PF_6]_4$	9.54	–	2.95
236 *trans*-$[Ru^{II}(NH_3)_4(PymQ^+)_2][PF_6]_4$	10.32	–	2.97
237 *trans*-$[Ru^{II}(NH_3)_4(MeQ^+)(PhQ^+)][PF_6]_4$	9.49[b]	–	2.92
238 *trans*-$[Ru^{II}(NH_3)_4(MeQ^+)(AcPhQ^+)][PF_6]_4$	9.53[b]	–	2.92
239 *trans*-$[Ru^{II}(NH_3)_4(MeQ^+)(PymQ^+)][PF_6]_4$	10.31[b]	–	2.94
138[c] $[Ru^{II}(NH_3)_5(MeQ^+)][PF_6]_3$	9.15	3.50	2.66
143[c] $[Ru^{II}(NH_3)_5(PhQ^+)][PF_6]_3$	9.33	3.60	2.70
148[c] $[Ru^{II}(NH_3)_5(AcPhQ^+)][PF_6]_3$	9.40	3.64	2.72
156[c] $[Ru^{II}(NH_3)_5(PymQ^+)][PF_6]_3$	10.17	3.75	2.74
[d] $[PymQ^+][PF_6]$	10.36	–	–

[a] Recorded in d_6-acetone on a Varian Gemini 200 spectrometer; all shifts referenced to $SiMe_4$. [b] Signals for ortho-H on *N*-aryl substituted ligand. [c] Ref 91. [d] Chapter 2.

The chemical shifts of the signals for the protons *ortho* to the quarternised nitrogen atom are dependent on the acceptor strength of the *N*-substituent. In each case, replacing an *N*-Me with an *N*-Ph substituent results in a downfield shift of this signal by *ca.* 0.2–0.3 ppm. The magnitude of this shift further increases as the acceptor strength of L_A increases, up to *ca.* 1.0–1.1 ppm in the $PymQ^+$ complex salts.

In each of the series, the signals for the ammine ligands are shifted downfield as the acceptor strength of L_A increases. The extent of this shifting is greatest (0.25 ppm) for the signals for the ammine ligand trans to L_A in the pentaammine complexes. In **229–232** the corresponding shift is 0.14 ppm.

5.4 Conclusion

The salts **229–232** have two broad MLCT absorptions in the visible region and fulfil the molecular requirements for large β values. They also exhibit interesting ligand-based electrochemistry, particularly **229** and **230** in which a degree of communication between the singly reduced ligands is observed. **233–239** also show broad visible MLCT absorptions, but **233–236** are not expected to exhibit NLO properties due to their symmetrical molecular structures. **237–239** however, are asymmetrically substituted and therefore should exhibit molecular NLO effects to some extent.

In all cases, the MLCT absorptions show a degree of tunability (see Chapter 2), red-shifting with increasing L_A acceptor strength.

5.5 Further Work

Due to the positions and broadness of the visible absorptions in **229–232**, only HRS with a fundamental wavelength of 800 nm (SH at 400 nm) is viable. However, electroabsorption (Stark) spectroscopy could be used to determine the contribution of each MLCT absorption to β. Other electrochemical techniques (*e.g.* a.c. or square wave voltammetry) could also be used to study in more detail the interesting inter-ligand interactions in **229–231**.

The MLCT absorptions in **237–239** are sufficiently low in energy to allow HRS at 1064 nm. However, as with previous systems (see section 2.5), the ligands used have not been optimised to give the largest possible β values. The work described here represents only the beginning of such endeavours.

References

[1] T. H. Maiman, *Nature (London)*, 1960, **187**, 493.

[2] (a) P. A. Franken, A. E. Hill, C. W. Peters, *Phys. Rev. Lett.*, 1961, **7(4)**, 118. (b) P. A. Franken and J. F. Ward, *Rev. Mod. Phys.*, 1963, **35**, 23. (c) J. A. Giordmaine and R. C. Miller, *Phys. Rev. Lett.*, 1965, **14**, 973. (d) R. W. Terhune, P. D. Maker and C. M. Savage, *Phys. Rev. Lett.*, 1962, **8**, 404.

[3] (a) P. D. Maker, R. W. Terhune, M. Nissenoff and C. M. Savage, *Phys. Rev. Lett.*, 1962, **8**, 21. (b) G. D. Boyd, R. C. Miller, K. Nassau, W. L. Bond and A. Savage, *Appl. Phys. Lett.*, 1964, **5(11)**, 234. (c) J. E. Geusic, H. J. Levinstein, J. J. Rubin, S. Singh and L. G. Van Uitert, *Appl. Phys. Lett.*, 1967, **11(9)**, 269.

[4] S. Allen in *Molecular Electronics,* ed. G. J. Ashwell, Wiley, New York, 1992, p. 216-218.

[5] S. K. Kurtz and T. T. Perry, *J. Appl. Phys.*, 1968, **39**, 3798.

[6] *Laser Focus*, August 1987 p. 30; *Laser Focus World*, September 1989 p. 36.

[7] R.W. Terhune, P. D. Maker and C. M. Savage, *Appl. Phys. Lett.*, 1963, **2**, 54.

[8] R. F. Belt, G. Gashurov and Y. S. Liu, *Laser Focus*, October 1985, 110.

[9] J. D. Bierlein, A. Ferretti, L. H. Brixner and W. Y. Hsu, *Appl. Phys. Lett.*, 1987, **50**, 1216; J. D. Bierlein and H. Vanherzeele, *J. Opt. Soc. Am. B.*, 1987, **6**, 622.

[10] S. R. Marder in *Inorganic Materials*, 2nd edition; Eds. D. W. Bruce and D. O'Hare; Wiley, Chichester, 1996.

[11] (a) K. D. Singer and A. F. Gorito, *J. Chem. Phys.*, 1981, **75**, 3572. (b) J. L. Oudar and H. Le Person, *Opt. Commun.*, 1975, **15**, 258. (c) B. F. Levine and C. G. Bethea, *Appl. Phys. Lett.*, 1974, **24**, 445. (d) L. T. Cheng, W. Tam. S. R. Marder, A. E. Steigman, G. Rikken and C. W. Spangler, *J. Phys. Chem.*, 1991, **95**, 10643.

[12] (a) K.Clays and A. Persoons, *Phys. Rev. Lett.*, 1991, **66**, 2980. (b) K.Clays and A. Persoons, *Rev. Sci. Instrum.*, 1992, **63**, 3285.

[13] (a) K. Clays, A. Persoons and L. De Maeyer, *Adv. Chem. Phys.*, 1994, **85**, 455. (b) S. J. Cyvin, J. E. Rauch and J. C. Decius, *J. Chem. Phys.*, 1965, **43**, 4083.

[14] R. L. Sutherland in *Handbook of Nonlinear Optics* ed. Marcel Dekker, New York, 1996.

[15] E. Hendickx, C. Dehu, K. Clays, J. L. Brédas, A. Persoons in *Polymers for Second Order Non Linear Optics* eds. G. A. Lindsay and K. D. Singer, American Chemical Society, Washington D. C. 1995, p 82.

[16] T. Verbiest, S. Houbrechts, M. Kauranan, K. Clays and A. Persoons, *J. Mater. Chem.*, 1997, **7**, 2175.

[17] (a) *Nonlinear Optical Properties of Organic and Polymeric Materials*, ed. D. J. Williams, *ACS Symp. Ser.* 233, 1983. (b) *Materials for Nonlinear Optics: Chemical Perspectives*, eds. S. R. Marder, J. E. Sohn, G. D. Stucky, *ACS Symp. Ser.* 1991, 455. (c) D. J. Williams, *Angew. Chem. Int. Ed.*, 1984, **23**, 690.

[18] S. R. Marder, D. N. Beretan, L. –T. Cheng, *Science*, 1991, **252**, 103.

[19] (a) J. L. Oudar and D.S. Chemla, *J. Phys. Chem.*, 1977, **66**, 2664. (b) J. L. Oudar, *J. Chem. Phys.*, 1977, **67**, 466. (c) J. L. Oudar and J. Zyss, *Phys. Rev. A*, 1982, **26**, 2016.

[20] A. Willets, J. E. Rice and D. M. Burland, *J. Phys. Chem.*, 1992, **97**, 7590.

[21] S. R. Marder, B. Kippelen, A. K. –Y. Jen and N. Peyghambarian, *Nature*, 1997, **388**, 845.

[22] (a) C. B. Gorman and S. R. Marder, *Proc. Natl. Acad. Sci. USA*, 1993, **90**, 11297. (b) F. Meyers, S. R. Marder, B. M. Pierce and J. L. Brédas, *J. Am. Chem. Soc.*, 1994, **116**, 10703.

[23] (a) C. Khun, *Synth. Met.*, 1991, **41-43**, 3681. (b) G. H. Chen and S. Mukamel, *J. Am. Chem. Soc.*, 1995, **117**, 4945. (c) C. Dehu, F. Meyers, E. Hendrickx, K. Clays, A. Persoons, S. R. Marder and J. L. Brédas, *J. Am. Chem. Soc.*, 1995, **117**, 10127. (d) D. Q. Lu, G. H. Chen, J. W. Perry and W. D. Goddard, *J. Am. Chem. Soc.*, 1994, **116**, 10685.

[24] G. Bourhill, J. L. Brédas, L. –T. Cheng, S. R. Marder, F. Meyers, J. W. Perry and B. G. Tiemann, *J. Am. Chem. Soc.*, 1994, **116**, 2619.

[25] S. R. Marder, L. –T. Cheng, B. G. Tiemann, A. G. Friedle, M. Blanchard-Desce, J. W. Perry and J. Skindhoj, *Science*, 1994, **263**, 511.

[26] T. L. Gilchrist, *Heterocyclic Chemistry,* Wiley, New York 1985.

[27] (a) A. K. –Y. Jen, V. P. Rao, K. Y. Wang and K. J. Drost, *J. Chem. Soc. Chem. Comm.*, 1993, 90. (b) V. P. Rao, A. K. –Y. Jen, K. Y. Wang and K. J. Drost, *J. Chem. Soc. Chem. Comm.*, 1993, 1118.

[28] I. D. L. Albert, T. J. Marks and M. A. Ratner, *J. Am. Chem. Soc.*, 1997, **119**, 6575.

[29] C.-F. Shu and Y. -K. Wang, *J. Mater. Chem.*, 1998, **8**, 833.

[30] (a) B. F. Levine and C. G. Bethea, *J. Chem. Phys.*, 1977, **66**, 1070. (b) S. J. Lalama and A. F. Gorito, *Phys. Rev. A*, 1979, **20**, 1179.

[31] M. Barazoukas, M. Blanchard-Desce, D. Josse, J. -M. Lehn and J. Zyss, *J. Chem. Phys.*, 1989, **133**, 323.

[32] A. Dulcic, C. Flytanis, C. L. Tang, D. Pepin, M. Fehzan and Y. Hoplilliard, *J. Chem. Phys.*, 1981, **74**, 1559.

[33] J. O. Morley, V. J. Docherty and D. Pugh, *J. Chem. Soc. Perkin Trans II*, 1987, 1351.

[34] J. F. Nicoud and R. J. Tweig in *Nonlinear Optical Properties of Organic Molecules, Vol 1.* Eds D. S. Chemla and J. Zyss, Academic Press, New York, 1987, p 227.

[35] (a) C. -F. Shu, W. -J. Tsai and A. K. -Y. Jen, *Tetrahedron lett.*, 1996, **37**, 7055. (b) C. -F. Shu, W. -J. Tsai, J. -Y. Chen, A. K. -Y. Jen, Y. Zhang and T. -A. Chen, *J. Chem. Soc. Chem. Commun.*, 1996, 2279. (c) G. Heilig and W. Lüttke, *Chem. Ber.*, 1987, **120**, 1963. (d) C. -F. Shu, Y. -C. Shu, Z. -H. Gong, S. -M. Peng, G. -H. Lee and A. K. -Y. Jen, *Chem. Mater.*, 1998, **10**, 3284.

[36] (a) J. Zyss, *Nonlinear Opt.*, 1991, **1**, 3; (b) J. Zyss and I. Ledoux, *Chem. Rev.*, 1994, **94**, 77; (c) J. L. Brédas, F. Meyers, B. M. Pierce and J. Zyss, *J. Am. Chem. Soc.*, 1992, **114**, 4928; (d) M. Joffre, D. Yaron, J. Silbey and J. Zyss, *J. Chem. Phys.*, 1992, **97**, 5607. (e) P. D. Maker, *Phys. Rev. A*, 1970, **1**, 923; (f) D. S. Chemla, J. L. Oudar, J. Jerphagnon, *Phys. Rev. B*, 1975, **12**, 4534; (g) I. Ledoux, J. Zyss, J. Siegel, J. Brienne, J. -M. Lehn, *Chem. Phys. Lett.*, 1990, **172**, 440.

[37] (a) Y. Luo, A. Cesar and H. Agren, *Chem. Phys. Lett.*, 1996, **252**, 389. (b) J. -L. Brédas, J. Duhu, F. Meyers, A. Persoons and J. Zyss, *Mol. Cryst. Liq. Cryst. Sci. Technol. Sect B*, 1994, **6**, 263. (c) K. K. Baldridge and J. S. Siegel, *J. Am. Chem. Soc.*, 1993, **115**, 10782. (d) I. G. Voigt-Martin, G. Li, A. Yakimanski, G. Schulz and J. J. Wolff, *J. Am. Chem. Soc.*, 1996, **118**, 12830.

[38] C. Lambert, G. Nöll, E. Schmälzlin, K. Meerholz and C. Bräuchle, *Chem. Eur. J.*, 1998, **4**, 2129.

[39] C. R. Moylan, R. J. Tweig, V. Y. Lee, S. A. Swanson, K. M. Betterton, R. D. Miller, *J. Am. Chem. Soc.*, 1993, **115**, 12599.

[40] J. Zyss and J. L. Oudar, *Phys. Rev. A*, 1982, **26**, 2028.

[41] R. Wortmann, C. Glanaia, P. Krämer, R. Matschiner, J. J. Wolff, S. Kraft, B. Treptow, E. Barbu, D. Längle and G. Görlitz, *Chem. Eur. J.*, 1997, **3**, 1765.

[42] S. Stadler, C. Bräuchle, S. Brandl, R. Gompper, *Chem. Mater.*, 1996, **8**, 676.

[43] J. J. Wolff, F. Siegler, R. Matschiner and R. Wortmann, *Angew. Chem. Int. Ed.*, 2000, **39**, 1436.

[44] (a)S. Brasslet, F. Cherioux, P. Audebert and J. Zyss, *Chem. Mater.*, 1999, **11**, 1915. (b) F. Cherioux, P. Audebert and P. Hapiot, *Chem. Mater.*, 1998, **10**, 1984.

[45] (a) M. Blanchard-Desce, J. –B. Baudin, O. Ruel, L. Jullien, S. Brasselet and J. Zyss, *Optic. Mat.*, 1998, **9**, 276. (b) M. Blanchard-Desce, J. –B. Baudin, L. Jullien, O. Ruel, S. Brasselet and J. Zyss, *Optic. Mat.*, 1999, **12**, 333.

[46] (a) J. Zyss, J. F. Nicoud and M. Coquillay, *J. Phys. Chem.*, 1984, **81**, 4160. (b) R.J. Tweig and K. Jain, *ACS Symp. Ser.*, 1983, **233**, 57.

[47] (a) J. Zyss and G.Berthier, *J. Chem. Phys.*, 1982, **77**, 3635. (b) M. C. Etter and G. M. Frankenbach, *Chem. Mater.*, 1989, **1**, 10.

[48] (a) R. H. Tredgold, M. C. J. Young, P. Hodge and E. Khoshdel, *Thin solid films*, 1987, **151**, 441; (b) R. H. Tredgold, M. C. J. Young, R. Jones, P. Hodge, P. Kolinsky and R. J. Jones, *Elect. lett.*, 1988, **24**, 308; (c) M. C. J. Young, R. H. Tredgold and P. Hodge in *Organic materials for Non Linear Optics* (eds. R. A. Hann and D. Bloor) p. 354-360. Royal Society of Chemistry, London (1989); (d) C. Bossard, G. Drecher, B. Tieke and P. Günter, *Proc. SPIE Int. Soc. Opt. Eng.*, 1989, **1017**, 141.

[49] D. M. Burland, R. D. Miller and C. A. Walsh, *Chem. Rev.*, 1994, **94**, 31.

[50] (a) B. J. Coe, S. Houbrechts, I. Asselberghs and A Persoons, *Angew. Chem. Int. Ed.*, 1999, **38**, 366. (b) B. J. Coe, *Chem. Eur. J.* 1999, **5**, 2464.

[51] (a) N. J. Long *Angew. Chem. Int. Ed. Engl.*, 1995, **34**, 21. (b) I. R. Whittal, A. M. McDonagh and M. G. Humphrey, *Adv. Organomet. Chem.*, 1998, **42**, 291.

[52] M. L. H. Green, S. R. Marder, M. E. Thompson, J. A. Bandy, D. Bloor, P. V. Kolinsky and R. J. Jones, *Nature (London)*, 1987, **330**, 360.

[53] G. G. A. Balavoine, J. –C. Daran, G. Iftime, P. G. Lacroix, E. Manoury, J. A. Delaire, I. Maltey-Fanton, K. Nakatani and S. Di Bella, *Organometallics*, 1999, **18**, 21.

[54] J. C. Calabrese, L. –T. Cheng, J. C. Green, S. R. Marder and W. Tam, *J. Am. Chem. Soc.*, 1991, **113**, 7227.

[55] S. R. Marder, J. W. Perry, W. P. Schaefer, B. G. Tiemann, P. C. Groves and K. J. Perry, *Proc. SPIE Int. Soc. Opt. Eng.*, 1989, **117**, 108.

[56] S. R. Marder, J. W. Perry, B. G. Tiemann and W. P. Schaefer, *Organometallics*, 1991, **10**, 1896.

[57] L. –T. Cheng, W. Tam, G. R. Meredith and S. R. Marder, *Mol. Cryst. Liq. Cryst.*, 1990, **189**, 137.

[58] (a) D. R. Kanis, M. A. Ratner and T. J. Marks, *J. Am. Chem. Soc.*, 1990, **112**, 8203. (b) D. R. Kanis, M. A. Ratner and T. J. Marks, *J. Am. Chem. Soc.*, 1992, **114**, 10338. (c) D. R. Kanis, M. A. Ratner and T. J. Marks, *Chem. Rev.*, 1994, **94**, 95.

[59] S. Barlow, H. E. Bunting, C. Ringham, J. C. Green, G. U. Bublitz, S. G. Boxer, J. W. Perry and S. R. Marder, *J. Am. Chem. Soc.*, 1999, **121**, 3715.

[60] K. R. Justin–Thomas, J. T. Lin ans Y. S. Wen, *J. Organomet. Chem.*, 1999, **575**, 301.

[61] (a) J. Mata, S. Ureil, E. Peris, R. Llusar, S. Houbrechts and A. Persoons, *J. Organometallic. Chem.*, 1998, **562**, 197. (b) U. Behrens, H. Brussard, U. Hagenau, J. Heck, E. Hendrickx, J. Kornich, J. G. M. van der Linden, A. Persoons, A. L. Spek, N. Veldman, B. Voss and H. wang, *Chem. Eur. J.*, 1996, **2**, 98. (c) U. Hagenau, J. Heck, E. Hendickx, A. Persoons, T. Schuld and H. Wang, *Inorg. Chem.*, 1996, **35**, 7863.

[62] V. Alain, A. Fort, M. Barzoukas, C. T. Chen, M. Blanchard-Desce, S. R. Marder and J. W. Perry, *Inorg. Chem. Acta.*, 1996, **242**, 43.

[63] M. Ahlheim, M. Barzoukas, P.V.Bedworth, M. Blanchard-Desce, A. Fort, Z. –Y. Hu, S. R. Marder, J. W. Perry, C. Runser, M. Staehelin and B. Zysset, *Science*, 1996, **271**, 335.

[64] W. Wenseleers, A. W. Gerbrandij, E. Goovaerts, M. H. Garcia, M. P. Robalo, P. J. Mendes, J. C. Rodrigues and A. Dias, *J. Mater. Chem.*, 1998, **8**, 925.

[65] (a) I.-Y. Wu, J. T. Lin, J. Luo, S. –S. Sun, C. -S. Li, K. J. Lin, C. Tsai, C. –C. Hsu and J. –L. Lin, *Organometallics*, 1997, **16**, 2038. (b) S. Houbrechts, K. Clays, A. Persoons, V. Cadierno, M. P. Gamasa and J. Gimeno, *Organometallics*, 1996, **15**, 5266. (c) I. R. Whittall, M. G. Humphrey, A. Persoons and S. Houbrechts, *Organometallics*, 1996, **15**, 1935. (d) R. H. Naulty, A. M. McDonagh, I. R. Whittall, M. P. Cifuentes, M. G. Humphrey, S. Houbrechts, J. Maes, A. Persoons, G. A. Heath and D. C. R. Hockless, *J. Organomet. Chem.*, 1998, **563**, 137. (e) A. M. McDonagh, M. G. Humphrey, M. Samoc, B. Luther-Davies, S. Houbrechts, T. Wada, H. Sasabe and A. Persoons, *J. Am. Chem. Soc.*, 1999, **121**, 1405. (f) I. R. Whittall, M. P. Cifuentes, M. G. Humphrey, N. Luther-Davies, M. Samoc, S. Houbrechts, A. Persoons, G. A. Heath and D. C. R. Hockless, *J. Organomet. Chem.*, 1997, **549**, 127. (g) I. R. Whittall, M. G. Humphrey, M. Samoc, J. Swiatkiewicz and B. Luther-Davies, *Organometallics*, 1995, **14**, 5493. (h) I. R. Whittall, M. G. Humphrey, D. C. R. Hockless, B. W. Skelton and A. H. White, *J. Organomet. Chem.*, 1995, **14**, 3970. (i) A. M. McDonagh, I. R. Whittall, M. G. Humphrey, B. W. Skelton and A. H. White, *J. Organomet. Chem.*, 1996, **519**, 229. (j) I. R. Whittall, M. P. Cifuentes, M. J. Costigan, M. G. Humphrey, S. C. Goh, B. W. Skelton and A. H. White, *J. Organomet. Chem.*, 1994, **471**, 193. (k) A. M. McDonagh, I. R. Whittall, M. G. Humphrey, D. C. R. Hockless, B. Skelton and A. H. White, *J. Organomet. Chem.*, 1996, **523**, 33. (l) A. M. McDonagh, M. P. Cifuentes, I. R. Whittall, M. G. Humphrey, M. Samoc, B. Luther-Davies and D. C. R. Hockless, *J. Organomet. Chem.*, 1996, **526**, 99. (m) I. R. Whittall, M. G. Humphrey, S. Houbrechts, J. Maes, A. Persoons, S. Schmid and D. C. R. Hockless, *J. Organomet. Chem.*, 1997, **544**, 277.

[66] (a) R. H. Naulty, M. P. Cifuentes, M. G. Humphrey, S. Houbrechts, C. Boutton, A. Persoons, G. A. Heath, D. C. R. Hockless, B. Luther-Davies and M. Samoc, *J. Chem. Soc. Dalton Trans.*, 1997, 4167. (b) I. R. Whittall, M. G. Humphrey, M. Samoc, B. Luther-Davies and D. C. R. Hockless, *J. Organomet. Chem.*, 1997, **544**, 189. (c) I. R. Whittall, M. G. Humphrey, S. Hobrechts, A. Persoons and D. C. R. Hockless, *Organometallics*, 1996, **15**, 5738.

[67] I. R. Whittall, M. P. Cifuentes, M. G. Humphrey, B. Luther-Davies, M. Samoc, S. Houbrechts, A. Persoons, G. A. Heath and D. Bogsányi, *Organometallics*, 1997, **16**, 2631.

[68] S. Houbrechts, K. Clays, A. Persoons, V. Cadierno, M. P. Gamasa, J. Gimeno, I. R. Whittall and M. G. Humphrey, *Proc. SPIE Int. Soc. Opt. Eng.*, 1996, **2852**, 98.

[69] J. Buey, S. Coco, L. Díez, P. Espinet, J. M. Martin-Alvarez, J. Miguel, S. García-Granda, A. Tesuro, I. Ledoux and J. Zyss, *Organometallics*, 1998, **17**, 1750.

[70] C. C. Frazier, M. A. Harvey, M. P. Cockerhan, H. M. Hand, E. A. Chauchard and C. H. Lee, *J. Phys. Chem.*, 1986, **90**, 5703.

[71] O. Briel, K. Sünkel, I. Krossing, H. Nöth, E. Schmälzlin, K. Meerholz, C. Bräuche and W. Beck, *Eur. J. Inorg. Chem.*, 1999, 483.

[72] C. –T. Chen, S. –Y. Liau, K. –J. Lin and L.-L Lai, *Adv. Mater.*, 1998, **3**, 334.

[73] (a) S. M. LeCours, H. –W. Guan, S. G. Dimagno, C. H. Wang and M. J. Therien, *J. Am. Chem. Soc.*, 1996, **118**, 1497. (b) S. Priyadarshy, M. J. Therien and D. N. Beratan, *J. Am. Chem. Soc.*, 1996, **118**, 1504. (c) A. Sen, P. C. Ray, P. K. Das and V. Krishnan, *J. Phys, Chem.*, 1996, **100**, 19611.

[74] G. Roth, H. Fischer, T. Meyer-Friedrichsen, J. Heck, S. Houbrechts and A. Persoons, *Organometallics*, 1998, **17**, 1511.

[75] J. Heck, S. Dabek, T. Meyer–Friedrichsen and H. Wang, *Coord. Chem. Rev.*, 1999, **190–192**, 1217.

[76] M. Tam, T. Bannenberg, K. Baum, R. Frölich, T. Steiner, T. Meyer–Friedrichsen and J. Heck, *Eur. J. Inorg. Chem.*, 2000, 1161.

[77] S. R. Marder, D. N. Beraton, B. G. Tiemann, L. T. Cheng and W. Tam in *Organic Materials for Nonlinear optics II*, eds. R. A. Hann and D. Bloor, Royal Society of Chemistry, London, 1991, p 165.

[78] Y. Yamakazi, K. Hosono, H. Matsuda, N. Minami, M. Asai and H. Nakanishi, *Biotechnol. Bioeng.* ,1991, **38**, 1218.

[79] (a) M. Bourgault, C. Mountassir, H. Le Bozec, I. Ledoux, G. Pucetti and J. Zyss, *J. Chem. Soc. Chem. Commun.*, 1993, 1623. (b) M. Bourgault, T. Renouard, B. Lognone, C. Mountassir and H. Le Bozec, *Can. J. Chem.*, 1997, **75**, 318.

[80] W. M. Laidlaw, R. G. Denning, T. Verbeist, E. Chauchard and A. Persoons, *Proc. SPIE.-Int. Soc. Opt. Eng.*, 1994, **2143**, 14.

[81] (a) I. D. Morrison, R. G. Denning, W. M. Laidlaw and M. A. Stammers, *Rev. Sci. Instrum.*, 1996, **67**, 1445. (b) W. M. Laidlaw, R. G. Denning, T. Verbeist, E. Chauchard and A. Persoons, *Nature (London)*, 1993, **363**, 59.

[82] J. Zyss, C. Dhenaut, T. Chauvan and I. Ledoux, *Chem. Phys. Lett.*, 1993, **206**, 409.

[83] A. Juris, V. Balzani, F. Burigelletti, S. Campagna, P. Belser and A. Van Zelewski, *Coord. Chem. Rev.*, 1998, **84**, 85.

[84] (a) P. Dupau, T. Renouard and H. Le Bozec, *Tet. Lett.*, 1996, **37**, 7503. (b) T. Renouard, Ph. D. Thesis, University of Rennes, 1998.

[85] C. Dhenaut, I. Ledoux, I. D. F. Samuel, J. Zyss, M. Bougault and H. Le Bozec, *Nature*, 1995, **374**, 339.

[86] (a) J. Zyss, C. Dhenaut, S. Brasselet and I. Ledoux, unpublished results. (b) H. Le Bozec and T. Renouard, *Eur. J. Inorg. Chem.*, 2000, 229.

[87] F. W. Vance and J. T. Hupp, *J. Am. Chem. Soc.*, 1999, **121**, 4047.

[88] H. Sakaguchi, H. Nakamura, T. Nagamura, T. Ogawa and T. Matsuo, *Chem. Lett.*, 1989, 1715.

[89] B. J. Coe, G. Chadwick, S. Houbrechts and A. Persoons, *J. Chem. Soc. Dalton Trans.*, 1997, 1705.

[90] B. J. Coe, M. C. Chamberlain, J. P. Essex-Lopresti, S. Gaines, J. C. Jeffery, S. Houbrechts and A. Persoons, *Inorg. Chem.*, 1997, **36**, 3284.

[91] B. J. Coe, J. A. Harris, L. J. Harrington, J. C. Jeffery, L. H. Rees, S. Houbrechts and A. Persoons, *Inorg. Chem.*, 1998, **37**, 3391.

[92] C. R. Moylan, *J. Phys. Chem.*, 1994, **98**, 13513.

[93] B. J. Coe, T. Beyer, J. C. Jeffery, S. J. Coles, T. Gelbrich, M. B. Hursthouse and M. E. Light, *J. Chem. Soc. Dalton Trans.*, 2000, 797.

[94] J. C. Curtis, B. P. Sullivan and T. J. Meyer, *Inorg. Chem.*, 1983, **22**, 224.

[95] A. J. Blacker, J. Jazwinski and J.-M. Lehn, *Helv. Chim. Acta.*, 1987, **70**, 1.

[96] E. D. Bergmann, F. E. Crane Jr. and R. M. Fuoss, *J. Am. Chem. Soc.*, 1952, **74**, 5981.

[97] E. Hendrickx, K. Clays, A. Persoons, C. Dehu and J. L. Brédas, *J. Am. Chem. Soc.*, 1995, **117**, 3547.

[98] S. Houbrechts, K. Clays, A. Persoons, Z. Pikramenou and J.-M. Lehn, *Chem. Phys. Lett.*, 1996, **258**, 485.

[99] M. Stähelin, D. M. Burland and J. E. Rice, *Chem. Phys. Lett.*, 1992, **191**, 245.

[100] E. Hendrickx, C. Dehu, K. Clays, J. L. Brédas and A. Persoons, *ACS Symp. Ser.*, 1995, **601**, 82.

[101] Collect: Data collection software, R. Hooft, Nonius B.V., 1998.

[102] Z. Otwinowski and W. Minor, *Methods in Enzymology*, Vol. 276: Macromolecular Crystallography, Part A, p. 307, C. W. Carter, Jr. and R. M. Sweet, Eds., Academic Press, 1997.

[103] (a) R. H. Blessing, *Acta. Crystallogr., Sect. A*, 1995, **51**, 33. (b) R. H. Blessing, *J. Appl. Crystallogr.*, 1997, **30**, 421.

[104] S. Mackay, C. J. Gilmore, C. Edwards, M. Tremayne, N. Stewart, K. Shankland. MaXus: a computer program for the solution and refinement of crystal structures from diffraction data.

[105] G. M. Sheldrick, *Acta Crystallogr., Sect. A*, 1990, **46**, 467.

[106] G. M. Sheldrick, SHELXL 97, Program for crystal structure refinement, University of Göttingen, Germany, 1997.

[107] D. W. Clack, J. C. Evans, C. R. Morris and C. R. Rowlands, *J. Chem. Soc. Perkin Trans. II*, 1988, 1541.

[108] M. Horner and S. Hünig, *Liebigs Ann. Chem.*, 1982, 1183.

[109] (a) P. J. Stang, D. H. Cao, S. Saito and A. M. Arif, *J. Am. Chem. Soc.*, 1995, **117**, 6273. (b) S. Hünig, J. Groß, E. F. Lier and H. Quast, *Liebigs Ann. Chem.*, 1973, 339.

[110] (a) P. Ford, De F. R. Rudd, R. Gaunder and H. Taube, *J. Am. Chem. Soc.*, 1968, **90**, 1187. (b) C. R. Johnson and R. E. Shepherd, *Inorg. Chem.*, 1983, **22**, 2439.

[111] See, for example: (a) P. Ford, De F. P. Rudd, R. Gaunder and H. Taube,. *J. Am. Chem. Soc.*, 1968, **90**, 1187–1194. (b) P. C. Ford, D. Wink and J. Di Benedetto, *Prog. Inorg. Chem.*, 1983, **30**, 213–271. (c) J. C. Curtis, B. P. Sullivan and T. J. Meyer, *Inorg. Chem.*, 1983, **22**, 224. (d) J. L. Winkler, T. L. Netzel, C. Creutz and N. Sutin, *J. Am. Chem. Soc.*, 1987, **109**, 2381. (e) J. R. Reimers and N. S. Hush, *J. Phys. Chem.*, 1991, **95**, 9773. (f) C. Creutz, M. D. Newton and N. Sutin, *J. Photochem. Photobiol. A: Chem.*, 1994, **82**, 47.

[112] G. Bublitz and S. G. Boxer, *Ann. Rev. Phys. Chem.*, 1997, **48**, 213.

[113] (a) D. H. Oh and S. G. Boxer, *J. Am. Chem. Soc.*, 1990, **112**, 8161. (b) D. H. Oh, M. Sano and S. G. Boxer, *J. Am. Chem. Soc.*, 1991, **113**, 6880.

[114] (a) Y. K. Shin, B. S. Brunschwig, C. Creutz and N. Sutin, *J. Am. Chem. Soc.*, 1995, **117**, 8668. (b) Y. K. Shin, B. S. Brunschwig, C. Creutz and N. Sutin, *J. Phys. Chem.*, 1996, **100**, 8157. (c) B. S. Brunschwig, C. Creutz and N. Sutin, *Coord. Chem. Rev.*,1998, **177**, 61.

[115] (a) B. J. Coe, J. P. Essex-Lopresti, J. A. Harris, S. Houbrechts and A. Persoons, *J. Chem. Soc. Chem. Commun.*, 1997, 1645. (b) B. J. Coe, J. A. Harris, I. Asselberghs, A. Persoons, J. C. Jeffery, L. H. Rees, T. Gelbrich and M. B. Hursthouse, *J. Chem. Soc., Dalton Trans.*, 1999, 3617.

[116] (a) F. W. Vance, L. Karki, J. K. Reigle, J. T. Hupp and M. A. Ratner, *J. Phys. Chem. A*, 1998, **102**, 8320. (b) G. U. Bublitz, W. M. Laidlaw, R. G. Denning and S. G. Boxer, *J. Am. Chem. Soc.*, 1998, **120**, 6068. (c) F. W. Vance, R. V. Slone, C. S. Stern and J. T. Hupp, *Chem. Phys.*, 2000, **253**, 313.

[117] G. U. Bublitz, R. Ortiz, S. R. Marder and S. G. Boxer, *J. Am. Chem. Soc.*, 1997, **119**, 3365.

[118] L. Karki, F. W. Vance, J. T. Hupp, S. M. LeCours and M. J. Therien, *J. Am. Chem. Soc.*, 1998, **120**, 2606.

[119] (a) H. Labhart, *Adv. Chem. Phys.*, 1967, **13**, 179. (b) W. Liptay, In *Excited States*; Ed. E. C. Lim, Academic Press: New York, 1974: Vol. 1, pp 129–229. (c) W. Baumann, In *Physical Methods of Chemistry*; Eds. B. W. Rossiter, J. F. Hamilton, Wiley: New York, 1989; Vol. IIIB, pp 45–131. (d) W. Baumann, Z. Nagy, A. K. Maiti, H. Reis, S. V. Rodriques, N. Detzer, In *Dynamics and Mechanism of Photoinduced Charge Transfer and Related Phenomena*; Eds. N. Mataga, T. Okada, H. Masuhara, Elsevier, Amsterdam, 1992; pp 211–229.

[120] MSI Cerius^2 v 4.2 modelling software from Molecular Simulation Inc.

[121] B. J. Coe, J. A. Harris and B. S. Brunschwig, *J. Phys. Chem.*, 2001 *in press*.

[122] S. R. Marder, J. W. Perry, W. P. Schaefer, *Science*, 1989, **245**, 626.

[123] (a) S. R. Marder, J. W. Perry, B. G. Tiemann, R. E. Marsh and W. P. Schaefer, *Chem. Mater.*, 1990, **2**, 685. (b) S. R. Marder, J. W. Perry and C. P. Yakymyshyn, *Chem. Mater.*, 1994, **6**, 1137.

[124] X. –M. Duan, S. Okada, H. Oikawa, N. Matsuda and H. Nakanishi, *Mol. Cryst. Liq. Cryst.*, 1995, **276**, 89.

[125] (a) P.G. Lacroix, R. Clément, K. Nakatani, J. Zyss and I. Ledoux, *Science*, 1994, **263**, 658. (b) T. Cordin, R. Clément, P.G. Lacroix and K. Nakatani, *Chem. Mater.*, 1996, **8**, 2153.

[126] (a) D. Dunne, P. Hodge, Z. Ali-Adib, N. B. McKeown and D. West, *J. Mater. Chem.*, 1998, **8**, 1391. (b) P. Hodge, Z. Ali-Adib, D. West and T. King, *Thin Solid Films*, 1994, **224**, 1007.

[127] G. J. Ashwell, R. C. Hargreaves, C. E. Balwin, G. S. Bahra and C. R. Brown, *Nature*, 1992, **357**, 393.

[128] (a) R. Andreu, I. Malfant, P. G. Lacroix, H. Gornitzka and K. Nakatani, *Chem. Mater.*, 1999, **11**, 840. (b) I. Malfant, R. Andreu, P.. G. Lacroix, C. Faulmann and P. Cassoux, *Inorg. Chem.*, 1998, **37**, 3361.

[129] (a) C. Bosshard, K. Shutter, P. Prêtre, J. Hulliger, M. Flörsheimer, P. Kaatz, P. Günter, *Organic Nonlinear Optical Materials, Vol 1* eds. Gordon and Breach, Amsterdam 1995 (b) G. Knöpfle, R. Schlesser, R. Duret, and P. Günter, *Adv. Mater.*, 1996, **8**, 591. (c) Q. Wu, X. –C. Zhang, *Appl. Phys. Lett.*, 1996, **68**, 1604. (d) S. Sohma, H. Takahashi, T. taniuchi and H. Ito, *Chem. Phys.*, 1999, **245**, 359.

[130] V. Alain, M. Blanchard-Desce, I. Ledoux-Rak and J. Zyss, *J. Chem. Soc. Chem. Commun.*, 2000, 353.

[131] K. Clays, K. Wostyn, G. Olbrechts, A. Persoons, A. Watanabe, K. Nogi, X. –M. Duan, S. Okada, H. Oikawa, H. Nakanishi, H. Vogel, D. Beljonne and J. –L. Brédas, *J. Opt. Soc. Am. B*, 2000, **17**, 256.

[132] O. –K. Kim, L. –S. Choi, H. –Y. Zhang, X. –H. He and Y. –H. Shih, *J. Am. Chem. Soc.*, 1996, **118**, 12220.

[133] K. Clays, G. Olbrechts, T. Munters, A. Persoons, O. –K. Kim and L. –S. Choi, *Chem. Phys. Lett.*, 1998, **293**, 337.

[134] (a) D. Li, M. A. Ratner, T. J. Marks, C. Zhang and G. K. Wong, *J. Am. Chem. Soc.*, 1990, **112**, 8034. (b) W. Lin, W. Lin, G. Wong and T. J. Marks, *J. Am. Chem. Soc.*, 1990, **112**, 7389.

[135] P. G. Lacroix and K. Nakatani, *Adv. Mater.*, 1997, **9**, 1105.

[136] Murrill, *J. Am. Chem. Soc.*, 1899, **21**, 835.

[137] A. N. Kost, A. K. Sheinkman and N. F. Kazarinova, *J. Gen. Chem. USSR*, 1964, **34**, 2059.

[138] M. G. Hutchings, *Tetrahedron*, 1984, **40**, 2061.

[139] A. P. Phillips, *J. Org. Chem.*, 1949, **14**, 302.

[140] J. L. R. Williams, R. E. Adel, J. M. Carlson, G. A. Reynolds, D. G. Barden and J. A. Ford Jr, *J. Org. Chem.*, 1963, **28**, 387.

[141] M. Matsui, S. Kawamura, K. Shibata and H. Muramatsu, *Bull. Chem. Soc. Jpn.*, 1992, **65**, 71.

[142] B. R. Baker, M. H. Doll, *J. Med. Chem.*, 1971, **14**, 793.

[143] G. Olbrechts, R. Strobbe, K. Clays, A. Persoons, *Rev. Sci. Instrum.*, 1998, **69**, 2233.

[144] G. Olbrechts, K. Wostyn, K. Clays, A. Persoons, *Optics Lett.*, 1999, **24**, 403.

[145] SHELXTL 5.03 program system, Siemens Analytical X-Ray Instruments, Madison, WI, 1995.

[146] Collect, Data collection software, R. Hooft, Nonius B.V., Delft, The Netherlands, 1998.

[147] Z. Otwinowski and W. Minor, *Methods Enzymol.*, 1997, **276**, 307.

[148] S. Mackay, C. J. Gilmore, C. Edwards, M. Tremayne, N. Stewart, and K. Shankland, MAXUS, a computer program for the solution and refinement of crystal structures from dffraction data, University of Glasgow, UK, Nonius B.V., Delft, The Netherlands and MacScience Co. Ltd., Yokohama, Japan, 1998.

[149] B. J. Coe, J. A. Harris, K. Clays, A. Persoons, K. Wostyn and B. S. Brunschwig, *Chem. Commun.*, 2001 *in press*.

[150] S. F. Nelsen, H. Q. Tran and M. A. Nagy, *J. Am. Chem. Soc.*, 1998, **120**, 298.

[151] P. Kaatz and D. P. Shelton, *J. Chem. Phys.*, 1996, **105**, 3918.

[152] R. Wortmann, P. Krämer, C. Glania, S. Lebus, N. Detzer, *Chem. Phys.*, 1993, **173**, 99.

[153] J. J. Wolff, D. Längle, D. Hillenbrand, R. Wortmann, R. Matschiner, C. Glania, P. Krämer, *Adv. Mater.*, 1997, **9**, 138.

[154] S. E. Boggs, R. E. Clarke and P. C. Ford, *Inorg. Chim. Acta.*, 1996, **247**, 129.

[155] (a) L. A. Pavanin, E. Giesbrecht and E Tfouni, *Inorg. Chem.*, 1985, **24**, 4444. (b) L. A. Pavanin, Z. Novais da Rocha, E. Giesbrecht and E Tfouni, *Inorg. Chem.*, 1991, **30**, 2185. (c) F. Salaymeh, S. Berhane, R. Yusof, R. de la Rosa, E. Y. Fung, R. Matamoros, K. W. Lau, Q. Zheng, E. M. Kober and J. C. Curtis, *Inorg. Chem.*, 1993, **32**, 3895.

[156] A. M. Zwickel and C. Creutz, *Inorg. Chem.*, 1971, **10**, 2395.

Appendix A: Copies of Selected Publications

Ruthenium(II) ammine centres as efficient electron donor groups for quadratic non-linear optics

Benjamin J. Coe,*[a] Jonathan P. Essex-Lopresti,[a] James A. Harris,[a] Stephan Houbrechts[a] and André Persoons[b,c]

[a] *Department of Chemistry, University of Manchester, Oxford Road, Manchester, UK M13 9PL*
[b] *Laboratory of Chemical and Biological Dynamics, Center for Research on Molecular Electronics and Photonics, University of Leuven, Celestijnenlaan 200D, B-3001 Leuven, Belgium*
[c] *Optical Sciences Center, University of Arizona, Tucson, Arizona, AZ 85721, USA*

Ruthenium(II) complex salts *trans*-$[Ru(NH_3)_4(L^D)(L^A)][PF_6]_3$ (L^D = an N-donor ligand, L^A = a 4,4′-bipyridinium ligand) exhibit large, tunable static first hyperpolarizabilities β_0 which are associated with intense, visible metal-to-ligand charge-transfer excitations.

Organic materials possessing non-linear optical (NLO) properties are the focus of much current research activity directed towards applications in advanced electronics systems.[1] Within this field, transition-metal organometallic and coordination complexes have attracted limited attention,[2] but their great potential as novel NLO materials is yet to be fully explored.

Solution measurements of hyperpolarizability coefficients allow the correlation of NLO properties with molecular structure. This facilitates the rational design and synthesis of efficient NLO chromophores which may subsequently be incorporated into active materials. Extensive data concerning the first (quadratic) hyperpolarizability β is now available for purely organic compounds,[1] but corresponding information for metal complexes is scarce.[2] This situation is gradually being rectified and β values have been determined for selected complexes including bimetallic sesquifulvalenes,[3] Schiff-base derivatives,[4] and σ-acetylides.[5]

Recent reports show that ruthenium mixed-valence,[6] 2,2′-bipyridine (bipy),[7] and σ-acetylide[8] complexes can possess large β values, although two-photon excited luminescence may explain these results for the bipy complexes.[9] Ruthenium(II) ammine complexes are promising candidates as high β molecules due to the strong π-donor ability of the d^6 metal centres.[10] Such complexes are structurally versatile, and their readily accessible $Ru^{III/II}$ redox couples may permit reversible, molecular-level modulation of NLO properties.

A series of complex salts *trans*-$[Ru^{II}(NH_3)_4(L^D)(L^A)][PF_6]_3$ [Fig. 1; L^D = NH_3, L^A = *N*-methyl-4,4′-bipyridinium (MeQ^+) **1**, *N*-phenyl-4,4′-bipyridinium (PhQ^+) **2** or *N*-(2,4-dinitrophenyl)-4,4′-bipyridinium ($DNPhQ^+$) **3**; L^D = 1-methylimidazole (mim), L^A = MeQ^+ **4** or PhQ^+ **5**; L^D = 4-dimethylaminopyridine (dmap), L^A = MeQ^+ **6** or PhQ^+ **7**] have been synthesized by using established coordination chemistry based on $[Ru^{II}(NH_3)_5(H_2O)][PF_6]_2$ or *trans*-$[Ru^{II}Cl(NH_3)_4(SO_2)]Cl$;[11,12] **1**, **4** and **6** are known,[11,13] but the other salts are new. [PhQ^+]Cl and [$DNPhQ^+$]Cl were synthesized by using a modification of a literature report for *N*,*N*′-diphenyl-4,4′-bipyridinium dichloride.[14] All of the compounds have been fully characterized by using various techniques including UV–VIS spectroscopy and cyclic voltammetry,† and the first molecular hyperpolarizabilities β of the complex salts have been determined *via* the hyper-Rayleigh scattering (HRS) technique.[15]

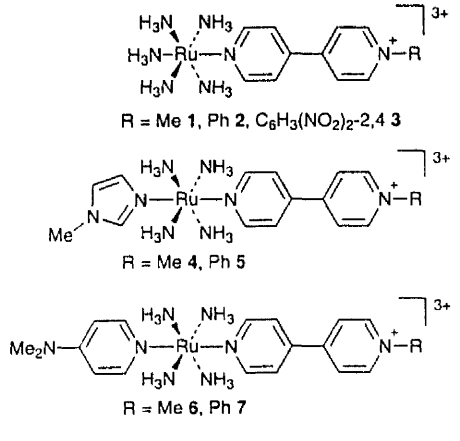

Fig. 1 Structures of the complex cations in 1–7

A common spectroscopic feature of low-valent ruthenium complexes of π-acceptor ligands are low-energy metal-to-ligand charge-transfer (MLCT) absorptions, the energies of which are governed by the electron-donor ability of the ruthenium centre and the ligand electron-acceptor capacity.[16] The exploitation of MLCT excited states as a basis for large β values has often been suggested,[2] but only very recently demonstrated.[8] The MeQ^+ ligand is a particularly effective π acceptor due to conjugation between the pyridyl rings.[17]

The complex salts show intense, broad $d_\pi(Ru^{II}) \rightarrow \pi^*(L^A)$ MLCT bands in the visible region (Table 1). For a given L^D, the MLCT energies decrease in the order L^A = MeQ^+ > PhQ^+ > $DNPhQ^+$, with a red-shift of 70 nm going from **1** to **3**. This is because the electron acceptor strength of the ligand increases as the conjugation pathlength is extended. In keeping with this, the potentials for ligand-based reduction obtained *via* cyclic voltammetry (Table 1) show that the lowest unoccupied molecular orbital energy of PhQ^+ is lower than that of MeQ^+ by 140–160 mV. With L^A fixed, the MLCT energies decrease in the order L^D = NH_3 > mim > dmap, with a red-shift of 30 nm going from **2** to **7** reflecting the increasing basicity of L^D. The reversible $Ru^{III/II}$ oxidation waves are at constant potential, showing that the energy of the metal-based highest occupied molecular orbital is unaffected by the ligand changes. The MLCT bands are highly solvatochromic, with the maximum for **6** occurring at 604 nm in $MeNO_2$ and at 706 nm in HMPA. Such behaviour, which often accompanies large β values in organic compounds,[18] confirms that the MLCT excitations are the primary contributors to β in these complexes.

The HRS setup and the method for derivation of β were as described in a recent report.[19] All samples were passed through a 0.45 mm filter, and were checked for fluorescence which can interfere with the HRS signal.[9,20] The β values obtained are extremely large (Table 1), and similar to those reported for ruthenium organometallics.[8] A much smaller HRS β_{1064} value of 78×10^{-30} esu was found for the mixed-valence salt **8** (Fig. 2) in which the $\{Ru^{III}(NH_3)_5\}^{3+}$ centre acts as an electron acceptor.[9] Since salts **1**–**7** absorb in the region of the second harmonic at 532 nm (Table 1), their β values are resonantly

Table 1 Electrochemical, UV–VIS and non-linear optical data in acetonitrile for the salts *trans*-$[Ru(NH_3)_4(L^D)(L^A)][PF_6]_3$

Salt	L^D	L^A	$E_{1/2}[Ru^{III/II}]$ (ΔE_p)/$E_{1/2}[L^{A+/0}]$ (ΔE_p) V vs. SCE/mV[a]		λ_{max}[MLCT]/nm (ε/nm dm^3 mol^{-1} cm^{-1})	ε_{532}[b] (%)	β_{1064} 10^{-30} esu	β_0
1	NH_3	MeQ^+	0.46 (75)	−0.91 (65)	590 (15 800)	61	750	123
2	NH_3	PhQ^+	0.46 (75)	−0.75 (70)	628 (19 300)	32	858	220
3	NH_3	$DNPhQ^+$	0.46[d]	−0.40[e]	660 (16 900)	23	871	289
4[f]	mim	MeQ^+	0.47 (75)	−0.88 (70)	602 (16 200)	55	523	100
5	mim	PhQ^+	0.46 (70)	−0.73 (70)	648 (21 500)	31	874	266
6[f]	dmap	MeQ^+	0.46 (70)	−0.87 (65)	614 (17 200)	47	587	130
7	dmap	PhQ^+	0.46 (75)	−0.73 (65)	658 (20 000)	28	794	260

[a] Measured in solution 0.1 M in $[NBu^n_4]PF_6$ at a Pt bead working electrode with a scan rate of 200 mV s^{-1} (ferrocene internal reference $E_{1/2}$ = 0.40 V, ΔE_p = 65 mV). [b] Extinction at 532 nm as a percentage of that at the MLCT maximum. [c] β_{1064} is the uncorrected first hyperpolarizability measured by using a 1064 nm Nd:YAG laser fundamental; β_0 is the static hyperpolarizability estimated by using the two-level model.[22] A relative error of ±15% is estimated for β values. The quoted cgs units (esu) are converted into SI units (C^3 m^3 J^{-2}) by dividing by a factor of 2.693×10^{20}. [d] E_{pa} for an irreversible oxidation process. [e] E_{pc} for an irreversible reduction process. [f] Ref.13.

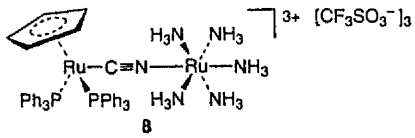

8

Fig. 2 Structure of the diruthenium salt **8**

enhanced, to the greatest extent for **1** and to the least extent for **3**. Correlations between β and the intramolecular charge-transfer (ICT) energy have been found for dipolar organics in which a single ICT absorption dominates β.[21] In similar fashion, β for these complexes clearly increases as the MLCT band shifts to lower energy. This trend is evident despite the concomitant decreasing extent of resonance enhancement.

Static first hyperpolarizabilities β_0, which provide an estimate of the intrinsic molecular hyperpolarizability with resonance effects removed, were obtained by application of the two-level model.[22] The β_0 values are very large and are in excess of those for most NLO-active molecules. By way of contrast, the organic dye Brilliant Green has an ICT maximum at 632 nm and a β_0 value of 97×10^{-30} esu derived from HRS in 5% MeOH–1,4-dioxane at 1064 nm.[23] A broad inverse correlation between β_0 and the MLCT energy is observed for **1**–**7**.

In conclusion, we have demonstrated that readily synthesized and structurally versatile ruthenium coordination complexes can exhibit very large β and β_0 values which are associated with low-energy MLCT excitations. The MLCT energy is readily tuned by ligand modifications, which will allow the maximization of β_0 and the establishment of further structure–property correlations for this novel class of NLO molecules.

Support from The Royal Society, from the Belgian National Fund for Scientific Research (G.2103.93 and 9.0011.92), the Belgian government (IUAP-16) and the University of Leuven (GOA/1/95) is acknowledged. S. H. is a Research Assistant of the Belgian National Fund for Scientific Research. Johnson Matthey plc are thanked for a loan of ruthenium trichloride.

Footnotes and References

* E-mail: b.coe@man.ac.uk

† The identity and purity of all of the ligands and complex salts were established by proton NMR spectroscopy and satisfactory elemental analyses.

1 *Nonlinear Optical Properties of Organic Molecules and Crystals*, ed. D. S. Chemla and J. Zyss, Academic Press, Orlando, 1987, vol. 1 and 2; *Molecular Nonlinear Optics*, ed. J. Zyss, Academic Press, New York, 1994.

2 S. R. Marder, in *Inorganic Materials*, ed. D. W. Bruce and D. O'Hare, Wiley, Chichester, 1992; N. J. Long, *Angew. Chem., Int. Ed. Engl.*, 1995, **34**, 21.

3 U. Behrens, H. Brussaard, U. Hagenau, J. Heck, E. Hendrickx, J. Körnich, J. G. M. van der Linden, A. Persoons, A. L. Spek, N. Veldman, B. Voss and H. Wong, *Chem. Eur. J.*, 1996, **2**, 98.

4 P. G. Lacroix, S. Di Bella and I. Ledoux, *Chem. Mater.*, 1996, **8**, 541.

5 P. Nguyen, G. Lesley, T. B. Marder, I. Ledoux and J. Zyss, *Chem. Mater.*, 1997, **9**, 406.

6 W. M. Laidlaw, R. G. Denning, T. Verbiest, E. Chauchard and A. Persoons, *Proc. SPIE, Int. Soc. Opt. Eng.*, 1994, **2143**, 14.

7 C. Dhenaut, I. Ledoux, I. D. W. Samuel, J. Zyss, M. Bourgault and H. Le Bozec, *Nature*, 1995, **374**, 339.

8 I. R. Whittall, M. G. Humphrey, A. Persoons and S. Houbrechts, *Organometallics*, 1966, **15**, 1935; S. Houbrechts, K. Clays, A. Persoons, V. Cadierno, M. P. Gamasa and J. Gimeno, *Organometallics*, 1996, **15**, 5266.

9 I. D. Morrison, R. G. Denning, W. M. Laidlaw and M. A. Stammers, *Rev. Sci. Instrum.*, 1996, **67**, 1445.

10 Y. K. Shin, B. S. Brunschwig, C. Creutz and N. Sutin, *J. Phys. Chem.*, 1996, **100**, 8157 and references therein.

11 J. C. Curtis, B. P. Sullivan and T. J. Meyer, *Inorg. Chem.*, 1983, **22**, 224.

12 E. Tfouni and P. C. Ford, *Inorg. Chem.*, 1980, **19**, 72.

13 B. J. Coe, M. C. Chamberlain, J. P. Essex-Lopresti, S. Gaines, J. C. Jeffery, S. Houbrechts and A. Persoons, *Inorg. Chem.*, 1997, in the press.

14 B. Emmert and N. Roh, *Ber.*, 1925, **58**, 503.

15 K. Clays and A. Persoons, *Phys. Rev. Lett.*, 1991, **66**, 2980; K. Clays and A. Persoons, *Rev. Sci. Instrum.*, 1992, **63**, 3285.

16 P. Ford, De F. P. Rudd, R. Gaunder and H. Taube, *J. Am. Chem. Soc.*, 1968, **90**, 1187; C. R. Johnson and R. E. Shepherd, *Inorg. Chem.*, 1983, **22**, 2439.

17 P. Chen, M. Curry and T. J. Meyer, *Inorg. Chem.*, 1989, **28**, 2271.

18 M. S. Paley and J. M. Harris, *J. Org. Chem.*, 1991, **56**, 568.

19 S. Houbrechts, K. Clays, A. Persoons, Z. Pikramenou and J.-M. Lehn, *Chem. Phys. Lett.*, 1996, **258**, 485.

20 E. Hendrickx, C. Dehu, K. Clays, J. L. Brédas and A. Persoons, *ACS Symp. Ser.*, 1995, **601**, 82; M. C. Flipse, R. de Jonge, R. H. Woudenberg, A. W. Marsman, C. A. van Walree and L. W. Jenneskens, *Chem. Phys. Lett.*, 1995, **245**, 297.

21 L.-T. Cheng, W. Tam, G. R. Meredith, G. Rikken and E. Meijer, *Proc. SPIE, Int. Soc. Opt. Eng.*, 1989, **1147**, 61; A. E. Stiegman, E. Graham, K. J. Perry, L. R. Khundkar, L.-T. Cheng and J. W. Perry, *J. Am. Chem. Soc.*, 1991, **113**, 7658.

22 J. L. Oudar and D. S. Chemla, *J. Chem. Phys.*, 1977, **66**, 2664; J. L. Oudar, *J. Chem. Phys.*, 1977, **67**, 446; J. Zyss and J. L. Oudar, *Phys. Rev. A*, 1982, **26**, 2016.

23 P. Kaatz and D. P. Shelton, *J. Chem. Phys.*, 1996, **105**, 3918.

Received in Basel, Switzerland, 18th April 1997; 7/02681A

Enhancement of Molecular Quadratic Hyperpolarizabilities in Ruthenium(II) 4,4′-Bipyridinium Complexes by N-Phenylation

Benjamin J. Coe*,† James A. Harris,† Lisa J. Harrington,† John C. Jeffery,‡ Leigh H. Rees,‡ Stephan Houbrechts,§ and André Persoons§,⊥

Department of Chemistry, University of Manchester, Oxford Road, Manchester M13 9PL, U.K., Department of Chemistry, University of Bristol, Cantock's Close, Bristol BS8 1TS, U.K., Laboratory of Chemical and Biological Dynamics, Center for Research on Molecular Electronics and Photonics, University of Leuven, Celestijnenlaan 200D, B-3001 Leuven, Belgium, and Optical Sciences Center, University of Arizona, Tucson, Arizona 85721

Received November 7, 1997

The new compounds *N*-phenyl-4,4′-bipyridinium (PhQ^+), *N*-(4-acetylphenyl)-4,4′-bipyridinium ($4\text{-}AcPhQ^+$), and *N*-(2,4-dinitrophenyl)-4,4′-bipyridinium ($2,4\text{-}DNPhQ^+$), together with the known ligand *N*-methyl-4,4′-bipyridinium (MeQ^+), have been used to prepare a series of Ru(II) complex salts *trans*-$[Ru(NH_3)_4(L^D)(L^A)](PF_6)_3$ [$L^D = NH_3$ and $L^A = MeQ^+$ (**1**), PhQ^+ (**2**), $4\text{-}AcPhQ^+$ (**3**), or $2,4\text{-}DNPhQ^+$ (**4**); L^D = 4-(dimethylamino)pyridine (dmap) and $L^A = PhQ^+$ (**7**) or $4\text{-}AcPhQ^+$ (**11**); L^D = 1-methylimidazole (mim) and $L^A = PhQ^+$ (**8**) or $4\text{-}AcPhQ^+$ (**12**); L^D = 4-(dimethylamino)benzonitrile (dmabn) and $L^A = PhQ^+$ (**9**) or $4\text{-}AcPhQ^+$ (**13**); L^D = phenothiazine (PTZ) and $L^A = PhQ^+$ (**10**) or $4\text{-}AcPhQ^+$ (**14**)]. These complexes display intense, visible metal-to-ligand charge-transfer (MLCT) absorptions, due to $d\pi(Ru^{II}) \rightarrow \pi^*(L^A)$ excitations. The MLCT energy decreases as the acceptor strength of L^A increases, in the order $MeQ^+ < PhQ^+ < 4\text{-}AcPhQ^+ < 2,4\text{-}DNPhQ^+$, and/or as the donor strength of L^D increases, in the order PTZ < dmabn < NH_3 < mim < dmap. X-ray crystal structure determinations have been carried out for $[PhQ^+]Cl\cdot 2H_2O$ and *trans*-$[Ru(NH_3)_4(PhQ^+)(PTZ)](PF_6)_3\cdot Et_2O$ (**10**·Et_2O). $[PhQ^+]Cl\cdot 2H_2O$, chemical formula $C_{16}H_{17}ClN_2O_2$, crystallizes in the triclinic system, space group $P\bar{1}$, with $a = 7.675(2)$ Å, $b = 9.895(2)$ Å, $c = 10.175(2)$ Å, $\alpha = 96.003(1)°$, $\beta = 104.74(2)°$, $\gamma = 90.398(1)°$, and $Z = 2$. **10**·Et_2O, chemical formula $C_{32}H_{44}F_{18}N_7OP_3RuS$, crystallizes in the triclinic system, space group $P\bar{1}$, with $a = 10.310(3)$ Å, $b = 10.698(2)$ Å, $c = 20.986(4)$ Å, $\alpha = 95.09(2)°$, $\beta = 91.49(2)°$, $\gamma = 105.53(2)°$, and $Z = 2$. The dihedral angles between the two pyridyl rings of the 4,4′-bipyridinium unit are 19.8° in $[PhQ^+]Cl\cdot 2H_2O$ and 2.6° in **10**·Et_2O. Molecular first hyperpolarizabilities β of the complex salts, obtained from hyper-Rayleigh scattering measurements at 1064 nm, are in the range $(698-1214) \times 10^{-30}$ esu. Static hyperpolarizabilities β_0 derived by using the two-level model are very large, with *trans*-$[Ru(NH_3)_4(4\text{-}AcPhQ^+)(dmap)](PF_6)_3$ (**11**) having the largest at 410×10^{-30} esu. When the MLCT absorption is sufficiently far from the second harmonic at 532 nm, both β and β_0 increase as the absorption energy decreases.

Introduction

The development of novel optoelectronic and photonic technologies requires organic materials possessing nonlinear optical (NLO) properties.[1] A thorough understanding of molecular hyperpolarizabilities is a prerequisite to the rational design and synthesis of efficient NLO chromophores for incorporation into active bulk structures. Structure−property correlations for the first (quadratic) hyperpolarizability β of purely organic compounds are now at an advanced stage of development,[1] but the molecular basis for NLO effects in organotransition metal complexes is relatively poorly understood.[2] Only very recently have studies begun to address this deficiency.[3-8]

Several reports concerning the quadratic NLO properties of ruthenium organometallic σ-acetylide[9] or allenylidene[10] complexes have appeared. We have chosen to investigate the NLO

* Author to whom correspondence should be addressed (e-mail, b.coe@man.ac.uk).
† University of Manchester.
‡ University of Bristol.
§ University of Leuven.
⊥ University of Arizona.

(1) (a) *Nonlinear Optical Properties of Organic Molecules and Crystals*; Chemla, D. S., Zyss, J., Eds.; Academic Press: Orlando, 1987; Vols. 1 and 2. (b) *Materials for Nonlinear Optics: Chemical Perspectives*; Marder, S. R., Sohn, J. S., Stucky, G. D., Eds.; ACS Symposium Series 455; American Chemical Society: Washington, DC, 1991. (c) *Molecular Nonlinear Optics*; Zyss, J., Ed.; Academic Press: New York, 1994. (d) Marder, S. R.; Kippelen, B.; Jen, A. K.-Y.; Peyghambarian, N. *Nature* **1997**, *388*, 845.
(2) (a) Marder, S. R. In *Inorganic Materials*; Bruce, D. W., O'Hare, D., Eds.; Wiley: Chichester, U.K., 1992. (b) Kanis, D. R.; Ratner, M. A.; Marks, T. J. *Chem. Rev.* **1994**, *94*, 195. (c) Long, N. J. *Angew. Chem., Int. Ed. Engl.* **1995**, *34*, 21.
(3) (a) Behrens, U.; Brussaard, H.; Hagenau, U.; Heck, J.; Hendrickx, E.; Körnich, J.; van der Linden, J. G. M.; Persoons, A.; Spek, A. L.; Veldman, N.; Voss, B.; Wong, H. *Chem. Eur. J.* **1996**, *2*, 98. (b) Hagenau, U.; Heck, J.; Hendrickx, E.; Persoons, A.; Schuld, T.; Wong, H. *Inorg. Chem.* **1996**, *35*, 7863.
(4) (a) Di Bella, S.; Fragala, I.; Ledoux, I.; Marks, T. J. *J. Am. Chem. Soc.* **1995**, *117*, 9481. (b) Lacroix, P. G.; Di Bella, S.; Ledoux, I. *Chem. Mater.* **1996**, *8*, 541.
(5) Nguyen, P.; Lesley, G.; Marder, T. B.; Ledoux, I.; Zyss, J. *Chem. Mater.* **1997**, *9*, 406.
(6) Cummings, S. D.; Cheng, L.-T.; Eisenberg, R. *Chem. Mater.* **1997**, *9*, 440.
(7) (a) Alain, V.; Fort, A.; Barzoukas, M.; Chen, C.-T.; Blanchard-Desce, M.; Marder, S. R.; Perry, J. W. *Inorg. Chim. Acta* **1996**, *242*, 43. (b) Wu, Z.; Ortiz, R.; Fort, A.; Barzoukas, M.; Marder, S. R. *J. Organomet. Chem.* **1997**, *528*, 217.

S0020-1669(97)01411-0 CCC: $15.00 © 1998 American Chemical Society
Published on Web 06/09/1998

properties of ruthenium(II) ammine complexes of pyridyl ligands, because these combine ideal, well-understood redox and charge-transfer absorption properties with synthetic versatility. The recently developed hyper-Rayleigh scattering (HRS) technique[11] allows the determination of β values of such complex salts. Initial studies have shown that *trans*-$\{Ru(NH_3)_4\}^{2+}$ complexes can possess large static hyperpolarizabilities β_0 which are associated with intense, low-energy metal-to-ligand charge-transfer (MLCT) absorptions.[12] The d^6 Ru(II) centers behave as powerful π donors, and the linear absorption and, hence, NLO properties are readily tuned via ligand modifications. Complexes of the *N*-methyl-4,4′-bipyridinium (MeQ^+) ligand have especially large β_0 values because MeQ^+ is a particularly effective π acceptor.

The present objectives of our research are fundamental in nature and include the maximization of β_0, together with the development of a detailed understanding of the origins of the NLO responses in Ru(II) 4,4′-bipyridinium chromophores. By analogy with dipolar organic molecules,[1] it is anticipated that the magnitude of the first hyperpolarizability will be increased by improving the π-electron-accepting ability of the 4,4′-bipyridinium ligand. The *N*,*N*′-diphenyl-4,4′-bipyridinium dication is more readily reduced than its dimethyl analogue by 150 mV,[13] as a result of extended conjugation. We hence reasoned that the *N*-phenyl-4,4′-bipyridinium (PhQ^+) ligand should be a better π acceptor than MeQ^+, and that substitution of the phenyl ring with electron-withdrawing groups will further enhance the acceptor strength. Although data for various highly NLO active pyridinium or *N*-methylpyridinium salts is available,[14] surprisingly it appears that no *N*-phenylpyridinium compounds have been investigated in this context. Some of the results reported herein have appeared recently as a preliminary communication.[15]

Experimental Section

Materials and Procedures. $RuCl_3 \cdot 2H_2O$ was supplied by Johnson Matthey plc. The salts $[Ru^{II}(NH_3)_5(H_2O)](PF_6)_2$, *trans*-$[Ru^{II}Cl(NH_3)_4(SO_2)]Cl$, and $[Ru^{II}(NH_3)_5(MeQ^+)](PF_6)_3$ (**1**) were prepared according to published procedures.[16] $[Ru^{II}(NH_3)_5(L^A)](PF_6)_3$ [L^A = PhQ^+ (**2**) or 4-$AcPhQ^+$ (**3**)] were prepared by following the procedure reported for their MeQ^+ analogue, but using $[PhQ^+]Cl$ or [4-$AcPhQ^+$]Cl, respectively, in place of $[MeQ^+]I$. All other reagents were obtained commercially and used as supplied. Products were dried overnight at room temperature in a vacuum desiccator ($CaSO_4$) prior to characterization.

Physical Measurements. ^1H NMR spectra were recorded on a Varian Gemini 200 spectrometer, and all shifts are referenced to TMS. The fine splitting of pyridyl or phenyl ring AA′BB′ patterns is ignored, and the signals are reported as simple doublets. Elemental analyses were performed by the Microanalytical Laboratory, University of Manchester. IR spectra were obtained as KBr disks with an ATI Mattson Genesis Series FTIR instrument. UV−visible spectra were recorded using a Hewlett-Packard 8452A diode array spectrophotometer.

Cyclic voltammetric measurements were carried out using an EG&G PAR model 173 potentiostat with an EG&G PAR model 175 universal programmer. A single-compartment cell was used with the SCE reference electrode separated by a salt bridge from the Pt bead working electrode and Pt wire auxiliary electrode. HPLC grade acetonitrile was used as received, and $[N(n\text{-}C_4H_9)_4]PF_6$, twice recrystallized from ethanol and dried in vacuo, was used as supporting electrolyte. Solutions containing ca. 10^{-3} M analyte (0.1 M electrolyte) were deaerated by N_2 purging. All $E_{1/2}$ values were calculated from $(E_{pa} + E_{pc})/2$ at a scan rate of 200 mV s^{-1}.

Synthesis of *N*-(2,4-Dinitrophenyl)-4,4′-bipyridinium Chloride, [2,4-DNPhQ$^+$]Cl. A solution of 2,4-dinitrochlorobenzene (13.16 g, 65 mmol) and 4,4′-bipyridine (10.00 g, 64 mmol) in ethanol (250 mL) was heated at reflux for 20 h. The solvent was reduced to a small volume in vacuo, diethyl ether was added, and the precipitate was filtered off and washed with diethyl ether. The crude product was dissolved through a frit in ethanol and reprecipitated by the slow addition of diethyl ether. The golden-brown microcrystalline product was filtered off, washed with diethyl ether, and dried: 10.33 g, 42%; δ_H (D_2O) 9.35 (1 H, d, $J_{3,5}$ = 2.5 Hz, H^3), 9.22 (2 H, d, J = 7.1 Hz, C_5H_4N−Ph), 8.90 (1 H, dd, $J_{5,6}$ = 8.7 Hz, $J_{3,5}$ = 2.5 Hz, H^5), 8.79 (2 H, d, J = 6.2 Hz, C_5H_4N), 8.65 (2 H, d, J = 7.1 Hz, C_5H_4N−Ph), 8.25 (1 H, d, $J_{5,6}$ = 8.7 Hz, H^6), 7.98 (2 H, d, J = 6.4 Hz, C_5H_4N); $\nu_{as}(NO_2)$ 1548 vs, $\nu_s(NO_2)$ 1345 vs cm^{-1}. Anal. Calcd for $C_{16}H_{11}ClN_4O_4 \cdot 0.5C_2H_5OH \cdot 0.25H_2O$: C, 52.86; H, 3.78; N, 14.50; Cl, 9.18. Found: C, 52.62; H, 3.75; N, 14.40; Cl, 9.25.

Synthesis of *N*-(2,4-Dinitrophenyl)-4,4′-bipyridinium Hexafluorophosphate, [2,4-DNPhQ$^+$]PF_6. [2,4-DNPhQ$^+$]$Cl \cdot 0.5C_2H_5OH \cdot 0.25H_2O$ (452 mg, 1.17 mmol) was dissolved in water (5 mL) and filtered into stirring aqueous NH_4PF_6. The precipitate was filtered off, washed with water, and dried to afford a pale golden solid: 334 mg, 60%; δ_H (CD_3COCD_3) 9.58 (2 H, d, J = 7.2 Hz, C_5H_4N−Ph), 9.29 (1 H, d, $J_{3,5}$ = 2.5 Hz, H^3), 9.06 (1 H, dd, $J_{5,6}$ = 8.6 Hz, $J_{3,5}$ = 2.5 Hz, H^5), 8.98 (2 H, d, J = 7.2 Hz, C_5H_4N−Ph), ca. 8.80 (2 H, br, C_5H_4N), 8.61 (1 H, d, $J_{5,6}$ = 8.6 Hz, H^6), 8.16 (2 H, d, J = 6.2 Hz, C_5H_4N); $\nu_{as}(NO_2)$ 1548 vs, $\nu_s(NO_2)$ 1345 vs cm^{-1}. Anal. Calcd for $C_{16}H_{11}F_6N_4O_4P \cdot 0.5H_2O$: C, 40.27; H, 2.53; N, 11.74. Found: C, 40.06; H, 2.28; N, 11.54. A small portion of this product was dissolved in acetone and metathesized back to [2,4-DNPhQ$^+$]Cl by the addition of an acetone solution of $[NBu_4]Cl$. Anal. Calcd for $C_{16}H_{11}ClN_4O_4 \cdot H_2O$: C, 51.01; H, 3.48; N, 14.87; Cl, 9.41. Found: C, 51.02; H, 3.47; N, 14.71; Cl, 9.34.

Synthesis of *N*-Phenyl-4,4′-bipyridinium Chloride, [PhQ$^+$]Cl. A solution of $[2,4\text{-DNPhQ}^+]Cl \cdot 0.5C_2H_5OH \cdot 0.25H_2O$ (5.00 g, 12.9 mmol) and aniline (5.00 g, 53.7 mmol) in ethanol (100 mL) was heated at reflux for 3 h. The solvent was reduced to a small volume in vacuo, water was added, and the precipitate of 2,4-dinitroaniline was filtered off and washed with water. The aqueous filtrate was evaporated to dryness and then dissolved in ethanol and precipitated by the addition of diethyl ether. The pale golden microcrystalline product was filtered off, washed with diethyl ether, and dried: 3.39 g, 86%; δ_H (D_2O) 9.14 (2 H, d, J = 7.0 Hz, C_5H_4N−Ph), 8.69 (2 H, br d, C_5H_4N), 8.48 (2 H, d, J = 7.0 Hz, C_5H_4N−Ph), 7.89 (2 H, d, J = 6.3 Hz, C_5H_4N), 7.74−7.64 (5 H, c m, Ph). Anal. Calcd for $C_{16}H_{13}ClN_2 \cdot 2H_2O$: C, 63.05; H, 5.62; N, 9.19; Cl, 11.63. Found: C, 63.29; H, 5.42; N, 9.48; Cl, 11.72.

Synthesis of *N*-(4-Acetylphenyl)-4,4′-bipyridinium Chloride, [4-AcPhQ$^+$]Cl. A solution of $[2,4\text{-DNPhQ}^+]Cl \cdot 0.5C_2H_5OH \cdot 0.25H_2O$

(8) (a) Whittall, I. R.; Humphrey, M. G.; Houbrechts, S.; Persoons, A.; Hockless, D. C. R. *Organometallics* **1996**, *15*, 5738. (b) Whittall, I. R.; Cifuentes, M. P.; Humphrey, M. G.; Luther-Davies, B.; Samoc, M.; Houbrechts, S.; Persoons, A.; Heath, G. A.; Bogsányi, D. *Organometallics* **1997**, *16*, 2631.
(9) (a) Whittall, I. R.; Humphrey, M. G.; Persoons, A.; Houbrechts, S. *Organometallics* **1996**, *15*, 1935. (b) Houbrechts, S.; Clays, K.; Persoons, A.; Cadierno, V.; Gamasa, M. P.; Gimeno, J. *Organometallics* **1996**, *15*, 5266. (c) Wu, I.-Y.; Lin, J. T.; Luo, J.; Sun, S.-S.; Li, C.-S.; Kuan, J. L.; Tsai, C.; Hsu, C.-C.; Lin, J.-L. *Organometallics* **1997**, *16*, 2038.
(10) Tamm, M.; Jentzsch, T.; Wernсke, W. *Organometallics* **1997**, *16*, 1418.
(11) (a) Clays, K.; Persoons, A. *Phys. Rev. Lett.* **1991**, *66*, 2980. (b) Clays, K.; Persoons, A. *Rev. Sci. Instrum.* **1992**, *63*, 3285. (c) Hendrickx, E.; Clays, K.; Persoons, A.; Dehu, C.; Brédas, J. L. *J. Am. Chem. Soc.* **1995**, *117*, 3547.
(12) Coe, B. J.; Chamberlain, M. C.; Essex-Lopresti, J. P.; Gaines, S.; Jeffery, J. C.; Houbrechts, S.; Persoons, A. *Inorg. Chem.* **1997**, *36*, 3284.
(13) Kuzuya, M.; Kondo, S.; Murase, K. *J. Phys. Chem.* **1993**, *97*, 7800.
(14) See, for example: (a) Marder, S. R.; Perry, J. W.; Yakymyshyn, C. P. *Chem. Mater.* **1994**, *6*, 1137. (b) Chauchard, E.; Combellas, C.; Hendrickx, E.; Mathey, G.; Suba, C.; Persoons, A.; Thiebault, A. *Chem. Phys. Lett.* **1995**, *238*, 47. (c) Duan, X.-M.; Okada, S.; Oikawa, H.; Matsuda, H.; Nakanishi, H. *Mol. Cryst. Liq. Cryst.* **1995**, *267*, 89.
(15) Coe, B. J.; Essex-Lopresti, J. P.; Harris, J. A.; Houbrechts, S.; Persoons, A. *Chem. Commun.* **1997**, 1645.
(16) Curtis, J. C.; Sullivan, B. P.; Meyer, T. J. *Inorg. Chem.* **1983**, *22*, 224.

(500 mg, 1.29 mmol) and 4-aminoacetophenone (1.88 g, 13.9 mmol) in ethanol (100 mL) was heated at reflux for 50 h. The solvent was reduced to a small volume in vacuo, water was added, and the precipitate of 2,4-dinitroaniline was filtered off and washed with water. The aqueous filtrate was evaporated to a small volume, acetone was added, and the solution was stored in a refrigerator for 24 h. The pale golden microcrystalline product was filtered off, washed with acetone, and dried: 360 mg, 81%; δ_H (D_2O) 9.23 (2 H, d, J = 7.0 Hz, C_5H_4N−AcPh), 8.75 (2 H, br d, J = 5.9 Hz, C_5H_4N), 8.56 (2 H, d, J = 7.0 Hz, C_5H_4N−AcPh), 8.25 (2 H, d, J = 8.8 Hz, C_6H_4−Ac), 7.95 (2 H, d, J = 6.3 Hz, C_5H_4N), 7.90 (2 H, d, J = 8.7 Hz, C_6H_4−Ac), 2.69 (3 H, s, Ac); ν(C=O) 1692 vs cm^{-1}. Anal. Calcd for $C_{18}H_{15}ClN_2O\cdot 2H_2O$: C, 62.34; H, 5.52; N, 8.08; Cl, 10.22. Found: C, 62.35; H, 5.40; N, 7.93; Cl, 10.39.

Data for $[Ru^{II}(NH_3)_5(MeQ^+)](PF_6)_3$ (1): δ_H (CD_3COCD_3) 9.15 (2 H, d, J = 7.0 Hz, C_5H_4N−Me), 9.04 (2 H, d, J = 6.9 Hz, C_5H_4N), 8.68 (2 H, d, J = 7.0 Hz, C_5H_4N−Me), 7.87 (2 H, d, J = 7.1 Hz, C_5H_4N), 4.53 (3 H, s, Me), 3.50 (3 H, s, *trans*-NH_3), 2.66 (12 H, s, 4 × *cis*-NH_3). Anal. Calcd for $C_{11}H_{26}F_{18}N_7P_3Ru\cdot 0.2C_3H_6O$: C, 17.33; H, 3.41; N, 12.20. Found: C, 17.31; H, 3.01; N, 12.57.

Data for $[Ru^{II}(NH_3)_5(PhQ^+)](PF_6)_3$ (2). Indigo solid: 73%; δ_H (CD_3COCD_3) 9.33 (2 H, d, J = 7.2 Hz, C_5H_4N−Ph), 9.21 (2 H, d, J = 7.1 Hz, C_5H_4N), 8.86 (2 H, d, J = 7.3 Hz, C_5H_4N−Ph), 8.01−7.94 (4 H, c m, C_5H_4N and Ph), 7.84−7.78 (3 H, c m, Ph), 3.60 (3 H, s, *trans*-NH_3), 2.70 (12 H, s, 4 × *cis*-NH_3). Anal. Calcd for $C_{16}H_{28}F_{18}N_7P_3Ru\cdot 0.5C_3H_6O$: C, 23.79; H, 3.54; N, 11.10. Found: C, 23.60; H, 3.39; N, 11.19.

Data for $[Ru^{II}(NH_3)_5(4\text{-}AcPhQ^+)](PF_6)_3$ (3). Indigo solid: 35%; δ_H (CD_3COCD_3) 9.40 (2 H, d, J = 7.2 Hz, C_5H_4N−Ph-4-Ac), 9.22 (2 H, d, J = 7.0 Hz, C_5H_4N), 8.89 (2 H, d, J = 7.2 Hz, C_5H_4N−Ph-4-Ac), 8.35 (2 H, d, J = 8.8 Hz, C_6H_4−Ac), 8.15 (2 H, d, J = 8.8 Hz, C_6H_4−Ac), 7.97 (2 H, d, J = 7.1 Hz, C_5H_4N), 3.64 (3 H, s, *trans*-NH_3), 2.72 (15 H, s, 4 × *cis*-NH_3 and Ac); ν(C=O) 1681 m cm^{-1}. Anal. Calcd for $C_{18}H_{30}F_{18}N_7OP_3Ru\cdot 0.3C_3H_6O$: C, 24.84; H, 3.51; N, 10.73. Found: C, 24.81; H, 3.29; N, 10.69.

Synthesis of $[Ru^{II}(NH_3)_5(2,4\text{-}DNPhQ^+)](PF_6)_3$ (4). A solution of $[Ru^{II}(NH_3)_5(H_2O)](PF_6)_2$ (250 mg, 0.506 mmol) and $[2,4\text{-}DNPhQ^+]PF_6\cdot 0.5H_2O$ (238 mg, 0.499 mmol) in acetone (5 mL) was stirred at room temperature for 2 h. The addition of diethyl ether afforded a dark precipitate, which was collected by filtration, washed with diethyl ether, and dried. Purification was effected by precipitation from acetone/aqueous NH_4PF_6 and then from acetone/diethyl ether followed by recrystallization from acetone/dichloromethane to afford a dark purple solid: 101 mg, 21%; δ_H (CD_3COCD_3) 9.37 (2 H, d, J = 7.2 Hz, C_5H_4N), 9.28−9.25 (3 H, c m, H^3 and C_5H_4N), 9.02 (1 H, dd, $J_{5,6}$ = 8.8 Hz, $J_{3,5}$ = 2.6 Hz, H^5), 8.97 (2 H, d, J = 7.4 Hz, C_5H_4N), 8.56 (1 H, d, $J_{5,6}$ = 8.7 Hz, H^6), 7.98 (2 H, d, J = 7.0 Hz, C_5H_4N), 3.74 (3 H, s, *trans*-NH_3), 2.75 (12 H, s, 4 × *cis*-NH_3); $\nu_{as}(NO_2)$ 1547 s, $\nu_s(NO_2)$ 1347 s cm^{-1}. Anal. Calcd for $C_{16}H_{26}F_{18}N_9O_4P_3Ru$: C, 20.35; H, 2.77; N, 13.35. Found: C, 21.09; H, 3.05; N, 13.00.

Synthesis of *trans*-$[Ru^{III}(SO_4)(NH_3)_4(PhQ^+)]Cl_2$ (5). A mixture of *trans*-$[Ru^{II}Cl(NH_3)_4(SO_2)]Cl$ (100 mg, 0.329 mmol) and $[PhQ^+]Cl\cdot 2H_2O$ (200 mg, 0.656 mmol) was dissolved in water (5 mL) and heated at ca. 45 °C under Ar for 30 min. Acetone (25 mL) was added to the dark brown solution, and the mauve precipitate was collected by filtration, washed with acetone, and dried to afford crude *trans*-$[Ru^{II}(NH_3)_4(SO_2)(PhQ^+)]Cl_3$: 180 mg, 96%. This material was then dissolved in water (ca. 10 mL) and oxidized by the addition of a 1/1 mixture of 30% aqueous H_2O_2 solution/2 M HCl (3 mL). After 5 min at room temperature, acetone (100 mL) was added to the yellow solution and the golden precipitate was collected by filtration, washed with acetone, and dried: 165 mg, 92%. The same quantity of this crude product was used in the subsequent syntheses of **7**−**10**.

Synthesis of *trans*-$[Ru^{III}(SO_4)(NH_3)_4(4\text{-}AcPhQ^+)]Cl_2$ (6). This was prepared similarly to **5** by using $[4\text{-}AcPhQ^+]Cl\cdot 2H_2O$ (229 mg, 0.660 mmol) in place of $[PhQ^+]Cl\cdot 2H_2O$ to afford a golden solid: 155 mg, 77%. The same quantity of this crude product was used in the subsequent syntheses of **11**−**14**.

Synthesis of *trans*-$[Ru^{II}(NH_3)_4(PhQ^+)(dmap)](PF_6)_3$ (7). A solution of **5** (165 mg, 0.290 mmol) in water (10 mL) was reduced over zinc amalgam (5 lumps) with Ar agitation for 5 min. This was then filtered under Ar into a flask containing 4-(dimethylamino)pyridine (dmap; 175 mg, 1.43 mmol), and the solution was stirred at room temperature in the dark under Ar for 3 h. The addition of aqueous NH_4PF_6 to the deep purple solution gave a dark precipitate, which was collected by filtration, washed with water, and dried. The product was purified by precipitation from acetone/$[NBu_4]Cl$ followed by precipitation from water/aqueous NH_4PF_6 to afford a dark indigo solid: 169 mg, 61%; δ_H (CD_3COCD_3) 9.38 (2 H, d, J = 7.1 Hz, C_5H_4N−Ph), 9.14 (2 H, d, J = 7.0 Hz, C_5H_4N), 8.86 (2 H, d, J = 7.1 Hz, C_5H_4N−Ph), 8.34 (2 H, d, J = 7.2 Hz, NC_5H_4−NMe_2), 8.06 (2 H, d, J = 7.0 Hz, C_5H_4N), 8.02−7.98 (2 H, c m, Ph), 7.82−7.79 (3 H, c m, Ph), 6.88 (2 H, d, J = 7.2 Hz, NC_5H_4−NMe_2), 3.17 (6 H, s, NMe_2), 2.78 (12 H, s, 4 × NH_3). Anal. Calcd for $C_{23}H_{35}F_{18}N_8P_3Ru$: C, 28.79; H, 3.68; N, 11.68. Found: C, 29.08; H, 3.43; N, 11.92.

Synthesis of *trans*-$[Ru^{II}(NH_3)_4(PhQ^+)(mim)](PF_6)_3$ (8). This was prepared and purified identically to **7** by using 1-methylimidazole (mim; 0.2 mL, 2.49 mmol) in place of dmap. A dark indigo solid was obtained: 205 mg, 77%; δ_H (CD_3COCD_3) 9.38 (2 H, d, J = 7.2 Hz, C_5H_4N−Ph), 9.21 (2 H, d, J = 7.0 Hz, C_5H_4N), 8.86 (2 H, d, J = 7.1 Hz, C_5H_4N−Ph), 8.24 (1 H, s, im), 8.05−7.97 (4 H, c m, C_5H_4N and Ph), 7.84−7.79 (3 H, c m, Ph), 7.48 (1 H, t, J = 1.4 Hz, im), 7.41 (1 H, t, J = 1.4 Hz, im), 3.93 (3 H, s, *Me*-im), 2.73 (12 H, s, 4 × NH_3). Anal. Calcd for $C_{20}H_{31}F_{18}N_8P_3Ru$: C, 26.13; H, 3.40; N, 12.19. Found: C, 26.26; H, 3.29; N, 12.11.

Synthesis of *trans*-$[Ru^{II}(NH_3)_4(PhQ^+)(dmabn)](PF_6)_3$ (9). This was obtained in crude form identically to **7** by using 4-(dimethylamino)-benzonitrile (dmabn; 210 mg, 1.44 mmol) in acetone (15 mL) in place of dmap. The product was purified by precipitation from acetone/diethyl ether to afford a dark burgundy solid: 110 mg, 39%; δ_H (CD_3COCD_3) 9.45 (2 H, d, J = 7.2 Hz, C_5H_4N−Ph), 9.21 (2 H, d, J = 6.9 Hz, C_5H_4N), 8.88 (2 H, d, J = 7.2 Hz, C_5H_4N−Ph), 8.15 (2 H, d, J = 7.0 Hz, C_5H_4N), 8.02−7.97 (2 H, c m, Ph), 7.85−7.80 (3 H, c m, Ph), 7.68 (2 H, d, J = 9.1 Hz, Me_2N−C_6H_4−CN), 6.86 (2 H, d, J = 9.2 Hz, Me_2N−C_6H_4−CN), 3.11 (6 H, s, NMe_2), 2.84 (12 H, s, 4 × NH_3). Anal. Calcd for $C_{25}H_{35}F_{18}N_8P_3Ru$: C, 30.53; H, 3.59; N, 11.39. Found: C, 30.54; H, 3.66; N, 11.24.

Synthesis of *trans*-$[Ru^{II}(NH_3)_4(PhQ^+)(PTZ)](PF_6)_3$ (10). A solution of **5** (165 mg, 0.290 mmol) in water (10 mL) was reduced over zinc amalgam (5 lumps) with Ar agitation for 5 min and then filtered under Ar into a flask containing acetone (200 mL). After refrigeration, the deep blue precipitate was collected by filtration, washed with acetone, and dried to yield a turquoise solid (145 mg). This was dissolved in water (5 mL) and added to solid NH_4PF_6 (1.5 g). After refrigeration, the deep purple precipitate was collected by filtration, dried, and then dissolved in acetone (10 mL), and phenothiazine (PTZ; 650 mg, 3.26 mmol) was added. The deep blue solution turned purple within minutes and was stirred in the dark under Ar for 1 h to yield a deep burgundy solution. The addition of diethyl ether afforded a dark precipitate, which was collected by filtration, washed with diethyl ether, and dried. Purification was effected by precipitation from acetone/aqueous NH_4PF_6 and then from acetone/diethyl ether to yield a dark red solid (ca. 95% pure by ^1H NMR): 135 mg, 45%; δ_H (CD_3COCD_3) 9.44 (2 H, d, J = 7.2 Hz, C_5H_4N−Ph), 8.93 (2 H, d, J = 6.9 Hz, C_5H_4N), 8.80 (2 H, d, J = 7.1 Hz, C_5H_4N−Ph), 8.71 (1 H, s, NH), 8.19 (2 H, d, J = 6.9 Hz, C_5H_4N), 8.00−7.95 (2 H, c m, Ph), 7.82−7.78 (3 H, c m, Ph), 7.57 (2 H, d, J = 7.7 Hz, PTZ), 7.44−7.36 (2 H, m, PTZ), 7.20−7.12 (4 H, m, PTZ), 2.60 (12 H, s, 4 × NH_3). Anal. Calcd for $C_{28}H_{34}F_{18}N_7P_3RuS$: C, 32.44; H, 3.31; N, 9.46; S, 3.09. Found: C, 32.86; H, 3.62; N, 8.94; S, 3.34.

Synthesis of *trans*-$[Ru^{II}(NH_3)_4(4\text{-}AcPhQ^+)(dmap)](PF_6)_3$ (11). This was prepared and purified identically to **7** by using **6** (155 mg, 0.253 mmol) in place of **5**. The product was precipitated once further from acetone/diethyl ether to afford an indigo solid: 158 mg, 62%; δ_H (CD_3COCD_3) 9.43 (2 H, d, J = 7.2 Hz, C_5H_4N−Ph-4-Ac), 9.14 (2 H, d, J = 7.0 Hz, C_5H_4N), 8.88 (2 H, d, J = 7.2 Hz, C_5H_4N−Ph-4-Ac), 8.38−8.32 (4 H, c m, C_6H_4−Ac and NC_5H_4−NMe_2), 8.14 (2 H, d, J = 8.8 Hz, C_6H_4−Ac), 8.06 (2 H, d, J = 7.0 Hz, C_5H_4N), 6.88 (2 H, d, J = 7.2 Hz, NC_5H_4−NMe_2), 3.16 (6 H, s, NMe_2), 2.77 (12 H, s, 4 × NH_3), 2.72 (3 H, s, Ac); ν(C=O) 1686 m cm^{-1}. Anal. Calcd for $C_{25}H_{37}F_{18}N_8OP_3Ru$: C, 29.98; H, 3.72; N, 11.19. Found: C, 29.77; H, 3.86; N, 11.22.

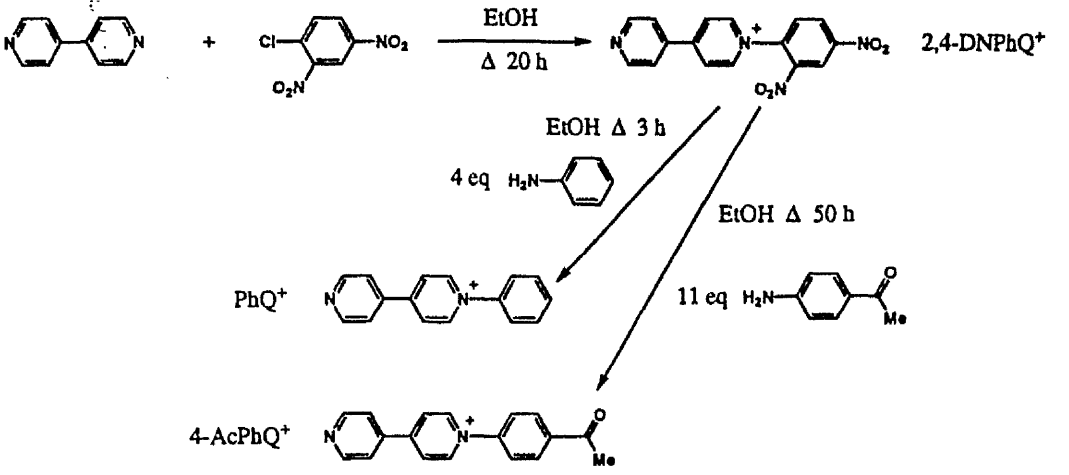

Figure 1. Synthesis of the ligands PhQ^+, 4-$AcPhQ^+$, and 2,4-$DNPhQ^+$.

Synthesis of *trans*-[$Ru^{II}(NH_3)_4$(4-$AcPhQ^+$)(mim)](PF_6)$_3$ (12). This was prepared and purified identically to **8** by using **6** (155 mg, 0.253 mmol) in place of **5** to afford an indigo solid: 160 mg, 66%; δ_H (CD_3COCD_3) 9.45 (2 H, d, J = 6.7 Hz, C_5H_4N−Ph-4-Ac), 9.23 (2 H, d, J = 6.8 Hz, C_5H_4N), 8.90 (2 H, d, J = 6.6 Hz, C_5H_4N−Ph-4-Ac), 8.36 (2 H, d, J = 8.6 Hz, C_6H_4−Ac), 8.26 (1 H, s, im), 8.15 (2 H, d, J = 8.7 Hz, C_6H_4−Ac), 8.05 (2 H, d, J = 6.8 Hz, C_5H_4N), 7.50 (1 H, s, im), 7.43 (1 H, s, im), 3.94 (3 H, s, *Me*-im), 2.75 (12 H, s, 4 × NH_3), 2.73 (3 H, s, Ac); ν(C=O) 1684 m cm^{-1}. Anal. Calcd for $C_{22}H_{33}F_{18}N_8OP_3Ru$: C, 27.48; H, 3.46; N, 11.65. Found: C, 27.74; H, 3.55; N, 11.75.

Synthesis of *trans*-[$Ru^{II}(NH_3)_4$(4-$AcPhQ^+$)(dmabn)](PF_6)$_3$ (13). This was prepared and purified identically to **9** by using **6** (155 mg, 0.253 mmol) in place of **5** to afford a purple solid: 161 mg, 62%; δ_H (CD_3COCD_3) 9.51 (2 H, d, J = 7.1 Hz, C_5H_4N−Ph-4-Ac), 9.23 (2 H, d, J = 6.9 Hz, C_5H_4N), 8.92 (2 H, d, J = 7.1 Hz, C_5H_4N−Ph-4-Ac), 8.37 (2 H, d, J = 8.8 Hz, C_6H_4−Ac), 8.18−8.13 (4 H, c m, C_5H_4N and C_6H_4−Ac), 7.68 (2 H, d, J = 9.1 Hz, Me_2N−C_6H_4−CN), 6.87 (2 H, d, J = 9.1 Hz, Me_2N−C_6H_4−CN), 3.11 (6 H, s, NMe_2), 2.86 (12 H, s, 4 × NH_3), 2.73 (3 H, s, Ac); ν(C=O) 1686 m cm^{-1}. Anal. Calcd for $C_{27}H_{37}F_{18}N_8OP_3Ru$: C, 31.62; H, 3.64; N, 10.93. Found: C, 31.67; H, 3.80; N, 10.80.

Synthesis of *trans*-[$Ru^{II}(NH_3)_4$(4-$AcPhQ^+$)(PTZ)](PF_6)$_3$ (14). This was prepared and purified identically to **10** by using **6** (155 mg, 0.253 mmol) in place of **5** to afford a deep red solid: 120 mg, 42%; δ_H (CD_3COCD_3) 9.50 (2 H, d, J = 7.1 Hz, C_5H_4N−Ph-4-Ac), 8.94 (2 H, d, J = 6.8 Hz, C_5H_4N), 8.83 (2 H, d, J = 7.1 Hz, C_5H_4N−Ph-4-Ac), 8.72 (1 H, s, NH), 8.36 (2 H, d, J = 8.8 Hz, C_6H_4−Ac), 8.20 (2 H, d, J = 6.9 Hz, C_5H_4N), 8.14 (2 H, d, J = 8.8 Hz, C_6H_4−Ac), 7.57 (2 H, d, J = 7.7 Hz, PTZ), 7.45−7.37 (2 H, m, PTZ), 7.21−7.13 (4 H, m, PTZ), 2.72 (3 H, s, Ac), 2.61 (12 H, s, 4 × NH_3); ν(C=O) 1685 m cm^{-1}. Anal. Calcd for $C_{30}H_{36}F_{18}N_7OP_3RuS\cdot 2H_2O$: C, 32.32; H, 3.62; N, 8.80; S, 2.88. Found: C, 32.50; H, 3.34; N, 8.86; S, 3.17.

X-ray Structural Determinations. Crystals of [PhQ^+]Cl·$2H_2O$ were grown by refrigeration of a water/acetone solution, and crystals of *trans*-[Ru(NH_3)$_4$(PhQ^+)(PTZ)](PF_6)$_3$·Et_2O (**10**·Et_2O) were grown by diffusion of diethyl ether into an acetone solution containing added PTZ at 4 °C in the dark. Crystallization in the absence of free PTZ leads to decomposition and production of a blue material.

Platelike crystals of [PhQ^+]Cl·$2H_2O$ (yellow) and **10**·Et_2O (red), having approximate dimensions of 0.50 × 0.40 × 0.2 mm and 0.20 × 0.20 × 0.02 mm, respectively, were mounted on glass fibers, and data were collected on a Siemens SMART CCD area-detector three-circle diffractometer at low temperature. For three settings of ϕ, narrow data "frames" were collected for 0.3° increments in ω. A total of 2082 and 2132 frames of data were collected, affording a sphere of data for [PhQ^+]Cl·$2H_2O$ and **10**·Et_2O, respectively. At the end of data collection the first 50 frames were re-collected to establish that crystal decay had not taken place. The substantial redundancy in data allows empirical absorption corrections to be applied using multiple measurements of equivalent reflections. Data frames were collected for 15s/frame for [PhQ^+]Cl·$2H_2O$ and 30 s/frame for **10**·Et_2O, giving overall data collection times of ca. 14 and ca. 25 h, respectively. The data frames were integrated using SAINT.[17]

The structures were solved by direct methods and refined by full-matrix least squares on all F_o^2 data using Siemens SHELXTL 5.03.[17] All non-hydrogen atoms were refined anisotropically. In the case of [PhQ^+]Cl·$2H_2O$, the protons of the two water molecules were located and refined with isotropic thermal parameters ca. 1.2 × the equivalent isotropic thermal parameters of their parent oxygen atoms. The NH hydrogen of the PTZ ligand in **10**·Et_2O was located and refined. All other hydrogen atoms were included in calculated positions with isotropic thermal parameters ca. 1.2 × (aromatic CH) or 1.5 × (Me) the equivalent isotropic thermal parameters of their parent carbon atoms. All calculations were carried out on Silicon Graphics Indy or Indigo computers. The asymmetric unit of [PhQ^+]Cl·$2H_2O$ contains one molecule of the cation, one chloride anion, and two water molecules in general positions. The asymmetric unit of **10**·Et_2O contains one molecule of the cation, three PF_6^- anions, and one molecule of diethyl ether in general positions. The diethyl ether solvent molecule and the anion PF_6^- (P2) were restrained to model perfect geometry.

ORTEP[18] diagrams showing views of [PhQ^+]Cl·$2H_2O$ and the complex cation in **10**·Et_2O are given in Figures 3 and 4. Crystallographic data and refinement details are presented in Table 3, and selected bond distances and angles in Tables 4 and 5. Additional material available from the Cambridge Crystallographic Data Centre comprises final atomic fractional coordinates, thermal parameters, and nonessential bond lengths and angles.

Hyper-Rayleigh Scattering. Details of the HRS experiment have been discussed previously,[11] and the experimental procedure used was as described recently.[19] β values were obtained by using the electric-field-induced second harmonic generation β_{1064} value for 4-nitroaniline of 29.2 × 10^{-30} esu in acetonitrile[20] as an external reference. All measurements were performed using the 1064 nm fundamental wavelength of an injection-seeded, Q-switched Nd:YAG laser (Quanta-Ray GCR-5, 8 ns pulses, 7 mJ, 10 Hz). Dilute acetonitrile solutions (10^{-4}−10^{-5} M) were used to ensure a linear dependence of $I_{2\omega}/I_\omega^2$ upon solute concentration, precluding the need for Lambert−Beer correction factors. All samples were passed through a 0.45 μm filter (Millipore)

(17) *SHELXTL 5.03 program system*; Siemens Analytical X-ray Instruments: Madison, WI, 1995.
(18) Johnson, C. K. *ORTEP: A Fortran Thermal Ellipsoid Plot Program*; Technical Report ORNL-5138; Oak Ridge National Laboratory: Oak Ridge, TN, 1976.
(19) Houbrechts, S.; Clays, K.; Persoons, A.; Pikramenou, Z.; Lehn, J.-M. *Chem. Phys. Lett.* **1996**, *258*, 485.
(20) Stähelin, M.; Burland, D. M.; Rice, J. E. *Chem. Phys. Lett.* **1992**, *191*, 245.

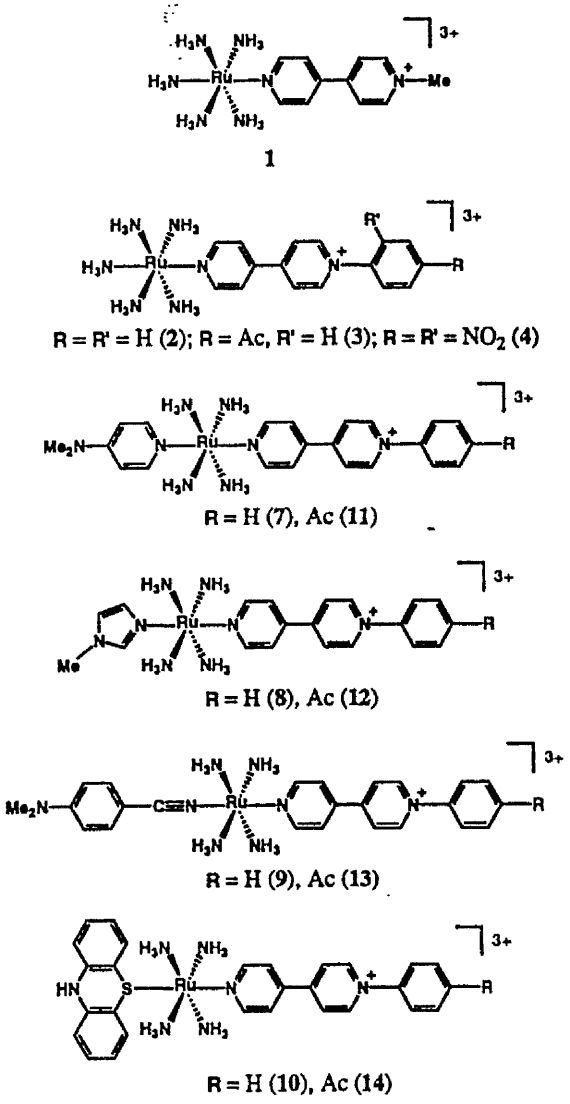

Figure 2. Structures of the complex cations in the salts **1**−**4** and **7**−**14**.

and were checked for fluorescence, which can interfere with the HRS signal.[21−24] One-dimensional hyperpolarizability is assumed, i.e., $\beta_{1064} = \beta_{333}$, and a relative error of ±15% is estimated.

Results and Discussion

Synthetic Studies. The new compounds [PhQ^+]Cl and [2,4-$DNPhQ^+$]Cl were synthesized by using modifications of a literature report for *N,N′*-diphenyl-4,4′-bipyridinium dichloride.[25] Nucleophilic attack by stoichiometric 4,4′-bipyridine on 2,4-dinitrochlorobenzene produces [2,4-$DNPhQ^+$]Cl in reasonable yield, and subsequent treatment with aniline affords [PhQ^+]Cl in high yield. Replacement of aniline by 4-aminoacetophenone produces [4-$AcPhQ^+$]Cl in high yield, but an extended reaction time and a larger excess of reagent are required due to the decreased basicity of the attacking nucleophile. Reaction of 4,4′-bipyridine with 2,4-dinitrofluorobenzene was found to be a much less efficient method for the synthesis of the 2,4-$DNPhQ^+$ cation. The syntheses of the new ligands are shown in Figure 1.

The new complex salts **2**−**14** were prepared by using established coordination chemistry based on either $[Ru(NH_3)_5(H_2O)](PF_6)_2$ or *trans*-$[RuCl(NH_3)_4(SO_2)]Cl$,[16,26,27] with previously described[12] and further modifications. Only 2 equiv of [PhQ^+]Cl·$2H_2O$ or [4-$AcPhQ^+$]Cl·$2H_2O$ was used in the syntheses of the intermediates **5** or **6** because the use of a 5-fold excess, as with [MeQ^+]I,[12] leads to precipitation of excess ligand salt together with the *trans*-$[Ru(NH_3)_4(SO_2)(L^A)]Cl_3$ (L^A = PhQ^+ or 4-$AcPhQ^+$) product. This excess ligand subsequently reacts with the intermediate aquo complexes in the reduction stages, causing contamination by symmetric *trans*-$\{Ru(NH_3)_4(L^A)_2\}^{4+}$ products. The use of only 1 equiv of [PhQ^+]Cl·$2H_2O$ or [4-$AcPhQ^+$]Cl·$2H_2O$ leads to incomplete reactions and reduced yields and purities of the final products. The structures of the complexes, except for **5** and **6**, are shown in Figure 2.

UV−Visible Studies. Spectra for all of the complex salts, except for the intermediates **5** and **6**, were recorded in acetonitrile, and results are presented in Table 1.

All of the complexes show intense, broad $d\pi(Ru^{II}) \rightarrow \pi^*(L^A)$ metal-to-ligand charge-transfer (MLCT) bands in the region 520−690 nm, the energies of which depend on the electron-donor ability of the Ru center and the electron-acceptor ability of L^A.[28,29] The complexes of dmap or dmabn also show a high-energy, $d\pi(Ru^{II}) \rightarrow \pi^*(L^D)$ band in the region 320−355 nm. Data for the visible MLCT bands are collected in Table 2, together with those for the related MeQ^+ complex salts for purposes of comparison.

For the pentaammine complex series ($L^D = NH_3$), the steady red-shifting of the MLCT maxima shows that the acceptor strength of L^A increases in the order MeQ^+ < PhQ^+ < 4-$AcPhQ^+$ < 2,4-$DNPhQ^+$. Parallel trends are also observed for the complexes of MeQ^+, PhQ^+, and 4-$AcPhQ^+$ when L^D is dmap, mim, dmabn, or PTZ. Clearly, N-phenylation does indeed cause the anticipated increase in the π-acceptor strength of the 4,4′-bipyridinium ligand, i.e., the ligand-based LUMOs are stabilized by increased delocalization. This effect is further enhanced by the placement of electron-withdrawing acetyl or nitro substituents on the phenyl ring. The average MLCT energy shift produced on replacing MeQ^+ by PhQ^+ is −0.14 eV, while that on going from PhQ^+ to 4-$AcPhQ^+$ is −0.06 eV. With a given L^A, the MLCT energy decreases as the donor strength of L^D increases, in the order PTZ < dmabn < NH_3 < mim < dmap, reflecting the destabilization of the Ru-based HOMOs.[12]

In addition to the MLCT bands, all of the complexes show intense, high-energy bands below 300 nm due to intraligand $\pi \rightarrow \pi^*$ excitations.

Electrochemical Studies. All of the complex salts, except for **5** and **6**, were studied by cyclic voltammetry in acetonitrile, and results are presented in Table 1.

All except for **4** and **10** exhibit reversible or quasi-reversible Ru(III/II) oxidation waves. For a given L^D, the $E_{1/2}$ values are independent of the nature of L^A, showing that the energy of the Ru-based HOMO is determined only by L^D. The donor abilities

(21) Hendrickx, E.; Dehu, C.; Clays, K.; Brédas, J. L.; Persoons, A. *ACS Symp. Ser.* **1995**, *601*, 82.
(22) Flipse, M. C.; de Jonge, R.; Woudenberg, R. H.; Marsman, A. W.; van Walree, C. A.; Jenneskens, L. W. *Chem. Phys. Lett.* **1995**, *245*, 297.
(23) Morrison, I. D.; Denning, R. G.; Laidlaw, W. M.; Stammers, M. A. *Rev. Sci. Instrum.* **1996**, *67*, 1445.
(24) Stadler, S.; Bourhill, G.; Bräuchle, C. *J. Phys. Chem.* **1996**, *100*, 6927.
(25) Emmert, B.; Roh, N. *Ber. Dtsch. Chem. Ges.* **1925**, *58*, 503.
(26) Tfouni, E.; Ford, P. C. *Inorg. Chem.* **1980**, *19*, 72.
(27) Chang, J. P.; Fung, E. Y.; Curtis, J. C. *Inorg. Chem.* **1986**, *25*, 4233.
(28) Ford, P.; Rudd, De F. P.; Gaunder, R.; Taube, H. *J. Am. Chem. Soc.* **1968**, *90*, 1187.
(29) Johnson, C. R.; Shepherd, R. E. *Inorg. Chem.* **1983**, *22*, 2439.

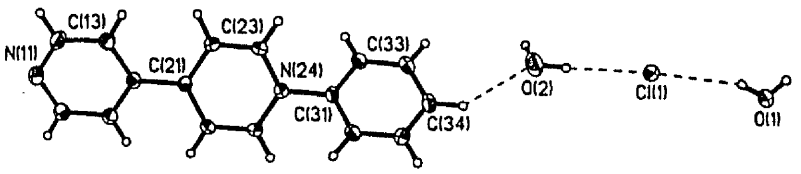

Figure 3. Structural representation of the salt $[PhQ^+]Cl\cdot 2H_2O$. The thermal ellipsoids correspond to 50% probability.

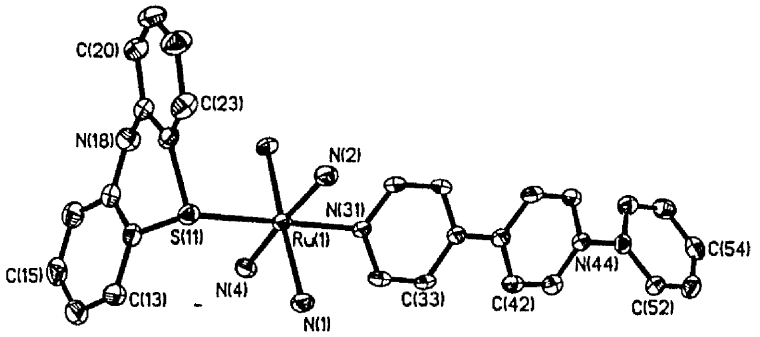

Figure 4. Structural representation of the cation in $10\cdot Et_2O$, *trans*-$[Ru(NH_3)_4(PhQ^+)(PTZ)]^{3+}$, with hydrogen atoms omitted. The thermal ellipsoids correspond to 50% probability.

Table 1. UV−Visible and Electrochemical Data in Acetonitrile

complex salt (no.)	$E_{1/2}$, V vs SCE (ΔE_p, mV)[a] Ru(III/II)	ligand waves	λ_{max}, nm (ϵ, M^{-1} cm^{-1})[b]	assignment
$[Ru(NH_3)_5(MeQ^+)](PF_6)_3$ (**1**)	0.46 (75)	−0.91 (70)	268 (16 300)	$\pi \rightarrow \pi^*$
		−1.52 (70)	590 (15 800)	$d\pi \rightarrow \pi^*$ (MeQ^+)
$[Ru(NH_3)_5(PhQ^+)](PF_6)_3$ (**2**)	0.46 (75)	−0.75 (70)	280 (18 500)	$\pi \rightarrow \pi^*$
		−1.35 (70)	628 (19 300)	$d\pi \rightarrow \pi^*$ (PhQ^+)
$[Ru(NH_3)_5(4\text{-}AcPhQ^+)](PF_6)_3$ (**3**)	0.47 (80)	−0.64 (75)	286 (20 300)	$\pi \rightarrow \pi^*$
		−1.17 (155)[c]	654 (18 000)	$d\pi \rightarrow \pi^*$ (4-$AcPhQ^+$)
$[Ru(NH_3)_5(2,4\text{-}DNPhQ^+)](PF_6)_3$ (**4**)	0.46[d]	−0.40[e]	270 (25 500)	$\pi \rightarrow \pi^*$
			660 (16 900)	$d\pi \rightarrow \pi^*$ (2,4-$DNPhQ^+$)
trans-$[Ru(NH_3)_4(PhQ^+)(dmap)](PF_6)_3$ (**7**)	0.46 (75)	−0.73 (70)	266 (24 000)	$\pi \rightarrow \pi^*$
		−1.32 (70)	ca. 352 (8400)	$d\pi \rightarrow \pi^*$ (dmap)
			658 (20 000)	$d\pi \rightarrow \pi^*$ (PhQ^+)
trans-$[Ru(NH_3)_4(PhQ^+)(mim)](PF_6)_3$ (**8**)	0.46 (70)	−0.73 (70)	280 (21 400)	$\pi \rightarrow \pi^*$
		−1.34 (70)	648 (21 500)	$d\pi \rightarrow \pi^*$ (PhQ^+)
trans-$[Ru(NH_3)_4(PhQ^+)(dmabn)](PF_6)_3$ (**9**)	0.69 (70)	−0.69 (70)	256 (16 800)	$\pi \rightarrow \pi^*$
		−1.26 (70)	290 (31 400)	$\pi \rightarrow \pi^*$
		1.30 (85)	326 (29 200)	$d\pi \rightarrow \pi^*$ (dmabn)
			572 (19 700)	$d\pi \rightarrow \pi^*$ (PhQ^+)
trans-$[Ru(NH_3)_4(PhQ^+)(PTZ)](PF_6)_3$ (**10**)	0.85 (200)	−0.64 (75)	244 (21 900)	$\pi \rightarrow \pi^*$
		−1.19 (70)	254 (20 700)	$\pi \rightarrow \pi^*$
			284 (22 500)	$\pi \rightarrow \pi^*$
			526 (10 200)	$d\pi \rightarrow \pi^*$ (PhQ^+)
trans-$[Ru(NH_3)_4(4\text{-}AcPhQ^+)(dmap)](PF_6)_3$ (**11**)	0.47 (75)	−0.63 (75)	282 (23 000)	$\pi \rightarrow \pi^*$
		−1.17 (80)	ca. 352 (7600)	$d\pi \rightarrow \pi^*$ (dmap)
			688 (18 600)	$d\pi \rightarrow \pi^*$ (4-$AcPhQ^+$)
trans-$[Ru(NH_3)_4(4\text{-}AcPhQ^+)(mim)](PF_6)_3$ (**12**)	0.48 (75)	−0.63 (70)	286 (23 000)	$\pi \rightarrow \pi^*$
		−1.16 (120)[c]	666 (19 500)	$d\pi \rightarrow \pi^*$ (4-$AcPhQ^+$)
trans-$[Ru(NH_3)_4(4\text{-}AcPhQ^+)(dmabn)](PF_6)_3$ (**13**)	0.70 (80)	−0.60 (70)	290 (40 600)	$\pi \rightarrow \pi^*$
		−1.12 (70)	320 (32 800)	$d\pi \rightarrow \pi^*$ (dmabn)
		1.33 (110)[c]	586 (21 800)	$d\pi \rightarrow \pi^*$ (4-$AcPhQ^+$)
trans-$[Ru(NH_3)_4(4\text{-}AcPhQ^+)(PTZ)](PF_6)_3$ (**14**)	0.87 (90)	−0.56 (70)	258 (23 000)	$\pi \rightarrow \pi^*$
		−1.07 (70)	286 (28 500)	$\pi \rightarrow \pi^*$
			538 (9800)	$d\pi \rightarrow \pi^*$ (4-$AcPhQ^+$)

[a] Measured in solutions ca. 10^{-3} M in analyte and 0.1 M in $[N(C_4H_9\text{-}n)_4]PF_6$ at a Pt bead working electrode with a scan rate of 200 mV s^{-1}. Ferrocene internal reference $E_{1/2} = 0.41$ V, $\Delta E_p = 70$ mV. [b] Solutions $1-4 \times 10^{-5}$ M. [c] Irreversible process as evidenced by $i_{pc} \neq i_{pa}$. [d] E_{pa} for an irreversible oxidation process. [e] E_{pc} for an irreversible reduction process.

of NH_3, dmap, and mim are sufficiently similar to give indistinguishable Ru(III/II) potentials, but the considerably less basic dmabn or PTZ ligands produce rather more positive $E_{1/2}$ values. The essentially irreversible oxidative behavior of **10** is similar to that previously observed for its MeQ^+ analogue, but **14** shows quasi-reversible behavior. The complexes in **9** and **13** each exhibit an additional, quasi-reversible wave assigned to oxidation of the dmabn ligands.

Rather more useful information is gained from examination of the ligand-based reduction waves. These data are collected in Table 2, together with those for the previously reported MeQ^+ complex salts.[12] In each complex, with the exception of **4**, the

Table 2. Visible Absorption, Ligand Reduction, and HRS Data for the Salts *trans*-$[Ru^{II}(NH_3)_4(L^D)(L^A)](PF_6)_3$ in Acetonitrile

no.	L^D	L^A	λ_{max}[MLCT], nm (ϵ, M^{-1} cm^{-1})	E_{max}[MLCT], eV	$E_{1/2}$, V vs SCE $L^{A+/0}$	$E_{1/2}$, V vs SCE $L^{A0/-}$	β_{1064}[a] × 10^{30} esu	β_0[a] × 10^{30} esu
1	NH_3	MeQ^+	590 (15 800)	2.10	−0.91	−1.52	750	123
2	NH_3	PhQ^+	628 (19 300)	1.97	−0.75	−1.35	858	220
3	NH_3	4-$AcPhQ^+$	654 (18 000)	1.90	−0.64	−1.17	1112	354
4	NH_3	2,4-$DNPhQ^+$	660 (16 900)	1.88	*b*	*b*	871	289
c	dmap	MeQ^+	614 (17 200)	2.02	−0.87	−1.46	587	130
7	dmap	PhQ^+	658 (20 000)	1.88	−0.73	−1.32	794	260
11	dmap	4-$AcPhQ^+$	688 (18 600)	1.80	−0.63	−1.17	1048	410
c	mim	MeQ^+	602 (16 200)	2.06	−0.88	−1.48	523	100
8	mim	PhQ^+	648 (21 500)	1.91	−0.73	−1.34	874	266
12	mim	4-$AcPhQ^+$	666 (19 500)	1.86	−0.63	−1.16	962	332
c	dmabn	MeQ^+	540 (17 700)	2.30	−0.85	−1.43	621	14
9	dmabn	PhQ^+	572 (19 700)	2.17	−0.69	−1.26	1273	141
13	dmabn	4-$AcPhQ^+$	586 (21 800)	2.12	−0.60	−1.12	1214	180
c	PTZ	MeQ^+	498 (8400)	2.49	−0.80	−1.32	419	40
10	PTZ	PhQ^+	526 (10 200)	2.36	−0.64	−1.19	698	12
14	PTZ	4-$AcPhQ^+$	538 (9800)	2.30	−0.56	−1.07	727	12

[a] β_{1064} is the uncorrected first hyperpolarizability measured using a 1064 nm Nd:YAG laser fundamental; β_0 is the static hyperpolarizability estimated by using the two-level model.[31] The quoted cgs units (esu) can be converted into SI units (C^3 m^3 J^{-2}) by dividing by a factor of 2.693 × 10^{20}. [b] Irreversible. [c] Reference 12.

Table 3. Crystallographic Data and Refinement Details for $[PhQ^+]Cl\cdot 2H_2O$ and $\mathbf{10}\cdot Et_2O$

	$[PhQ^+]Cl\cdot 2H_2O$	$\mathbf{10}\cdot Et_2O$
empirical formula	$C_{16}H_{17}ClN_2O_2$	$C_{32}H_{44}F_{18}N_7OP_3RuS$
M_r	304.77	1110.78
cryst syst	triclinic	triclinic
space group	$P\bar{1}$	$P\bar{1}$
a, Å	7.675(2)	10.310(3)
b, Å	9.895(2)	10.698(2)
c, Å	10.175(2)	20.986(4)
α, deg	96.003(1)	95.09(2)
β, deg	104.74(2)	91.49(2)
γ, deg	90.398(1)	105.53(2)
V, Å^3	742.7(3)	2218.3(8)
Z	2	2
D_c, g cm^{-3}	1.363	1.663
T, °C	−100(2)	−100(2)
λ, Å	0.710 73 (Mo Kα)	0.710 73 (Mo Kα)
F(000)	320	1120
μ, cm^{-1}	0.263	0.622
scan type	φ	φ
θ range	2.07−27.47°	1.95−27.48°
h,*k*,*l* ranges	−9/9, −12/12, −13/13	−13.13, −13/13, −27/27
no. of reflns collected	7592	23 184
no. of unique reflns (R_{int})	3353 (0.0207)	10 055 (0.0459)
data, restraints, parameters	3352, 0, 202	10 054, 52, 577
final *R* indices [$I > 2\sigma(I)$][a,b]	R_1= 0.0322, wR_2 = 0.0865	R_1= 0.0532, wR_2 = 0.1281
weighting factors (*x*, *y*)[b]	0.0537, 0	0.0735, 0
goodness of fit, *S*	0.971	1.022
peak and hole, e Å^{-3}	0.247, −0.245	1.205, −0.692

[a] Structure was refined on F_o^2 using all data; the value of R_1 is given for comparison with older refinements based on F_o with a typical threshold of $F_o > 4\sigma(F_o)$. [b] $wR_2 = [\Sigma w(F_o^2 - F_c^2)^2/\Sigma w(F_o^2)^2]^{1/2}$; $S = [\Sigma w(F_o^2 - F_c^2)^2/(M - N)]^{1/2}$ where M = number of reflections and N = number of parameters; $w^{-1} = [\sigma^2(F_o^2) + (xP)^2 + yP]$ and $P = [\max(F_o^2, 0) + 2F_c^2]/3$.

4,4′-bipyridinium ligands give rise to two reversible or quasi-reversible, one-electron-reduction waves assigned to the $L^{A+/0}$ and $L^{A0/-}$ redox couples. For a given L^D, both of these potentials become less negative in the order MeQ^+ < PhQ^+ < 4-$AcPhQ^+$, confirming the stabilization of the ligand-based LUMOs shown in the visible absorption spectra (vide supra). Replacement of the methyl substituent of MeQ^+ by phenyl produces average positive shifts of 150 mV in both potentials, while substitution of the phenyl ring with a 4-acetyl group produces average positive shifts of 100 and 150 mV in the first and second reduction potentials, respectively. As expected, these shifts for the first reduction potentials correlate reasonably well with the changes in the MLCT maximum energies (vide supra).

Structural Determinations. Single-crystal X-ray structures were obtained for $[PhQ^+]Cl\cdot 2H_2O$ and $\mathbf{10}\cdot Et_2O$. Representations of $[PhQ^+]Cl\cdot 2H_2O$ and the cation in $\mathbf{10}\cdot Et_2O$ are shown in Figures 3 and 4.

The cation in $[PhQ^+]Cl\cdot 2H_2O$ adopts a twisted conformation, with torsion angles C(13)−C(14)-C(21)−C(22) = −19.8° and C(23)−N(24)−C(31)−C(32) = −39.7°. Hydrogen bonding is observed between the aromatic hydrogen H(34) of the PhQ^+ cation and the oxygen atom O(2) of one of the water molecules, with a bond length of 2.392 Å. Hydrogen bonding is also

Table 4. Selected Bond Distances (Å) and Angles (deg) for $[PhQ^+]Cl\cdot 2H_2O$

N(11)–C(16)	1.334(2)	C(23)–N(24)	1.358(2)
N(11)–C(12)	1.345(2)	N(24)–C(25)	1.356(2)
C(12)–C(13)	1.386(2)	N(24)–C(31)	1.460(2)
C(13)–C(14)	1.387(2)	C(25)–C(26)	1.374(2)
C(14)–C(15)	1.398(2)	C(31)–C(36)	1.388(2)
C(14)–C(21)	1.487(2)	C(31)–C(32)	1.389(2)
C(15)–C(16)	1.385(2)	C(32)–C(33)	1.388(2)
C(21)–C(26)	1.394(2)	C(33)–C(34)	1.386(2)
C(21)–C(22)	1.402(2)	C(34)–C(35)	1.388(2)
C(22)–C(23)	1.373(2)	C(35)–C(36)	1.389(2)
C(16)–N(11)–C(12)	116.26(12)	C(25)–N(24)–C(23)	120.24(11)
N(11)–C(12)–C(13)	123.59(13)	C(25)–N(24)–C(31)	119.59(11)
C(12)–C(13)–C(14)	119.61(12)	C(23)–N(24)–C(31)	120.16(10)
C(13)–C(14)–C(15)	117.20(12)	N(24)–C(25)–C(26)	120.35(12)
C(13)–C(14)–C(21)	121.80(11)	C(25)–C(26)–C(21)	121.00(11)
C(15)–C(14)–C(21)	121.00(12)	C(36)–C(31)–C(32)	121.94(12)
C(16)–C(15)–C(14)	118.91(13)	C(36)–C(31)–N(24)	118.97(11)
N(11)–C(16)–C(15)	124.39(12)	C(32)–C(31)–N(24)	119.09(12)
C(26)–C(21)–C(22)	117.21(12)	C(33)–C(32)–C(31)	118.69(13)
C(26)–C(21)–C(14)	121.31(11)	C(34)–C(33)–C(32)	120.26(12)
C(22)–C(21)–C(14)	121.47(12)	C(33)–C(34)–C(35)	120.22(13)
C(23)–C(22)–C(21)	120.41(12)	C(34)–C(35)–C(36)	120.48(13)
N(24)–C(23)–C(22)	120.78(11)	C(31)–C(36)–C(35)	118.41(12)

Table 5. Selected Bond Distances (Å) and Angles (deg) for $\mathbf{10}\cdot Et_2O$

Ru(1)–N(1)	2.146(3)	Ru(1)–N(4)	2.139(3)
Ru(1)–N(2)	2.140(3)	Ru(1)–N(31)	2.097(3)
Ru(1)–N(3)	2.144(3)	Ru(1)–S(11)	2.3350(12)
N(1)–Ru(1)–N(2)	85.75(14)	N(3)–Ru(1)–N(4)	88.30(13)
N(1)–Ru(1)–N(3)	177.50(13)	N(3)–Ru(1)–N(31)	88.38(13)
N(1)–Ru(1)–N(4)	93.21(14)	N(3)–Ru(1)–S(11)	92.31(9)
N(1)–Ru(1)–N(31)	89.69(13)	N(4)–Ru(1)–N(31)	87.59(13)
N(1)–Ru(1)–S(11)	89.62(10)	N(4)–Ru(1)–S(11)	92.53(10)
N(2)–Ru(1)–N(3)	92.65(14)	N(31)–Ru(1)–S(11)	179.31(9)
N(2)–Ru(1)–N(4)	176.79(13)	C(12)–S(11)–Ru(1)	111.19(14)
N(2)–Ru(1)–N(31)	89.37(14)	C(24)–S(11)–Ru(1)	109.42(14)
N(2)–Ru(1)–S(11)	90.49(11)	C(12)–S(11)–C(24)	98.0(2)

observed between the hydrogen atom H(2B), the anion Cl(1), and hydrogen atom H(1B). The lengths of the hydrogen bonds Cl(1)–H(1B) and Cl(1)–H(2B) are 2.535 and 2.363 Å, respectively. This is the first *N*-phenyl-4,4′-bipyridinium compound and only the second hetero-*p*-terphenyl analogue to be structurally characterized. The recently reported structure of borabenzene-4-phenylpyridine shows a twisted conformation similar to that of $[PhQ^+]Cl\cdot 2H_2O$.[30]

The structure of the complex in $\mathbf{10}\cdot Et_2O$ resembles that of its MeQ^+ analogue.[12] In the latter the torsion angle between the two pyridyl rings of the MeQ^+ ligand is 9.6°, whereas in $\mathbf{10}\cdot Et_2O$ the equivalent angle is only 2.6°. This compares with 19.8° in $[PhQ^+]Cl\cdot 2H_2O$. These data indicate that the extent of electronic delocalization between the two pyridyl rings in the solid state is greater in $\mathbf{10}\cdot Et_2O$ than in its MeQ^+ analogue, and that complexation of the PhQ^+ ligand enhances inter-ring electronic coupling. The twisting between the phenyl and pyridinium rings in $\mathbf{10}\cdot Et_2O$ is similar to that in $[PhQ^+]Cl\cdot 2H_2O$, with the C(45)–N(44)–C(51)–C(52) torsion angle being 135°.

Nonlinear Optical Studies. The first hyperpolarizabilities β of the new complexes were measured in acetonitrile using the HRS technique[11,19] with a 1064 nm Nd:YAG laser fundamental. Static hyperpolarizabilities were obtained by application of the two-level model,[31] and results are presented in Table 2. The β_0 values for **10** and **14** are grossly underestimated because a neglect of damping renders the two-level model invalid when the absorption maximum is sufficiently close to the second-harmonic frequency (532 nm).

The large resonance-enhanced β values obtained are comparable to those previously reported for ruthenium organometallics.[9,10] More significantly, the β_0 values are also extremely large and those for the 4-$AcPhQ^+$ complexes in **3**, **11**, and **12** are somewhat greater than those measured for Ru(II) σ-acetylide complexes, for which the highest value reported to date is 232 $\times 10^{-30}$ esu.[9a] Indeed, the β_0 for **11** of 410 $\times 10^{-30}$ esu is almost the largest yet found for a metal-containing chromophore. Although a substituted $[Ru(bpy)_3]^{2+}$ derivative (bpy = 2,2′-bipyridine) was claimed to possess a β_0 value in excess of 10^{-27} esu,[32] it appears that this observation may be primarily due to two-photon excited luminescence, rather than harmonic scattering.[23] A push–pull arylethynyl zinc porphyrin has a β_0 of 800 $\times 10^{-30}$ esu,[33] but the extent of involvement of the metal in the NLO response of such systems is unclear. Within the realm of purely organic NLO molecules, significantly larger β_0 values have been reported only for donor–acceptor polyenes.[34]

The effects of increasing the acceptor strength of L^A while keeping L^D fixed, observed in the visible absorption spectra (vide supra), are also shown in the β_0 values, which consistently increase in the order $L^A = MeQ^+ < PhQ^+ < 4\text{-}AcPhQ^+$. The single complex of 2,4-$DNPhQ^+$ (**4**) provides an apparent, unexpected exception to this trend, but the difference in β_0 between **4** and **3** may not be significant. A 2,4-dinitrophenyl group is evidently more electron deficient than its 4-acetyl counterpart, so the lower β_0 for **4** can most likely be traced to a reduction in delocalization through the *N*-phenylpyridinium unit arising from the steric effect of the *o*-NO_2 group. The crystallographic studies (vide supra), which indicate that the extent of electronic delocalization within the 4,4′-bipyridinium unit is greater in $\mathbf{10}\cdot Et_2O$ than in its MeQ^+ analogue, are consistent with the larger β_0 values for the PhQ^+ complexes with respect to their MeQ^+ counterparts.

For a given L^A, although the MLCT energies always decrease in the order $L^D = NH_3 >$ mim > dmap (vide supra), the corresponding differences in the β_0 values are small and no clear trends are evident. This indicates that the presence of a trans N-heterocyclic ligand is not especially important in producing a large hyperpolarizability. It is likely that inter-ligand π–π coupling occurs through the metal centers,[26,35] but the potential benefits of this in terms of extending the overall conjugation are clearly minor. Furthermore, the dmap complexes exhibit a second, high-energy MLCT transition which opposes the low-energy MLCT process. As indicated by the Ru(III/II) reduction potentials (vide supra), the role of L^D is primarily to determine the amount of electron density at the Ru(II) center and hence its π-donor strength toward L^A.

According to the two-level model,[31] the dominant component of β is proportional to both $\Delta\mu$ (the dipole moment change

(30) Qiao, S.; Hoic, D. A.; Fu, G. C. *Organometallics* **1997**, *16*, 1501.

(31) (a) Oudar, J. L.; Chemla, D. S. *J. Chem. Phys.* **1977**, *66*, 2664. (b) Oudar, J. L. *J. Chem. Phys.* **1977**, *67*, 446. (c) Zyss, J.; Oudar, J. L. *Phys. Rev. A* **1982**, *26*, 2016.

(32) Dhenaut, C.; Ledoux, I.; Samuel, I. D. W.; Zyss, J.; Bourgault, M.; Le Bozec, H. *Nature* **1995**, *374*, 339.

(33) LeCours, S. M.; Guan, H.-W.; DiMagno, S. G.; Wang, C. H.; Therien, M. J. *J. Am. Chem. Soc.* **1996**, *118*, 1497.

(34) See, for example: (a) Blanchard-Desce, M.; Alain, V.; Bedworth, P. V.; Marder, S. R.; Fort, A.; Runser, C.; Barzoukas, M.; Lebus, S.; Wortmann, R. *Chem. Eur. J.* **1997**, *3*, 1091. (b) Hsu, C.-C.; Shu, C.-F.; Huang, T.-H.; Wang, C. H.; Lin, J.-L.; Wang, Y.-K.; Zang, Y.-L. *Chem. Phys. Lett.* **1997**, *274*, 466.

(35) (a) Zwickel, A. M.; Creutz, C. *Inorg. Chem.* **1971**, *10*, 2395. (b) Wishart, J. F.; Zhang, X.; Isied, S. S.; Potenza, J. A.; Schugar, H. J. *Inorg. Chem.* **1992**, *31*, 3179.

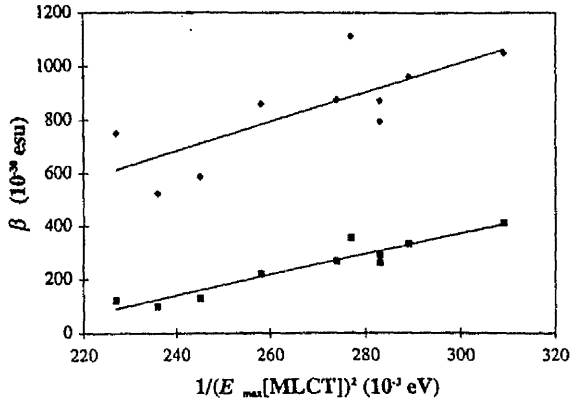

Figure 5. Plot of the first hyperpolarizability against the inverse square of the MLCT energy for the salts **1**−**4**, **7**, **8**, **11**, **12**, and *trans*-[Ru(NH$_3$)$_4$(MeQ$^+$)(L^D)](PF$_6$)$_3$ (L^D = dmap or mim)[12] (◆ = β; ■ = β_0).

between the ground and excited states) and μ_{ge}^2 (the square of the transition oscillator strength) and inversely proportional to E_{ge}^2 (the square of the energy gap between the two states). A linear correlation between β and $1/E_{ge}^2$ has previously been found for donor−acceptor diphenylacetylenes,[36] indicating that the charge-transfer energy plays a more significant role in determining β than does $\Delta\mu$ or μ_{ge} in such molecules. A similar analysis reveals a relatively poor correlation for β_{1064}, but a much better linear trend for β_0 for the present compounds (Figure 5). The data for the dmabn or PTZ complexes are excluded because their β and β_0 values are less reliable due to the combined effects of resonance enhancement and the limitations of the two-level model. The observed correlation confirms that the visible MLCT excitations are indeed responsible for the large hyperpolarizabilities, as indicated by our earlier results.[12] Furthermore, the product $\Delta\mu(\mu_{ge}^2)$ apparently remains relatively constant within this group of complexes.

(36) Stiegman, A. E.; Graham, E.; Perry, K. J.; Khundkar, L. R.; Cheng, L.-T.; Perry, J. W. *J. Am. Chem. Soc.* **1991**, *113*, 7658.

Conclusions

Dipolar ruthenium(II) tetra- or pentaammine complexes of N-substituted 4,4′-bipyridinium ligands exhibit β_0 values larger than those of most other organotransition metal complexes or organic molecules investigated previously. Intense, low-energy MLCT absorptions are the basis for these extremely large quadratic hyperpolarizabilities which can be tuned by rational changes in ligand structure. We have clearly demonstrated that N-phenylation of 4,4′-bipyridinium ligands is an effective means to increase β_0 in MLCT-based chromophores, and we anticipate that such an approach will also be applicable to purely organic compounds.

It should be emphasized that the properties of these complexes are currently by no means optimized. Present synthetic work includes variations in ligand structures in order to allow the maximization of β_0 and the development of further structure−property correlations. The effects of the conformation of L^A on β_0 and the direct comparison of the donor properties of Ru(II) ammine centers with traditional electron-rich organic groups are of particular interest. The use of Ru(III/II) redox couples as a means to achieve reversible modulation of molecular NLO properties is also an immediate goal. Aspects of importance for potential practical applications such as stability and transparency at relevant wavelengths are also to be addressed.

Acknowledgment. S.H. is a Research Assistant of the Fund for Scientific Research−Flanders. This work was supported by research grants from The Royal Society, from the Belgian National Fund for Scientific Research (G.0308.96), from the Belgian government (IUAP-P4/11), and from the University of Leuven (GOA/1/95). Thanks are due to Johnson Matthey plc for a generous loan of ruthenium trichloride.

Supporting Information Available: Tables of final atomic fractional coordinates, thermal parameters, and nonessential bond lengths and angles (9 pages). Ordering information is given on any current masthead page.

IC971411S

DALTON
FULL PAPER

Tuning of charge-transfer absorption and molecular quadratic non-linear optical properties in ruthenium(II) ammine complexes †

Benjamin J. Coe,*[a] James A. Harris,[a] Inge Asselberghs,[b] André Persoons,[b,c] John C. Jeffery,[d] Leigh H. Rees,[d] Thomas Gelbrich[e] and Michael B. Hursthouse[e]

[a] *Department of Chemistry, University of Manchester, Oxford Road, Manchester, UK M13 9PL. E-mail: b.coe@man.ac.uk*
[b] *Laboratory of Chemical and Biological Dynamics, Center for Research on Molecular Electronics and Photonics, University of Leuven, Celestijnenlaan 200D, B-3001 Leuven, Belgium*
[c] *Optical Sciences Center, University of Arizona, Tucson, Arizona, AZ 85721, USA*
[d] *Department of Chemistry, University of Bristol, Cantock's Close, Bristol, UK BS8 1TS*
[e] *EPSRC X-ray Crystallography Service, Department of Chemistry, University of Southampton, Highfield, Southampton, UK SO17 1BJ*

Received 13th July 1999, Accepted 1st September 1999

The ligands *N*-methyl-2,7-diazapyrenium (Medap$^+$), *N*-(2-pyrimidyl)-4,4′-bipyridinium (PymQ$^+$), *N*-methyl-4-[*trans*-2-(4-pyridyl)ethenyl]pyridinium (Mebpe$^+$) and *N*-phenyl-4-[*trans*-2-(4-pyridyl)ethenyl]pyridinium (Phbpe$^+$) have been used to prepare a series of complex salts *trans*-[Ru^{II}(NH$_3$)$_4$(L^D)(L^A)][PF$_6$]$_3$ [L^D = NH$_3$ and L^A = Medap$^+$ **1**, PymQ$^+$ **2**, Mebpe$^+$ **3** or Phbpe$^+$ **4**; L^D = pyridine (py) and L^A = Medap$^+$ **8**, PymQ$^+$ **9**, Mebpe$^+$ **10** or Phbpe$^+$ **11**; L^D = 1-methylimidazole (mim) and L^A = Medap$^+$ **12**, PymQ$^+$ **13**, Mebpe$^+$ **14** or Phbpe$^+$ **15**]. The salt *trans*-[Ru^{II}(NH$_3$)$_4$(py)(4,4′-bpy)][PF$_6$]$_2$ (4,4′-bpy = 4,4′-bipyridine) **16** has also been prepared. The dipolar complexes in **1–4** and **8–15** exhibit intense d$_\pi$(Ru^{II})→π*(L^A) metal-to-ligand charge-transfer (MLCT) absorptions in the region 560–700 nm. For a given L^A, the MLCT energy decreases as the donor strength of L^D increases, in the order py < NH$_3$ < mim. Within the pairs of Medap$^+$/PymQ$^+$ complexes, the energy of the Ru-based HOMO is constant and the MLCT energy decreases by *ca.* 0.3 eV as the acceptor strength of L^A increases on going from Medap$^+$ to PymQ$^+$. The complexes of Mebpe$^+$ or Phbpe$^+$ also have similar HOMO energies which are lower than those of their Medap$^+$/PymQ$^+$ counterparts due to the increased basicity of L^A. Replacement of Mebpe$^+$ by Phbpe$^+$ decreases the MLCT energy by *ca.* 0.1 eV due to the greater electron-withdrawing ability of Phbpe$^+$. Single-crystal structures of **8**·4MeCN and **16**·2MeCN have been determined. Molecular first hyperpolarizabilities β of **1–4** and **8–15**, obtained from hyper-Rayleigh scattering measurements at 1064 nm, are in the range (579–1068) × 10^{-30} esu. Static hyperpolarizabilities β_0 derived by using the two-level model are also very large, with **13** having the largest at 336 × 10^{-30} esu. In general, β_0 increases as the absorption energy decreases, in keeping with the two-level model.

Introduction

Molecular materials possessing non-linear optical (NLO) properties are of great interest for applications in optoelectronic and photonic devices of the 21st century.[1] Organotransition metal complexes form an important sub-class of NLO materials which have recently attracted increasing attention.[2] Such compounds are promising because polarizable d electrons can contribute to enhanced NLO responses, and redox activity provides extensive opportunities for modulation of NLO properties. The creation of materials for quadratic (second order) NLO applications begins with the molecular engineering of chromophores possessing large first hyperpolarizabilities, β. Detailed structure–activity relationships for β of purely organic compounds are well established,[1] but comparable understanding for organotransition metal complexes is poorly developed.[2] Systematic investigations into the quadratic NLO activity of metal complexes are hence timely.

The quadratic NLO properties of ruthenium complexes have proven an especially popular research topic, and large β responses have been reported.[3–8] Most of these studies have involved organometallic σ-acetylide or allenylidene complexes with {Ru^{II}(η^5-L′)L$_2$}$^+$ [L′ = cyclopentadienyl or indenyl; L$_2$ = mono- or bi-dentate phosphine ligand(s)] or *trans*-{Ru^{II}Cl(dppm)$_2$}$^+$ [dppm = bis(diphenylphosphino)methane] electron donor groups.[5–8] We are investigating the quadratic NLO behaviour of ruthenium ammines which combine synthetic accessibility with especially well understood redox and spectroscopic properties. Initial studies have shown that {Ru^{II}(NH$_3$)$_5$}$^{2+}$ or *trans*-{Ru^{II}(NH$_3$)$_4$L}$^{2+}$ (L = 4-dimethylaminopyridine or 1-methylimidazole) complexes of *N*-methyl/aryl-4,4′-bipyridinium ligands possess very large β values.[9] In such dipolar molecules the d^6 ruthenium(II) centre acts as a powerful π donor whilst the pyridinium ring is an acceptor. These complexes hence exhibit intense, low energy metal-to-ligand charge-transfer (MLCT) absorptions, and a good correlation exists between β_0 (the static first hyperpolarizability) and $1/E^2$ where E is the MLCT energy.[9c] This is in accord with the two-level model which is often used to relate charge-transfer absorption and NLO properties in classical dipolar organic chromophores.[10] Furthermore, the NLO responses of the {Ru^{II}(NH$_3$)$_5$}$^{2+}$ complexes can be reversibly and very effectively switched *via* Ru$^{III/II}$ redox.[11]

We have begun to develop a versatile family of complexes, the MLCT absorptions and quadratic NLO responses of which are readily controlled. The subject of this report is the further tuning of these properties in ruthenium(II) ammine complexes,

† *Supplementary data available*: rotatable 3-D crystal structure diagram in CHIME format. See http://www.rsc.org/suppdata/dt/1999/3617/

This journal is © The Royal Society of Chemistry 1999

principally by changing the structure of the acceptor-substituted ligand. Previous work with NLO-active transition metal complexes has often borrowed "molecular engineering" concepts from purely organic molecules,[2] for example by simply replacing an amino donor with an electron-rich metal centre. We are seeking to develop novel approaches towards modifying the properties of MLCT chromophores which have no existing counterparts in simple organics. The results of these studies are of direct relevance to the design of other transition metal-based NLO compounds and also related organic chromophores.

Experimental

Materials and procedures

The compound $RuCl_3 \cdot 2H_2O$ was supplied by Johnson Matthey plc. The salts $[Ru^{II}(NH_3)_5(H_2O)][PF_6]_2$,[12] *trans*-$[Ru^{II}Cl(NH_3)_4(SO_2)]Cl$,[12] *trans*-$[Ru^{III}(SO_4)(NH_3)_4(py)]Cl$,[12] *N*-methyl-2,7-diazapyrenium chloride ([Medap$^+$]Cl)[13] and *N*-methyl-4-[*trans*-2-(4-pyridyl)ethenyl]pyridinium iodide ([Mebpe$^+$]I)[14] were prepared according to published procedures. The latter two salts were metathesized to [Medap$^+$]PF_6 and [Mebpe$^+$]PF_6, respectively, by precipitation from water–aqueous NH_4PF_6. 2,7-Diazapyrene was prepared by using a combination of published procedures,[15,16] with one simple modification: in the synthesis of the intermediate 1,3,6,8-tetrahydro-2,7-dimethyldiazapyrene we found that extraction into boiling methanol affords a higher yield of a purer product compared with the published THF extraction method.[16] All other reagents were obtained commercially and used as supplied. Products were dried overnight at room temperature in a vacuum desiccator ($CaSO_4$) prior to characterization.

Physical measurements

Proton NMR spectra were recorded on a Varian Gemini 200 spectrometer and all shifts are referenced to $SiMe_4$. The fine splitting of pyridyl or phenyl ring AA′BB′ patterns is ignored and the signals are reported as simple doublets, with *J* values referring to the two most intense peaks. Solvents of crystallization were detected as singlets at δ 2.86 (water) or 2.09 (acetone) in acetone-d_6 solutions. Elemental analyses were performed by the Microanalytical Laboratory, University of Manchester and UV/VIS spectra were obtained by using a Varian Cary 1E spectrophotometer.

Cyclic voltammetric measurements were carried out by using an EG&G PAR model 173 potentiostat/galvanostat with a model 175 universal programmer. A single-compartment cell was used with the saturated calomel reference electrode (SCE) separated by a salt bridge from the platinum-bead working electrode and platinum-wire auxiliary electrode. Acetonitrile (HPLC grade) was used as received and tetra-*n*-butylammonium hexafluorophosphate, twice recrystallized from ethanol and dried *in vacuo*, as supporting electrolyte. Solutions containing *ca.* 10^{-3} mol dm^{-3} analyte (0.1 mol dm^{-3} electrolyte) were deaerated by purging with N_2. All $E_{1/2}$ values were calculated from $(E_{pa} + E_{pc})/2$ at a scan rate of 200 mV s^{-1}.

Syntheses

4-Methyl-*N*-phenylpyridinium chloride, [Phpic$^+$]Cl. A solution of 4-methylpyridine (2.4 cm^3, 25 mmol) and chloro-2,4-dinitrobenzene (5 g, 25 mmol) in ethanol (25 cm^3) was heated at reflux for 2 h. After cooling to room temperature, diethyl ether was added and the black precipitate filtered off, washed with diethyl ether and dried. The crude product was purified by precipitation from boiling ethanol–diethyl ether to afford a grey solid which was filtered off, washed with diethyl ether and dried: 3.68 g. $\delta_H(D_2O)$ 9.31 (1 H, d, *J* 2.5 Hz, H^3), 8.89–8.83 (3 H, m, H^5 + C_5H_4N), 8.19–8.06 (3 H, m, H^6 + C_5H_4N) and 2.79 (3 H, s, Me). This material was dissolved in boiling ethanol (30 cm^3), aniline (5.6 cm^3, 61 mmol) was added and the resulting solution heated at reflux for 3 h. The solution was cooled to room temperature and reduced to half volume *in vacuo*. On addition of water a green material precipitated which was filtered off, washed with water and discarded. The filtrate was reduced to dryness and dissolved in ethanol. The addition of diethyl ether afforded a golden-brown precipitate which was filtered off, washed with diethyl ether and dried: yield 2.24 g (39%). $\delta_H(D_2O)$ 8.85 (2 H, d, *J* 6.6, C_5H_4N), 7.99 (2 H, d, *J* 6.9 Hz, C_5H_4N), 7.67 (5 H, s, Ph) and 2.71 (3 H, s, Me) (Found: C, 63.30; H, 6.06; N, 6.23. Calc. for $C_{12}H_{12}ClN \cdot 1.25H_2O$: C, 63.16; H, 6.40; N, 6.14%).

***N*-Phenyl-4-[*trans*-2-(4-pyridyl)ethenyl]pyridinium chloride, [Phbpe$^+$]Cl.** A mixture of [Phpic$^+$]Cl·1.25H_2O (3.08 g, 13.5 mmol), pyridine-4-carbaldehyde (1.5 cm^3, 15.8 mmol) and piperidine (0.4 cm^3) in ethanol (3 cm^3) was heated at reflux for 15 min. The resulting solution was cooled in an ice-bath, causing formation of a solid mass. A black liquid was decanted off and the residue dissolved in ethanol and precipitated by addition of diethyl ether. The pink solid was filtered off, washed with diethyl ether and dried: yield 1.04 g (23%). $\delta_H(D_2O)$ 8.94 (2 H, d, *J* 6.8, C_5H_4N), 8.48 (2 H, d, *J* 5.9, C_5H_4N), 8.19 (2 H, d, *J* 6.7, C_5H_4N), 7.71 (1 H, d, *J* 16.4, CH), 7.69 (5 H, s, Ph), 7.59 (2 H, d, *J* 6.2, C_5H_4N) and 7.51 (1 H, d, *J* 16.4 Hz, CH) (Found: C, 64.19; H, 5.38; N, 8.06. Calc. for $C_{18}H_{15}ClN_2 \cdot 2.25H_2O$: C, 64.48; H, 5.86; N, 8.35%).

***N*-Phenyl-4-[*trans*-2-(4-pyridyl)ethenyl]pyridinium hexafluorophosphate, [Phbpe$^+$]PF_6.** The salt [Phbpe$^+$]Cl·2.25H_2O (200 mg, 0.596 mmol) was dissolved in the minimum volume of water and aqueous NH_4PF_6 added dropwise. The white precipitate was filtered off, washed with water and dried: yield 210 mg (87%). $\delta_H(CD_3COCD_3)$ 9.31 (2 H, d, *J* 6.8, C_5H_4N), 8.71 (2 H, d, *J* 6.1, C_5H_4N), 8.57 (2 H, d, *J* 6.8, C_5H_4N), 8.16 (1 H, d, *J* 16.4, CH), 8.00–7.95 (2 H, m, Ph), 7.94 (1 H, d, *J* 16.4, CH), 7.82–7.78 (3 H, m, Ph) and 7.72 (2 H, d, *J* 6.0 Hz, C_5H_4N) (Found: C, 53.56; H, 3.77; N, 6.72. Calc. for $C_{18}H_{15}F_6N_2P$: C, 53.48; H, 3.74; N, 6.93%).

***N*-(2-Pyrimidyl)-4,4′-bipyridinium chloride, [PymQ$^+$]Cl.** A mixture of 4,4′-bipyridine (2.06 g, 13.2 mmol) and 2-chloropyrimidine (1.00 g, 8.73 mmol) was heated quickly to *ca.* 70 °C. Upon solidification, the green material was dissolved in ethanol (5 cm^3) and heated at reflux for 6 h. Addition of diethyl ether afforded a green precipitate which was filtered off, washed with diethyl ether and dried: yield 1.30 g (55%). $\delta_H(D_2O)$ 10.08 (2 H, d, *J* 7.3, C_5H_4N), 9.10 (2 H, d, *J* 4.9, $C_4H_3N_2$), 8.74 (2 H, d, *J* 6.1, C_5H_4N), 8.61 (2 H, d, *J* 7.3, C_5H_4N), 7.96 (2 H, d, *J* 6.3, C_5H_4N) and 7.85 (1 H, t, *J* 5.0 Hz, $C_4H_3N_2$) (Found: C, 61.94; H, 4.42; N, 20.39. Calc. for $C_{14}H_{11}ClN_4$: C, 62.11; H, 4.10; N, 20.70%).

***N*-(2-Pyrimidyl)-4,4′-bipyridinium hexafluorophosphate, [PymQ$^+$]PF_6.** The salt [PymQ$^+$]Cl (500 mg, 1.85 mmol) was dissolved in the minimum volume of water and aqueous NH_4PF_6 added dropwise. The white precipitate was filtered off, washed with water and dried: yield 665 mg (95%). $\delta_H(CD_3COCD_3)$ 10.36 (2 H, d, *J* 7.4, C_5H_4N), 9.29 (2 H, d, *J* 4.8, $C_4H_3N_2$), 8.96–8.91 (4 H, m, C_5H_4N), 8.14 (2 H, d, *J* 6.3, C_5H_4N) and 8.04 (1 H, t, *J* 4.8 Hz, $C_4H_3N_2$) (Found: C, 44.36; H, 2.93; N, 14.88. Calc. for $C_{14}H_{11}F_6N_4P$: C, 44.22; H, 2.92; N, 14.73%).

[$Ru^{II}(NH_3)_5$(Medap$^+$)][PF_6]$_3$ 1. A solution of [$Ru^{II}(NH_3)_5(H_2O)$][PF_6]$_2$ (250 mg, 0.505 mmol) and [Medap$^+$]PF_6 (188 mg, 0.516 mmol) in Ar-degassed acetone (5 cm^3) was stirred at room temperature under Ar for 2 h. The addition of diethyl ether afforded a dark precipitate which was filtered off, washed with diethyl ether and dried. Purification was effected by

precipitations from acetone–aqueous NH_4PF_6 and then from acetone–diethyl ether to afford a dark purple solid: yield 137 mg (32%). $\delta_H(CD_3COCD_3)$ 10.05 (2 H, s, $C_{14}H_8N_2$), 9.83 (2 H, s, $C_{14}H_8N_2$), 8.54 (2 H, d, *J* 9.2, $C_{14}H_8N_2$), 8.48 (2 H, d, *J* 9.2 Hz, $C_{14}H_8N_2$), 4.89 (3 H, s, Me), 3.59 (3 H, s, *trans*-NH_3) and 2.81 (12 H, s, 4 × *cis*-NH_3) (Found: C, 21.10; H, 3.08; N, 11.49. Calc. for $C_{15}H_{26}F_{18}N_7P_3Ru$: C, 21.44; H, 3.12; N, 11.67%).

$[Ru^{II}(NH_3)_5(PymQ^+)][PF_6]_3$ 2. This was prepared in identical manner to salt **1** by using $[Ru^{II}(NH_3)_5(H_2O)][PF_6]_2$ (100 mg, 0.202 mmol) and $[PymQ^+]PF_6$ (77 mg, 0.203 mmol) in place of $[Medap^+]PF_6$. Purification was effected by several precipitations from acetone–diethyl ether to afford a dark blue solid: yield 75 mg (42%). $\delta_H(CD_3COCD_3)$ 10.17 (2 H, d, *J* 7.5, C_5H_4N), 9.28–9.22 (4 H, m, $C_5H_4N + C_4H_3N_2$), 8.94 (2 H, d, *J* 7.5 Hz, C_5H_4N), 8.03–7.96 (3 H, m, $C_5H_4N + C_4H_3N_2$), 3.75 (3 H, s, *trans*-NH_3) and 2.74 (12 H, s, 4 × *cis*-NH_3) (Found: C, 19.15; H, 3.14; N, 13.76. Calc. for $C_{14}H_{26}F_{18}N_9P_3Ru \cdot 2H_2O$: C, 18.84; H, 3.39; N, 14.13%).

$[Ru^{II}(NH_3)_5(Mebpe^+)][PF_6]_3$ 3. This was prepared in similar manner to salt **2** by using $[Mebpe^+]I$ (79 mg, 0.244 mmol) in place of $[PymQ^+]PF_6$ and 1:1 water–acetone (5 cm^3) in place of acetone. The addition of aqueous NH_4PF_6 afforded a dark precipitate which was filtered off, washed with water and dried. Purification was effected by precipitations from acetone–diethyl ether, acetone–NBu^n_4Cl and finally water–aqueous NH_4PF_6 to afford a dark purple solid: yield 58 mg (35%). $\delta_H(CD_3COCD_3)$ 8.94 (4 H, d, *J* 6.9, C_5H_4N), 8.33 (2 H, d, *J* 7.0, C_5H_4N), 8.02 (1 H, d, *J* 16.4, CH), 7.89 (1 H, d, *J* 16.4, CH), 7.54 (2 H, d, *J* 6.8 Hz, C_5H_4N), 4.49 (3 H, s, Me), 3.41 (3 H, s, *trans*-NH_3) and 2.65 (12 H, s, 4 × *cis*-NH_3) (Found: C, 19.28; H, 3.18; N, 11.68. Calc. for $C_{13}H_{28}F_{18}N_7P_3Ru$: C, 19.08; H, 3.45; N, 11.98%).

$[Ru^{II}(NH_3)_5(Phbpe^+)][PF_6]_3$ 4. This was prepared in identical manner to salt **2** by using $[Phbpe^+]PF_6$ (83 mg, 0.205 mmol) in place of $[PymQ^+]PF_6$. The product was purified as for **3** with one further precipitation from acetone–diethyl ether to afford a dark blue solid: yield 113 mg (62%). $\delta_H(CD_3COCD_3)$ 9.25 (2 H, d, *J* 7.0, C_5H_4N), 8.97 (2 H, d, *J* 6.3, C_5H_4N), 8.51 (2 H, d, *J* 6.9, C_5H_4N), 8.18 (1 H, d, *J* 16.2, CH), 8.04 (1 H, d, *J* 16.2, CH), 7.99–7.94 (2 H, m, Ph), 7.81–7.77 (3 H, m, Ph), 7.58 (2 H, d, *J* 6.9 Hz, C_5H_4N), 3.44 (3 H, s, *trans*-NH_3) and 2.65 (12 H, s, 4 × *cis*-NH_3) (Found: C, 25.28; H, 3.52; N, 10.51. Calc. for $C_{18}H_{30}F_{18}N_7P_3Ru \cdot 0.3C_3H_6O$: C, 25.28; H, 3.57; N, 10.92%).

***trans*-$[Ru^{III}(SO_4)(NH_3)_4(mim)]Cl$ 5.** A mixture of *trans*-$[Ru^{II}Cl(NH_3)_4(SO_2)]Cl$ (100 mg, 0.329 mmol) and 1-methylimidazole (mim, 0.2 cm^3, 2.51 mmol) was dissolved in water (5 cm^3) and heated at *ca.* 45 °C under Ar for 30 min. Acetone (100 cm^3) was added to the brown solution and a white precipitate filtered off, washed with acetone and dried to afford crude *trans*-$[Ru^{II}(NH_3)_4(mim)(SO_2)]Cl_2$ (124 mg, 98%). This material was dissolved in water (5 cm^3) and oxidized by the addition of a 1:1 mixture of 30% aqueous H_2O_2–2 M HCl (2 cm^3). After 5 min at room temperature, acetone (200 cm^3) was added and the golden precipitate filtered off, washed with acetone and dried: crude yield 111 mg (88%).

***trans*-$[Ru^{III}(SO_4)(NH_3)_4(Medap^+)]Cl_2$ 6.** This salt was prepared in identical manner to that of **5** by using $[Medap^+]Cl$ (167 mg, 0.656 mmol) in place of mim. The addition of acetone (30 cm^3) to the brown solution afforded a mauve precipitate which was filtered off, washed with acetone and dried to yield crude *trans*-$[Ru^{II}(NH_3)_4(Medap^+)(SO_2)]Cl_3$ (151 mg, 82%). The oxidation was carried out by using water (10 cm^3) to dissolve the SO_2 salt and acetone (100 cm^3) to precipitate the golden product: crude yield: 108 mg (59%).

***trans*-$[Ru^{III}(SO_4)(NH_3)_4(Mebpe^+)]Cl_2$ 7.** This was prepared in identical manner to that of salt **6** by using $[Mebpe^+]I$ (214 mg, 0.660 mmol) in place of $[Medap^+]Cl$ to afford a golden solid: crude yield 135 mg (77%).

***trans*-$[Ru^{II}(NH_3)_4(py)(Medap^+)][PF_6]_3$ 8.** A solution of *trans*-$[Ru^{III}(SO_4)(NH_3)_4(py)]Cl$ (108 mg, 0.284 mmol) in water (5 cm^3) was reduced over zinc amalgam (5 lumps) with argon agitation for 15 min. This was filtered under Ar into a flask containing $[Medap^+]Cl$ (360 mg, 1.41 mmol) and the solution was stirred at room temperature in the dark under Ar for 6 h. The addition of acetone (100 cm^3) to the deep blue solution gave a dark precipitate which was filtered off, washed with acetone and dried (crude *trans*-$[Ru^{II}(NH_3)_4(py)(Medap^+)]Cl_3$). This material was purified by precipitation from water–acetone and then metathesized to its PF_6^- salt by precipitation from water–aqueous NH_4PF_6. Further purification was effected by several precipitations from acetone–diethyl ether to afford a dark blue solid: yield 99 mg (39%). $\delta_H(CD_3COCD_3)$ 10.15 (2 H, s, $C_{14}H_8N_2$), 9.99 (2 H, s, $C_{14}H_8N_2$), 9.00 (2 H, d, $H^{2,6}$), 9.12 (2 H, d, *J* 9.1, $C_{14}H_8N_2$), 8.63 (2 H, d, *J* 9.2 Hz, $C_{14}H_8N_2$), 8.03 (1 H, t, H^4), 7.65 (2 H, t, $H^{3,5}$), 5.01 (3 H, s, Me) and 2.83 (12 H, s, $4NH_3$) (Found: C, 26.78; H, 3.09; N, 10.61. Calc. for $C_{20}H_{28}F_{18}N_7P_3Ru$: C, 26.62; H, 3.13; N, 10.86%).

***trans*-$[Ru^{II}(NH_3)_4(py)(PymQ^+)][PF_6]_3$ 9.** This was prepared in identical manner to that of salt **8** by using *trans*-$[Ru^{III}(SO_4)(NH_3)_4(py)]Cl$ (103 mg, 0.271 mmol) and $[PymQ^+]Cl$ (367 mg, 1.36 mmol) in place of $[Medap^+]Cl$. Purification was effected by precipitation from acetone–diethyl ether to afford a dark blue solid: yield: 172 mg (69%). $\delta_H(CD_3COCD_3)$ 10.28 (2 H, d, *J* 7.4, C_5H_4N), 9.27 (2 H, d, *J* 4.9, $C_4H_3N_2$), 9.26 (2 H, d, *J* 7.0, C_5H_4N), 8.99–8.93 (4 H, m, $C_5H_4N + H^{2,6}$), 8.19 (2 H, d, *J* 7.0 Hz, C_5H_4N), 8.06–7.98 (2 H, m, $H^4 + C_4H_3N_2$), 7.63 (2 H, t, $H^{3,5}$) and 2.88 (12 H, s, $4NH_3$) (Found: C, 25.16; H, 3.10; N, 13.32. Calc. for $C_{19}H_{28}F_{18}N_9P_3Ru$: C, 24.85; H, 3.07; N, 13.73%).

***trans*-$[Ru^{II}(NH_3)_4(py)(Mebpe^+)][PF_6]_3$ 10.** This was prepared in similar manner to that of salt **8** by using **7** (135 mg, 0.253 mmol) in place of *trans*-$[Ru^{III}(SO_4)(NH_3)_4(py)]Cl$ and pyridine (0.1 cm^3, 1.24 mmol) in place of $[Medap^+]Cl$. The solution was stirred for 3 h in the dark and addition of aqueous NH_4PF_6 gave a dark precipitate which was filtered off, washed with water and dried. Purification was effected by precipitation from acetone–diethyl ether to afford a dark blue solid: yield 81 mg (36%). $\delta_H(CD_3COCD_3)$ 8.98–8.92 (4 H, m, $C_5H_4N + H^{2,6}$), 8.88 (2 H, d, *J* 6.5, C_5H_4N), 8.36 (2 H, d, *J* 6.9, C_5H_4N), 8.09 (1 H, d, *J* 16.5, CH), 7.95 (1 H, t, H^4), 7.93 (1 H, d, *J* 16.4, CH), 7.74 (2 H, d, *J* 6.8 Hz, C_5H_4N), 7.56 (2 H, t, $H^{3,5}$), 4.53 (3 H, s, Me) and 2.78 (12 H, s, $4NH_3$) (Found: C, 24.72; H, 3.50; N, 10.85. Calc. for $C_{18}H_{30}F_{18}N_7P_3Ru$: C, 24.56; H, 3.43; N, 11.14%).

***trans*-$[Ru^{II}(NH_3)_4(py)(Phbpe^+)][PF_6]_3$ 11.** This was prepared in identical manner to that of salt **8** by using *trans*-$[Ru^{III}(SO_4)(NH_3)_4(py)]Cl$ (109 mg, 0.287 mmol) and $[Phbpe^+]Cl \cdot 2.25H_2O$ (424 mg, 1.26 mmol) instead of $[Medap^+]Cl$. Purification was effected by precipitation from acetone–diethyl ether to afford a dark blue solid: yield 163 mg (58%). $\delta_H(CD_3COCD_3)$ 9.30 (2 H, d, *J* 6.9, C_5H_4N), 8.98 (2 H, d, *J* 6.6, C_5H_4N), 8.90 (2 H, d, $H^{2,6}$), 8.55 (2 H, d, *J* 7.0, C_5H_4N), 8.25 (1 H, d, *J* 16.2, CH), 8.07 (1 H, d, *J* 16.2 Hz, CH), 8.00–7.93 (3 H, m, Ph + H^4), 7.82–7.78 (5 H, m, Ph + C_5H_4N), 6.90 (2 H, t, $H^{3,5}$) and 2.81 (12 H, s, $4NH_3$) (Found: C, 30.18; H, 3.39; N, 9.64. Calc. for $C_{23}H_{32}F_{18}N_7P_3Ru \cdot 0.5C_3H_6O$: C, 30.29; H, 3.63; N, 10.09%).

***trans*-$[Ru^{II}(NH_3)_4(mim)(Medap^+)][PF_6]_3$ 12.** This was prepared in similar manner to that of salt **8** by using **6** (108 mg, 0.194 mmol) in place of *trans*-$[Ru^{III}(SO_4)(NH_3)_4(py)]Cl$ and mim (0.2 cm^3, 2.51 mmol) in place of $[Medap^+]Cl$. The solution

was stirred for 3 h in the dark and addition of aqueous NH_4PF_6 afforded a dark precipitate which was filtered off, washed with water and dried. Purification was effected by sequential precipitations from acetone–NBu^n_4Cl, water–aqueous NH_4PF_6 and finally from acetone–diethyl ether: yield 69 mg (39%). $\delta_H(CD_3COCD_3)$ 10.10 (2 H, s, $C_{14}H_8N_2$), 9.88 (2 H, s, $C_{14}H_8N_2$), 8.59 (2 H, d, *J* 8.8, $C_{14}H_8N_2$), 8.53 (2 H, d, *J* 9.2 Hz, $C_{14}H_8N_2$), 8.31 (1 H, s, $C_3N_2H_3$), 7.51 (1 H, s, $C_3N_2H_3$), 7.47 (1 H, s, $C_3N_2H_3$), 4.93 (3 H, s, $C_{14}H_8N_2$-*Me*), 3.95 (3 H, s, $C_3N_2H_3$-*Me*) and 2.85 (s, 12 H, $4NH_3$) (Found: C, 26.02; H, 3.20; N, 11.98. Calc. for $C_{19}H_{29}F_{18}N_8P_3Ru\cdot0.3C_3H_6O$: C, 25.90; H, 3.36; N, 12.14%).

***trans*-[$Ru^{II}(NH_3)_4$(mim)(PymQ$^+$)][PF_6]$_3$ 13.** This salt was prepared and purified in identical manner to that of **12** by using **5** (109 mg, 0.285 mmol) in place of **6** and [PymQ$^+$]Cl (385 mg, 1.42 mmol) in place of mim. A dark blue solid was obtained: yield 76 mg (28%). $\delta_H(CD_3COCD_3)$ 10.22 (2 H, d, *J* 7.5, C_5H_4N), 9.27–9.24 (4 H, m, C_5H_4N + $C_4H_3N_2$), 8.95 (2 H, d, *J* 7.4, C_5H_4N), 8.28 (1 H, s, $C_3N_2H_3$), 8.08 (2 H, d, *J* 6.6, C_5H_4N), 8.03 (1 H, t, *J* 4.1 Hz, $C_4H_3N_2$), 7.50 (1 H, s, $C_3N_2H_3$), 7.44 (1 H, s, $C_3N_2H_3$), 3.95 (3 H, s, Me) and 2.78 (12 H, s, $4NH_3$) (Found: C, 24.03; H, 3.46; N, 14.68. Calc. for $C_{18}H_{29}F_{18}N_{10}P_3Ru\cdot0.3C_3H_6O$: C, 24.18; H, 3.31; N, 14.92%).

***trans*-[$Ru^{II}(NH_3)_4$(mim)(Mebpe$^+$)][PF_6]$_3$ 14.** This salt was prepared and purified in identical manner to that of **12** by using **7** (104 mg, 0.195 mmol) in place of **6**. A dark purple solid was obtained: yield 64 mg (37%). $\delta_H(CD_3COCD_3)$ 8.94 (4 H, d, *J* 5.1, C_5H_4N), 8.35 (2 H, d, *J* 6.5, C_5H_4N), 8.18 (1 H, s, $C_3N_2H_3$), 8.06 (1 H, d, *J* 16.4, CH), 7.91 (1 H, d, *J* 16.5, CH), 7.62 (2 H, d, *J* 6.6 Hz, C_5H_4N), 7.45 (1 H, s, $C_3N_2H_3$), 7.37 (1 H, s, $C_3N_2H_3$), 4.51 (3 H, s, C_5H_4N-*Me*), 3.91 (3 H, s, $C_3N_2H_3$-*Me*) and 2.65 (12 H, s, $4NH_3$) (Found: C, 23.44; H, 3.56; N, 12.41. Calc. for $C_{17}H_{31}F_{18}N_8P_3Ru$: C, 23.11; H, 3.54; N, 12.68%).

***trans*-[$Ru^{II}(NH_3)_4$(mim)(Phbpe$^+$)][PF_6]$_3$ 15.** This salt was prepared in identical manner to that of **12** by using **5** (115 mg, 0.300 mmol) in place of **6** and [Phbpe$^+$]Cl·2.25H_2O (445 mg, 1.33 mmol) in place of mim. Purification was effected by precipitation from acetone–diethyl ether to give a dark blue solid: yield 97 mg (34%). $\delta_H(CD_3COCD_3)$ 9.26 (2 H, d, *J* 6.9, C_5H_4N), 8.96 (2 H, d, *J* 5.6, C_5H_4N), 8.52 (2 H, d, *J* 6.9, C_5H_4N), 8.23 (1 H, d, *J* 16.2, CH), 8.18 (1 H, s, $C_3N_2H_3$), 8.04 (1 H, d, *J* 16.2, CH), 8.00–7.96 (2 H, m, Ph), 7.81–7.78 (3 H, m, Ph), 7.68 (2 H, d, *J* 5.9 Hz, C_5H_4N), 7.45 (1 H, s, $C_3N_2H_3$), 7.39 (1 H, s, $C_3N_2H_3$), 3.94 (3 H, s, Me) and 2.67 (12 H, s, $4NH_3$) (Found: C, 28.51; H, 3.94; N, 11.08. Calc. for $C_{22}H_{33}F_{18}N_8P_3Ru\cdot0.3C_3H_6O$: C, 28.56; H, 3.64; N, 11.64%).

***trans*-[$Ru^{II}(NH_3)_4$(py)(4,4′-bpy)][PF_6]$_2$ 16.** This salt was prepared in similar manner to that of **8** by using *trans*-[$Ru^{III}(SO_4)(NH_3)_4$(py)]Cl (200 mg, 0.527 mmol) and 4,4′-bipyridine (2.06 g, 13.2 mmol) in acetone (10 cm^3) in place of [Medap$^+$]Cl. The crude product was precipitated by addition of aqueous NH_4PF_6/Na_2CO_3, followed by removal of the acetone *in vacuo*. Two reprecipitations from acetone–diethyl ether afforded a red, microcrystalline solid: yield 215 mg (59%). $\delta_H(CD_3COCD_3)$ 9.00 (2 H, d, *J* 6.8, C_5H_4N), 8.88 (2 H, d, $H^{2,6}$), 8.74 (2 H, d, *J* 6.1 Hz, C_5H_4N), 7.95–7.84 (5 H, c m, $2C_5H_4N$ and H^4), 7.55 (2 H, t, $H^{3,5}$) and 2.81 (12 H, s, $4NH_3$) (Found: C, 25.95; H, 3.69; N, 13.94. Calc. for $C_{15}H_{25}F_{12}N_7P_2Ru$: C, 25.95; H, 3.63; N, 14.12%).

Hyper-Rayleigh scattering

Details of the hyper-Rayleigh scattering (HRS) experiment have been discussed elsewhere,[17] and the experimental procedure used was as described previously.[18] β Values were determined by using the electric-field-induced second harmonic generation β_{1064} for *p*-nitroaniline (29.2×10^{-30} esu in acetonitrile)[19] as an external reference. All measurements were performed by using the 1064 nm fundamental wavelength of an injection-seeded, Q-switched Nd-YAG laser (Quanta-Ray GCR-5, 8 ns pulses, 7 mJ, 10 Hz). The use of dilute acetonitrile solutions (10^{-5}–10^{-6} mol dm^{-3}) ensured a linear dependence of $I_{2\omega}/I_\omega^2$ upon solute concentration, precluding the need for Lambert–Beer correction factors. Samples were passed through a 0.45 μm filter (Millipore), and checked for fluorescence.[20,21] One-dimensional hyperpolarizability is assumed, *i.e.* $\beta_{1064} = \beta_{333}$, and a relative error of ±15% is estimated.

Crystal structure determinations

Crystals of salts **8**·4MeCN and **16**·2MeCN were obtained by slow diffusion of diethyl ether vapour into acetonitrile solutions. A red-brown crystal of **8**·4MeCN of approximate dimensions 0.1 × 0.1 × 0.15 mm and a red-orange crystal of **16**·2MeCN with dimensions 0.2 × 0.1 × 0.05 mm were chosen for diffraction studies.

Data collection details are as follows: for **8**·4MeCN, data were collected on a Nonius Kappa CCD area-detector diffractometer controlled by the COLLECT software package.[22] Images were processed by DENZO[23] and the data corrected for absorption by using the empirical method employed in SORTAV[24] from within the MAXUS suite of programs.[25] For **16**·2MeCN, data were collected on a Siemens SMART CCD area-detector diffractometer. An empirical absorption correction was applied and the data frames were integrated using SAINT.[26] The structure of **8**·4MeCN was solved by direct methods and refined by full-matrix least squares on all F_o^2 data using SHELXS 97[27] and SHELXL 97.[28] The same approach was used for **16**·2MeCN, but using Siemens SHELXTL 5.03.[26] In both cases, all non-hydrogen atoms, including those of the PF_6^- anions and the acetonitrile molecules of crystallization, were refined anisotropically. Crystallographic data and refinement details are presented in Table 3.

CCDC reference number 186/1638.

See http://www.rsc.org/suppdata/dt/1999/3617/ for crystallographic files in .cif format.

Results and discussion

Molecular design and synthesis

This report constitutes an extension of our previous studies in which we have found that complexes *trans*-[$Ru^{II}(NH_3)_4(L^D)$-(L^A)]$^{3+}$ in which L^A is a *N*-R-4,4′-bipyridinium ligand exhibit large β_0 responses which increase in the order R = Me < Ph < 4-MeCOPh.[9c] The new complexes in the salts **1**–**4** and **8**–**15** were designed to probe the effects of several further molecular structural changes on the electronic absorption and quadratic NLO properties. These changes can be summarized as follows. *(i)* The complexes of *N*-methyl-2,7-diazapyrenium (Medap$^+$) in **1**, **8** and **12** feature fixed, coplanar L^A rings and 4 additional π electrons when compared with their 4,4′-bipyridinium analogues. *(ii)* The 2-pyrimidyl ring in the complexes of *N*-(2-pyrimidyl)-4,4′-bipyridinium (PymQ$^+$) in **2**, **9** and **13** is considerably more electron deficient than the *N*-aryl substituents used previously. *(iii)* The complexes of *N*-methyl-4-[*trans*-2-(4-pyridyl)ethenyl]pyridinium (Mebpe$^+$) and *N*-phenyl-4-[*trans*-2-(4-pyridyl)ethenyl]pyridinium (Phbpe$^+$) (in **3**, **4**, **10**, **11**, **14**, **15**) are similar to their predecessors containing *N*-methyl-4,4′-bipyridinium (MeQ$^+$) or *N*-phenyl-4,4′-bipyridinium (PhQ$^+$), but have planar and extended conjugated systems. The salt **16** is included in this report primarily to allow crystal structural comparisons (see later).

The salt [PymQ$^+$]Cl has been reported previously, but without details.[29] This compound is prepared by nucleophilic attack of 4,4′-bipyridine upon 2-chloropyrimidine, and it was found that initial melt reactions improve the yields of subsequent reactions in refluxing ethanol. The ion Phbpe$^+$ was obtained

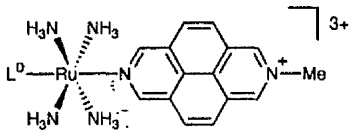

L^D = NH_3 **1**, py **8**, mim **12**

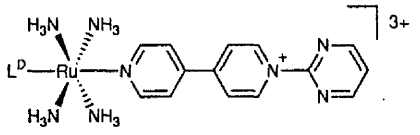

L^D = NH_3 **2**, py **9**, mim **13**

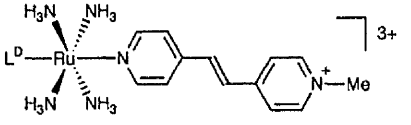

L^D = NH_3 **3**, py **10**, mim **14**

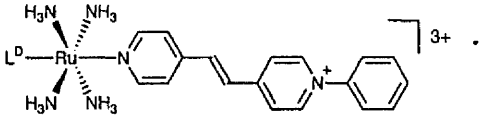

L^D = NH_3 **4**, py **11**, mim **15**

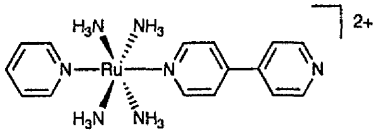

16

from the condensation of 4-methyl-*N*-phenylpyridinium chloride with pyridine-4-carbaldehyde using piperidine as a base catalyst. The yield of this reaction diminishes with increasing reflux times, in similar fashion to the related, published preparation of Mebpe$^+$.[30] The new complex salts were synthesized and purified by using previously described procedures,[9] with some minor modifications. In the syntheses of the salts **8**–**16** the sequences of ligand complexations described are those which give the optimum product yields and purities.

Electronic spectroscopy studies

Electronic absorption spectra for all of the new complex salts, except for the sulfatoruthenium(III) intermediates **5**–**7**, were recorded in acetonitrile and results are presented in Table 1. Complexes **1**–**4** and **8**–**15** show intense, broad $d_\pi(Ru^{II})\rightarrow\pi^*(L^A)$ (L^A = pyridinium-substituted ligand) MLCT bands in the region 560–700 nm, the energies of which depend on the relative energies of the Ru-based HOMO and of the L^A-based LUMO.[31] The MLCT band of **16** is found at considerably higher energy due to the weaker electron-accepting nature of 4,4′-bpy compared with the pyridinium ligands. The pyridine complexes in **8**–**11** and **16** also show less intense, high energy, $d_\pi(Ru^{II})\rightarrow\pi^*$(py) MLCT bands at *ca.* 385 nm, although this absorption is obscured by a more intense UV band for **8** and overlaps with the $d_\pi(Ru^{II})\rightarrow\pi^*$(4,4′-bpy) band for **16**. All of the complexes also show one or more intense UV absorptions due to intraligand $\pi\longrightarrow\pi^*$ excitations. Data for the visible MLCT bands of **1**–**4** and **8**–**15** are collected in Table 2, together with those for the related salts of the ligands MeQ$^+$, PhQ$^+$, *N*-(4-acetylphenyl)-4,4′-bipyridinium (4-AcPhQ$^+$) and *N*-(2,4-dinitrophenyl)-4,4′-bipyridinium (2,4-DNPhQ$^+$) for purposes of comparison.[9b,c]

The MLCT band maxima of the Medap$^+$ complexes in **1** and **12** are blue-shifted by 0.03 eV with respect to those of their MeQ$^+$ counterparts.[9] The maxima of the PymQ$^+$ complexes in **2** and **13** are red-shifted by *ca.* 0.3 eV with respect to those of their Medap$^+$ analogues and red-shifted by 0.06–0.08 eV with respect to those of their 4-AcPhQ$^+$ analogues.[9c] Given an almost constant HOMO energy (see later), this shows that PymQ$^+$ has the lowest LUMO energy of the 4,4′-bipyridinium ligands studied, in keeping with the highly electron-deficient nature of the 2-pyrimidyl group. The acceptor strength of L^A hence increases in the order MeQ$^+$ < PhQ$^+$ < 4-AcPhQ$^+$ < 2,4-DNPhQ$^+$ < PymQ$^+$. The MLCT energies of the complexes of Mebpe$^+$ (in **3** and **14**) and Phbpe$^+$ (in **4** and **15**) are very similar to those of their analogues featuring MeQ$^+$ or PhQ$^+$, respectively.[9]

Comparison of the MLCT data for the pairs **3**/**4**, **10**/**11** and **14**/**15** reveals shifts of *ca.* −0.1 eV on replacing an N–Me with an N–Ph substituent. This shows that Phbpe$^+$ is a considerably stronger acceptor than Mebpe$^+$, in keeping with the previously noted difference between PhQ$^+$ and MeQ$^+$.[9c] With a given L^A, the MLCT energy decreases as the net donor strength of L^D increases, in the order py < NH_3 < mim, reflecting a progressive destabilization of the Ru-based HOMO.

Electrochemical studies

All of the new complex salts, except for **5**–**7**, were studied by cyclic voltammetry in acetonitrile and results are presented in Table 1. All exhibit reversible or quasi-reversible $Ru^{III/II}$ oxidation waves, together with generally irreversible ligand-based reduction processes. By contrast, the related complexes of MeQ$^+$, PhQ$^+$ or 4-AcPhQ$^+$ each show two reversible or quasi-reversible ligand reduction waves.[9a,c] Selected electrochemical data for **1**–**4** and **8**–**15** and for previously reported complex salts are included in Table 2.

The $Ru^{III/II}$ $E_{1/2}$ values for **1** and **12** are shifted by *ca.* +40 mV with respect to those of their MeQ$^+$ analogues,[9] due to the lower basicity of Medap$^+$ caused by increased delocalization. The accompanying blue shifts in the MLCT bands (see earlier) can hence be attributed largely to a slight stabilization of the Ru-based HOMOs in the Medap$^+$ complexes. By contrast, the $Ru^{III/II}$ $E_{1/2}$ values for **3**, **4**, **14** and **15** are shifted by *ca.* −40 mV with respect to those of their MeQ$^+$ or PhQ$^+$ analogues,[9] due to the mildly electron-donating character of the ethylene units. Comparison of the $Ru^{III/II}$ $E_{1/2}$ values for the pairs **3**/**4**, **10**/**11** and **14**/**15** reveals negligible shifts on replacing an N–Me with an N–Ph substituent, whilst the ligand E_{pc} values show large positive shifts. The corresponding red shifts in the MLCT bands (see earlier) are hence purely a result of stabilization of the ligand-based LUMOs. With a given L^A, the $Ru^{III/II}$ $E_{1/2}$ values become less positive as the donor strength of L^D increases, in the order py < mim ≈ NH_3, reflecting the HOMO destabilization indicated by the MLCT data (see earlier).

Comparison of the ligand reduction potentials for **2** and **13** with those of the previously reported complexes confirms that the PymQ$^+$ ligand is a considerably stronger electron acceptor than MeQ$^+$, PhQ$^+$ or 4-AcPhQ$^+$, in keeping with the MLCT data (see earlier). The accompanying variations in the $Ru^{III/II}$ $E_{1/2}$ values are only small, showing that the HOMO energy is relatively insensitive to changes in the substituent at N. Complex **9** also exhibits a relatively anodic reduction wave attributed to the PymQ$^+$ ligand.

Crystallographic studies

Single crystal structures were obtained for salts **8**·4MeCN and **16**·2MeCN, and representations of the molecular struc-

Table 1 Electrochemical and UV/VIS data for complex salts in acetonitrile

Complex salt	$E_{1/2}$/V *vs.* SCE (ΔE_p/mV)[a]		λ_{max}/nm (ε/dm^3 mol^{-1} cm^{-1})[b]	Assignment
	$Ru^{III/II}$	Ligand waves		
1 $[Ru^{II}(NH_3)_5(Medap^+)][PF_6]_3$	0.50 (70)	−0.98[c]	581 (14 800)	$d_\pi \longrightarrow \pi^*(Medap^+)$
			397 (10 900)	$\pi \longrightarrow \pi^*$
			376 (7800)	$\pi \longrightarrow \pi^*$
			335 (24 900)	$\pi \longrightarrow \pi^*$
			241 (37 200)	$\pi \longrightarrow \pi^*$
2 $[Ru^{II}(NH_3)_5(PymQ^+)][PF_6]_3$	0.49 (100)	−0.45 (200)[d]	673 (18 000)	$d_\pi \longrightarrow \pi^*(PymQ^+)$
			285 (21 500)	$\pi \longrightarrow \pi^*$
3 $[Ru^{II}(NH_3)_5(Mebpe^+)][PF_6]_3$	0.41 (70)	−0.85[c]	595 (16 100)	$d_\pi \longrightarrow \pi^*(Mebpe^+)$
			312 (23 800)	$\pi \longrightarrow \pi^*$
4 $[Ru^{II}(NH_3)_5(Phbpe^+)][PF_6]_3$	0.42 (90)	−0.66[c]	628 (17 200)	$d_\pi \longrightarrow \pi^*(Phbpe^+)$
			329 (25 800)	$\pi \longrightarrow \pi^*$
8 *trans*-$[Ru^{II}(NH_3)_4(py)(Medap^+)][PF_6]_3$	0.65 (75)	−0.95[c]	564 (12 300)	$d_\pi \longrightarrow \pi^*(Medap^+)$
			397 (11 300)	$\pi \longrightarrow \pi^*$
			378 (10 900)	$\pi \longrightarrow \pi^*$
			334 (19 100)	$\pi \longrightarrow \pi^*$
			242 (33 100)	$\pi \longrightarrow \pi^*$
9 *trans*-$[Ru^{II}(NH_3)_4(py)(PymQ^+)][PF_6]_3$	0.67 (80)	−0.41 (90)[d]	644 (16 800)	$d_\pi \longrightarrow \pi^*(PymQ^+)$
		−1.10 (100)[d]	385 (5800)	$d_\pi \longrightarrow \pi^*(py)$
			283 (24 500)	$\pi \longrightarrow \pi^*$
10 *trans*-$[Ru^{II}(NH_3)_4(py)(Mebpe^+)][PF_6]_3$	0.60 (70)	−0.75 (150)[d]	563 (14 800)	$d_\pi \longrightarrow \pi^*(Mebpe^+)$
			386 (5900)	$d_\pi \longrightarrow \pi^*(py)$
			311 (23 800)	$\pi \longrightarrow \pi^*$
11 *trans*-$[Ru^{II}(NH_3)_4(py)(Phbpe^+)][PF_6]_3$	0.61 (90)	−0.64[c]	591 (17 100)	$d_\pi \longrightarrow \pi^*(Phbpe^+)$
			387 (sh) (6900)	$d_\pi \longrightarrow \pi^*(py)$
			328 (30 000)	$\pi \longrightarrow \pi^*$
12 *trans*-$[Ru^{II}(NH_3)_4(mim)(Medap^+)][PF_6]_3$	0.51 (70)	−0.97[c]	593 (16 700)	$d_\pi \longrightarrow \pi^*(Medap^+)$
			398 (12 000)	$\pi \longrightarrow \pi^*$
			377 (9300)	$\pi \longrightarrow \pi^*$
			337 (27 600)	$\pi \longrightarrow \pi^*$
			242 (33 100)	$\pi \longrightarrow \pi^*$
13 *trans*-$[Ru^{II}(NH_3)_4(mim)(pymQ^+)][PF_6]_3$	0.52 (90)	−0.41 (120)[d]	698 (18 700)	$d_\pi \longrightarrow \pi^*(PymQ^+)$
		−1.17 (100)[d]	285 (24 300)	$\pi \longrightarrow \pi^*$
14 *trans*-$[Ru^{II}(NH_3)_4(mim)(Mebpe^+)][PF_6]_3$	0.42 (80)	−0.86[d]	604 (16 200)	$d_\pi \longrightarrow \pi^*(Mebpe^+)$
			310 (23 000)	$\pi \longrightarrow \pi^*$
15 *trans*-$[Ru^{II}(NH_3)_4(mim)(Phbpe^+)][PF_6]_3$	0.43 (70)	−0.66[c]	638 (17 600)	$d_\pi \longrightarrow \pi^*(Phbpe^+)$
			329 (28 400)	$\pi \longrightarrow \pi^*$
16 *trans*-$[Ru^{II}(NH_3)_4(py)(4,4'\text{-bpy})][PF_6]_2$	0.60 (80)		464 (17 000)	$d_\pi \longrightarrow \pi^*(4,4'\text{-bpy})$
			378 (sh) (2800)	$d_\pi \longrightarrow \pi^*(py)$
			246 (17 600)	$\pi \longrightarrow \pi^*$

[a] Measured in solutions *ca.* 10^{-3} mol dm^{-3} in analyte and 0.1 mol dm^{-3} in $NBu^n_4PF_6$ at a platinum-bead working electrode with a scan rate of 200 mV s^{-1}. Ferrocene internal reference $E_{1/2} = 0.41$ V, $\Delta E_p = 90$ mV. [b] Solutions (5–7) × 10^{-5} mol dm^{-3}. [c] E_{pc} for an irreversible reduction process. [d] Irreversible process as evidenced by $i_{pc} \neq i_{pa}$.

Table 2 Electrochemical, visible MLCT absorption and HRS data for the salts *trans*-$[Ru^{II}(NH_3)_4(L^D)(L^A)][PF_6]_3$ in acetonitrile

Salt	L^D	L^A	$E_{1/2}$/V *vs.* SCE		λ_{max}[MLCT]/nm (ε/dm^3 mol^{-1} cm^{-1})	E_{max}[MLCT]/eV	β_{1064}[a]	β_0[a]
			$Ru^{III/II}$	$L^{A\,+/0}$				
1	NH_3	$Medap^+$	0.50		581 (14 800)	2.13	660	89
2	NH_3	$PymQ^+$	0.49	−0.45	673 (18 000)	1.84	640	230
3	NH_3	$Mebpe^+$	0.41		595 (16 100)	2.08	828	142
4	NH_3	$Phbpe^+$	0.42		628 (17 200)	1.97	751	192
[b]	NH_3	MeQ^+	0.46	−0.91	590 (15 800)	2.10	750	123
[b]	NH_3	PhQ^+	0.46	−0.75	628 (19 300)	1.97	858	220
[b]	NH_3	4-$AcPhQ^+$	0.47	−0.64	654 (18 000)	1.90	1112	354
[b]	NH_3	2,4-$DNPhQ^+$			660 (16 900)	1.88	871	289
8	py	$Medap^+$	0.65		564 (12 300)	2.20	579	51
9	py	$PymQ^+$	0.67	−0.41	644 (16 800)	1.93	774	228
10	py	$Mebpe^+$	0.60	−0.75	563 (14 800)	2.20	904	78
11	py	$Phbpe^+$	0.61		591 (17 100)	2.10	936	151
12	mim	$Medap^+$	0.51		593 (16 700)	2.09	756	126
13	mim	$PymQ^+$	0.52	−0.41	698 (18 700)	1.78	818	336
14	mim	$Mebpe^+$	0.42		604 (16 200)	2.05	857	168
15	mim	$Phbpe^+$	0.43		638 (17 600)	1.93	1068	310
[c]	mim	MeQ^+	0.47	−0.88	602 (16 200)	2.06	523	100
[b]	mim	PhQ^+	0.46	−0.73	642 (21 500)[d]	1.93	874	254
[b]	mim	4-$AcPhQ^+$	0.48	−0.63	666 (19 500)	1.86	962	332

[a] The value of β_{1064} ($\times 10^{30}$ esu) is the uncorrected first hyperpolarizability measured using a 1064 nm Nd-YAG laser fundamental (15% error); β_0 is the static hyperpolarizability estimated by using the two-level model.[10] The quoted cgs units (esu) can be converted into SI units (C^3 m^3 J^{-2}) by dividing by a factor of 2.693×10^{20}. [b] Ref. 9(*c*). [c] Ref. 9(*a*). [d] λ_{max} slightly altered from value quoted in ref. 9(*c*).

Table 3 Crystallographic data and refinement details for complexes **8**·4MeCN and **16**·2MeCN

	8·4MeCN	**16**·2MeCN
Formula	$C_{28}H_{40}F_{18}N_{11}P_3Ru$	$C_{19}H_{31}F_{12}N_9P_2Ru$
M	1066.69	776.54
Crystal system	Orthorhombic	Monoclinic
Space group	$Pna2_1$	$C2/c$
a/Å	12.8413(3)	16.296(4)
b/Å	23.9689(3)	22.383(3)
c/Å	14.0305(5)	8.683(1)
β/°	90	108.33(2)
U/Å^3	4318.47(19)	3006.4(10)
Z	4	4
T/K	150(2)	173(2)
μ/mm^{-1}	0.589	0.731
Reflections collected	45910	15164
Independent reflections (R_{int})	8434 (0.1226)	3458 (0.0215)
Final $R1$, $wR2$ [$I > 2\sigma(I)$][a]	0.0482, 0.0867	0.0324, 0.0914
(all data)	0.0972, 0.0979	0.0374, 0.0940

[a] Structures were refined on F_o^2 using all data; the value of $R1$ is given for comparison with older refinements based on F_o with a typical threshold of $F_o > 4\sigma(F_o)$.

Table 4 Selected interatomic distances (Å) and angles (°) for salts **8**·4MeCN and **16**·2MeCN

8·4MeCN			
Ru1–N2	2.046(3)	Ru1–N5	2.138(5)
Ru1–N1	2.083(3)	Ru1–N7	2.147(5)
Ru1–N4	2.127(4)	Ru1–N6	2.154(4)
N2–Ru1–N1	177.2(2)	N4–Ru1–N7	90.72(19)
N2–Ru1–N4	91.18(16)	N5–Ru1–N7	179.4(2)
N1–Ru1–N4	87.37(16)	N2–Ru1–N6	90.85(15)
N2–Ru1–N5	87.9(2)	N1–Ru1–N6	90.68(16)
N1–Ru1–N5	89.7(2)	N4–Ru1–N6	177.21(19)
N4–Ru1–N5	88.8(2)	N5–Ru1–N6	93.18(19)
N2–Ru1–N7	91.7(2)	N7–Ru1–N6	87.30(19)
N1–Ru1–N7	90.6(2)		
16·2MeCN			
Ru(1)–N(11)	2.076(3)	Ru(1)–N(2)	2.140(2)
Ru(1)–N(21)	2.077(3)	Ru(1)–N(1^I)	2.149(2)
Ru(1)–N(2^I)	2.140(2)	Ru(1)–N(1)	2.149(2)
N(11)–Ru(1)–N(21)	180.0	N(2^I)–Ru(1)–N(1^I)	87.74(10)
N(11)–Ru(1)–N(2^I)	90.54(5)	N(2)–Ru(1)–N(1^I)	92.27(10)
N(21)–Ru(1)–N(2^I)	89.46(5)	N(11)–Ru(1)–N(1)	89.20(5)
N(11)–Ru(1)–N(2)	90.53(5)	N(21)–Ru(1)–N(1)	90.80(5)
N(21)–Ru(1)–N(2)	89.47(5)	N(2^I)–Ru(1)–N(1)	92.27(10)
N(2^I)–Ru(1)–N(2)	178.93(10)	N(2)–Ru(1)–N(1)	87.74(10)
N(11)–Ru(1)–N(1^I)	89.20(5)	N(1^I)–Ru(1)–N(1)	178.40(11)
N(21)–Ru(1)–N(1^I)	90.80(5)		

Symmetry transformation used to generate equivalent atoms: I $1-x$, y, $-z+\frac{1}{2}$.

tures of the cations are shown in Figs. 1 and 2, bond lengths and angles in Table 4.

In salt **16**·2MeCN the torsion angle C(22)–N(21)–N(11)–C(12) between the py ligand and the co-ordinated pyridyl ring of the 4,4′-bpy is 12.2°, and the planes of the co-ordinated rings approximately bisect the H_3N–Ru–NH_3 angles. Similar arrangements have also been found in *trans*-[$Ru^{III}(NH_3)_4$(Him)(isn)][CF_3CO_2]$_3$·Pr^iOH (Him = imidazole, isn = isonicotinamide)[32] and *trans*-[$Ru^{III}(NH_3)_4(Him)_2$]Cl_3·H_2O.[33] and it has been suggested that the quasi-coplanarity of the *trans* rings may allow π coupling through the Ru.[32] As expected, steric repulsions between the 2,2′-hydrogens cause the 4,4′-bpy ligand in **16**·2MeCN to twist, with a C(32A)–C(31)–C(24)–C(23) torsion of 38.5°. This compares with torsion angles between the pyridyl rings of the 4,4′-bipyridinium ligands in *trans*-[$Ru^{II}(NH_3)_4$(MeQ^+)(PTZ)][PF_6]$_3$·Me_2CO[9a] (PTZ = phenothiazine) and *trans*-[$Ru^{II}(NH_3)_4$(PhQ^+)(PTZ)][PF_6]$_3$·Et_2O,[9c] of 9.6 and 2.6°, respectively. The marked contrast with **16**·2MeCN can be ascribed to increased delocalization in the latter two complexes due to the greater electron-withdrawing capabilities of MeQ^+ and PhQ^+ with respect to 4,4′-bpy. The bond distances Ru(1)–N(11) and Ru(1)–N(21) in **16**·2MeCN are equivalent and *ca.* 0.07 Å shorter than the average of the Ru–NH_3 distances.

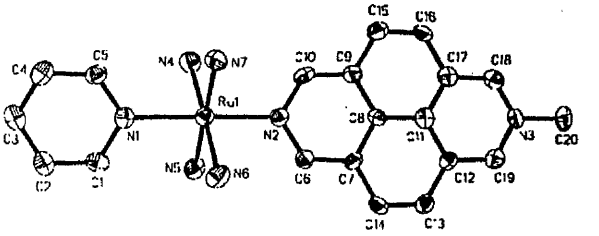

Fig. 1 Structural representation of the complex cation in the salt **8**·4MeCN (50% probability ellipsoids).

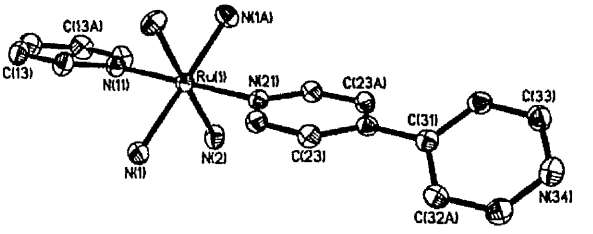

Fig. 2 Structural representation of the complex cation in the salt **16**·2MeCN (50% probability ellipsoids).

The structure of the cation in salt **8**·4MeCN resembles that in **16**·2MeCN in that the *trans* ligands are almost coplanar [C1–N1–N2–C6 9.8°], with the co-ordinated rings approximately bisecting the H_3N–Ru–NH_3 angles. However, in **8**·4MeCN the Ru1–N2 distance is *ca.* 0.05 Å shorter than Ru1–N1, indicating more extensive π-back bonding to $Medap^+$ than to the py ligand; Ru1–N2 is also *ca.* 0.03 Å shorter than the Ru1–N21 distance in **16**·2MeCN. These observations are in keeping with $Medap^+$ being a considerably stronger π acceptor than either py or 4,4′-bpy. The ammine ligands in **8**·4MeCN are hydrogen bonded to one PF_6^- anion and four acetonitrile molecules of crystallization.

Salt **16**·2MeCN adopts the centrosymmetric space group $C2/c$, whilst that of **8**·4MeCN ($Pna2_1$) is non-centrosymmetric. However, crystal packing diagrams of **8**·4MeCN reveal that the complex dipoles (as represented by the Ru(1)–N(3) vectors) are orientated almost completely antiparallel. This precludes the likelihood of this particular crystalline form of **8** exhibiting macroscopic quadratic NLO effects, in spite of the very large β_0 value determined in solution (see later).

Non-linear optical studies

The first hyperpolarizabilities β of the new complex salts **1**–**4** and **8**–**15** were measured in acetonitrile by using the HRS technique[17,18] with a 1064 nm Nd-YAG laser fundamental. Estimated static hyperpolarizabilities β_0 were obtained by application of the two-level model,[10] and results are presented in Table 2, together with data for a selection of previously reported complex salts.[9b,c] It should be noted that the utility of comparisons between these data is limited by the relatively large experimental errors in the HRS β values (±15%).

All of the new complexes show very large β and β_0 values which are comparable to those we have determined for related complexes,[9] and several of these values are amongst the largest found for metal-containing chromophores. Comparison of the data for the $Medap^+$ complexes in **1** and **12** with their MeQ^+

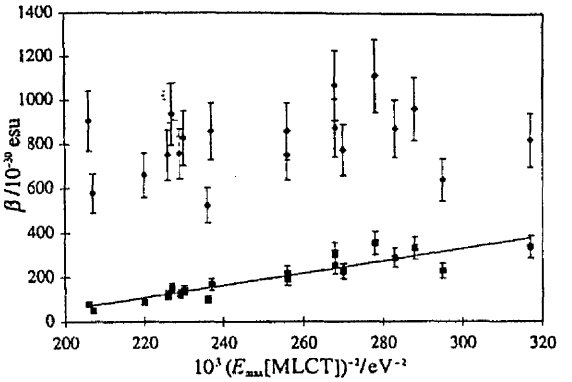

Fig. 3 Plot of the first hyperpolarizability against the inverse square of the MLCT energy for the salts **1–4**, **8–15** and other salts included in Table 2[9b,c] (◆ = β_{1064}; ■ = β_0).

analogues shows that for $L^D = NH_3$ the Medap$^+$ complex has a slightly smaller β_0, whilst when L^D = mim the reverse may be true. However, the differences are small and so it is reasonable to conclude that fixing the planarity of the 4,4′-bipyridinium rings does not greatly affect β_0. This is consistent with crystallographic studies which show that the MeQ$^+$ ligand adopts a quasi-planar configuration, and a similar situation is likely to pertain in solution due to strong donor–acceptor electronic coupling.[9a]

Although the visible absorption and electrochemical data clearly show that PymQ$^+$ is the strongest electron acceptor of the 4,4′-bipyridinium ligands studied (see earlier), this does not result in the anticipated increases in β_0 for the complexes where $L^D = NH_3$ (in **2**) or mim (in **13**). The β_0 values of **2** and **13** are, respectively, smaller than and equal to those of their 4-AcPhQ$^+$ analogues. At present, we cannot explain this apparent anomaly, but tentatively suggest that the β_0 values of the 4-AcPhQ$^+$ complexes are boosted by the presence of the acetyl groups. Clearly, further experiments are required in order to clarify this matter.

The complexes of Mebpe$^+$ and Phbpe$^+$, with the exception of **14**, have β_0 values indistinguishable from those of their 4,4′-bipyridinium analogues, providing little evidence for enhancement of the NLO response upon addition of a *trans*-ethylene unit. This contrasts with the situation in related organics where extension of conjugated bridges typically leads to increased first hyperpolarizabilites.[1] For example, the β_0 values determined *via* electric-field-induced second harmonic generation at 1907 nm for 4-(dimethylamino)-4′-nitrobiphenyl and *trans*-4-(dimethylamino)-4′-nitrostilbene are 40 and 55×10^{-30} esu, respectively.[34] However, in the latter case the addition of an ethylene unit also causes a 0.3 eV red shift in the intramolecular charge-transfer absorption band, whilst the same structural change does not significantly affect the MLCT maxima of the present complexes (see earlier).

The marked red-shifting of the MLCT bands due to the greater acceptor strength of Phbpe$^+$ with respect to Mebpe$^+$ (see earlier) also gives rise to increases in β_0 between the pairs **3/4**, **10/11** and **14/15**. This is in keeping with the previously noted difference between complexes of PhQ$^+$ and MeQ$^+$.[9c] For a given L^A, the MLCT energy increases in the order L^D = mim < NH_3 < py (see earlier), and the β_0 values broadly decrease in the opposite order.

According to the two-level model,[10] the dominant component of β is inversely proportional to E_{ge}^2 (the square of the energy gap between the ground state and first charge-transfer excited state). We have previously demonstrated a good linear correlation between β_0 and $1/E_{ge}^2$,[9c] and Fig. 3 shows that the data for the new complex salts fit reasonably well with this trend. Hence, decreasing the MLCT energy of these ruthenium(II) chromophores generally corresponds to an increase in the first hyperpolarizability. However, it should be noted that this correlation is only partial, and this may be explained by the fact that β_0 is also influenced by a number of other factors such as the oscillator strength of the charge-transfer transition.

Conclusion

The MLCT absorption properties of dipolar ruthenium(II) ammine complexes of pyridinium-substituted ligands show a fine degree of tunability. The associated large molecular first hyperpolarizabilities β_0 of these complexes are also tunable, although perhaps to a lesser extent. In general, β_0 increases as the MLCT absorption energy decreases, in keeping with the two-level model. Notably, extension of the conjugated bridge in these complexes neither significantly alters the MLCT energies nor leads to increases in β_0.

Acknowledgements

We are grateful to EPSRC for provision of a studentship (to J. A. H.). This work was supported by research grants from The Royal Society, from the Belgian National Fund for Scientific Research (G.0308.96), from the Belgian government (IUAP-P4/11) and from the University of Leuven (GOA/1/95). Thanks are due to Johnson Matthey plc for a generous loan of ruthenium trichloride.

References

1 *Nonlinear Optical Properties of Organic Molecules and Crystals*, eds. D. S. Chemla and J. Zyss, Academic Press, Orlando, 1987, vols. 1 and 2; J. Zyss, *Molecular Nonlinear Optics: Materials, Physics and Devices*, Academic Press, Boston, 1994; S. R. Marder, B. Kippelen, A. K.-Y. Jen and N. Peyghambarian, *Nature (London)*, 1997, **388**, 845; T. Verbiest, S. Houbrechts, M. Kauranen, K. Clays and A. Persoons, *J. Mater. Chem.*, 1997, **7**, 2175.

2 S. R. Marder, in *Inorganic Materials*, eds. D. W. Bruce and D. O'Hare, Wiley, Chichester, 1992; D. R. Kanis, M. A. Ratner and T. J. Marks, *Chem. Rev.*, 1994, **94**, 195; N. J. Long, *Angew. Chem., Int. Ed. Engl.*, 1995, **34**, 21; I. R. Whittall, A. M. McDonagh, M. G. Humphrey and M. Samoc, *Adv. Organomet. Chem.*, 1998, **42**, 291.

3 W. M. Laidlaw, R. G. Denning, T. Verbiest, E. Chauchard and A. Persoons, *Nature (London)*, 1993, **363**, 58; *Proc. SPIE, Int. Soc. Opt. Eng.*, 1994, **2143**, 14; F. W. Vance and J. T. Hupp, *J. Am. Chem. Soc.*, 1999, **121**, 4047.

4 J. Zyss, C. Dhenaut, T. Chauvan and I. Ledoux, *Chem. Phys. Lett.*, 1993, **206**, 409; C. Dhenaut, I. Ledoux, I. D. W. Samuel, J. Zyss, M. Bourgault and H. Le Bozec, *Nature (London)*, 1995, **374**, 339.

5 I. R. Whittall, M. G. Humphrey, A. Persoons and S. Houbrechts, *Organometallics*, 1996, **15**, 1935; R. H. Naulty, A. M. McDonagh, I. R. Whittall, M. P. Cifuentes, M. G. Humphrey, S. Houbrechts, J. Maes, A. Persoons, G. A. Heath and D. C. R. Hockless, *J. Organomet. Chem.*, 1998, **563**, 137.

6 S. Houbrechts, K. Clays, A. Persoons, V. Cadierno, M. P. Gamasa and J. Gimeno, *Organometallics*, 1996, **15**, 5266; V. Cadierno, S. Conejero, M. P. Gamasa, J. Gimeno, I. Asselberghs, S. Houbrechts, K. Clays, A. Persoons, J. Borge and S. García-Granda, *Organometallics*, 1999, **18**, 582.

7 M. Tamm, T. Jentzsch and W. Werncke, *Organometallics*, 1997, **16**, 1418.

8 I.-Y. Wu, J. T. Lin, J. Luo, S.-S. Sun, C.-S. Li, K. J. Lin, C. Tsai, C.-C. Hsu and J.-L. Lin, *Organometallics*, 1997, **16**, 2038; I.-Y. Wu, J. T. Lin, J. Luo, C.-S. Li, C. Tsai, Y.-S. Wen, C.-C. Hsu, F.-F. Yeh and S. Liou, *Organometallics*, 1998, **17**, 2188.

9 (*a*) B. J. Coe, M. C. Chamberlain, J. P. Essex-Lopresti, S. Gaines, J. C. Jeffery, S. Houbrechts and A. Persoons, *Inorg. Chem.*, 1997, **36**, 3284; (*b*) B. J. Coe, J. P. Essex-Lopresti, J. A. Harris, S. Houbrechts and A. Persoons, *Chem. Commun.*, 1997, 1645; (*c*) B. J. Coe, J. A. Harris, L. J. Harrington, J. C. Jeffery, L. H. Rees, S. Houbrechts and A. Persoons, *Inorg. Chem.*, 1998, **37**, 3391.

10 J. L. Oudar and D. S. Chemla, *J. Chem. Phys.*, 1977, **66**, 2664; J. Zyss and J. L. Oudar, *Phys. Rev. A*, 1982, **26**, 2016.

11 B. J. Coe, S. Houbrechts, I. Asselberghs and A. Persoons, *Angew. Chem., Int. Ed.*, 1999, **38**, 366; B. J. Coe, *Chem. Eur. J.*, 1999, **5**, 2464.

12 J. C. Curtis, B. P. Sullivan and T. J. Meyer, *Inorg. Chem.*, 1983, **22**, 224.
13 A. J. Blacker, J. Jazwinski and J.-M. Lehn, *Helv. Chim. Acta*, 1987, **70**, 1.
14 E. D. Bergmann, F. E. Crane, Jr. and R. M. Fuoss, *J. Am. Chem. Soc.*, 1952, **74**, 5981.
15 P. J. Stang, D. H. Cao, S. Saito and A. M. Arif, *J. Am. Chem. Soc.*, 1995, **117**, 6273.
16 S. Hünig, J. Groß, E. F. Lier and H. Quast, *Liebigs Ann. Chem.*, 1973, 339.
17 K. Clays and A. Persoons, *Phys. Rev. Lett.*, 1991, **66**, 2980; *Rev. Sci. Instrum.*, 1992, **63**, 3285; E. Hendrickx, K. Clays, A. Persoons, C. Dehu and J. L. Brédas, *J. Am. Chem. Soc.*, 1995, **117**, 3547.
18 S. Houbrechts, K. Clays, A. Persoons, Z. Pikramenou and J.-M. Lehn, *Chem. Phys. Lett.*, 1996, **258**, 485.
19 M. Stähelin, D. M. Burland and J. E. Rice, *Chem. Phys. Lett.*, 1992, **191**, 245.
20 E. Hendrickx, C. Dehu, K. Clays, J. L. Brédas and A. Persoons, *ACS Symp. Ser.*, 1995, **601**, 82.
21 I. D. Morrison, R. G. Denning, W. M. Laidlaw and M. A. Stammers, *Rev. Sci. Instrum.*, 1996, **67**, 1445.
22 Collect, Data collection software, R. Hooft, Nonius B.V., Delft, The Netherlands, 1998.
23 Z. Otwinowski and W. Minor, *Methods Enzymol.*, 1997, **276**, 307.
24 R. H. Blessing, *Acta Crystallogr., Sect. A*, 1995, **51**, 33; *J. Appl. Crystallogr.*, 1997, **30**, 421.
25 S. Mackay, C. J. Gilmore, C. Edwards, M. Tremayne, N. Stewart and K. Shankland, MAXUS, a computer program for the solution and refinement of crystal structures from diffraction data, University of Glasgow, UK, Nonius B.V., Delft, The Netherlands and MacScience Co. Ltd., Yokohama, Japan, 1998.
26 SHELXTL 5.03 program system, Siemens Analytical X-Ray Instruments, Madison, WI, 1995.
27 G. M. Sheldrick, *Acta Crystallogr., Sect. A*, 1990, **46**, 467.
28 G. M. Sheldrick, SHELXL 97, Program for crystal structure refinement, University of Göttingen, 1997.
29 D. W. Clack, J. C. Evans, C. R. Morris and C. R. Rowlands, *J. Chem. Soc., Perkin Trans. 2*, 1988, 1541.
30 M. Horner and S. Hünig, *Liebigs Ann. Chem.*, 1982, 1183.
31 P. Ford, De F. P. Rudd, R. Gaunder and H. Taube, *J. Am. Chem. Soc.*, 1968, **90**, 1187; C. R. Johnson and R. E. Shepherd, *Inorg. Chem.*, 1983, **22**, 2439.
32 J. F. Wishart, X. Zhang, S. S. Isied, J. A. Potenza and H. J. Schugar, *Inorg. Chem.*, 1992, **31**, 3179.
33 K. J. LaChance-Galang, P. E. Doan, M. J. Clarke, U. Rao, A. Yamano and B. M. Hoffman, *J. Am. Chem. Soc.*, 1995, **117**, 3529.
34 L.-T. Cheng, W. Tam, S. R. Marder, A. E. Stiegman, G. Rikken and C. W. Spangler, *J. Phys. Chem.*, 1991, **95**, 10643.

Paper 9/05652A

Acta Crystallographica Section C
Crystal Structure Communications
ISSN 0108-2701

trans-4-[4-(Dimethylamino)phenyliminomethyl]-*N*-phenylpyridinium hexafluorophosphate

Benjamin J. Coe,[a]* James A. Harris,[a] Thomas Gelbrich[b] and Michael B. Hursthouse[b]

[a]Department of Chemistry, University of Manchester, Manchester M13 9PL, England, and [b]EPSRC X-ray Crystallography Service, Department of Chemistry, University of Southampton, Highfield, Southampton SO17 1BJ, England
Correspondence e-mail: b.coe@man.ac.uk

Received 24 July 2000
Accepted 12 September 2000

The crystal structure of the dipolar chromophoric title compound, $C_{20}H_{20}N_3^+ \cdot PF_6^-$, is described. The phenylene and pyridyl rings are almost coplanar [dihedral angle 7.5 (2)°], but the phenyl substituent forms a dihedral angle of 56.6 (1)° with the pyridyl ring. The compound crystallizes in the non-centrosymmetric space group *Cc* and is a likely candidate for the display of quadratic non-linear optical effects.

Comment

The discovery of new molecular materials possessing non-linear optical (NLO) properties is crucial for the development of future optoelectronic and photonic devices (Bosshard *et al.*, 1995; Chemla & Zyss, 1987; Nalwa & Miyata, 1997). It is well established that the creation of efficient quadratic NLO materials requires the optimization of both molecular and bulk properties. The majority of promising candidates consist of dipolar donor–π–acceptor (*D*–π–*A*) molecules which must exist in a non-centrosymmetric macroscopic arrangement if quadratic NLO effects, such as frequency doubling (second harmonic generation, SHG), are to be observed.

Although NLO organics are usually neutral molecules, various charged compounds also exhibit NLO behaviour. Hemicyanine dyes, such as the *p*-toluenesulfonate salt of *trans*-4′-(dimethylamino)-*N*-methyl-4-stilbazolium (DAST), are particularly attractive for quadratic NLO applications (Marder *et al.*, 1989, 1994). The NLO properties of related Schiff base chromophores such as *trans*-4-[4-(dimethylamino)phenyliminomethyl]-*N*-methylpyridinium have also been studied (Coradin *et al.*, 1996). We have recently found that the molecular quadratic NLO responses of *N*-arylstilbazolium chromophores are larger than those of their *N*-methyl counterparts (Coe *et al.*, 2000). Hence, dipolar *N*-arylpyridinium Schiff base derivatives are also of interest as potential novel NLO materials. The title compound, (I), was synthesized by a base-catalyzed condensation reaction of *N*-phenylpicolinium chloride hydrate [prepared from the reaction of picoline with 2,4-dinitrochlorobenzene, followed by treatment with aniline, according to a procedure previously published by Coe *et al.* (1998)] with *N*,*N*′-dimethyl-4-nitrosoaniline, and its structure is presented here.

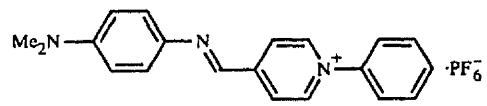

(I)

The cation in (I) is a *D*–π–*A* molecule and shows an intense visible absorption band at λ_{max} = 534 nm in acetonitrile. By comparison with existing related molecules, this band is ascribed to a $\pi \rightarrow \pi^*$ intramolecular charge transfer (ICT) from the highest occupied molecular orbital (primarily localized on the electron-rich NMe_2 group) to the lowest unoccupied molecular orbital, localized on the electron-deficient pyridinium unit. Such low-energy ICT bands are typically associated with large molecular quadratic NLO responses (Bosshard *et al.*, 1995; Chemla & Zyss, 1987; Nalwa & Miyata, 1997). The ICT band in (I) is red-shifted by *ca* 0.14 eV, but is roughly half as intense when compared with the corresponding absorption in *trans*-4′-(dimethylamino)-*N*-phenyl-4-stilbazolium hexafluorophosphate (Coe *et al.*, 2000; data in acetonitrile).

The molecular structure of the cation in (I) is as indicated by ^{1}H NMR spectroscopy, with the phenylene and pyridyl rings adopting the expected *trans* disposition about the iminomethyl group. The small dihedral angle of 7.5 (2)° defined by the ring planes C13–C18 and N1/C7–C11 is consistent with substantial π-electronic coupling through the *D*–π–*A* framework. The phenyl substituent is twisted with respect to the pyridyl ring, with a dihedral angle of 56.6 (1)° between the planes N1/C7–C11 and C1–C6. As expected, the dipolar cation in (I) shows some evidence for polarization in the ground state, both the pyridyl and phenylene rings being partially quinoidal. For example, the average of the distances C14—C15 and C17—C18 is *ca* 0.03 Å less than the average of the other phenylene C—C distances. Also, N3—C16 shows appreciable double-bond character, being *ca* 0.08 Å shorter than N1—C1.

To the best of our knowledge, no crystallographic studies of purely organic compounds closely related to (I) have been reported previously. The only structures containing 4-[(4-*R*-phenyl)iminomethyl]-*N*-*R*′-pyridinium fragments (*R* and *R*′ are any substituent) are cluster complexes of Rh (Lahoz *et al.*, 1991) or Os (Wong *et al.*, 1995, 1996). The geometric parameters of the diaryl Schiff base unit in (I) are similar to those found in $[Os_3(\mu\text{-}H)_2(CO)_9(\mu_3\text{-}CNC_5H_4CH{=}NC_6H_4\text{-}4\text{-}O\text{-}n\text{-}C_{16}H_{33})]$ (Wong *et al.*, 1996).

The crystal packing structure of (I) is of primary importance in relation to quadratic NLO properties. The well studied compound DAST crystallizes in the non-centrosymmetric space group *Cc* and is highly SHG active (Marder *et al.*, 1989). Although the presence of *p*-toluenesulfonate anions generally

 © 2000 International Union of Crystallography • Printed in Great Britain – all rights reserved

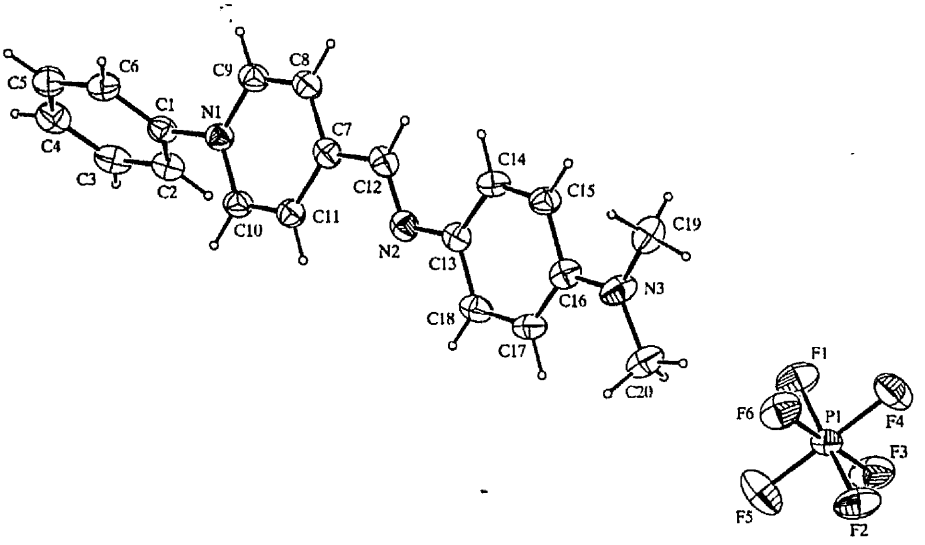

Figure 1
A representation of the molecular structure of (I), with 50% probability displacement ellipsoids. H atoms are drawn as small spheres of arbitrary radii.

appears to encourage stilbazolium salts to adopt packing motifs favourable for quadratic NLO effects (Marder *et al.*, 1994), the PF_6^- salt (I) also crystallizes in *Cc*.

The pseudo-planar *trans*-4-[4-(dimethylamino)phenyliminomethyl]pyridinium portions of the cations of (I) align head-to-tail and stack in an essentially parallel fashion, forming polar sheets within a macroscopically polar structure. The plane of the pyridinium ring (N1/C7–C11) in a given molecule and the phenylene ring plane (C13–C18) in the adjacent molecule generated by the symmetry operation $(x, 1-y, z+\frac{1}{2})$ form an angle of 1.5° with an interplanar separation of 3.29 Å, suggestive of π-stacking interactions. The PF_6^- anions lie in between the cationic sheets and are located close to the electron-deficient pyridinium moieties. The shortest intermolecular contact involving the PF_6^- anion is C9—H···F3(x, $y+1$, $z-1$), with H···F3 = 2.43 Å. The anions are arranged in channels which run parallel to the *c* axis. Similar packing structures have been observed in DAST and related compounds, in which it has been suggested that the intervening anions act to reduce dipole–dipole interactions which would otherwise cause the polar cationic sheets to align antiparallel (Marder *et al.*, 1989, 1994).

In (I), the angle θ_m between the dipolar axis (approximated as the N1—N3 vector) and the crystallographic *b* axis is 74.33°. The optimal θ_m value for SHG phase matching in the *m* symmetry point group is 35.26° (Zyss & Oudar, 1982). Hence, although the structure is not optimized for SHG, it is anticipated that (I) will exhibit substantial bulk quadratic NLO effects, especially electro-optic behaviour.

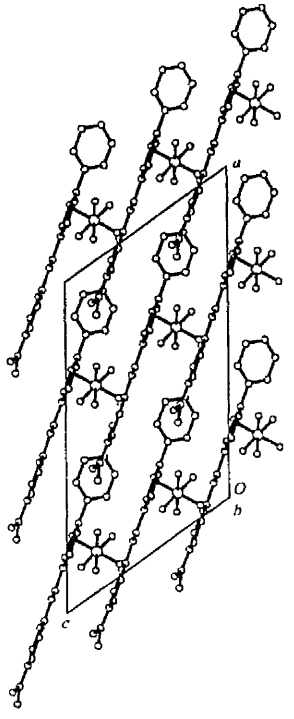

Figure 2
A crystal packing diagram for (I), viewed along the *b* axis.

Experimental

A solution of *N*-phenylpicolinium chloride hydrate (220 mg, 0.878 mmol), *N*,*N*′-dimethyl-4-nitrosoaniline (Aldrich; 219 mg, 1.458 mmol) and piperidine (Lancaster Synthesis; 2 drops) in methanol (Merck; 15 ml) was heated under reflux for 1.5 h. The resulting purple solution was reduced to dryness on a rotary evaporator. The crude chloride salt was metathesized to the PF_6^- salt by precipitation from water/aqueous NH_4PF_6 (Acros) and purified by column chromatography [silica gel, 70–230 mesh (Aldrich), acetone (Merck)/dichloromethane (Merck) 1:10], followed by precipitation from acetone/diethyl ether (yield 59 mg, 14%). Analysis calculated for $C_{20}H_{20}F_6N_3P$: C 53.69, H 4.51, N 9.39%; found: C 53.99, H 4.57, N 9.21%. Spectroscopic analysis, ^{1}H NMR (200 MHz, CD_3CN, δ, p.p.m.): 9.31 (2H, *d*, J = 7.0 Hz, C_5H_4N), 9.07 (1H, *s*, CH), 8.66 (2H, *d*, J = 7.0 Hz, C_5H_4N), 8.01–7.96 (2H, *m*, Ph), 7.84–7.79 (3H, *m*, Ph), 7.61 (2H, *d*, J = 9.1 Hz, C_6H_4), 6.87 (2H, *d*, J = 9.2 Hz, C_6H_4), 3.11 (6H, *s*, NMe_2); MS, *m*/*z*: 302: $[M-PF_6^-]^+$; λ_{max}/nm (ε/M^{-1} dm^3): 534 (32,900), 284 (16,500). Crystals of (I) suitable for single-crystal X-ray diffraction measurements were obtained by slow evaporation of an acetonitrile (Rathburn) solution at room temperature.

Crystal data

$C_{20}H_{20}N_3^+ \cdot PF_6^-$
$M_r = 447.36$
Monoclinic, Cc
$a = 19.3044$ (4) Å
$b = 10.6009$ (3) Å
$c = 11.6549$ (3) Å
$\beta = 125.527$ (2)°
$V = 1941.10$ (8) Å^3
$Z = 4$
$D_x = 1.531$ Mg m^{-3}
Mo $K\alpha$ radiation
Cell parameters from 3729 reflections
$\theta = 2.9$–40.2°
$\mu = 0.210$ mm^{-1}
$T = 150$ (2) K
Block, black
0.1 × 0.1 × 0.1 mm

Data collection

Nonius KappaCCD area-detector diffractometer
φ scans and ω scans to fill Ewald sphere
Absorption correction: multi-scan (*SORTAV*; Blessing, 1995)
$T_{min} = 0.979$, $T_{max} = 0.979$
6150 measured reflections
1909 independent reflections (with 1331 Friedel-related reflections)
2945 reflections with $I > 2\sigma(I)$
$R_{int} = 0.028$
$\theta_{max} = 25.98°$
$h = -23 \rightarrow 23$
$k = -12 \rightarrow 13$
$l = -13 \rightarrow 12$

Refinement

Refinement on F^2
$R[F^2 > 2\sigma(F^2)] = 0.036$
$wR(F^2) = 0.092$
$S = 0.998$
3240 reflections
292 parameters
H-atom parameters constrained
$w = 1/[\sigma^2(F_o^2) + (0.0611P)^2]$ where $P = (F_o^2 + 2F_c^2)/3$
$(\Delta/\sigma)_{max} < 0.001$
$\Delta\rho_{max} = 0.22$ e Å^{-3}
$\Delta\rho_{min} = -0.21$ e Å^{-3}
Extinction correction: *SHELXL97* (Sheldrick, 1997)
Extinction coefficient: 0.0126 (13)
Absolute structure: Flack (1983)
Flack parameter = 0.01 (9)

Table 1
Selected geometric parameters (Å, °).

N1—C9	1.353 (3)	N2—C13	1.392 (3)
N1—C10	1.361 (3)	N3—C16	1.363 (3)
N1—C1	1.443 (3)	N3—C20	1.445 (4)
N2—C12	1.288 (3)	N3—C19	1.459 (3)
C9—N1—C10	119.8 (2)	N1—C9—C8	120.7 (2)
C9—N1—C1	120.8 (2)	N1—C10—C11	121.2 (2)
C10—N1—C1	119.3 (2)	N2—C12—C7	119.5 (2)
C12—N2—C13	121.9 (2)	N2—C13—C18	116.7 (2)
C16—N3—C20	120.3 (2)	N2—C13—C14	126.2 (2)
C16—N3—C19	121.1 (2)	N3—C16—C17	122.4 (2)
C20—N3—C19	118.6 (2)	N3—C16—C15	120.4 (2)

All H atoms were refined in idealized positions using a riding model (C—H 0.93 and 0.96 Å) and their isotropic displacement parameters were allowed to refine freely.

Data collection: *DENZO* (Otwinowski & Minor, 1997) and *COLLECT* (Hooft, 1998); cell refinement: *DENZO* and *COLLECT*; data reduction: *DENZO* and *COLLECT*; program(s) used to solve structure: *SHELXS97* (Sheldrick, 1997); program(s) used to refine structure: *SHELXL97* (Sheldrick, 1997); molecular graphics: *PLATON* (Spek, 1990).

Thanks are due to the EPSRC for provision of a studentship (JAH) and X-ray facilities.

Supplementary data for this paper are available from the IUCr electronic archives (Reference: SX1113). Services for accessing these data are described at the back of the journal.

References

Blessing, R. H. (1995). *Acta Cryst.* A**51**, 33–38.
Bosshard, Ch., Sutter, K., Prêtre, Ph., Hulliger, J., Flörsheimer, M., Kaatz, P. & Günter, P. (1995). *Organic Nonlinear Optical Materials* (*Advances in Nonlinear Optics*, Vol. 1). Amsterdam: Gordon and Breach.
Chemla, D. S. & Zyss, J. (1987). Editors. *Nonlinear Optical Properties of Organic Molecules and Crystals*, Vols. 1 and 2. Orlando: Academic Press.
Coe, B. J., Harris, J. A., Asselberghs, I., Olbrechts, G., Wostyn, K., Clays, K., Persoons, A., Jeffery, J. C., Reeves, Z. R., Coles, S. J. & Hursthouse, M. B. (2000). In preparation.
Coe, B. J., Harris, J. A., Harrington, L. J., Jeffery, J. C., Rees, L. H., Houbrechts, S. & Persoons, A. (1998). *Inorg. Chem.* **37**, 3391–3399.
Coradin, T., Clement, R., Lacroix, P. G. & Nakatani, K. (1996). *Chem. Mater.* **8**, 2153–2158.
Flack, H. D. (1983). *Acta Cryst.* A**39**, 876–881.
Hooft, R. (1998). *COLLECT*. Nonius BV, Delft, The Netherlands.
Lahoz, F. J., Martin, A., Esteruelas, M. A., Sola, E., Serrano, J. L. & Oro, L. A. (1991). *Organometallics*, **10**, 1794–1799.
Marder, S. R., Perry, J. W. & Schaefer, W. P. (1989). *Science*, **245**, 626–628.
Marder, S. R., Perry, J. W. & Yakymyshyn, C. P. (1994). *Chem. Mater.* **6**, 1137–1147.
Nalwa, H. S. & Miyata, S. (1997). Editors. *Nonlinear Optics of Organic Molecules and Polymers*. Boca Raton: CRC Press.
Otwinowski, Z. & Minor, W. (1997). *Methods Enzymol.* **276**, 307–326.
Sheldrick, G. M. (1997). *SHELXS97* and *SHELXL97*. University of Göttingen, Germany.
Spek, A. L. (1990). *Acta Cryst.* A**46**, C-34.
Wong, W.-Y., Chan, S. & Wong, W.-T. (1996). *J. Chem. Soc. Dalton Trans.* pp. 2293–2297.
Wong, W.-Y., Wong, W.-T. & Cheung, K.-K. (1995). *J. Chem. Soc. Dalton Trans.* pp. 1379–1387.
Zyss, J. & Oudar, J. L. (1982). *Phys. Rev. A*, **26**, 2028–2048.

JOHN RYLANDS UNIVERSITY LIBRARY OF MANCHESTER